NEW METHODS IN GRAVITATIONAL AND SEISMIC REFLECTION EXPLORATION

XIN QUAN MA B. sc.

A thesis submitted for the degree of Doctor of Philosophy at the Department of Geology & Applied Geology, University of Glasgow.

April 1990.

ProQuest LLC.
789 East Eisenhower Parkway
P.O. Box 1346
Ann Arbor, MI 48106 – 1346

Dedicated to my parents

Contents

Declaration

The material presented herein is the result of my independent research undertaken between April 1987 and April 1990 at the Department of Geology & Applied Geology, University of Glasgow. It has not previously been submitted for any degree.

Any published or unpublished results of other workers have been given full acknowledgment in the text.

April 1990.

Acknowledgments

This research was carried out at the Department of Geology & Applied Geology, University of Glasgow. I am indebted to Professor B. E. Leake, the head of the department, for allowing me the use of the facilities of the department during this research.

I would like to thank my supervisor Dr. Doyle R. Watts for his guidance and support especially on gravity work. His considerable help in conducting the seismic survey in the field, in providing constructive comments and criticisms on seismic work, and in correcting the drafts of this thesis are invaluable. His friendliness and hospitality at all times made me feel very much at home. This project would have never completed on time without his help.

I would like to thank my supervisor Professor Dave K. Smythe for his initiating and supervising seismic work. His patient guidance, stimulating discussion and encouragement and assistance with field work from the second year of the project are extremely important for this research. His correcting the drafts of this thesis greatly improves the grammar.

This project has benefited much from comments and suggestions by Dr. J. J. Doody of the department. His assistance in computing and in field work is acknowledged with thanks.

My appreciation goes to the technical staff at the Department of Geology & Applied Geology; in particular to Eddie Spiers and Kenny Roberts for their assistance throughout many long, often wet, windy and cold, days of field work, to George Gordon for designing, maintaining and repairing field equipment and to Roddy Morrison and Bob Cumberland for efficiently supplying the maps and other materials.

My thanks are due to my postgraduate student colleagues and some undergraduate students of the Department of Geology & Applied geology,

University of Glasgow; in particular, Fawzy Ahmed, Zayd Kamaliddin, Emil Said, Mohammed Boulfoul, Paul Nicholson and Morgan Sullivan, who helped me in the field work.

My gratitude is extended to the British Geological Survey, Nottinghamshire, for generously providing the gravity data of the Northern Britain, and to the British Geological Survey, Edinburgh, for allowing me the use of their seismic modelling package. The project has also benefited from Mr. Min Lou, a postgraduate student in the BGS who helped me generate synthetic seismic data.

Britoil plc (now BP Exploration plc) in Glasgow helped me demutilplex seismic data. The Signal Processing Division of Electrical and Electronic Engineering Department, University of Strathclyde allowed me to access the computer, in particular Dr. J. L. Bowie in the Division helped me to use the seismic data processing package. They are all here acknowledged with thanks.

The field work was carried out only with kind permission of landowners throughout the survey area. I am also grateful to them.

I would like to thank the China National Oil & Gas Cooperation for financing my study in Glasgow.

I am grateful to my wife Aiping for her love and encouragement and also to my daughter Maning who spent hours with me at the department.

Preface

The original project was defined as "Gravitational and Seismic Investigations in the Southern Uplands of Scotland". That was to develop a new terrain correction method, reprocess and model gravity data, and to conduct a seismic refraction survey to derive crustal structure in the Southern Uplands of Scotland. However, the seismic refraction survey was obstructed by infrequent quarry blasts and the lack of cooperation of quarry managers on notification of times of blasting, so that the research had to be redirected to another field.

In February 1988, it was agreed that my research could be redirected towards the new field as "New Methods in Gravitational and Seismic Reflection Exploration", which then forms the present thesis.

Summary

For the purpose of regional gravity survey, a completely automatic terrain correction method has been developed. The advantages of previous methods developed by others have been taken over with some modifications, also a new idea for the inner zone correction has been presented. At first, the whole area under investigation is divided into a grid of equal squares of convenient size for the automatic computation. The terrain effect of the far distant zone ($r>50$ km) is neglected. The terrain effect of the distant zone ($30<r\leq50$ km) is evaluated by approximating the prism as a vertical line with all mass centred on it, so, the line mass formula is used for this computation. The terrain correction of the intermediate zone ($2<r\leq30$ km) is estimated by approximating prism as a segment of a hollow cylinder of different sizes. Specifically, the side of the prism is treated as 4 km in the zone ($20<r\leq30$ km), 2 km in the zone ($15<r\leq20$ km) and 1 km in the zone ($2<r\leq15$ km). The terrain effect of near zone 2 ($0.5<r\leq2$ km) is calculated by approximating the terrain as a vertical prism with a horizontal lower face and an upper face constantly sloping towards the station. A simplified formula is used for this computation. The terrain effect of near zone 1 ($r\leq0.5$ km), that is, the square with the gravity station inside, is obtained by triangulating that square with an additional four elevation values provided at the four corners of the square. Since these four heights are read directly from four points on the Ordnance Survey map, they are relatively accurate, so that the triangulated prisms will more approach the real terrain. The gravitational effect of individual prisms in near zone 1 is obtained by integrating gravity over the volume. As a result, the rather complicated formulae are derived. The software MATERRAIN has been developed on the VAX/UNIX operating system not only to make terrain corrections, but to make the free-air and Bouguer corrections. The output from the program is a Bouguer anomaly. The method is tested by the gravity data in the Southern Uplands of Scotland and the results are satisfactory. It is found

that some of the original terrain corrections provided by the BGS are underestimated and need to be modified. The method is entirely automatic and easy to use.

With respect to reflection seismology, a new experiment was conducted aimed at understanding the wave propagation in volcanic rocks, finding new means of obtaining conventional reflection seismic data, and extracting the weak signals in the presence of noise. To accommodate this, a new areal 'RAZOR' array was designed. Three-component geophones lie on one of two concentric circles of radii 75 and 130 m. The determination of the array dimension is based on several factors such as the wavelength of signal, the true dip of deep reflectors. Three-component seismic data were acquired over the basalt in the Midland Valley of Scotland using an MDS-10 Data System. The SEG-Y data were transformed into an ASCII-coded format and then rotated onto a new coordinate system. The study of characteristics of field data shows that 3-component seismograms are characterised by strong reverberations lasting as long as 500 ms. The reverberation patterns vary from station to station. The horizontal components exhibit larger amplitudes and lower frequency than the vertical component. Furthermore, the data from the inner stations are believed to be more affected by surface conditions than the data from the outer stations. The display of the vertical and radial components from the outer stations shows a line of reflection events at about 420 ms; there are no clear events on the transverse section. By applying a spatial directional filter to each component of seismic data, it is shown that there is more information in the horizontal component passing through the filter than the vertical component. This is attributed to the far larger amplitudes of the horizontal components, which may dominate the polarisation direction of particle motions. The energy variation diagram of each shot shows quantitatively that the radial component receives much more energy than the others.

In order to extract weak signals in the presence of noise, a bandpass frequency filter with a low cut-off of 20 Hz and a slope of 30 dB/octave, and a high cut-off of 60 Hz and a slope of 70 dB/octave is applied. The filtered data reveal that the filter can reject part of the low frequency reverberations (<20

Hz) and high frequency noise. For most of high reverberations within the bandwidth, the filter does little to improve the data. Predictive deconvolution filtering shows that it is very good at compressing the wavelets and attenuating the amplitude of reverberations. Since both multiples and reflections are not clear on the sections, the predictive deconvolution filter has to be used with great care, otherwise it degrades the useful signals. A signal enhancement polarisation filter was developed, based on a covariance matrix method. Both random noise and field data tests demonstrate that it can be used to remove the random noise and part of the surface waves arriving from different directions. From the interpretation point of view, the base of the Clyde Plateau Lavas in the area investigated is found to be at about 930 m below the surface.

To test the newly developed signal enhancement polarisation filter and the optimisation of array designing, synthetic 3-component seismic data were generated in both isotropic and anisotropic media. The application of the signal enhancement polarisation filter to those data is successful in terms of suppressing random noise and enhancing signals. In addition, stacking the filtered data based on the areal 'RAZOR' array provides a highly resolved seismic section. The study of effect of added random noise on filtering shows that, if the noise entirely changes the polarisation direction of particle motions of reflection wavelets. The filter may thus not be able to extract very weak signals from noise, however, by reducing the root mean square variance of random noise to a certain degree such that the noise mixed data exhibit a better polarisation, the filter can then extract very weak signals.

A new approach of using slant-slack processing to image structure based on the areal array has been demonstrated using synthetic data from a simple geological model. The result further proves that the dimension of the aerial array is appropriate for receiving the reflected plane waves from deep interfaces. The true dip and dip direction of a reflector can possibly be derived from τ-p images and τ-x images respectively, supposing that the velocity of the upper layer is known. This method can additionally be used to optimise the polarisation filtering, which keeps and enhances compressional waves of interest according to the polarisation directions of waves.

List of Figures

Chapter 1

Chapter 2

Chapter 5

List of Tables

PART ONE: GRAVITY

Chapter 1 Automatic Terrain Correction Method for Regional Gravity Survey

1.1 Introduction

In general, the Bouguer anomaly is determined by

$$g_{ba} = g_{ob} - g_o + g_f - g_b + g_t \qquad (1.1)$$

where g_{ba} is Bouguer anomaly,

g_{ob} is observed gravity value,

g_o is normal gravity calculated by an international formula,

g_f is free-air correction,

g_b is Bouguer correction,

g_t is terrain correction.

The values g_o, g_f, g_b can easily be determined, if all gravity station data such as coordinates, elevations and rock densities are available. However, determining the terrain correction g_t is the most tedious task and is a very important part of the Bouguer anomaly, especially in rugged terrain. Because of that, many authors have placed more emphasis on developing various methods to calculate the terrain correction since the 1950's.

Bott pioneered methods of terrain correction using the electronic digital computer [Bott, 1958]. His method was to divide the region under investigation into a grid of equal squares of convenient size, take the elevations at the centres of the squares as the average heights of these prisms, determine the gravity attraction of a prism at a station by calculating the

gravity value produced by a segment of a hollow vertical cylinder, sum the incremental contributions from all squares except those less than 1 km from the station. The corrections from the inner squares are calculated using the Hammer zone chart method and finally added to the computer correction value. This method was a milestone for calculations made by computer, which not only increased accuracy but also saved time. However, the main disadvantage is the time-consuming terrain correction for the inner squares.

Karlemo [1963] developed a similar method mainly used for local gravity investigation on the condition that the points of observation are regularly distributed in a definite system and the distance between points is rather small. He used a symmetrical pattern of radial elevation profiles, each representing a sector of the terrain. The gravity attraction in the inner zone ($r<250$ m) is estimated by calculating the value produced by 68 segments. The terrain corrections for the intermediate and distant zones are estimated in a similar way, but the spacing of points in these zones is increased in order to reduce the calculation time. The formulae used for calculation are very complicated. Such a method seems very accurate and reliable for small scale prospecting. However, it is rather impractical for regional gravity surveys; here stations are irregularly and sparsely distributed, because of logistical problems which make data collection in a regular grid difficult.

Blais and Ferland [1983] approximated a distant prism as a vertical line with the total mass of the prism, so the line mass formula is used to give the gravimetric terrain correction. The intermediate zones are treated in the same way as the distant zones, except for using the rigorous rectangular prism formula for regular flat-top prisms centred at the grid points. The inner zones with regular elevation data are treated as a number of smaller prisms with horizontal lower faces and sloping upper faces. The zones with irregular elevation data have to be triangulated, the corresponding boundary definition for triangulation is determined using contribution levels of the individual flat-top rectangular prisms. The gravimetric terrain corrections are obtained by calculating the effects from the triangular prisms with sloping upper

faces. This method uses a rigorous rectangular prism formula which increases accuracy for the intermediate zone contributions. However, the computation time will be increased by the 24-term formula. Above all, the boundary for triangulation defined by the contribution levels of the individual flat-top rectangular prisms is not accurate enough since the heights of the prisms are often read from contour maps, for instance, the Ordnance Survey map with a scale of 1:25000 in Britain, and are average values partly depending on a person's subjective judgment. The maximum height difference in a hilly area read by different persons can sometimes reach 30 m, which of course will affect the total correction value.

Lagios [1978] approximated the inner zones by fitting multiquadric surfaces or paraboloids to additional heights read from a map and height of a station taken as control. The more heights that are provided, the more closely does the fitting surface approach the real topography. He calculated the terrain correction for a 100×100 m block with a horizontal upper face using the approximated formula for a segment of a hollow cylinder whose height is decided by fitting surface equations to the station at the centre. The accuracy of this computation largely depends on the number of heights provided for fitting the surfaces. In practice, however, it is difficult to give a large number of elevation data for the neighborhood of stations, especially in regional gravity surveys, in which there may be thousands of stations to process.

In this chapter, an automatic terrain correction method is presented which is partly based on the previous methods, with more refined calculations for the inner zone corrections.

1.2 New approach to an automatic terrain correction method

The advantages of previous methods developed by others have been taken over with some modifications, with a new contribution for the inner zone correction being presented. The basic procedures are similar to the others. That is, the whole area under investigation is divided into a grid of equal squares of convenient size for the automatic computation. The terrain

effect of the far distant zone (r>50 km) is neglected. The terrain effect of the distant zone (30<r≤50 km) is evaluated by approximating the prism as a vertical line with all mass centred on it, so, the line mass formula is used for this computation. The terrain correction of the intermediate zone (2<r≤30 km) is estimated by approximating a prism as a segment of a hollow cylinder of different sizes. Specifically, the size of the prism is treated as 4 km in the zone where 20<r≤30 km, 2 km in the zone where 15<r≤20 km and 1 km in the zone where 2<r≤15 km. The terrain effect of near zone 2 (0.5<r≤2 km) is calculated by approximating the terrain as a vertical prism with a horizontal lower face and an upper face constantly sloping towards the station. A simplified formula is used for this computation. The terrain effect of near zone 1 (r≤0.5 km), that is, the square with the gravity station inside, is obtained by triangulating that square with an additional four elevation values provided at the four corners of the square. Since these four heights are read directly from four points on the Ordnance Survey map, the values are relatively accurate, so that the triangulated prisms will more closely approach the real terrain.

1.3 Distant zone contribution

To achieve the terrain correction by computer, the terrain has to be divided into a grid of equal squares of convenient size. For instance, in Great Britain, the size of a square for the computation is usually adapted the same as the National Grid square, which is one square kilometre. The gravitational effect is usually obtained by summing the incremental contributions from the individual prisms. With respect to the computation time and accuracy, the terrain is again divided by different zones, within each zone different approximations of terrain and formulae are applied (see Fig. 1.3.1).

The definition of the distant zone given by the author means the area which is 30 km or further from a station. For regional gravity surveys, the terrain effect caused by this large area is certainly significant. On the other hand, according to Newton's gravitational law, the gravity attraction of any mass to a certain point is inversely proportional to the square of the distance

from the mass to the point, in other words, the further the mass from the point, the less gravity attraction it will exert. So, we investigate what kind of formula is acceptable for the corrections in this distant zone. Let us suppose that the distant zone consists of a number of vertical flat-top prisms, in order to choose the appropriate formula for shortening the calculation time, but without losing much accuracy, the vertical line mass formula (1.2) and the rigorous formula of a right rectangular prism given by Nagy [1966], which contains 24-term mathematical expressions, are studied.

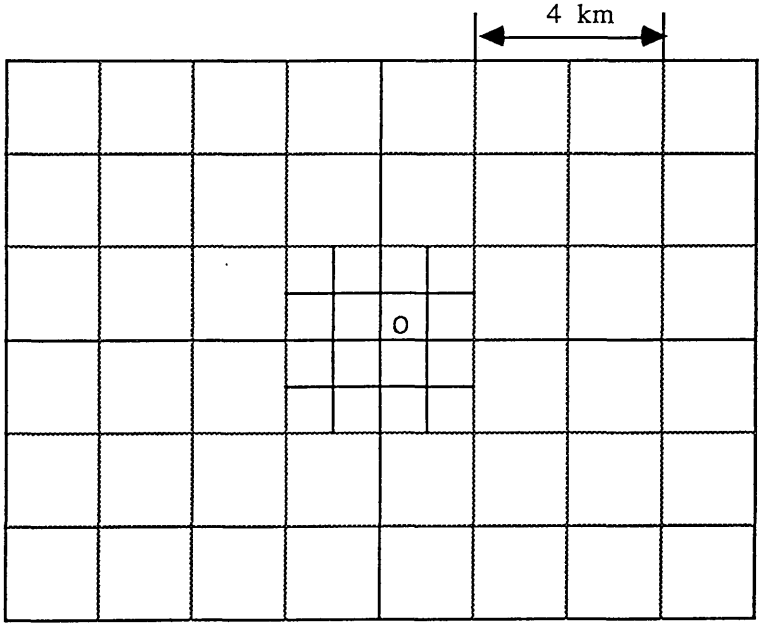

Fig. 1.3.1 Division of topography for the computerized terrain correction. The station is at the centre (o).

$$\Delta g = G\,\rho A \int_0^h \frac{z\,dz}{\sqrt{(r^2+z^2)^3}} = G\,\rho A\,(\frac{1}{r} - \frac{1}{\sqrt{r^2+h^2}}) \qquad (1.2)$$

Where r is distance from station to centre of square,

h is height difference between square and station,

A is area of square,

ρ is density of the rocks.

We calculate the gravitational effect of a height-fixed, vertical prism as

a function of the distance from the station. The results given by the rigorous prism formula are plotted in Fig. 1.3.2 (curve 1). Those given by the approximated line mass formula are shown in the same figure (curve 2). The approximation is so made that the height and mass of the line are the same as the prism's. We can see that the gravity attraction produced by the line mass at any location is always smaller than that produced by the prism. Furthermore, the difference between them decreases with increasing distance from the line mass or prism to the station. Quantitatively, Fig. 1.3.3 shows that the relative difference approaches zero when the distance between line mass or prism and a station reaches 12 km. Therefore, the line mass formula is an acceptable approximation for this distant area (r>30 km).

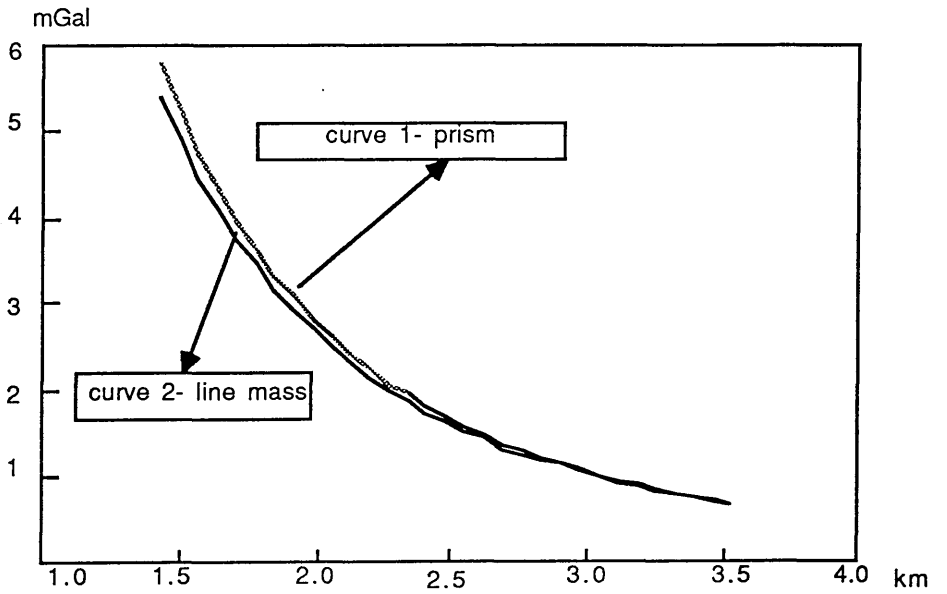

Fig. 1.3.2 Diagram showing gravity in mGal of a prism and a line mass. Both have the same mass.

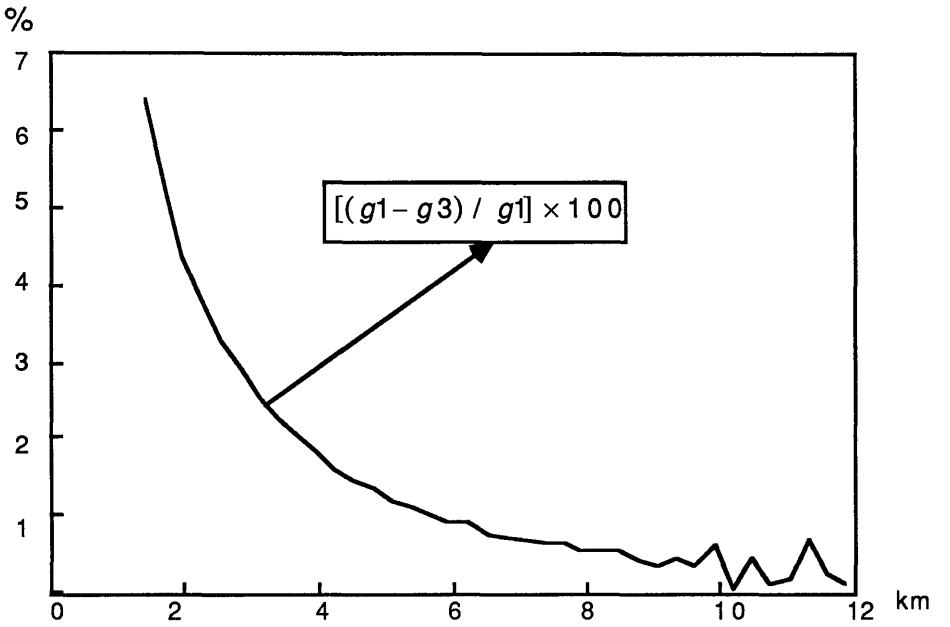

Fig. 1.3.3 Comparison of the terrain effect of a prism and a line mass. g1 is the effect of a prism, g3 is the effect of a line mass. The computation is made by [(g1-g3)/g1] ×100.

1.4 Intermediate zone contribution

This zone covers the area at a radius of 2 km to 30 km. Bott [1959] showed that substituting a prism with a segment of hollow cylinder is an excellent approximation. The gravitational attraction from a segment of a hollow cylinder (α) with an inner radius r_1 and an outer radius r_2 is given by

$$\Delta g = G\rho\alpha\left(r_2 - r_1 + \sqrt{r_1^2 + h^2} - \sqrt{r_2^2 + h^2} \right)$$

The above formula is further approximated. That is, the square root is expanded in a power series and the terms with high power are neglected,

$$\sqrt{r^2 + h^2} \approx r\left(1 + \frac{1}{2}\frac{h^2}{r^2}\right)$$

If we now replace r_2 and r_1 by r+p and r-p, α by A/2rp (A is area of the square, r is distance from station to centre of square and p is half length of

square side), the terrain correction for a prism can be approximated as

$$\Delta g = \frac{G \rho A}{2} \cdot \frac{h^2}{r(r^2 - p^2)} \qquad (1.3)$$

where definitions of G, ρ, A, h, are the same as those given in formula (1.2).

A considerable amount of computation time will be saved if many squares which are beyond a certain distance from a station are grouped and treated as a single square. In the area where $20<r\leq30$ km, sixteen squares are treated as one square. In the area where $15<r\leq20$ km, four squares are treated as a single square (here p=1 km). In the area where $2<r\leq15$ km, a single square with 1 km sides is used to calculate the terrain correction.

1.5 Near zone 2 contribution

The term 'near zone' is sometimes called the inner zone, and may mean different sizes of an area to different authors. The near zone is defined here as the area whose radius is less than or equal to 2 km. This zone is sub-divided into two zones named near zone 1 ($0.0<r\leq0.5$ km) and near zone 2 ($0.5<r\leq2$ km).

We can see from Fig. 1.3.3 that an error will reach more than 6% when a line mass is used to approximate a prism within near zone 2. Substitution of a prism by a segment of a hollow cylinder will also introduce an error. Furthermore, when the upper face of a prism is sloping, an even bigger error will be introduced. Hence not only a rigorous formula like the prism formula is required, but the slope of terrain must also be taken into consideration.

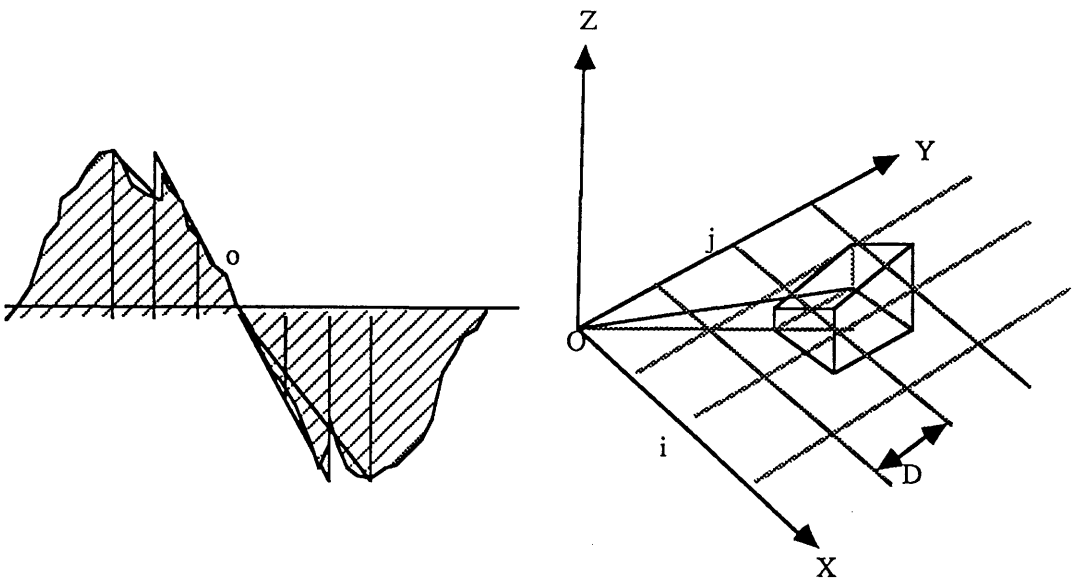

Fig. 1.5.1 (a) Presentation of the terrain in near zone 2. (b) Diagram to show one prism with an upper face constantly sloping towards the station.

To solve this problem, the terrain is divided into a number of rectangular prisms with the horizontal lower faces and sloping upper faces which are determined by the heights at the centres of prisms and heights of neighbouring locations. The gravitational effect of a rectangular prism with the horizontal upper and lower faces and vertical sides has already been derived by Nagy [1966]. The modification is made to include a sloping top given by an equation of form: z=ax+by+c, where a and b are the slope coefficients in x and y respectively. Hence the terrain correction for a single prism can be given as

$$\Delta g = G\rho \int_{y_1}^{y_2} dy \int_{x_1}^{x_2} dx \int_{0}^{ax+by+c} \frac{z\,dz}{\sqrt{(x^2+y^2+z^2)^3}} \qquad (1.4)$$

If the lower face of the prism is horizontal at the level of origin, the upper face slopes with a constant slope towards the origin, the sides of prism

have a unit length D, the gravitational attraction at the origin (0, 0) of the volume element dv, can be integrated over the volume of the prism, which has its vertical axis at x=iD and y=jD (see Fig. 1.5.1. (b)), the integers i and j are the indexes along the x-axis and the y-axis. The result from integrating (1.4) is given as [Ketelaar, 1976]

$$\Delta g = G\,\rho \iiint_{v} \frac{z}{r^3}\,dv = G\,\rho(1-\cos\,\alpha)\,D\,K(i,j) \qquad (1.5)$$

where G is gravitational constant,

ρ is density of the rocks,

D is unit length,

K(i, j) is position matrix,

α is arctg(h/r).

In order to give a quantitative idea, the terrain effect of a prism in the vicinity of a station is calculated using three different formulae assuming that the prism is at the fixed location (2.12 km from the station) with different heights (Δg_1 is for a prism with the horizontal upper and lower faces, Δg_2 for a prism with a horizontal lower face and a sloping upper face constantly towards the station and Δg_3 for a line mass). The gravitational effects of a prism computed by three formulae are listed in Table 1.5.1, from which we can see that, no matter how variable the height of the prism, the formula for the prism with the horizontal upper and lower faces always gives the biggest values. The result from the line mass formula is always underestimated. The relative difference between Δg_1 and Δg_2 decreases with the increasing height. We also calculate the terrain effect of a prism with a fixed height (1.0 km) as a function of the distance from the station. The results are listed in Table 1.5.2, which indicates that the relative difference between Δg_1 and Δg_2 decreases with the increasing distance from the station. It is assumed that topography in near zone 2 would be better represented by a prism with a sloping upper face. Table 1.5.1 demonstrates that a flat top prism will systematically overestimate gravity correction, and a line mass would be an underestimate. It is better to

use a prism with a sloping upper face to approximate real terrain in near zone 2, although problems may arise for areas of very rapid changes of topography.

h	0.5	0.8	1.0	1.5	2.0	3.0 km
Δg_1	0.246	0.589	0.868	1.643	2.411	3.689
Δg_2	0.228	0.552	0.819	1.574	2.336	3.626
Δg_3	0.226	0.546	0.811	1.558	2.313	3.589
%	7.100	6.300	5.700	4.200	3.100	1.700

Table 1.5.1 Terrain corrections for prisms of 1×1 km^2 with different heights by three different formulae. The prism is located at r=2.12 km. $\%=100 \times(\Delta g_1-\Delta g_2)/\Delta g_1$.

r	1.41	2.12	2.83	3.54	4.24	6.36 km
Δg_1	2.657	0.868	0.380	0.198	0.116	0.003
Δg_2	2.396	0.819	0.366	0.193	0.113	0.003
Δg_3	2.337	0.811	0.364	0.192	0.113	0.003
%	9.800	5.700	3.600	2.400	1.700	0.900

Table 1.5.2 Terrain corrections for prisms of 1×1 km^2 with a fixed height (1.0 km) at different distances from the station. $\%=100 \times(\Delta g_1-\Delta g_2)/\Delta g_1$.

1.6 Near zone 1 contribution

This zone covers the area with a radius of less than or equal to 0.5 km. The gravity effect of this near zone is extremely important. Table 1.6.1 lists the gravity contributions of 4 stations from 3 different zones in the Southern Uplands of Scotland. We can see that although it occupies a small area, its gravity effect is significant. Station 55 shows that the gravity effect of near zone 1 contributes up to 48 % of the total terrain correction.

No.	gt1	gt2	gt3	gt	%
55	1.39	1.15	0.35	2.89	48
107	3.98	4.35	5.11	3.44	29
164	2.77	1.86	1.05	5.69	48
494	1.31	1.36	0.76	3.41	38

Table 1.6.1 Gravity contributions from different zones. N- station number, gt1- mGal from Near zone 1, gt2 - mGal from near zone 2, gt3- mGal from rest of area, gt- mGal, total terrain correction. % = 100 ×(gt-gt1)/gt.

It is obviously time-consuming to use the Hammer zone chart for the terrain correction in this area. We develop a new method which not only achieves the correction automatically but provides higher accuracy. The basic idea is to establish a new coordinate system whose origin is at the station location, then to triangulate the station-contained square with an additional four elevation values at the four corners of the square, and the elevation of the station itself taken as control. Fig. 1.6.1 (a) shows four triangular prisms with horizontal lower faces and sloping upper faces. The gravitational attraction of individual prisms can be obtained by integrating gravity over the volume of the triangular prism. The effects of the four prisms are summed together, and the result is eventually added to the total terrain correction for that station.

Suppose that four elevations at the four corners of the square are all higher than the station elevation. Based on this assumption, the terrain effects of the four triangular prisms are considered individually as follows.

Let us take the first triangular prism $OP_1P_2Z_2Z_1$ as an example to show how the terrain effect is obtained. The basic formula for the calculation is a simple integration over volume v:-

$$g_1 = G\rho \iiint_v \frac{z\,dx\,dy\,dz}{\sqrt{(x^2+y^2+z^2)^3}} \qquad (1.6)$$

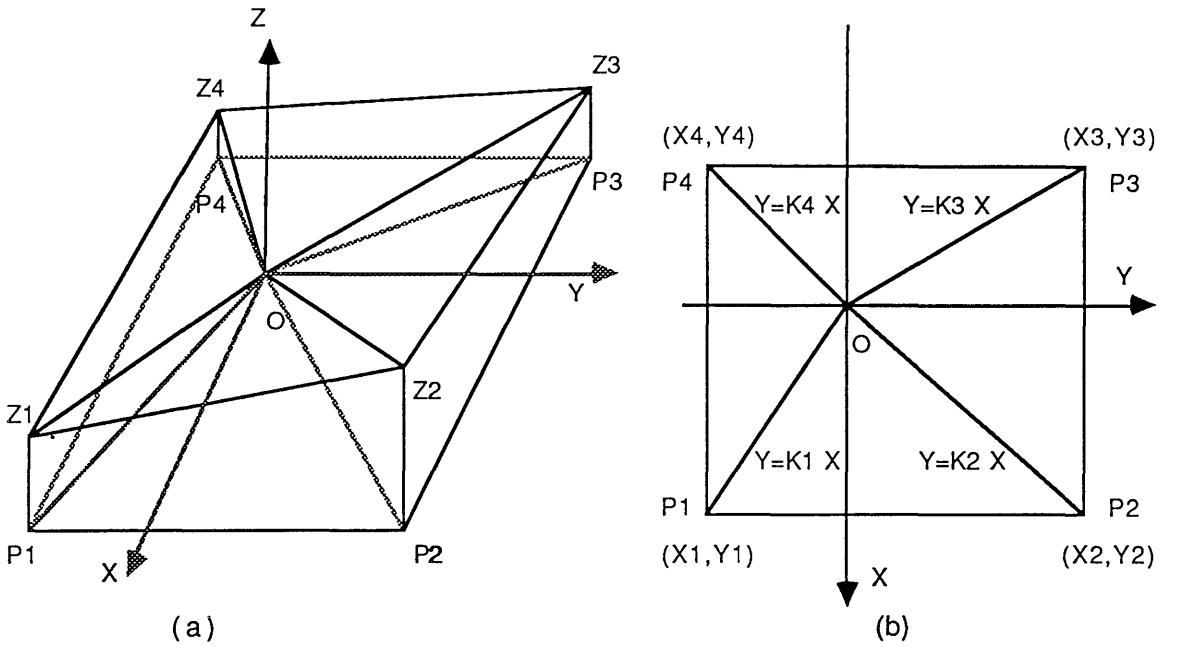

Fig. 1.6.1 (a) Triangulation of near zone 1 in perspective view when P1Z1, P2Z2, P3Z3 and P4Z4 are positive. (b) Projection of (a) onto the X-Y plane.

The integration limits are shown in Fig. 1.6.1 (a) and (b). The equations of line OP_1 and line OP_2 and plane OZ_1Z_2 are $y=k_1x$ and $y=k_2x$ and $z=a_1x+b_1y$ respectively. Therefore, the integration can be written as

$$g_1 = G\rho \int_0^{x_1} dx \int_{k_1 x}^{k_2 x} dy \int_0^{ax+by} \frac{z\,dz}{\sqrt{(x^2+y^2+z^2)^3}} \qquad (1.7)$$

Since we already know the coordinates at P_1 and P_2, the heights Z_1P_1 and Z_2P_2, the line and plane equations can exclusively be determined by the following coefficients,

$$a_1 = \frac{\begin{vmatrix} z_1 & y_1 \\ z_2 & y_2 \end{vmatrix}}{\begin{vmatrix} x_1 & y_1 \\ x_2 & y_2 \end{vmatrix}} \qquad b_1 = \frac{\begin{vmatrix} x_1 & z_1 \\ x_2 & z_2 \end{vmatrix}}{\begin{vmatrix} x_1 & y_1 \\ x_2 & y_2 \end{vmatrix}}$$

$$k_1 = \frac{y_1}{x_1} \qquad k_2 = \frac{y_2}{x_2}$$

Hence the gravitational effect of the triangular volume $OP_1P_2Z_2Z_1$ is obtained by integrating (1.7). We get

$$g_1 = G\rho \int_0^{x_1} dx \int_{k_1 x}^{k_2 x} dy \int_0^{a_1 x + b_1 y} \frac{z\,dz}{\sqrt{(x^2 + y^2 + z^2)^3}}$$

$$= G\rho \int_0^{x_1} dx \int_{k_1 x}^{k_2 x} dy \left(\frac{1}{\sqrt{x^2 + y^2}} - \frac{1}{\sqrt{x^2 + y^2 + (a_1 x + b_1 y)^2}} \right)$$

$$= G\rho \int_0^{x_1} dx \left(\int_{k_1 x}^{k_2 x} \frac{dy}{\sqrt{x^2 + y^2}} - G\rho \int_{k_1 x}^{k_2 x} \frac{dy}{\sqrt{x^2 + y^2 + (a_1 x + b_1 y)^2}} \right)$$

$$= G\rho \int_0^{x_1} dx \left(\ln \frac{k_2 + \sqrt{1 + k_2^2}}{k_1 + \sqrt{1 + k_1^2}} - \right.$$

$$\left. \frac{G\rho}{\sqrt{1 + b_1^2}} \left[\ln \frac{k_2 + \frac{a_1 b_1}{1 + b_1^2} + \sqrt{\left(k_2 + \frac{a_1 b_1}{1 + b_1^2}\right)^2 + \frac{1 + a_1^2}{1 + b_1^2} - \frac{a_1^2 b_1^2}{(1 + b_1^2)^2}}}{k_1 + \frac{a_1 b_1}{1 + b_1^2} + \sqrt{\left(k_1 + \frac{a_1 b_1}{1 + b_1^2}\right)^2 + \frac{1 + a_1^2}{1 + b_1^2} - \frac{a_1^2 b_1^2}{(1 + b_1^2)^2}}} \right] \right)$$

$$= G\rho x_1 \ln \frac{k_2 + \sqrt{1+k_2^2}}{k_1 + \sqrt{1+k_1^2}} -$$

$$\frac{G\rho X_1}{\sqrt{1+b_1^2}} \left[\ln \frac{k_2 + \frac{a_1 b_1}{1+b_1^2} + \sqrt{(k_2 + \frac{a_1 b_1}{1+b_1^2})^2 + \frac{1+a_1^2}{1+b_1^2} - \frac{a_1^2 b_1^2}{(1+b_1^2)^2}}}{k_1 + \frac{a_1 b_1}{1+b_1^2} + \sqrt{(k_1 + \frac{a_1 b_1}{1+b_1^2})^2 + \frac{1+a_1^2}{1+b_1^2} - \frac{a_1^2 b_1^2}{(1+b_1^2)^2}}} \right] \quad (1.8)$$

Formula (1.8) is used to calculate the terrain effect for the first triangular prism $OP_1P_2Z_2Z_1$. The other three triangular prisms can be treated in the same way, that is, suppose the equations of planes OZ_2Z_3, OZ_3Z_4, and OZ_4Z_1 are $z=a_2x+b_2y$, $z=a_3x+b_3y$ and $z=a_4x+b_4y$ respectively, the coefficients a_2, b_2, a_3, b_3, a_4, and b_4 can also be obtained in a similar way. For simplicity, below are given only three results obtained from integrating (1.7) over three different triangular prisms.

$$g_2 = G\rho y_2 \ln \frac{k_2' + \sqrt{1+k_2'^2}}{k_3' + \sqrt{1+k_3'^2}} -$$

$$\frac{G\rho y_2}{\sqrt{1+a_2^2}} \left[\ln \frac{k_2' + \frac{a_2 b_2}{1+a_2^2} + \sqrt{(k_2' + \frac{a_2 b_2}{1+a_2^2})^2 + \frac{1+b_2^2}{1+a_2^2} - \frac{a_2^2 b_2^2}{(1+a_2^2)^2}}}{k_3' + \frac{a_2 b_2}{1+a_2^2} + \sqrt{(k_3' + \frac{a_2 b_2}{1+a_2^2})^2 + \frac{1+b_2^2}{1+a_2^2} - \frac{a_2^2 b_2^2}{(1+a_2^2)^2}}} \right] \quad (1.9)$$

$$g_3 = -G\rho x_3 \ln \frac{k_3 + \sqrt{1+k_3^2}}{k_4 + \sqrt{1+k_4}} + \frac{G\rho x_3}{\sqrt{1+a_3^2}} \left[\ln \frac{k_3 + \frac{a_3 b_3}{1+a_3^2} + \sqrt{(k_3 + \frac{a_3 b_3}{1+a_3^2})^2 + \frac{1+b_3^2}{1+a_3^2} - \frac{a_3^2 b_3^2}{(1+a_3^2)^2}}}{k_4 + \frac{a_3 b_3}{1+a_3^2} + \sqrt{(k_4 + \frac{a_3 b_3}{1+a_3^2})^2 + \frac{1+b_3^2}{1+a_3^2} - \frac{a_3^2 b_3^2}{(1+a_3^2)^2}}} \right] \quad (1.10)$$

$$g_4 = -G\rho y_1 \ln \frac{k_1' + \sqrt{1+k_1'^2}}{k_4' + \sqrt{1+k_4'}} + \frac{G\rho y_1}{\sqrt{1+b_4^2}} \left[\ln \frac{k_1' + \frac{a_4 b_4}{1+b_4^2} + \sqrt{(k_1' + \frac{a_4 b_4}{1+b_4^2})^2 + \frac{1+a_4^2}{1+b_4^2} - \frac{a_4^2 b_4^2}{(1+b_4^2)^2}}}{k_4' + \frac{a_4 b_4}{1+b_4^2} + \sqrt{(k_4' + \frac{a_4 b_4}{1+b_4^2})^2 + \frac{1+a_4^2}{1+b_4^2} - \frac{a_4^2 b_4^2}{(1+b_4^2)^2}}} \right] \quad (1.11)$$

Where $k_2'=1/k_2$ and $k_3'=1/k_3$.

The terrain correction of near zone 1 is obtained by summing 4 incremental contributions for the 4 triangular prisms. Thus we get

$$g=g_1+g_2+g_3+g_4 \quad (1.12)$$

As stated before, the value g is based on an assumption that the four elevation values Z_1P_1, Z_2P_2, Z_3P_3, and Z_4P_4 are all positive. However, in reality, these four positions in the square can be either higher or lower than the gravity station. One example is shown in Fig. 1.6.2 in which Z_1P_1 is negative, the others remain positive. Here, if (1.8) is taken as the terrain effect of triangular prism 1, the correction will be overestimated. Specifically, the real terrain being considered should be the triangular prism $OQ_1P_1Z_1'$ and $OQ_1P_2Z_2$

instead of $OP_1P_2Z_2Z_1$. Because of symmetry, the volume of the prism $OQ_1P_1Z_1'$ is equal to that of the prism $OQ_1P_1Z_1$, that is, integrating over the volume $OQ_1P_1Z_1'$ is equivalent to integrating over the volume $OQ_1P_1Z_1$. Therefore, the terrain effect of two triangular prisms $OQ_1P_1Z_1'$ and $OQ_1P_2Z_2$ can be obtained by subtracting the effect produced by the central prism $OQ_1Z_1Z_2$ from the overall effect produced by the triangular prism $OP_1P_2Z_2Z_1$.

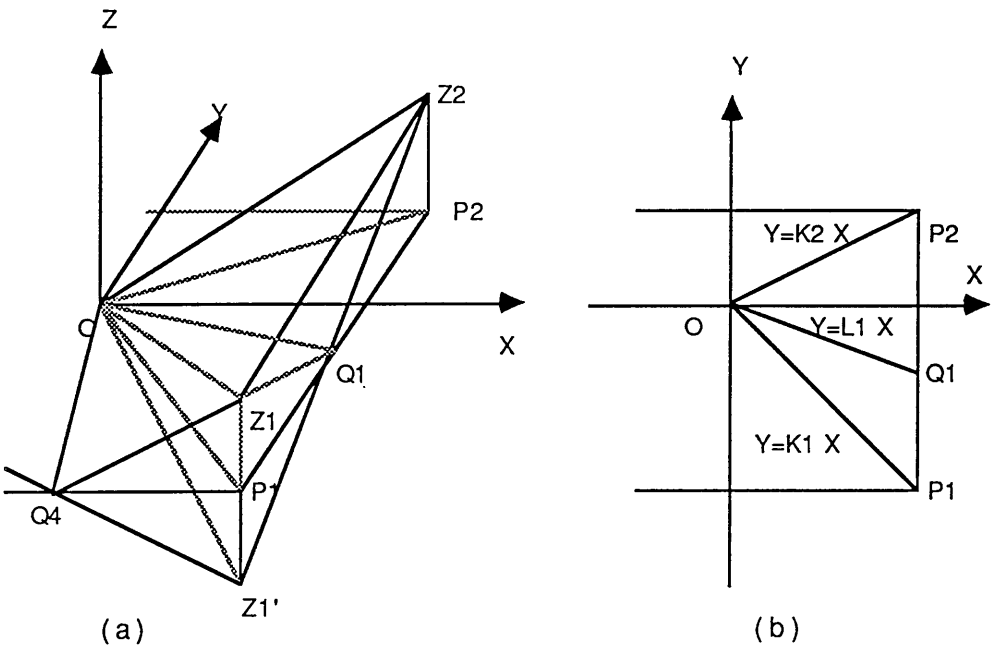

Fig. 1.6.2 (a) Triangulation of near zone 1 when P1Z1 is negative. (b) Projection of (a) onto the X-Y plane.

To calculate the gravitational effect (F_1) of the triangular prism $OQ_1Z_2Z_1$, the equations of plane OZ_1Q_1 and OZ_2Q_1 must be known. Let $z=c_1x+d_2y$ and $z=c_2x+d_2y$ be equations of planes OZ_1Q_1 and OZ_2Q_1 respectively. The coefficients c_1, d_1, c_2 and d_2 can easily be determined. We get

$$c_1 = \frac{\begin{vmatrix} z_1 & y_1 \\ -z_2 & y_2 \end{vmatrix}}{\begin{vmatrix} x_1 & y_1 \\ x_2 & y_2 \end{vmatrix}} \qquad d_1 = \frac{\begin{vmatrix} x_1 & z_1 \\ x_2 & -z_2 \end{vmatrix}}{\begin{vmatrix} x_1 & y_1 \\ x_2 & y_2 \end{vmatrix}}$$

$$c_2 = \frac{\begin{vmatrix} -z_1 & y_1 \\ z_2 & y_2 \end{vmatrix}}{\begin{vmatrix} x_1 & y_1 \\ x_2 & y_2 \end{vmatrix}} \qquad d_2 = \frac{\begin{vmatrix} x_1 & -z_1 \\ x_2 & z_2 \end{vmatrix}}{\begin{vmatrix} x_1 & y_1 \\ x_2 & y_2 \end{vmatrix}}$$

$$l_1 = -c_1 / d_1$$

Integrating (1.6) over the volume $OQ_1Z_2Z_1$ gives

$$F_1 = G\rho\{\int_0^{x_1} dx \int_{k_1 x}^{l_1 x} dy \int_{c_1 x + d_1 y}^{a_1 x + b_1 y} \frac{z\,dz}{\sqrt{(x^2+y^2+z^2)^3}} + \int_0^{x_1} dx \int_{l_1 x}^{k_2 x} dy \int_{c_2 x + d_2 y}^{a_1 x + b_1 y} \frac{z dz}{\sqrt{(x^2+y^2+z^2)^2}}\}$$

$$= \frac{G\rho X_1}{\sqrt{1+d_1^2}} \left[\ln \frac{l_1 + \frac{c_1 d_1}{1+d_1^2} + \sqrt{(l_1 + \frac{c_1 d_1}{1+d_1^2})^2 + \frac{1+c_1^2}{1+d_1^2} - \frac{c_1^2 d_1^2}{(1+d_1^2)^2}}}{k_1 + \frac{c_1 d_1}{1+d_1^2} + \sqrt{(k_1 + \frac{c_1 d_1}{1+d_1^2})^2 + \frac{1+c_1^2}{1+d_1^2} - \frac{c_1^2 d_1^2}{(1+d_1^2)^2}}} \right]$$

$$- \frac{G\rho X_1}{\sqrt{1+b_1^2}} \left[\ln \frac{l_1 + \frac{a_1 b_1}{1+b_1^2} + \sqrt{(l_1 + \frac{a_1 b_1}{1+b_1^2})^2 + \frac{1+a_1^2}{1+b_1^2} - \frac{a_1^2 b_1^2}{(1+b_1^2)^2}}}{k_1 + \frac{a_1 b_1}{1+b_1^2} + \sqrt{(k_1 + \frac{a_1 b_1}{1+b_1^2})^2 + \frac{1+a_1^2}{1+b_1^2} - \frac{a_1^2 b_1^2}{(1+b_1^2)^2}}} \right]$$

$$+\frac{G\rho X_1}{\sqrt{1+d_2^2}}\left[\ln\frac{k_2+\frac{c_2d_2}{1+d_2^2}+\sqrt{(k_2+\frac{c_2d_2}{1+d_2^2})^2+\frac{1+c_2^2}{1+d_2^2}-\frac{c_2^2d_2^2}{(1+d_2^2)^2}}}{l_1+\frac{c_2d_2}{1+d_2^2}+\sqrt{l_1+\frac{c_2d_2}{1+d_2^2})^2+\frac{1+c_2^2}{1+d_2^2}-\frac{c_2^2d_2^2}{(1+d_2^2)^2}}}\right]$$

$$-\frac{G\rho X_1}{\sqrt{1+b_1^2}}\left[\ln\frac{k_2+\frac{a_1b_1}{1+b_1^2}+\sqrt{(k_2+\frac{a_1b_1}{1+b_1^2})^2+\frac{1+a_1^2}{1+b_1^2}-\frac{a_1^2b_1^2}{(1+b_1^2)^2}}}{l_1+\frac{a_1b_1}{1+b_1^2}+\sqrt{(l_1+\frac{a_1b_1}{1+b_1^2})^2+\frac{1+a_1^2}{1+b_1^2}-\frac{a_1^2b_1^2}{(1+b_1^2)^2}}}\right] \quad (1.13)$$

Formula (1.13) gives a final result for evaluating the terrain effect caused by the prism $OQ_1Z_2Z_1$. We can also calculate the terrain effects (F_2, F_3, F_4) produced by other three triangular prisms $OQ_2Z_2Z_3$, $OQ_3Z_3Z_4$ and $OQ_4Z_4Z_1$ (these three triangular prisms are not shown in Fig. 1.6.2). Therefore, the terrain effect of near zone 1 can be expressed as

$$\begin{aligned} g&=(g_1-F_1)+g_2+g_3+(g_4-F_4)\\ &=g_1+g_2+g_3+g_4-F_1-F_4\\ &=g-F_1-F_4 \end{aligned} \quad (1.14)$$

In a practical situation, any of the four elevations can be either positive or negative. In order to calculate the terrain correction automatically by computer, all the cases must be considered. Fig. 1.6.3 illustrates 16 cases which may happen in reality. Up-lines indicate the terrain is higher than the station, down-lines indicate the terrain is lower than the station. The formula corresponding to each case is listed below the diagram. A computer program can determine where it goes, and which formula therefore to be applied. For

example, if, Z1<0, Z2>0, Z3<0, Z4 >0, the program will read four heights and judge the signs and search for a formula from the flow chart as shown in Fig. 1.6.4, which is formula 10.

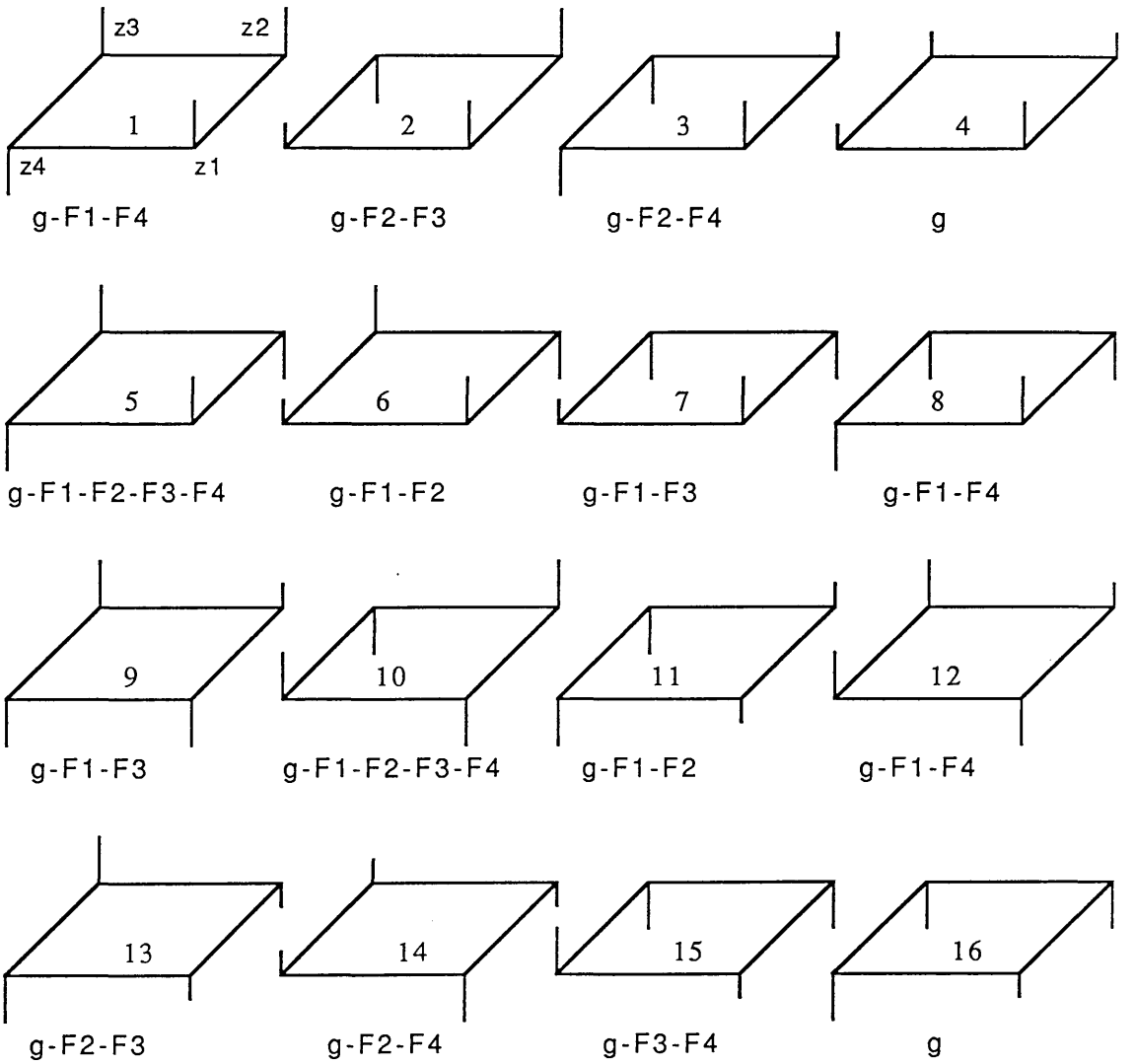

Fig. 1.6.3 16 cases of possible terrain near the station in near zone 1 and their corresponding formulae.

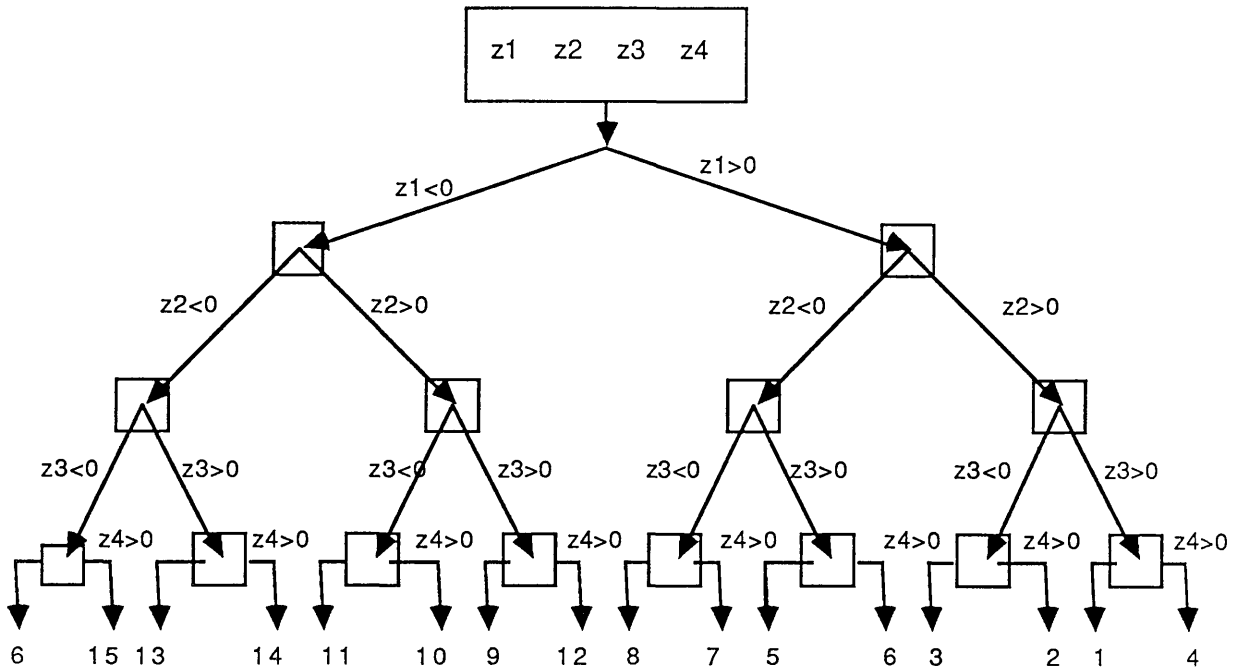

Fig. 1.6.4 Flow chart of possible terrain for the computer to choose appropriate formulae.

1.7 Fortran-77 program MATERRAIN

A Fortran-77 program (see Appendices; Fortran-77 program 1) was written by the author for the evaluation of the gravimetric terrain correction, free-air correction and Bouguer correction. The general flow chart of the program is illustrated in Fig. 1.7.1. The explanation of the various boxes are as follows:

Box 1 is a station file, consisting of station number (No.), latitude (LATI in degrees), coordinates in National Grid (X, Y in metres), elevation of the station (H in metres), elevations at the four corners of a square (Z1, Z2, Z3 and Z4 in metres), rock density (DEN in g/cm^3) and observed gravity value (g_{ob} in mGal). The data format is shown in Table 1.7.1.

Box 2 is an elevation file, consisting of block numbers (No.), coordinates of block centres (X, Y), densities (DEN), 16 elevation values of individual squares (16 squares are grouped as one block). The format of block data is shown in Table 1.7.2.

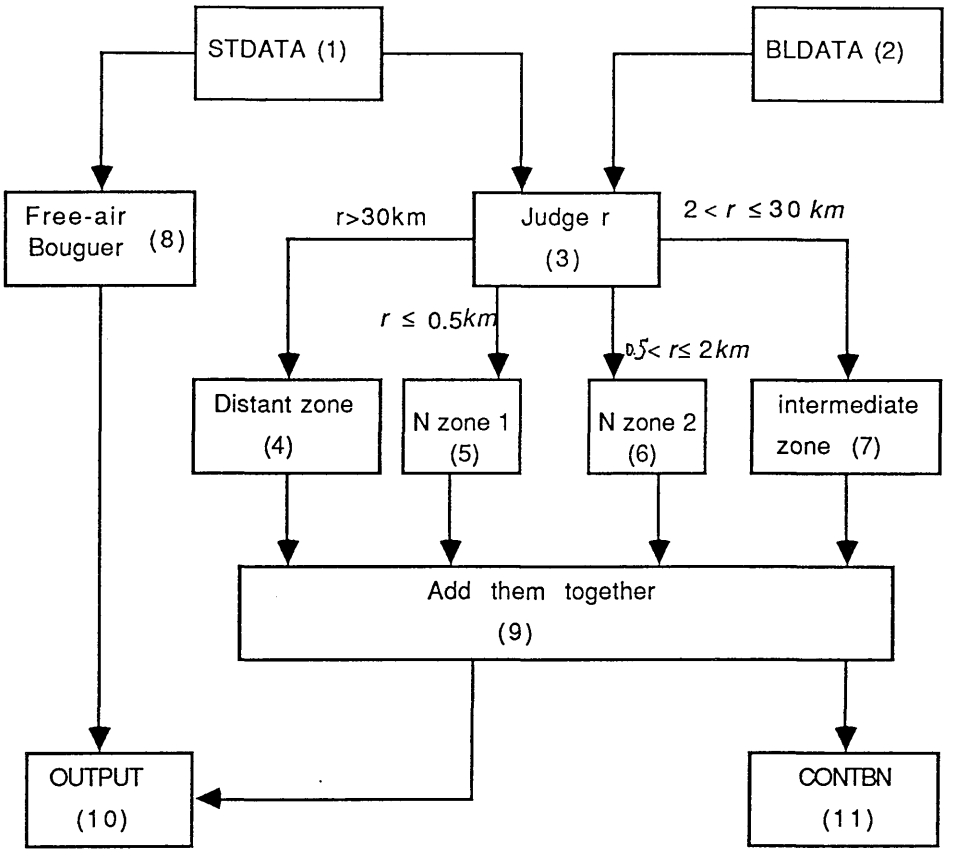

Fig. 1.7.1 Flow chart of Fortran-77 program MATERRAIN.

No	LATI	X	Y	H	Z1	Z2	Z3	Z4	DEN	gob
50	55.5175	292220	626100	259.7	234.7	320.0	274.3	236.2	2.72	1513.13
65	55.5328	296990	627780	439.5	327.7	414.5	313.9	304.8	2.72	1476.30
132	55.6225	301740	637660	269.1	228.6	304.8	274.3	251.5	2.72	1516.70
197	55.5607	305290	641820	270.6	243.8	259.1	281.9	274.3	2.72	1516.96
329	55.7370	316410	650090	225.6	292.6	219.5	237.7	221.0	2.72	1529.09
461	55.3673	256050	610500	240.2	304.8	221.0	222.5	335.3	2.72	1500.21

Table 1.7.1 The station data file format. The actual observed gravity value is $(980000+g_{ob})$ mGal.

No	X	Y	Den	h1	h2	h3	h4	.....	h16
99	222000	560000	2.73	225	225	375	280	.....	300
133	238000	584000	2.72	600	580	650	825	.....	1250
198	240000	566000	2.73	140	50	175	60	.....	460
330	270000	590000	2.72	850	970	1000	900	.....	800
430	286000	586000	2.75	300	300	400	265	.....	475
514	306000	570000	2.33	43	37	46	50	.....	47

Table 1.7.2 Block file data format.

Box 3 reads the station data and block data from Box 1 and Box 2 and calculates the distance from the station for every block. If r>30 km, it goes to Box 4. If 2<r ≤30 km, it goes to Box 7. If r ≤0.5 km, it goes to Box 5, and so on.

Box 4 calculates the terrain effect for the distant zone, where a line mass formula (1.2) is used.

Box 5 evaluates the terrain effect for near zone 1 which involves many calculations. Since the formulae (1.8), (1.9), (1.10), (1.11) and (1.13) are similar in pattern, subroutines NEARZONE1 and NEARZONE2 are used so that the main program can call them many times, each with different coefficient values.

Box 6 evaluates the terrain effect for near zone 2, where formula (1.5) is used.

Box 7 evaluates the terrain effect for the intermediate zone, where formula (1.3) is used.

Box 8 evaluates the free-air and Bouguer corrections.

Box 9 adds the contributions from different zones together to give the total terrain correction.

Box 10 produces an output file showing station number, coordinate, elevation, total terrain correction, free-air correction, Bouguer correction, normal gravity, observed gravity and finally Bouguer anomaly. The output format is shown in Table 1.7.3.

Box 11 produces a file showing the contributions of terrain corrections

from different zones. The output format is illustrated in Table 1.7.4, where gt1 is from near zone 1, gt2 is from near zone 2, gt3 is from the distant and intermediate zones, and gt is the total terrain correction for that station.

No	X	Y	H	gt	gf	gb	go	gob	gba
1	273350	625460	516.9	2.35	159.52	58.95	1460.00	1549.63	13.31
64	297960	629060	384.7	1.89	118.72	43.87	1488.40	1552.81	12.25
196	305290	641820	270.6	0.12	83.51	30.86	1516.96	1562.56	7.13
328	316410	650090	225.6	0.37	69.62	25.73	1529.09	1569.13	4.19
1131	319750	613870	677.9	5.52	2.9.20	77.31	1406.86	1541.63	2.63

Table 1.7.3 Format of output file OUTPUT. The actual normal gravity is (980000+go) mGal. The actual observed gravity value is (980000+g_{ob}) mGal.

No	$gt1 (r \leq 0.5\ km)$	$gt2 (0.5 < r \leq 2\ km)$	gt3(r>2 km)	gt (total)
1	0.6531	0.7503	0.9473	2.3512
131	0.0723	0.2457	0.1030	0.4210
208	2.8616	3.3325	1.9163	8.1104
263	1.3266	1.5234	0.9469	3.7969
395	0.0014	0.0693	0.2003	0.2710
500	0.3674	0.7596	0.4520	1.5780

Table 1.7.4 Format of output file CONTBN.

This software has been run on the VAX11/750 computer with the Unix operating system at the Department of Geology and Applied Geology, University of Glasgow. The time for processing one station is about five seconds. It will certainly be reduced if the software is run on the more modern workstations and/or mainframes which have replaced it.

1.8 Real gravity data test and accuracy consideration

The British Geological Survey, Nottinghamshire, kindly gave us gravity data for the areas of the Southern Uplands, Midland Valley and Grampian

Highlands. For the purpose of testing the new method, 4526 gravity station in the western Southern Uplands, which occupies 11,000 km^2, were read from the magnetic tape. The area was digitized for the terrain correction. There are in total 11,328 elevation data read from the Ordnance Survey (OS) map for 708 blocks, each block having 16 squares inside. In addition, 18,104 more elevation data were also read from the OS map in order to calculate the terrain correction for near zone 1. The organisation of elevation data is shown in Table 1.7.1 and Table 1.7.2.

In creating block file BLDATA, the densities in the fourth column are adapted from previous papers by Mansfield [1963], Bott [1960] and Parslow & Randall [1973]. Specifically, the density for lower Palaeozoic rocks is 2.72-2.73 g/cm^3, 2.33 g/cm^3 for New Red Sandstone rocks, 2.62 g/cm^3 for granite, 1.03 g/cm^3 for sea water. In order to check these densities determined by the sample measurement, Nettleton's method [1939] is used here for three areas in the Southern Uplands where there are simple rock types and low relief topography. According to Nettleton's theory, the correct density is measured simply by making a special tra-verse of gravimetric stations across the topographic feature, reducing these stations for several densities and finding the density value for which the reduced curve has a minimum correlation with the topography. A Fortran-77 program was written by the author to pick up those stations which have to be not only along a short straight profile line, but also in places where the geology is simple. The first density profile, passing through the National Grid NX39 (see Fig. 1.8.1, line a), lies in the northern belt of the Southern Uplands. The area is composed of greywackes and shales (Ordovician). The second and third profile lines, passing through NX77, NX87, NX88, and NX76, NX87 respectively. Both trend NE-SW and lie in the central belt of the Southern Uplands (see Fig. 1.8.1, lines b and c). Rock exposures are greywackes, shales and sandstone (Silurian). The relief of the topography along three lines is in the region of 60-190 m. The correct densities from three figures seem to be in the region of 2.70-2.73 g/cm^3 because the curves reduced by those densities are nearly horizontal,

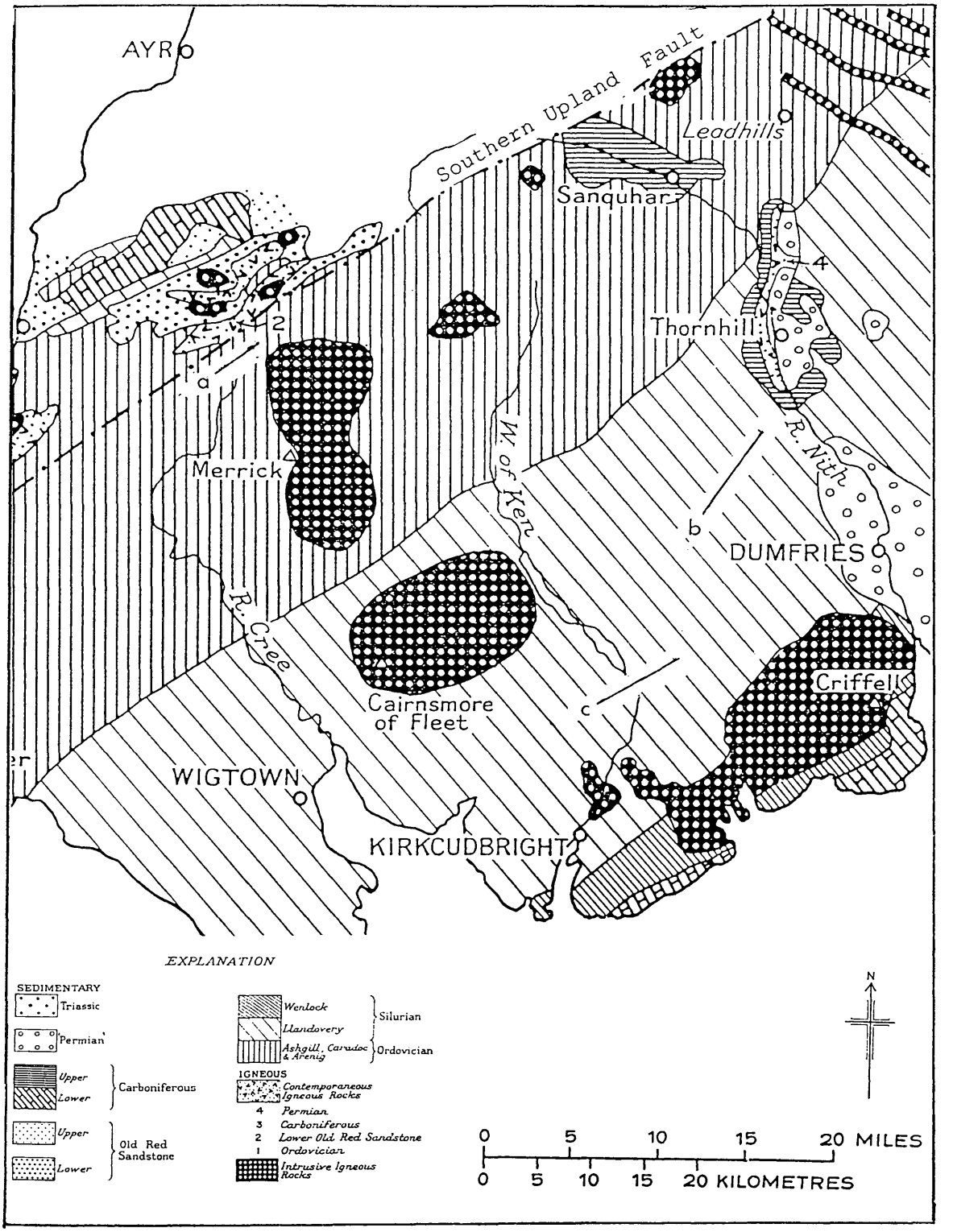

Fig. 1.8.1 Geological map of the Southern Uplands of Scotland, showing the sites of three density profile lines a, b and c.

in other words, they have the minimum correlation with topography (see Fig. 1.8.2 (a), (b), (c)).

However, densities determined by the Nettleton's method have not been used for the terrain correction, but are taken as the tests. To obtain more precise density values, many short-length profiles along which gravity stations have to be densely located are required.

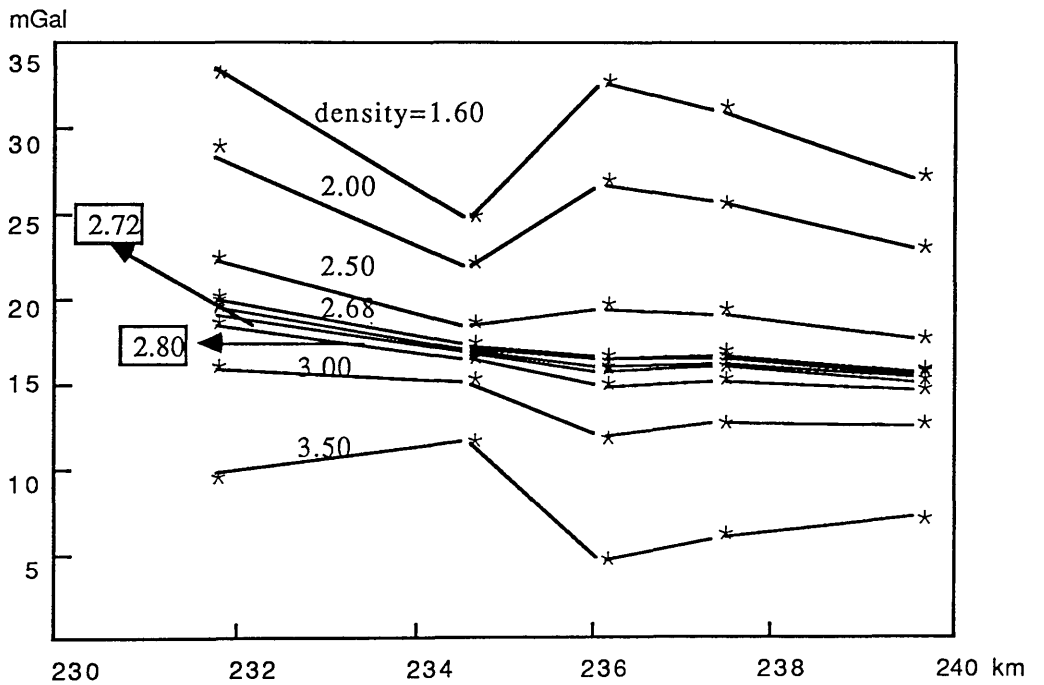

Fig. 1.8.2 (a) Density profile 1 in the Southern Uplands of Scotland.

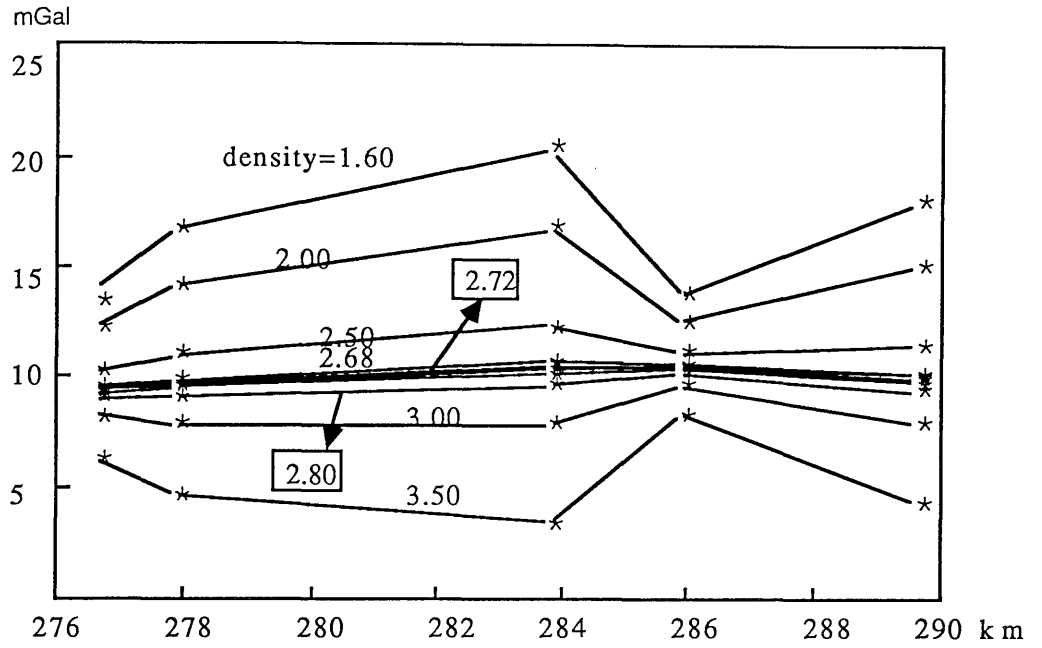

Fig. 1.8.2 (b) Density profile 2 in the Southern Uplands of Scotland.

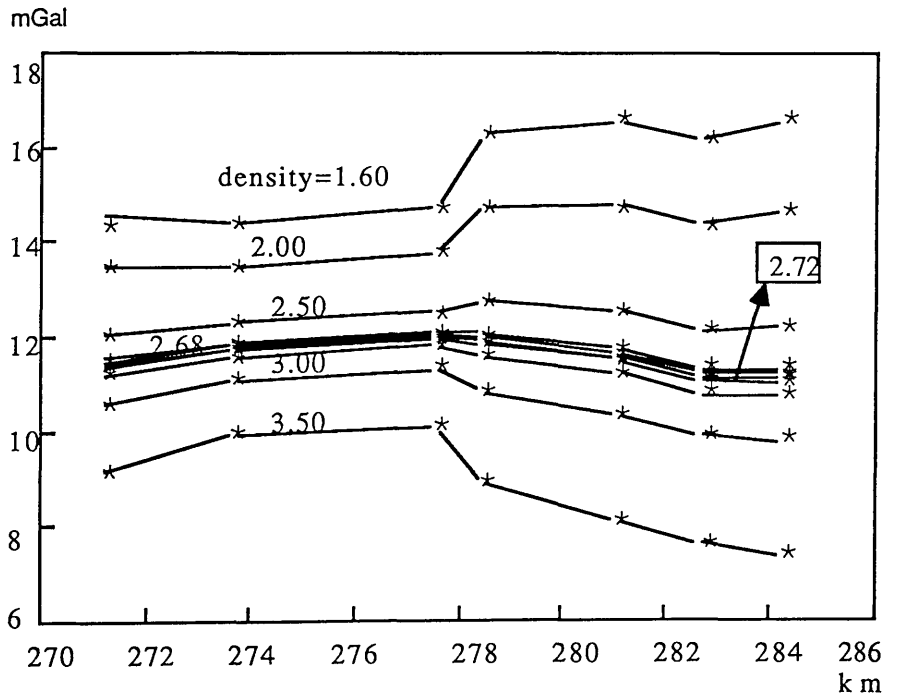

Fig. 1.8.2 (c) Density profile 3 in the Southern Uplands of Scotland.

The error in terrain correction can arise from many factors, such as inaccurate elevations of the stations and squares read from the OS map and inexact determination of rock densities. The method is tested by comparing the new corrections with those made by the BGS for the same station. We arbitrarily pick up 10 stations for the test. It has been found that most of the new terrain corrections are near to the original values, the relative difference is about 2-9% (see Table 1.8.1). On the other hand, there are some stations whose new terrain corrections are very different from the original ones, the relative difference being up to 50%. To examine the problem, the Hammer zone chart method is used to perform the corrections. The Hammer zone chart available in the department has the zones from D to K, corresponding to the area with a radius from 53.3 to 9902.5 m. Three stations (2444, 2657 and 2659) are checked. Station 2444 on the National Grid NX48 is located at the top of a hill (808 m). On either side of the hill, 1 km away, is the valley with elevation of about 300 m. This large difference in topography should give rise to a great terrain correction. The old correction by the BGS, however, was 6.29 mGal compared to the new correction of 15.74 mGal by the above software. The value by the Hammer zone chart method, on the other hand, is 14.90 mGal (see Table 1.8.2). The minor difference between the new and Hammer's values is because of the neglect of the terrain effects from zones A-D and L-M. The other two stations are also located at the top of a hill on the National Grid NX 56. From Table 1.8.2, we see that the old corrections by the BGS are also underestimated. Therefore, some original data at stations, where the topography changes dramatically, need to be modified.

NO	X	Y	gt (old)	gt (new)	error%
107	295280	634380	13.25	13.60	2.6
168	306530	631480	10.07	10.09	2.0
487	264240	601040	5.61	5.99	6.8
825	289020	610710	5.95	7.18	3.3
1061	314160	608940	5.18	5.28	1.9
1122	314690	611100	7.41	7.65	3.2
1888	227420	596860	2.34	2.12	9.0
2159	233520	591080	5.24	5.68	8.4

Table 1.8.1 Comparison of new corrections with old ones. gt (old) is provided by the BGS, gt (new) is produced by the new terrain computation method.

Station No.	X (m)	Y (m)	H (m)	Old (mGal)	Hammer (D-K) (mGal)	NEW (mGal)
2444	249680	588360	808	6.29	14.90	15.74
2657	250100	566460	655	5.52	6.76	8.21
2659	250940	565390	657	8.43	10.15	12.81

Table 1.8.2 Comparison of terrain correction among the old, Hammer and new values.

In order to show overall influence of terrain correction upon the Bouguer anomaly, Bouguer anomaly contour maps from the original data and new data are drawn in Fig. 1.8.3 (a) and (b). They show that the general patterns of two contour maps are quite similar to each other. Specifically, they both show gravity lows over the Loch Doon Pluton, Cairnsmore of Fleet Granite, Criffell Granodiorite, Stranraer Sedimentary Basin and the New Red Sandstone deposits near Dumfries. The data by the new method appears to provide somewhat better resolution.

1.9 Summary

A new method of terrain correction has been developed for regional gravity survey. The basic idea is to divide the terrain into different zones,

within each zone, different formulae with certain approximations are applied. The main contributions to the old methods are made particularly for the near zone 1 correction, where new formulae are derived from integrations. The software MATERRAIN is tested by the gravity data in the Southern Uplands of Scotland. It has been found that some of the old corrections by the BGS are likely to be underestimated. The new method is entirely automatic and easy to use.

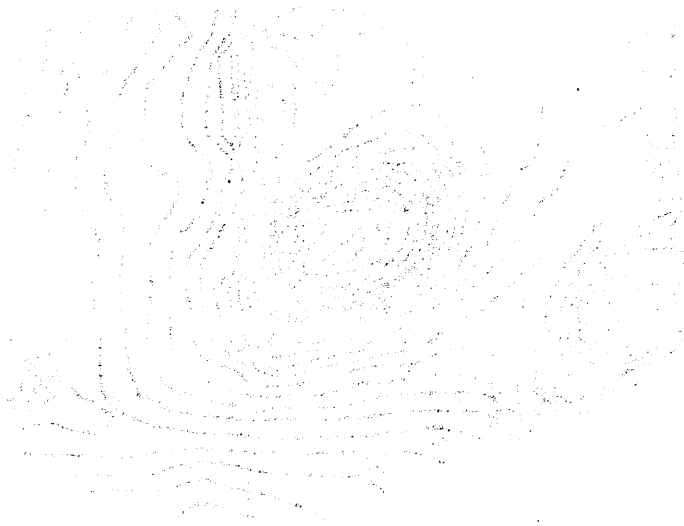

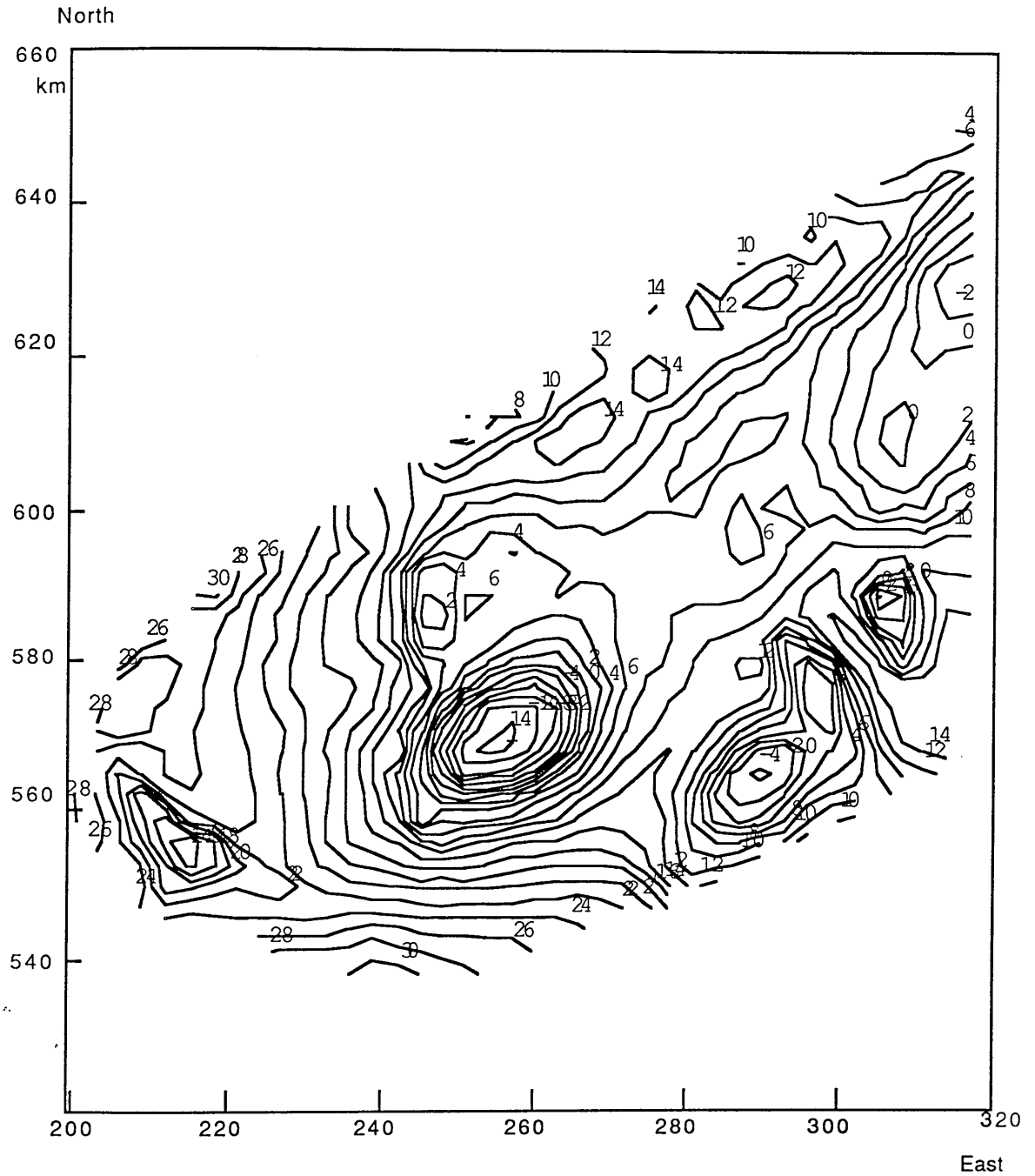

Fig. 1.8.3 (a) The original Bouguer anomaly map for the Southern Uplands of Scotland provided by the BGS.

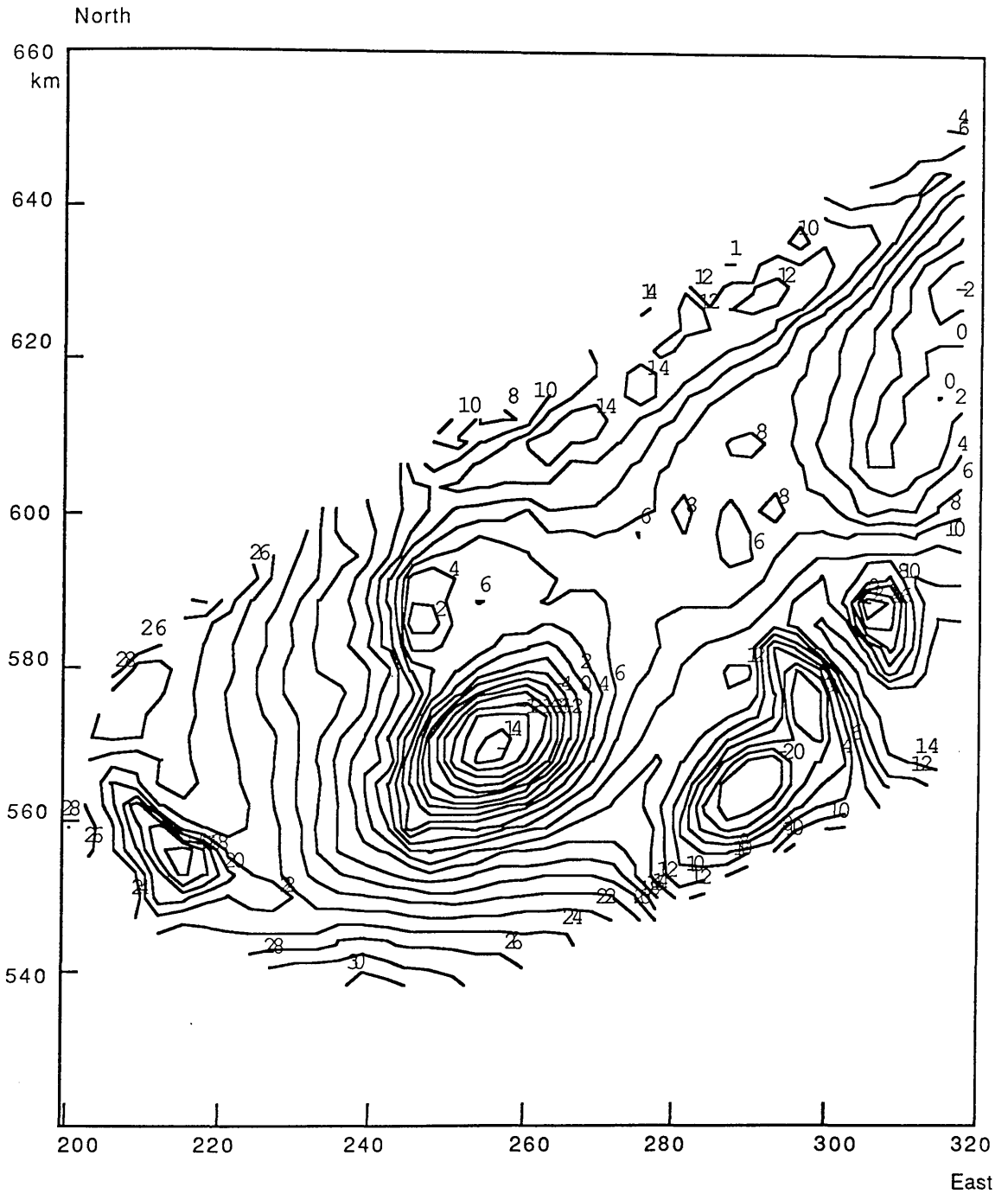

Fig. 1.8.3 (b) New Bouguer anomaly map for the Southern Uplands of Scotland, produced using the new terrain correction computation method.

PART TWO: REFLECTION SEISMOLOGY

Chapter 2 Methodology and Approach of New Seismic Reflection Experiment

2.1. Introduction

The conventional seismic survey is usually conducted by placing a number of vertical geophones along a profile line. After a shot is fired, the whole array is successively moved forward. This is the most widely used seismic data acquisition technique to cancel multiples and random noise. However, in areas characterised by high velocity volcanic rocks (about 5.0 km/s) sandwiched between low velocity surface materials at the top and sediments at the bottom, many problems such as high level noise and reverberations are encountered. In such a setting, the conventional method usually fails in terms of data quality and results derived from it. In this chapter, we describe a new approach of collecting seismic data using a special areal array and 3-component geophones specifically designed for basalt-covered areas.

2.2 Review of noise problems on basalt-covered areas studied by previous authors

The University of Wyoming Volcanic Reflection Research Group (UW VRRG) has carried out an integrated approach to understand wave propagation in volcanic rocks and to find means of obtaining usable seismic reflection data in areas covered by volcanic rocks overlying sedimentary rocks [Smithson, 1986]. In order to reach the target, VSP (Vertical Seismic Profile) and CDP

(Common Depth Point) data have been acquired in different areas covered by volcanic rocks where boreholes were available. The CDP line data in such areas show that practically all P-wave energy at take-off angles greater than several degrees (5-10^{o}, depending on the area) from the source is trapped in the surface layer and contributes to the organised noise. In other words, most of the P-wave energy is returned to the surface as organised noise rather than passing into the earth to interfaces of interest. This noise problem in the CDP field records is caused by reverberating first arrivals. These reverberations represent the worst kind of organised noise because of their long duration and high horizontal velocity. Wave tests show that the amplitude of reverberations in correlated surface seismic data do not decay significantly with time at a fixed distance from the source, but with increasing distance from the source. In areas where basalts are near the surface, there are several important phenomena affecting the seismic wavelets. One is that the input signal in such areas is really a train of wavelets lasting as long as a second instead of a single wavelet, i.e., the downgoing wavefield is long and complicated. This is probably caused by reverberations in the near surface where low velocity material overlies basalt. The other phenomenon is that the basic wavelet and its reverberations change dramatically as the source location is changed, which will severely degrade the continuity of reflections.

Attenuation in basalt has been studied by a spectral ratio method applied to the first break [Smithson, 1986]. The ratio of amplitude of the first break at specific depth to the reference amplitude has been calculated, and the procedure is repeated for several frequencies. The results show that attenuation in volcanic rocks is not unusually large or very different from those in sedimentary rocks, demonstrating that volcanic rocks do not attenuate the energy of seismic wave propagating through them at a higher rate than sedimentary rocks.

Apart from the conventional processing techniques applied to the data such as frequency filtering, inverse filtering and velocity filtering, some new techniques have been developed by the UW VRRG group, with the aim of

extracting weak signals in the presence of noise. One is the τ-p transform, which is based on the theory that the linear reverberations in the τ-p domain are well separated from the zone in which the reflections are located. The τ-p transform does diminish the amplitude of reverberations, but artifacts are still a problem. Another technique is that before cross-correlation, the synthetic reflection record is summed with field record. The summed record is then compared to the synthetic record, so as to suppress the contribution of samples with low signal-to-noise ratio in the summed record. The summed record is then cross-correlated with the appropriate sweep.

Although much effort has been made to acquire high quality data and to develop new processing techniques, the noise problem in basalt-covered areas has not yet fully been solved.

2.3 Array design

A new shot-receiver array was designed by D. K. Smythe for a proposed BIRPS piggy-back experiment to accompany the WISPA line in 1988. This section is based on Smythe's note [Smythe, 1988]. An array pattern is chosen as shown in Fig. 2.3.1, with the shot point at the centre. Three-component geophones lie on one of two concentric circles of radii 75 and 130 m. The shot point spacing is 75 m.

The determination of array dimension is based on several factors. They are described in detail as follows:-

(1) For a maximum phase shift of half a wavelength, the radius of the array for events of interest should be of the order 200-300 m. Let us consider a normal-incidence ray leaving a reflector, which dips at an angle θ in the lower crust (see Fig. 2.3.2). If the P-wave velocity of the crust is V, the horizontal slowness p is

$$p = \sin \theta / V$$

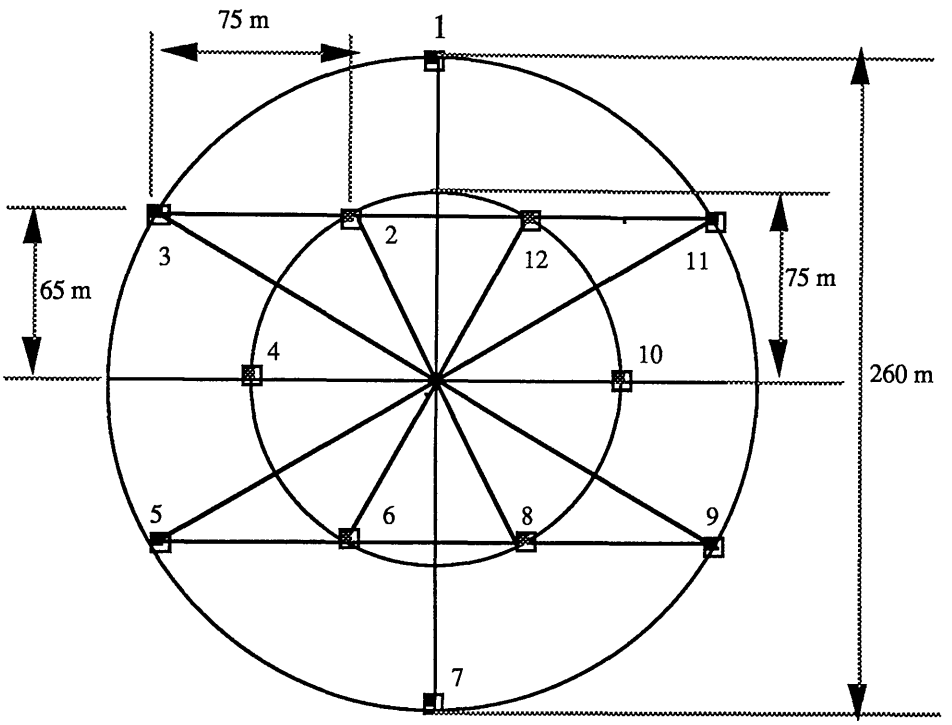

Fig. 2.3.1 Field areal 'RAZOR' array pattern for seismic survey.

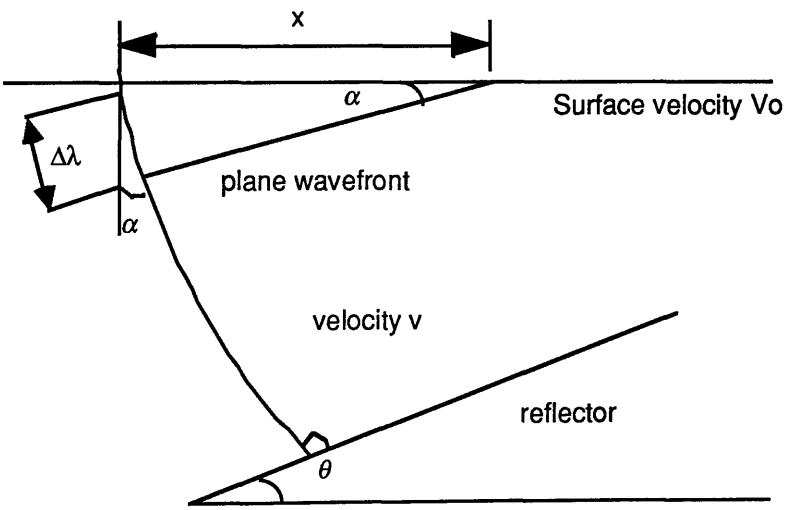

Fig. 2.3.2 Geometry of a normal-incidence ray from a lower crustal reflector dipping at θ. Plane wavefront is incident across an array of receivers of horizontal dimension x.

The ray emerges at an angle of incidence α, corresponding to a planar wavefront dipping at the same α. We require a suitable dimension of x, the width of the array, over which the phase difference of a planar arrival will not differ by more than half a wavelength. The path difference across the array is

$$\Delta\lambda = V_0 \, \Delta t$$

where V_0 is the velocity at the surface, and Δt is the time delay. Snell's law says that the quantity $\sin\theta/v$, which is the inverse of the horizontal phase velocity, is constant along any raypath in a horizontally stratified medium. Thus the same horizontal slowness p applies at the surface. We get

$$p = \sin \alpha \, / V_0 = \Delta\lambda/(x \, V_0).$$

Substituting and re-arranging, we get

$$x = V \, \Delta t \, / \sin \theta \, .$$

For a half-cycle of a 25 Hz wavelet, Δt = 40/2 =20 ms. Taking a lower crustal velocity of V = 6.5 km/s, and a typical dip of an event of 30^o, we get

$$x = 20 \times 6.5 \, / \, \sin 30^o = 260 \; m.$$

(2) The station spacing of 75 m is big enough so that different near surface ground conditions will be sampled. Rogue stations can be identified by comparison with other stations, and rejected from the beam-steered stack.

(3) The 75 m radius of the inner circle is large enough so that the stations will not interfere with the firing of the shots; there is no station at the shot point.

(4) Summation of 12 stations produces a respectable signal-to-noise increase of 3.5, after polarisation filtering of each 3-component station separately. This provides zero-offset (coincident source-receiver) 3-component 12 fold reflection sections.

(5) During shooting, only 6 of the 12 stations have to be shifted between each shot point, two stations (9, 11) are used 4 times, another two stations (8, 12) are used 3 times, three stations (2, 6, 10) are used twice and only 3 stations (1, 4, 7) are used once. Thus the preparation of sites for planting the geophones is minimised.

(6) This particular array allows slant-stack processing to be carried out along a straight line of a varied azimuth through the shot point, after 12 stations are projected on it. The transformed-sections can be "turned" to maximise the amplitude of reflections from any directions, both in-line and cross-line, and supply 3-dimensional information.

(7) Geophones with small offsets to a shot point will record good shear waves with near-vertical incidence.

The array has subsequently been given the acronym "RAZOR", for Roll-Along Zero Offset Receiver array [Smythe, pers. comm., 1989].

2.4 Three-component seismic data acquisition

2.4.1 Area chosen for the investigation

Interpretation of gravity data in terms of gradual lateral variations by McLean and others is largely unsuccessful in the Greenock-Strathaven area, SW of Glasgow, because of the lack of surface geological control and the multiplicity of density and magnetic susceptibility contrasts present in the area. A particularly frustrating ambiguity is caused by the low density (2.3-2.6 $\times 10^3$ kg/m^3) of Old Red Sandstone sediments sandwiched between the lavas (2.7×10^3 kg/m^3) and the lower Palaeozoic rocks (2.7×10^3 kg/m^3). Hall [1974] had carried out a detailed seismic survey in an attempt to detect the depth to the base of the Clyde Plateau Lavas. A contour map and an isopach map of the Clyde Plateau Lavas were constructed.

We chose this area (hard volcanic rocks nearly at the surface), SW of Glasgow, as a site for the experiment to try to develop an alternative or auxiliary new method for seismic survey and to solve the reflection problems in basalt-covered areas. However, in retrospect it was a risk to select such an area for the experiment at the early stage.

2.4.2 Instrumentation

Initially we intended to use the analogue FM cassette type recorders available in the department for this experiment. After a 2 day survey in the

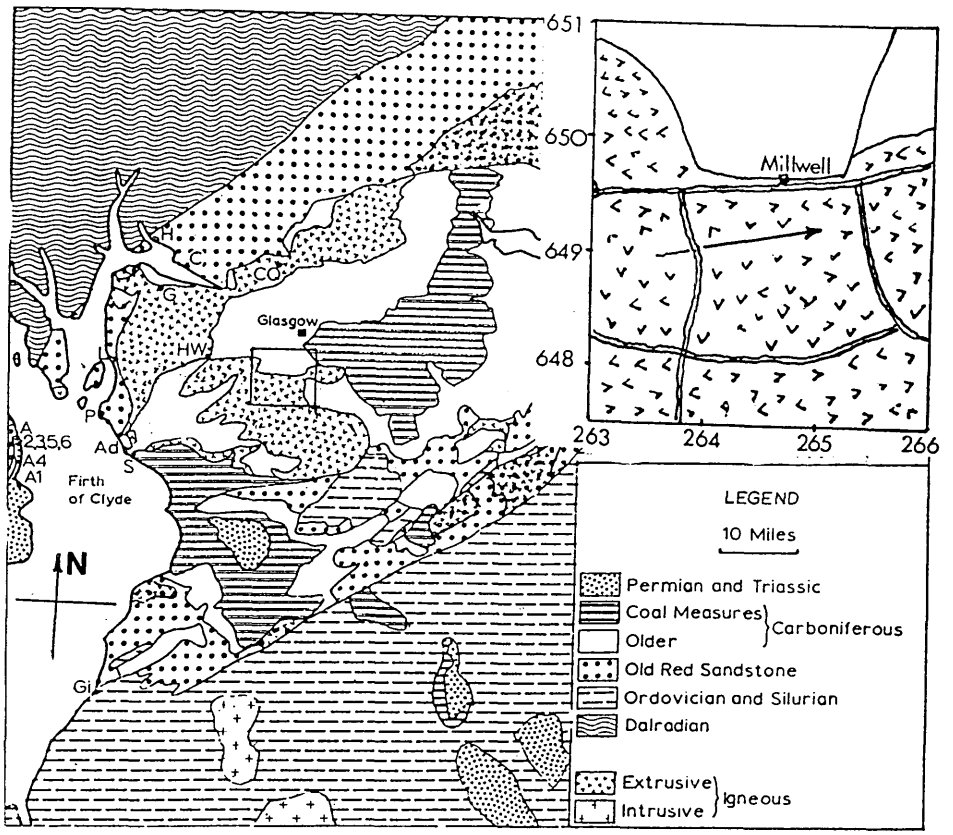

Fig. 2.4.1 Geological map of part of the Midland Valley, showing the site of the seismic experiment in the rectangle to the South-west of Glasgow. Inset map with national grid coordinates shows the precise location of seismic line.

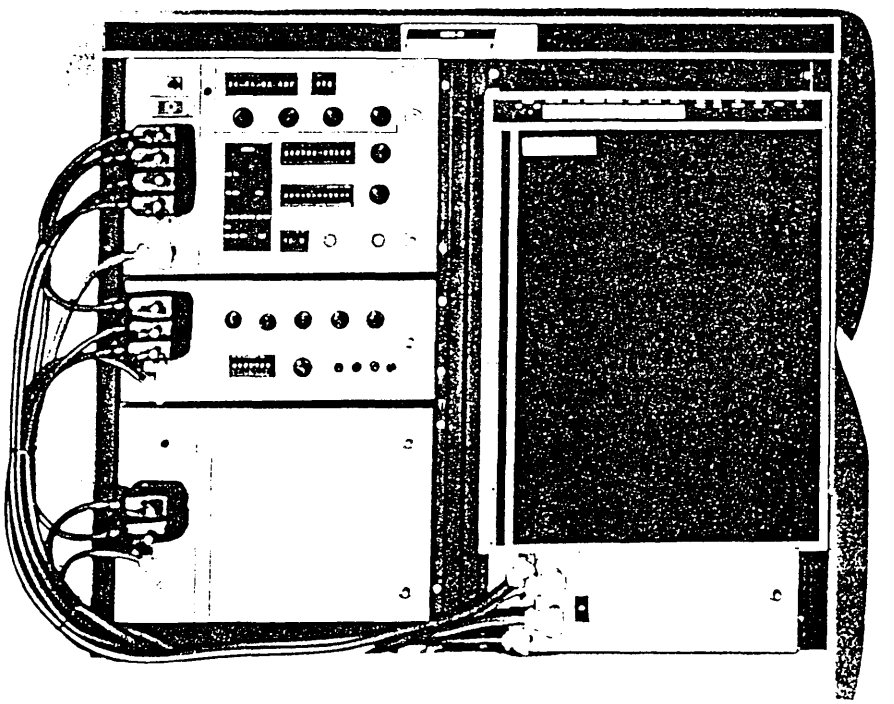

Fig. 2.4.2 MDS-10 Data System Units, Rack-mounted.

area, we collected data from two shots with different sizes of explosive using these recorders in early June, 1988. Twelve vertical component traces were recorded from each shot.

The recordings obtained from the seismometers were played back using an analogue facility and converted to digital form. Arrivals were picked up from the analogue playbacks and arrival times were calculated using the MSF pulses as a time scale. By inspecting the collected data carefully, we found that the seismic signals were overloaded, and the time error of up to 20 ms was unacceptable if the data are to be stacked. In fact, to image structure from the time difference introduced by the dipping of reflectors, we require that the error brought by the equipment should be less than 5 ms, otherwise this experiment would lose its significance.

The department subsequently acquired a second-hand MDS-10 (see Fig. 2.4.2) in 1988. This equipment can meet our requirements. The basic electronic modules of the MDS-10 Seismic Data System are the printed circuit plug-in cards containing an assemblage of linear and digital integrated circuits. These cards are housed in modular card racks which may be mounted in several different configurations depending on the type of exploration work required. The basic modules of Preamp, IFP Amplifier, Digital Controller, Power Supply, and Tape Transport form the core of a Seismic Data Acquisition System. System capabilities are expandable to 96 data channels by the addition of a second Preamp module, and to field data stacking by the addition of a Mass Memory Unit and card modules in the Digital Control Unit (Service Manual, 1977).

The Preamp Unit (see Fig. 2.4.3) is the analog input to the system. It is capable of handling up to 96 seismic inputs. The seismic input is normally channelled to the Preamp Unit by an input switching unit to allow for needed functions such as geophone testing, leakage testing, CDP switching, etc. In the operating mode of this Input Unit, the Preamps are connected directly to the geophones. The functions performed by the Preamp Unit include: amplification of the signal, low-cut filtering, 50/60 Hz notch filtering, anti-aliasing filtering, and multiplexing of the data channels to the IFP Unit.

The IFP Amplifier Unit contains: the Track & Hold circuit which samples the multiplexed signals from the Preamp, the IFP Amplifier which raises the held sample to an analog level near full scale of the converter, and the Analog-to-Digital Converter which converts the analog signal to 14 bits plus sign.

The Digital Control Unit contains the system master clock and associated logic for system timing and control functions. Primary data flow concerns movement of the converted data bits from the A/D converter and gain bits from the IFP Controller Logic to the Tape Formatter. Data are arranged according to the SEG-B Format and written to tape under the control of the Tape Controller Logic in the Digital Unit. Other functions performed by the Digital Controller include I/O signals for operation of remote firing system, defloating and conversion circuits for driving a Monitor Camera, formatting and controlling a Digital Correlator for display of vibroseis data, and formatting and controlling a Mass Memory device for data stacking, when the optional stacking features are ordered with the system.

The geophones used here have a natural frequency of 7.5 Hz. The coil resistance is 600 ohms. To obtain uniform coupling, the 3 geophones (two horizontal and one vertical) were fixed in one cluster, the horizontal geophones being oriented towards North and East respectively. Twelve such clusters were used.

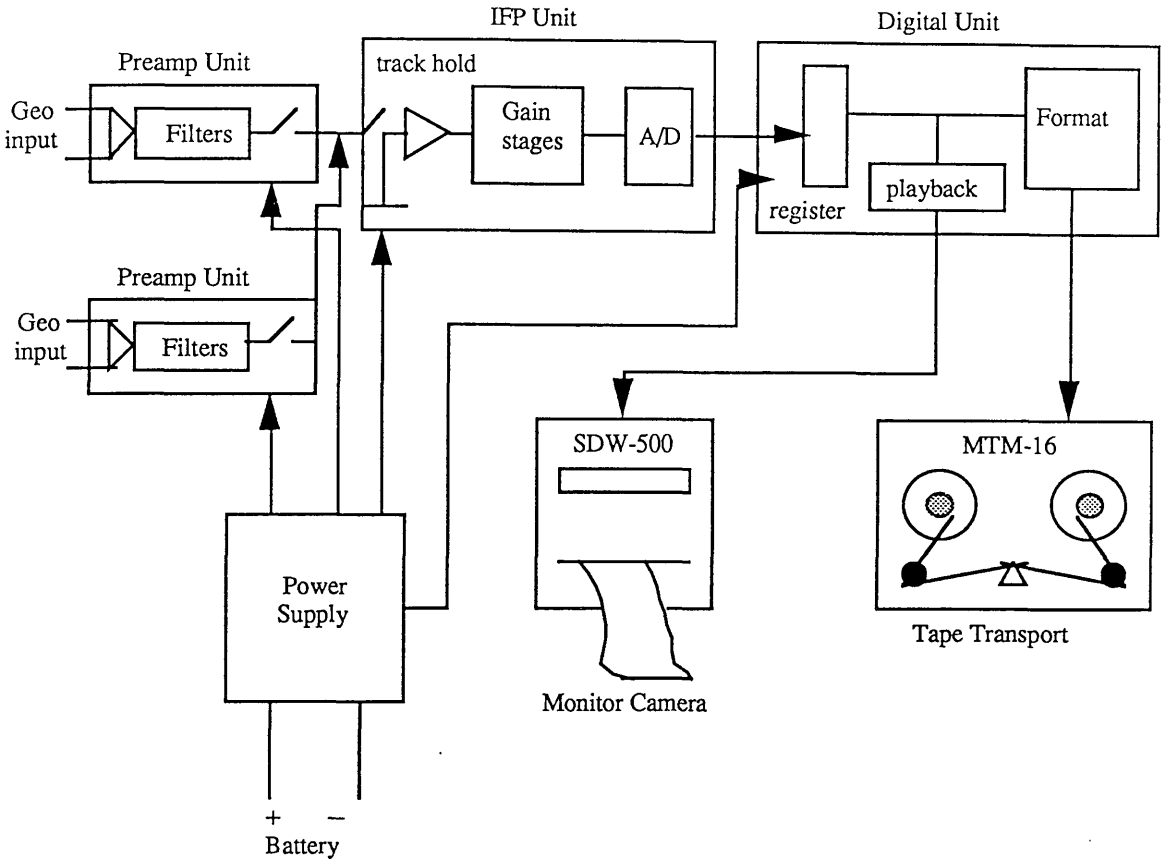

Fig. 2.4.3 MDS-10 data system block diagram.

2.4.3 Field survey

The area we chose for this experiment is relatively flat and covered by a close network of roads or tracks, along which the rapid laying of cables is possible. It was also thought to be easier for drilling because the surface is covered by drift several metres deep.

The areal field pattern was surveyed by taping and levelling in September, 1988. It was found tedious and time-consuming to measure 12 different azimuths for each array pattern, hence we surveyed 5 parallel lines with a distance gap of 65 m between two adjacent lines, with an increment of 75 m between adjacent stations along a line (see Fig. 2.3.1). The accuracy for setting up the aerial array was within ± 2 m.

2.4.4 *Field work preparation*

To carry out the experiment, the following equipment was needed:-

Vehicle	2
MDS-10 seismic data system	1
12 V Batteries	6
Vertical geophones	12
Horizontal geophones	24
150 m D10 cables	15
200 m extension cables	6
Junction boxes	2
Drilling equipment	1
Firing system	1

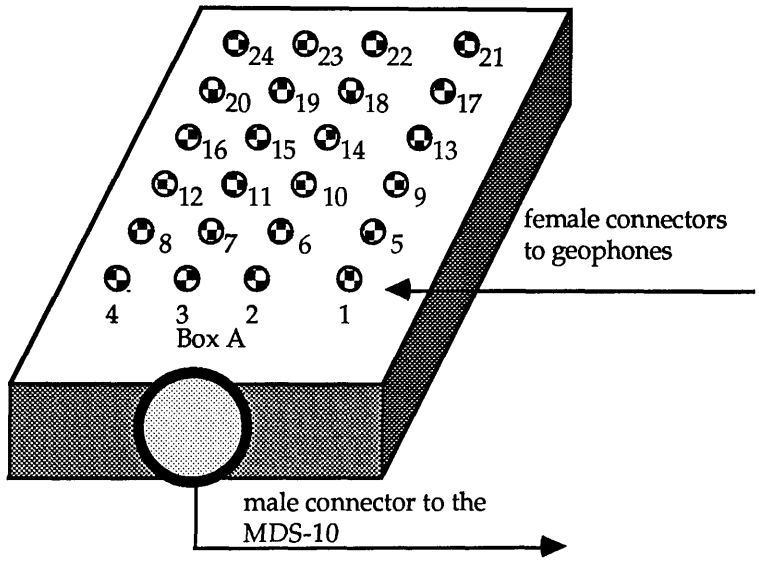

Fig. 2.4.4 Junction Box designed for connecting geophones to the MDS-10.

The plan for the connection between geophones and the input switching board on the MDS-10 was in two phases. Firstly, the 18 channels from 6 stations (1-6) are connected to the Junction Box A located at station 4, another 18 channels from 6 stations (7-12) are connected to the Junction Box B located at station 10 (see Fig. 2.4.5). This connection was supposed to save 6 150

m D10 cables; that is, the 3 channels from station 4 and another 3 channels from station 10 are directly connected to the Junction Box A and Box B respectively without using extra cables for the connections between geophones to the Junction Boxes. Secondly, the Junction Boxes were connected to the input switching board by the extension cables which can be extended up to 600 m (see Fig. 2.4.5).

The MDS-10 Data System testing was in two phases. First, it was tested by writing pulses and sine waves with different frequencies to tape in the SEG-B format and then displaying the demultiplexed data to see if they are as expected. In addition, we tested the system by completing the circuits from geophones to the input switching board. The geophones were set on supports in the corridor, and a hammer was used as a seismic source. By inspecting the playback from the monitor camera, we could isolate the dead traces, identify problems either in the MDS-10 recorder, cables or geophones. Secondly, testing of the blaster was carried out in the field.

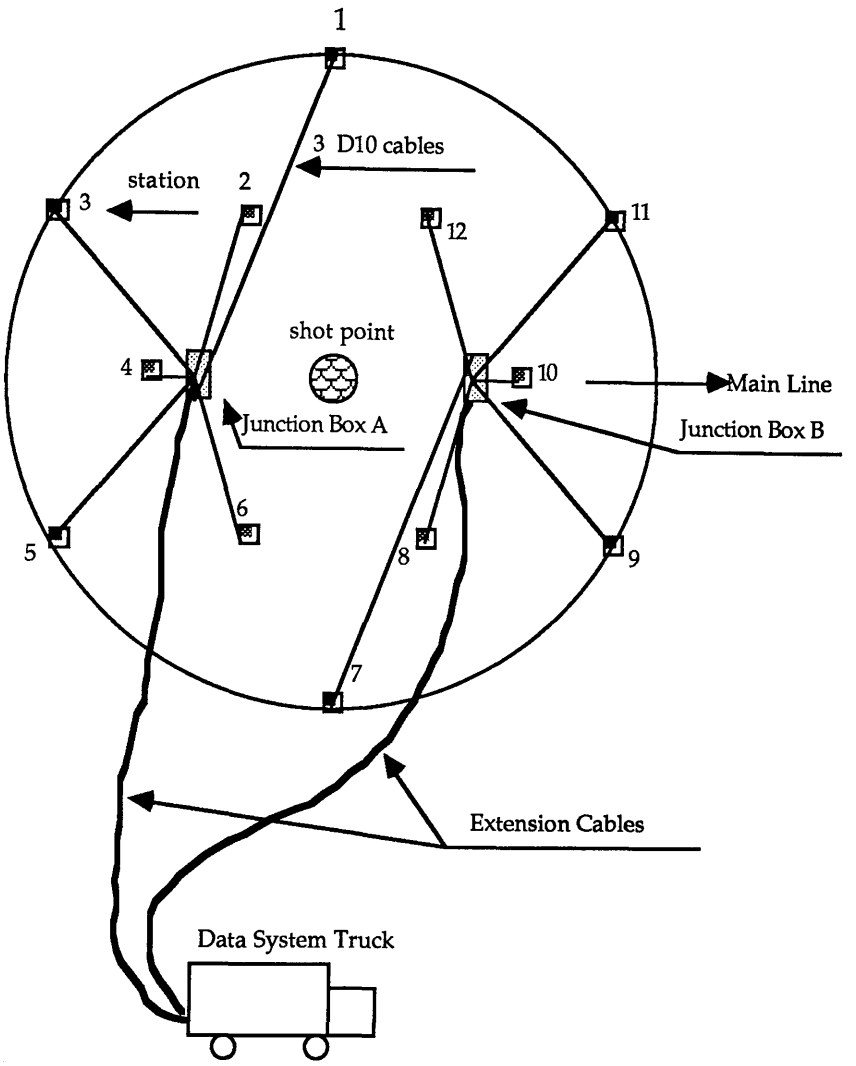

Fig. 2.4.5 Field lay-out and connections of the areal array experiment.

2.4.5 Field work procedures

To carry out field work, all the equipment had to be checked and loaded one day before the experiment, and field crew kept well informed and prepared. In the field, four people drilled shot holes, two planted geophones and a further two laid out cables and made all the connections.

Shot-hole drilling was the most difficult and time-consuming business. We used a pointed bulb-head hand drill which was made in the department 20 years ago. The drill is rhythmically plunged to the base of the drift, or to 2 m

length of the drill shaft by means of a hand percussion bore and filled, after loading, with mud and water. The 4 cm diameter drill head makes a hole wide enough to take the 3 cm wide gelignite inserting device which comprises an open-bottomed sleeve to hold the stick, within which there is a plunger to push the stick out at the bottom of the shot hole. Four holes in a polygonal pattern about 1 m apart are drilled and made ready for loading dynamite.

Sticks or part sticks of I.C.I polar ammon gelignite, about 20 cm in length and 3 cm in diameter, are placed individually in holes drilled to the base of the drift at the depth of about 2 m. The test was first conducted at the same location by different sizes of explosive, say 4 half sticks in 4 holes and 2 half sticks in 2 holes. By comparison of the seismograms from the two shots, it was found the first shot did not look any better than the second shot (see the details in chapter 3). Therefore, two half sticks were used in the majority of shots.

The HS-200 blaster was used as a remote firing system which is connected to the Digital Control Unit on the MDS-10 system. The firing signal comes from the main system after pressing the "start" button, the blaster then generates a 150-V firing pulse, which is conducted along a firing cable to the series-connected detonators. Two 200 m-long twin core steel cables with a total resistance of 40 ohms were used to complete the circuit. The blast creates a cavity around the shot which is filled and flattened immediately after shooting.

Two people planted the geophones. A shallow hole of about 50 cm in depth was dug, and one geophone cluster was planted in the hole. A compass was used to orient one of the horizontal geophones towards North, and the other towards East. The holes were usually filled with soft clay afterwards.

The D10 cables were divided into two groups according to their length (100 m or 150 m) having been tested and marked in the laboratory. Therefore, six long cables could be used to connect stations 1 and 7 at the far ends, 30 short cables could be used t o connect other 10 stations around the stations 4 and 10 where the two Junction Boxes were placed. The person who

made all the connections had to be sure that all the stations had been connected to the proper channels marked on the Junction Boxes. If one of the connections was found to be faulty, he had to either swap the channels on the Junction Box or take down the mis-connected channels for later change by software. It was found that channel 24 did not work properly, so that this channel had to be jumped over. In the field, channels 6-23 and channels 25-42 were used.

The MDS-10 operator is the key person in charge of the field work. He is responsible for directing the field crew, testing the connections, giving the signals to the firing system operator and to an observer who is stationed in the vicinity of the shot to warn the shooter of any hazard. Generally speaking, if everything went all right in the field, it would take at least 3 hours to finish one shot. In fact, we never succeeded in firing two shots in one day at the beginning of the experiment, although the second shot would only take half the time of the first. The work was slowed down by many factors; for instance, checking the dead channels again and again, and repairing the tape transport and firing systems. These unexpected problems had to be sorted out in the field. Sometimes, the weather before Christmas was too bad to proceed the work.

2.5 Interaction with the seismic data processing package SKS

2.5.1 Introduction to the SKS package

The collected seismic data were processed partly with the SKS (Seismic Kernel System) package, so that it is necessary to give a brief introduction to the package.

The Merlin SKS system consists of over 60 standard seismic processors, which are called using MGL, Merlin Geophysical Language. MGL is a seismic data processing language in which the geophysicist codes requests for seismic data processes to be performed on seismic data. It has sophisticated plain-English definition and comprehensive error reporting facilities, and includes facilities to recognize the various kinds of block processing which are

required in seismic data processing.

A seismic job coded in MGL is translated into the ESSR, Execution Stage Seismic Run, by MGLTRAN, the Merlin Geophysical Language Translator. MGLTRAN is a four pass compiler which is able to recognize a wide number of incorrect setups as well as optimize inefficient ones, and convert the requests in the seismic job into a Fortran-77 program which is then compiled and run in the normal way.

A seismic processor in SKS consists of two subroutines: (a) PPS (Pre-processing Subroutine), which is loaded by the translator, MGLTRAN, in response to the appearance of the corresponding processor name in seismic job coded in MGL. Each processor has a number of verbs which define the various functions of the processor. The PPS checks for the presence of the verbs and the values of their arguments given in the seismic job. The PPS then defines the system requirements for the SPS, and sets or resets variables in the process common blocks. (b) SPS (Seismic Processing Subroutine) which does the actual processing of the seismic data is executed as a subroutine call from within the Fortran-77 program produced as the output of MGLTRAN.

The SKS package used was that installed in the Signal Processing Division, Department of Electrical & Electronic Engineering, University of Strathclyde, by kind permission of Professor T. Durrani.

2.5.2 *Change of SEG-Y format into free ASCII-coded format*

A major problem is dealing with various tape formats. Seismic field tapes are recorded in a number of standard formats, SEG-A, SEG-B, SEG-C, and SEG-D, corresponding to the A, B, C and D formats of the Society of Exploration Geophysicists (SEG). Different machines with different software use different formats. However, all formats are simple if the computer on which the tape is being read is an IBM machine, as both the characters and numeric formats are based on IBM standards. A SEG-Y file, which is commonly used in the exploration industry is a file that contains a number of traces stored sequentially. Each trace contains a number of data samples. A SEG-Y file

always begins with an identification header of 3600 bytes, followed by trace data blocks which also contain a trace header area and a data area (see Fig. 2.5.1).

file identification header	trace header block	trace data block 1	trace header block	trace data block 2	.....	trace header block	trace data block n

Fig. 2.5.1 SEG-Y tape format.

As described in Section 2.4.2, the recording equipment used is the Geosource MDS-10 Data System which can record up to 96 channels although only 48 channels were used in our experiment. The time-ordered multiplexed seismic data were written to tape in the SEG-B format. The demultiplexing package we used, by courtesy of Britoil plc (now BP Exploration plc), demultiplexes seismic data and produces output as a SEG-Y file.

The SKS package was designed to process demultiplexed CDP marine and land seismic data collected in the normal way. However, the purpose of our experiment is to detect structure using 3-component seismic data collected in a novel way, in terms of the field array and the types of geophones. Therefore, it requires different processing techniques like polarisation filtering, and slant-stack processing, which are not available in the SKS package. In spite of that, we still need to use the SKS package to do the basic processing like data editing, application of automatic gain control, bandpass frequency filtering, predictive deconvolution filtering and so on.

In order to apply a polarisation filter and a spatial directional filter to the data, we firstly had to interact with the SKS system, that is, to read SEG-Y data files into a buffer which can then be read and processed by a Fortran-77 program under the VAX/VMS operating system. A new program called MASEGY to do this job is based on Hansen's program [1988] which has been modified to suit our case.

The program MASEGY uses the SKS subroutines to open, read, decode and close SEG-Y files. The subroutines are as follows:-

DDKOPN opens the SEGY file in such way as to guarantee being able to read the reel number, but not necessarily be able to read the data traces.

DSKHED reads the reel header, decodes it into a work common block and then determines the required number of traces and record length for this file. The file is automatically closed and reopened with the correct record length parameters.

DSKTIN reads the trace headers and traces into arrays in the required formats.

DSKFMT decodes the trace from tape into an array HOST(K).

MASEGY sets the data in the HOST(K) into another array BUFFER(I, J) and then writes them into a new file in a required format.

The program MASEGY (see Appendices; Fortran-77 program 2) has several advantages over ISAN (an interactive program with facilities for the manipulation and analysis of time series and frequency domain data) and other packages, in that it can read any number of traces in any part of a data file and read any number of samples in any part of a trace. When we run the program, it shows the length of header, number of traces in the file, and number of samples in one trace. Several questions then have to be answered, as shown by the following example. Program prompts follow the $ sign.

```
$  INPUT QUALIFIER
   MA
$  INPUT FILE NAME
   RAGCDT
$  TRACE COMMON LENGTH (UTRCLN) = 160
$  LENGTH OF TRACE HEADER (RHWTHL)= 100
$  SAMPLES PER TRACE = 501
$  NUMBER OF TRACES IN FILE (RHWNRC)=192
$  INPUT FIRST TRACE YOU WANT TO READ
   45
$  INPUT LAST TRACE YOU WANT TO READ
```

```
    96
$   INPUT FILE NAME FOR OUTPUT
    RESMPDT
$   NO. OF TRACES TO READ = 48
$   TRACE      1    COMPLETED
$   TRACE     48    COMPLETED
$   FORTRAN STOP
```

As shown in Table 2.5.1, the data have finally been written into a file that contains three columns: trace number, sample number and sample data.

In order to get 10 separate output files, we had to run the program 10 times, each file corresponding to a single shot. Part of the output data have been checked using the processor IMEG in the ISAN package, which reads the SEG-Y file into a workfile. The data from both outputs are identical.

channel no.	sample no.	samples
1	1	-0.31208420E+04
1	2	-0.23770420E+04
1	3	0.72183459E+03
....	....	.....
2	1	0.4.940039E+03
2	2	-0.24473999E+02
2	3	-0.12872484E+04
....	....	.....
3	1	-0.33545245E+03
3	2	0.53580952E+04
3	3	-0.79183521E+04
...	...	.....
48	1	0.73537378E+03

Table 2.5.1. Output data format from the program MASEGY.

2.6 *Three-component data transformation*

2.6.1 *Theory and method of transformation*

For recording 3-component seismograms, it is always ideal to point one of the horizontal geophones towards the radial direction (R) which is located on the line containing both shot point and station, another horizontal geophone towards the transverse direction (T) which is perpendicular to the radial direction, the third vertical geophone points downwards (V). Thus, three geophones are supposed to record source-generated and mode-converted SH, SV and P-waves with the highest response.

In the field, the 12 3-component geophones were set on two circles with an inner radius of 75 m and an outer radius of 130 m. Two adjacent stations are separated by an azimuth of 30^{o}. To keep 36 geophones in the ideal orientations (R, T, V) with error less than 0.5^{o} in the wet, muddy field was difficult and time-consuming. It was very convenient, however, to orient geophones towards magnetic North, East and vertical direction with a compass. Field crew in this case would be able to set up one station in 2-3 minutes. In order to satisfy ideal orientations, we can perform the vector transformation in the lab by computer.

Suppose that we now have two coordinate systems O_1 and O_2, here O_1 is a field system (N, E, V), N standing for North, E standing for East, V for vertical. O_2 is a required coordinate system (R, T, V), R standing for radial, T for transverse, V for vertical. If the origins of two systems are at the same point with coinciding vertical axis V, it is more efficient to do a rotation on the plane. For a vector $F = (X_0, Y_0)$, where X_0 is its component in N axis, Y_0 is the component in E axis. The projections of that vector on the new coordinate system obtained by rotating the field system with an angle of α to the N axis clockwise have X and Y components. β is an angle of the vector F to the N axis (see Fig. 2.6.1), so we get:-

$$X_0 = F\cos(\beta)$$

$$Y_0 = F\sin(\beta)$$

$$X = F\cos(\beta-\alpha) = F\cos(\beta)\cos(\alpha) + F\sin(\beta)\sin(\alpha)$$

$$= X_0 \cos(\alpha) + Y_0 \sin(\alpha)$$

$$Y = F \sin(\beta - \alpha) = F \sin(\beta) \cos(\alpha) - F \cos(\beta) \sin(\alpha)$$

$$= -X_0 \sin(\alpha) + Y_0 \cos(\alpha)$$

Seismic energy travels down as a wave from a source, strikes various interfaces and reflects upwards to the surface. The wave received at one station at time T can be expressed by a vector in space which has not only quantity but direction. For a 3 second seismic trace with the sampling interval of 4 ms, the seismic wave can be represented by 751 vectors. Using the above formula, 3 components of a vector taken from 3 seismograms at one time in the field coordinate system (N, E, V) can exactly be represented by 3 components of the vector in the new coordinate system (R, T, V).

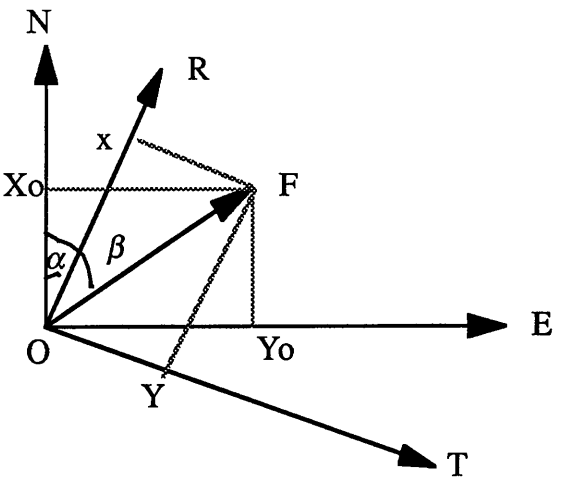

Fig. 2.6.1 Two coordinate systems with origins at the same point.

The orientation of the main profile in our seismic reflection experiment has been surveyed and is at an angle of 76.5° from North towards East. The symmetry of the array makes it easy to evaluate the 12 angles of radial directions from North. Table 2.6.1 below gives the values. The first row shows 12 station numbers, the second row gives the angles of 12 radial directions from North.

No.	1	2	3	4	5	6	7	8	9	10	11	12
α	346.5	316.5	286.5	256.5	226.5	196.5	166.5	136.5	106.5	76.5	46.5	16.5

Table 2.6.1 The angles of 12 radial directions from North.

To demonstrate how the transformation is performed, let us take station 11 (refer to Fig. 2.3.1 on page 37) as an example. We already know the orientation of the main line relative to North, 76.5^{o}, and we can then derive the angle of the radial direction from North, 46.5^{o}, which is the value of angle α in Table. 2.6.1. We also know the values of X_0 and Y_0 so that the values of X and Y in the new coordinate system can easily be calculated using the above formula.

2.6.2. Fortran-77 program MATRAN

A Fortran-77 program called MATRAN (see Appendices; Fortran-77 program 3) was written by the author to perform these transformations. As shown in Fig. 2.6.2 below, the program firstly reads 3-component data into an array XYZ(I, J) after a user inputs data file name, number of traces, and so on. Successively, it carries out the transformation for every station by calling a subroutine TRANLT. The transformed results are written into a new file with different order (see Table 2.6.2).

When the program is run under VAX/VMS, the user has to answer the following questions:-

```
$  INPUT FILE NAME TO BE TRANSFORMED
   SHOT09
$  INPUT FILE NAME FOR OUTPUT
   TRST09
$  INPUT NO. OF TRACES IN THE FILE
   48
```

```
$  START READING DATA INTO ARRAY
$  INPUT STATION NUMBER TO START(TYPE 0 TO STOP)
   1
$  INPUT STATION NUMBER TO START(TYPE 0 TO STOP)
   0
$  START WRITING TRANSFORMED DATA INTO NEW FILE
$  FORTRAN STOP
```

Data from 10 shots have been transformed by running the program 10 times. Part of the results from this program have been checked both by manual calculation and map drawing.

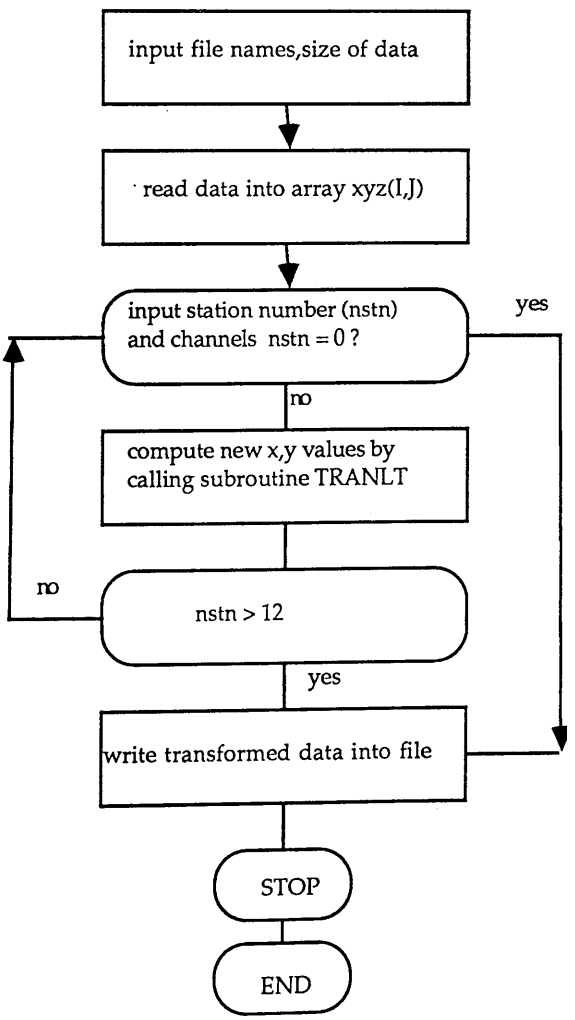

Fig. 2.6.2 Flow diagram of Fortran-77 program MATRAN.

I	J	R	T	V
2	30	0.43721714E+04	-0.24265833E+04	-0.66208169E+04
2	31	0.20342482E+04	-0.86845978E+03	-0.31671978E+04
2	32	-0.89819867E+03	0.12185277E+04	0.18010933E+04
2	33	-0.17012490E+04	0.17980367E+04	0.51663369E+04
2	34	0.16894063E+03	0.21042696E+03	0.51132510E+04
2	35	0.22622275E+04	-0.10723242E+04	0.38682339E+04
2	36	0.21623433E+04	0.22828473E+03	0.38494138E+04
2	37	0.75670850E+03	0.21057329E+04	0.40104707E+04
2	38	0.26581714E+03	0.13405616E+04	0.26566113E+04
2	39	0.30066162E+02	-0.72609741E+03	0.73537378E+03
2	40	-0.21853218E+04	-0.46790924E+03	-0.49363110E+03
2	41	-0.59391719E+04	0.13882744E+04	-0.40073503E+04
2	42	-0.36328962E+04	-0.17063904E+03	-0.46824844E+04

Table 2.6.2 Transformed data format from the program MATRAN.

2.7 Seismic data display using the UNIRAS package

2.7.1 Introduction to the UNIRAS package

The original SEG-Y data were edited and resampled using the SKS package in the Signal Processing Division, Department of Electrical & Electronic Engineering, University of Strathclyde. After the data were reformatted using the MASEGY program into ASCII coded decimal data, they were transferred through the computer network from the VAX 11/750 at the University of Strathclyde to the VAX cluster at the Glasgow University Computer Centre for the reasons of accessibility and higher computing speed. To obtain the seismic trace plots, the UNIRAS package was used to display seismic traces on the screen, which are then dumped to a laser printer. Therefore, it is worthwhile mentioning how the seismic wiggle traces are produced outside the SKS environment.

UNIRAS, standing for Universal Raster software, is a multipart package comprising interactive, menu-driven programs and also subroutine libraries for inclusion in programs. It will analyse data and produce a wide range of graphics display, including line charts, piecharts, histograms, 2D, 3D and 4D surface, solid modelling, and seismic data.

UNIRAS is a graphics package which is composed of two basic parts, the

first being the interactive programs. These provide facilities to draw charts and maps of all kinds without the need to write your own program. UNIGRAPH is for drawing charts and graphs, while UNIMAP is for contour maps and surface views etc. The third interactive is UNIEDIT which allows pictures drawn by the other two to be modified. The second main section of UNIRAS is the subroutine libraries which are routines which can be called from a user's own program in the similar manner to the NAG Graphics Library. Two levels of subroutine library exist, one for high level routines which correspond to the interactive programs, and a low level library. SEISPAK is a subroutine library for the display of seismic data.

SEISPAK consists of many library subroutines which can be called in a user's own program to display many kinds of seismic record sections. It can display seismic traces, variable area traces in vertical or horizontal direction as a user requires. It can drive many kinds of terminals and plotters. Furthermore, the seismic data can also be displayed in colour if a colour terminal and a colour plotter are available. The package itself can enhance a seismic section either by reprocessing data or by using colours. Finally, SEISPAK can also display seismic data in 3 dimensions.

2.7.2 *Plotting seismic traces in the normal way*

In order to make use of available packages for our own purposes, the author has written a Fortran-77 program called MAPLOT (see Appendices; Fortran-77 program 4) to display 3-component seismic data in various kinds of ways. The program permits the display of any one trace of 3-component data which exists as one of 3 columns in a data file. It can display traces or variable area wiggle traces and filled wiggle variable area without wiggle lines.

2.7.3 *Combination of a gain control program with the plotting package*

Seismic reflection data collected in our experiment exhibit different characteristics, as we deliberately selected the complex area with the intention

of solving problems associated with basalts. The recorded seismic traces show large amplitudes at the beginning of the traces (see the detailed description in Chapter 3). In contrast, the later parts of the traces are scaled down to a nearly invisible level. This makes it difficult to recognise any reflection events at the later part of the traces.

The general method of solving the above problem is to apply a gain to each trace. The gain itself should have small amplitudes at the beginning and large amplitudes at the later part. Furthermore, it has to change with the variation of the trace amplitudes. A program called MAGNPL (see Appendices; Fortran-77 program 5) was written by the author for the purpose of solving the above problem. The program calculates a gain function for each trace separately. At first, it computes a mean amplitude $\overline{A}$ for the time window $L_1 \times \Delta t$ (where L_1 is the number of samples and Δt is the sampling interval), all amplitudes of the gain function in that window are now taken as the same as the mean value $\overline{A}$, the time window moves down for the next computation until the end of the trace (windows are not overlapped). In order to get a smooth gain function, we set another time window $L_2 \times \Delta t$ (for instance, 160 ms), and sum all the calculated mean amplitudes (these amplitudes can be different) over the window $L_2 \times \Delta t$ and then divide it by the window length L_2, the final value is used as the amplitude for the centre point of the window. The window then moves one sample down for the next computation until whole trace has been finished. The scaled gain function exhibits large amplitudes at the beginning and small amplitudes towards the end (see Fig. 2.7.1 (c)). To scale down the large amplitudes and scale up the small amplitudes in the traces, we have to multiply the original traces by the inversed gain functions; i.e., we divide the original traces by the gain functions. Fig. 2.7.1 (a) shows the original unscaled seismic traces (12 vertical traces from shot 2), (b) shows the scaled seismic traces, and (c) shows the gain functions for the same data. By comparing Fig. 2.7.1 (a) with (b), we see that the frequency characteristics in the original traces are retained in the gain-applied traces; for instance, the large amplitudes appearing at 1100 and 1650 ms in (a) can still be seen in (b).

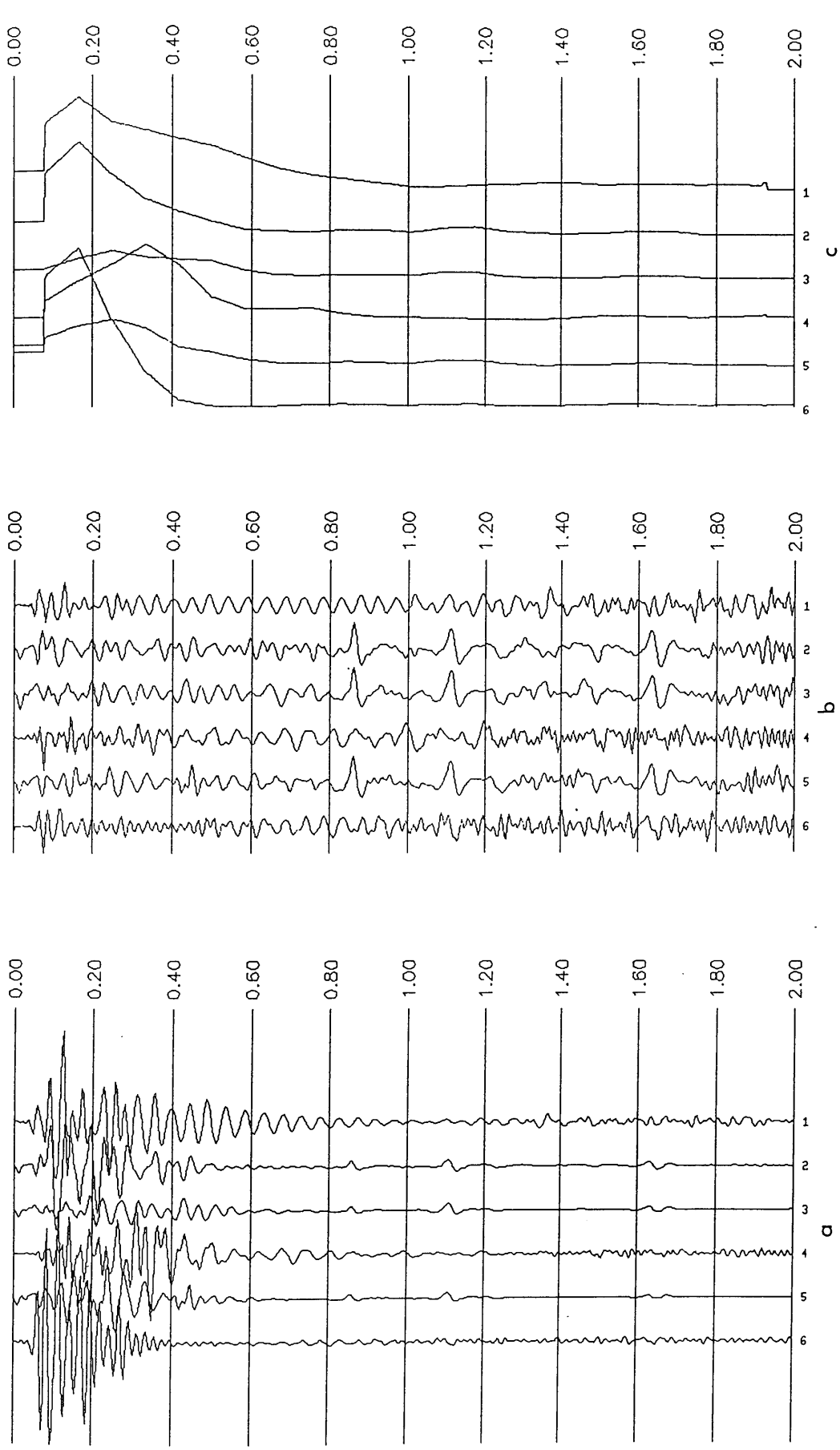

Fig. 2.7.1 (a) Original unscaled seismic traces from shot 2. (b) Scaled seismic traces after a gain is applied.
(c) The gain functions.

The window lengths are empirically determined to produce the optimum coherence of seismic events.

The combination of the gain-control program with the plotting package saves much computer memory, since there are no temporary files needed for output from the gain-control program. This program reads the data, scales and plots the data in one program run, which makes it possible for the user quickly to examine the data. The program can also display seismic data in various ways, such as wiggle line display, variable area plus wiggle line display or variable area display without wiggle lines.

2.8 Static correction

In order to obtain a seismic section which shows seismic reflectors representing the actual geological structure, reflection times must be reduced to a defined reference datum. This is normally taken to correspond to a horizontal plane fixed at a certain known elevation. Static correction is essentially a time-shift introduced to each trace, reducing the observed reflection time to the chosen datum plane.

The value of total static correction (Δt) depends on the following factors [Al-Sadi, 1980]:-

(1) The vertical distance of the source from the datum plane.

(2) The surface topography, that is the vertical distance of the detector from the datum.

(3) The velocity variation of the surface layer along the seismic line.

(4) Thickness variation of the surface layer.

The total static correction Δt (Fig. 2.8.1) is made up of two parts, the source correction Δt_s and the receiver correction Δt_r, where

$$\Delta t = \Delta t_s + \Delta t_r = \frac{d_s + d_r - 2d_1 - d}{V_o} + \frac{2d_1}{V_1}$$

Δt_s Source static correction,

Δt_r Receiver static correction,

d_s Distance between the source location at the surface and datum

plane,

d_r Distance between the receiver location at the surface and the datum plane,

d_1 Thickness of the second consolidated layer,

d Depth of a shot hole,

V_o Velocity of the weathered layer,

V_1 Velocity of the consolidated layer,

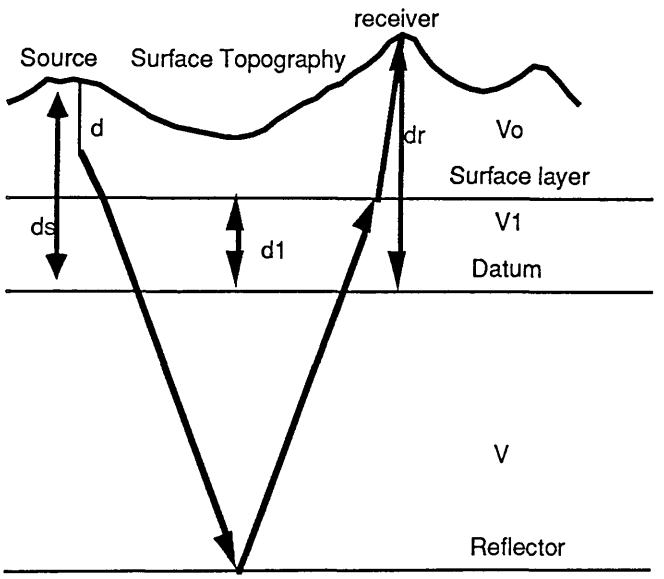

Fig. 2.8.1 Definitions of source and receiver static corrections.

The area chosen for this experiment is relatively flat - the elevation difference between adjacent shot points is less than 10 m, the biggest difference between the lowest and highest shot points along the profile line is about 15 m. The relief of the terrain along the line is illustrated in Fig. 2.8.2. To apply the static corrections to the data, the principle is the same as described above, that is, to introduce a time shift to each trace using the above formula. A local datum was chosen as a horizontal plane 5 m beneath the lowest shot point (shot point 1) along the profile line, above which is the surface layer with a constant velocity of V_o. Therefore, all observed reflection times are reduced to this local datum.

The relative elevations of 12 stations to each shot point and relative elevations of adjacent shot points were surveyed. To calculate the time shift for each trace, the depth of source (d) is approximated as 2 m, which is the depth of the shot hole. The effect of the depth of receivers, about 50 cm, is neglected because it introduces less than 1 ms time reduction. The velocity V_0 of weathered layer (boulder clay), about 2100 m/s, is taken from Hall [1971].

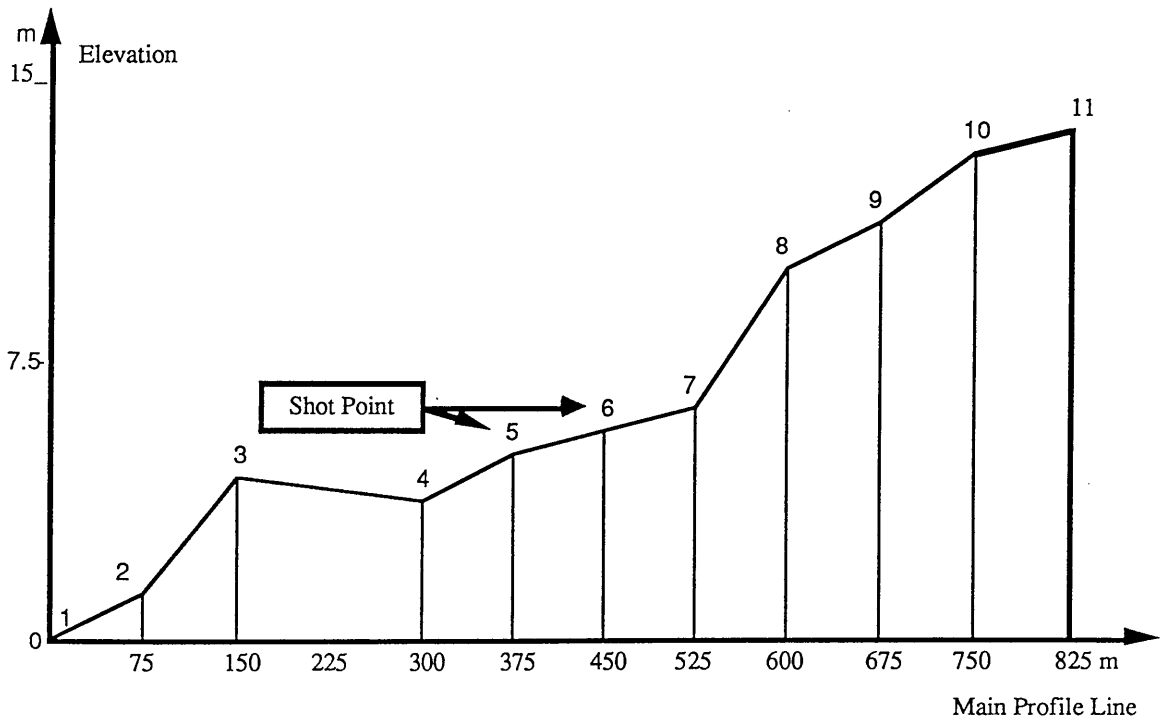

Fig. 2.8.2 The topography along the main profile line (elevation value is exaggerated).

It was found that we cannot easily access the processors in the SKS package to apply the static corrections to such data, because the package mainly deals with the CDP data. Therefore, we made manual calculations which proved to be easier for the 9 shot records. The time shifts are obtained using the following simplified formula,

$$\Delta t = \Delta t_s + \Delta t_r = \frac{d_s + d_r - d}{V_0}$$

in which the velocity of the surface layer V_0 is equal to the velocity of the second layer V_1. In fact, this assumption is valid because the local datum is just 15 m beneath the surface, within this layer the materials can be considered to be the same. The distances (dr) between the various stations to the local datum are listed in Table 2.8.1, the time shifts (t) applied to the stations are also listed in the table. From the table, we can see that the variation in time shift between adjacent stations is less than 5 ms, but the variation between shots can reach up to 13 ms, which would introduce a large phase shift for reflection signals. In practice, these time shifts were first converted to the nearest number divisible by 4 because of the sampling interval 4 ms, and lastly were subtracted from the orientation-transformed data.

sp	st	1	2	3	4	5	6	7	8	9	10	11	12
1	dr	2.4	4.3	4.6	5.8	7.0	6.6	12.2	7.1	9.0	6.1	5.0	4.9
	t	2.6	3.5	3.6	4.2	4.8	4.6	7.2	4.8	5.7	4.3	3.8	3.7
2	dr	3.2	4.4	5.0	5.2	6.5	6.4	11.7	9.3	8.5	9.1	7.2	5.7
	t	3.5	4.1	4.3	4.4	5.1	5.0	7.5	6.4	6.0	6.3	5.4	4.7
3	dr	4.2	5.2	5.0	6.1	8.0	7.9	11.2	8.7	9.3	6.8	4.4	4.7
	t	5.4	5.9	5.8	6.3	7.2	7.2	8.7	7.5	7.8	6.6	5.5	5.6
4	dr	3.4	4.1	4.4	6.9	9.2	10.0	10.6	8.7	10.2	9.6	6.0	5.0
	t	4.7	5.1	5.2	5.4	7.5	7.9	8.2	7.3	8.0	7.7	6.0	5.5
5	dr	4.7	6.1	5.1	9.0	10.0	10.0	12.1	10.5	12.7	10.4	9.2	5.6
	t	5.9	6.5	6.0	7.9	8.4	8.3	9.4	8.6	9.7	8.6	8.0	6.3
6	dr	6.1	7.5	6.7	9.8	10.1	10.6	13.1	13.1	13.5	11.7	13.1	9.3
	t	6.9	7.6	7.2	8.7	8.8	9.1	10.2	10.2	10.4	9.6	10.2	8.4
7	dr	9.2	9.2	6.8	10.7	10.1	13.2	14.8	14.1	14.6	14.7	15.6	14.1
	t	9.0	9.0	7.8	9.7	9.4	10.9	11.7	11.3	11.6	11.6	12.0	11.3
8	dr	13.4	13.9	9.4	11.4	13.6	13.9	15.9	15.2	17.1	16.3	16.7	16.1
	t	12.4	12.6	10.5	11.5	12.5	12.6	13.6	13.3	14.2	13.8	14.0	13.7
9	dr	15.5	16.6	14.0	14.9	14.1	14.9	16.7	17.6	18.4	18.1	17.0	17.5
	t	14.2	14.7	13.5	13.9	13.5	13.9	14.8	15.2	15.6	15.4	14.9	15.1

Table 2.8.1 Static corrections applied to all the stations (st- station number, sp-shot number, dr- distance between receiver and the datum in metres, t- time shift in milliseconds).

Chapter 3 Characterization of 3-component Seismic Data from a Basalt-covered Area

3.1 Introduction

Seismic reflection CDP and VSP data are often of poor quality when recorded in areas where volcanic rocks are present at or near the surface. They are both characterised by large-amplitude reverberations caused by seismic energy trapped in the upper layers [Pujol, 1989]. In this chapter, we present the major characteristics of seismic reflection data recorded using the areal array and 3-component geophones in a basalt-covered area of the Midland Valley of Scotland. We then investigate the energy distribution on geophones at different orientations by applying a specially designed filter.

3.2. Correlation between the penetration of seismic energy and charge size

As it is the first trial of shooting in a basalt-covered area, we had to carry out some tests before the real experiment started. One of the tests was to find out the correlation between the penetration of seismic energy and size of explosive. This test aims at determining the minimum size of explosive without substantial signal degradation. As described in Section 2.4.5, there is a limit to the number of shots that can be fired together due to the properties of the blaster and firing lines. The size of a cavity produced by a blast which is proportional to size of explosive, and therefore has to be minimised. The total resistance of the firing circuit should be kept to below 75 ohms to maintain the current of about 2 A to fire seismic detonators. Therefore, it is advised to shoot fewer than five charges together.

Four half-sticks of dynamite (each weighing 1/8 kg), in four holes,

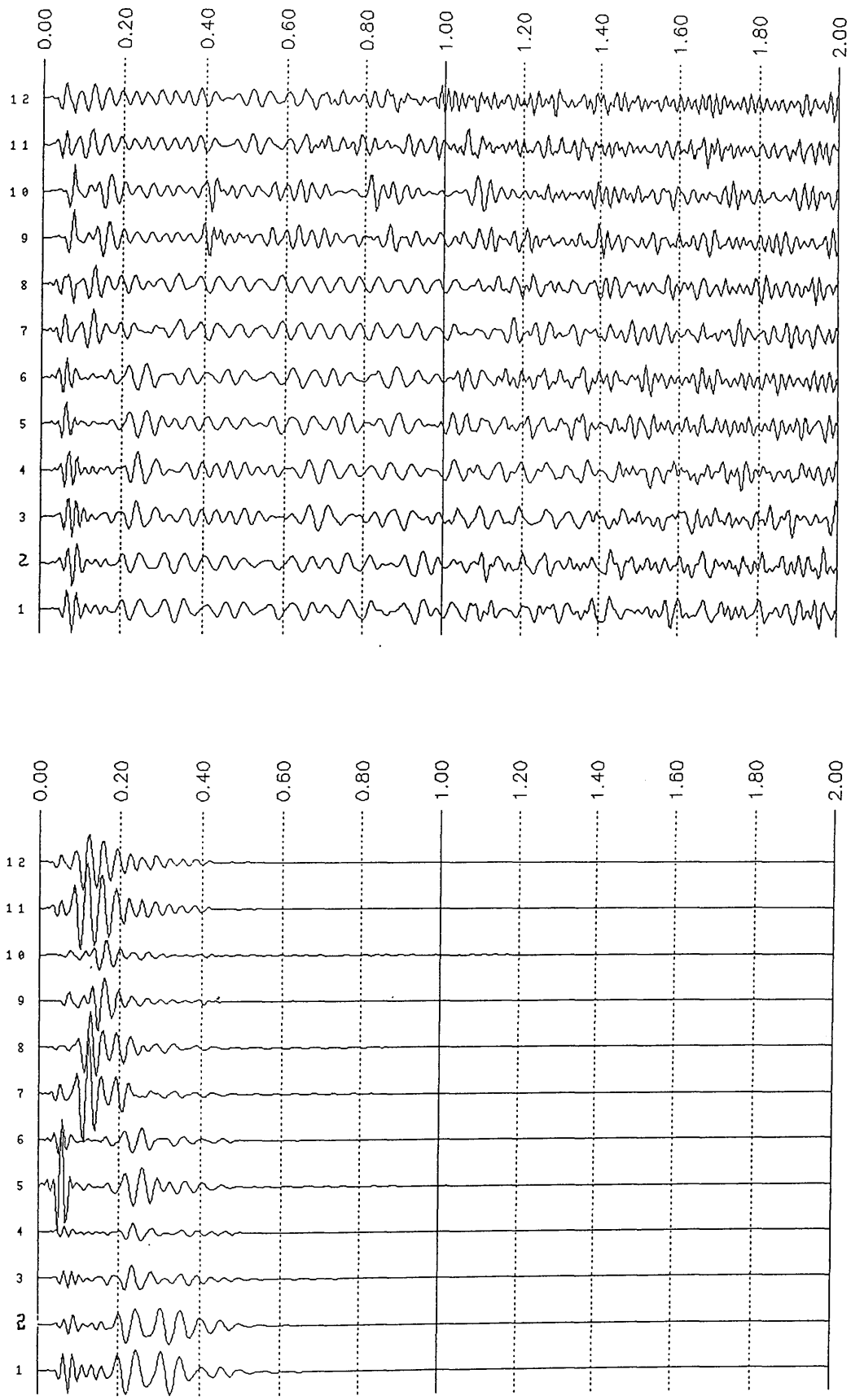

Fig. 3.2.1 (a) Six vertical traces (channels 1, 3, 5, 7, 9, 11) from stations 1, 2, 6, 8, 9, 10 at shot 1 and six vertical traces (channels 2, 4, 6, 8, 10, 12) at shot 2 (shot 1 and shot 2 are test shots at the same location). (b) Same data as those in Fig. 3.3.1 (a) after gain functions are applied.

were used for the first shot, and two half-sticks of dynamite, in two holes, were used for the second shot at the same location. A comparison is made by displaying six vertical traces from 6 stations (1, 2, 6, 8, 9, 10) at shot 1 and also 6 vertical traces at the same location at shot 2. As shown in Fig. 3.2.1 (a), 2 traces from 2 shots are plotted together; that is, trace 1 is from station 1 at shot 1, trace 2 is from station 1 at shot 2, and so on. From the amplitude and frequency characteristics of 6 pairs of traces, we can see that they are comparable down to 500 ms. To make a detailed comparison, these 12 traces are scaled using the program MAGNPL (refer to Section 2.7.3) and then are plotted in Fig. 3.2.1 (b), here we can see that any pair of traces are comparable down to 1600 ms.

For the purpose of this experiment; that is to detect reflectors beneath the basalt (about 500-1500 m beneath the surface), 2 s two-way travel time (TWT) is a long enough record. Since a doubled charge size does not improve the data, two half-sticks of dynamite in two separate holes were used in the majority of shots.

3.3 Characteristics of seismic reflection data in a basalt-covered area

Fig. 3.3.1 (a) shows 3-component seismograms (vertical, north and east) from station 8 at shot 6, 3 traces are all dominated by strong reverberations with large amplitudes and low frequencies, lasting up to 600 ms. The maximum difference between amplitudes in a trace can be up to 80 dB. Fig. 3.3.1 (b) shows the amplitude spectra of the V and N component time series. We see that the maximum of the horizontal component versus frequency (dashed curve) is much larger than the maximum of the vertical component (plain curve). Two amplitude peaks for the horizontal component are at 17 and 25 Hz. In contrast, two peaks for the vertical component are at 23 and 33 Hz. The lowest amplitudes of both components at 50 Hz is due to the use of a notch filter in the MDS-10, which removes the 50 Hz component. The amplitudes beyond 45 Hz are very small. Thus reflection signals with higher frequency are masked and difficult to extract. Moreover, the reverberation patterns vary from trace to trace and from station to station. In order to show the general features of

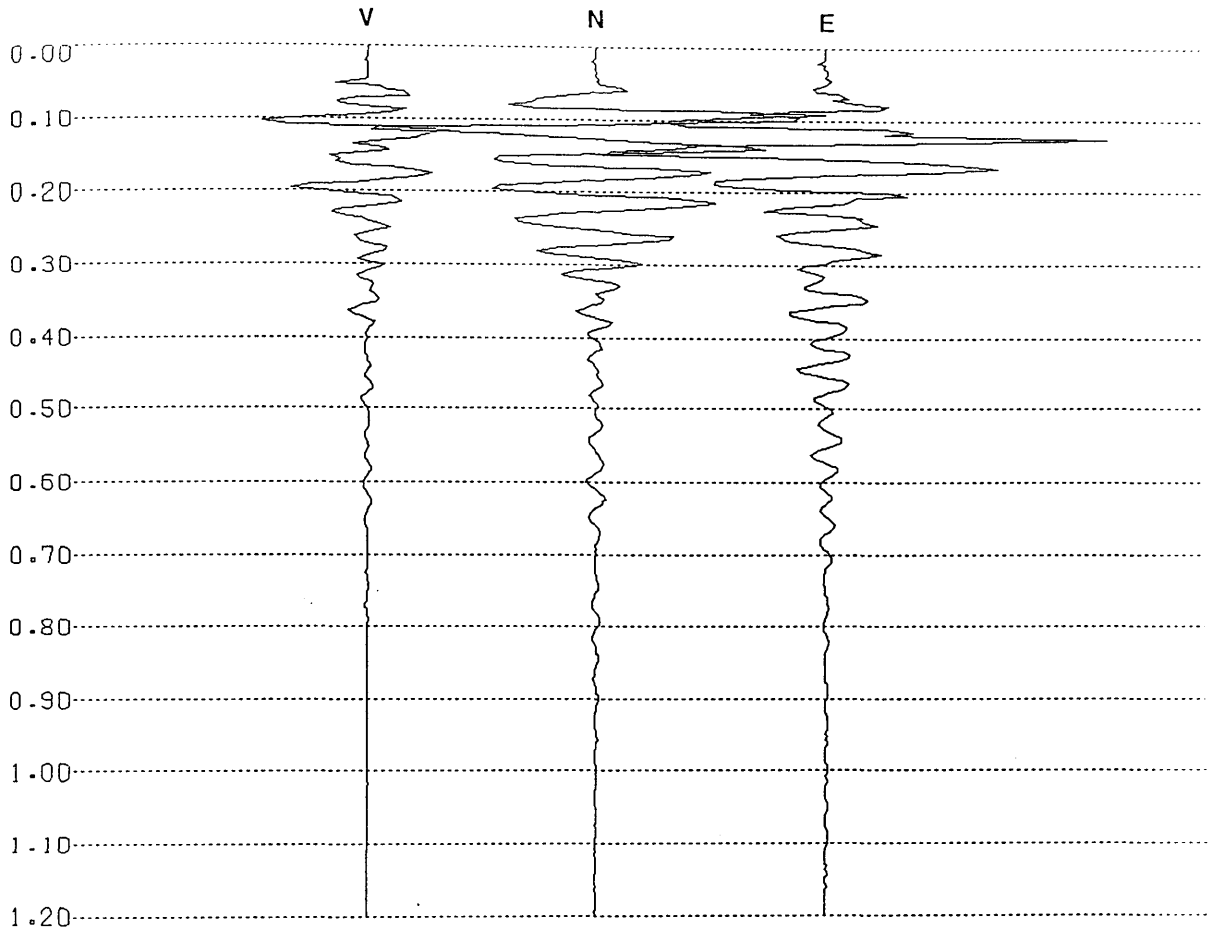

Fig. 3.3.1 (a) Three component seismic traces from station 8 at shot 6 (V - vertical, N - North, E - East).

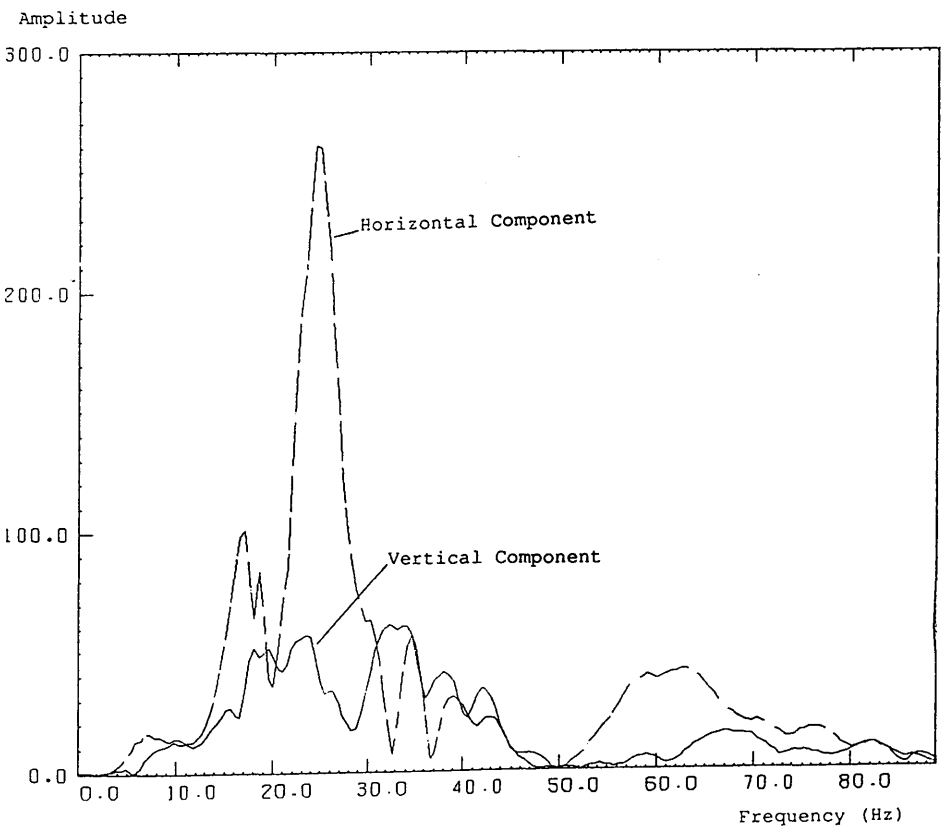

Fig. 3.3.1 (b) The amplitude spectra of two time series- vertical (V) and horizontal (N) components as shown in (a).

such data, several traces from different shots are plotted together (Fig. 3.3.2). Half of them are from the stations in the inner circles and half are from the stations in the outer circles (refer to Fig. 2.3.1). It was found that the data from the inner circles all have much larger amplitudes than those from the outer circles in the same time region. It is likely that the data from the inner circles are much more affected by organised noise than those from the outer circles. In fact, the attenuation difference by spherical divergence and absorption in seismic energy reflected from the deep layers, say 2 km, is minor between the stations with small distance (say 65 m). Thus the great attenuation between two offsets cannot be attributed to spherical divergence and absorption. It is, however, caused by surface conditions in the area where basalt is near the surface. Strong reverberations, as trapped modes in the upper layer, are generated. The reverberations are attenuated dramatically with increase of the distance from a shot point. In other words, the data from small offset stations (75 m) are obscured more severely than those from long offset stations. Additionally, two horizontal components are more noisy than the vertical component, and their reverberation duration lasts longer than the vertical component. In fact, the basalt at the shallow depth gives rise to a critical angle of less than 20^{o}, and a corresponding distance at the surface is less than 50 m. Therefore, stations in this area are all located beyond the critical distance from a shot point, which may cause the data degradation.

Seismic reflection signals are believed to be random. The organised noise-reverberations, however, might be periodic. Auto-correlation of seismic traces is used here to investigate the periodicity of organised noise. Therefore, a number of seismic traces including both the vertical and horizontal components are auto-correlated. The auto-correlation functions show a striking change in strength and period of reverberations, this must be related to surface effects at the source. Fig. 3.3.3 shows one of the auto-correlation functions which mostly represents the periodicity (40 ms) or the frequency (25 Hz) of such organised noise in such a basalt-covered area. The frequency of such noise varies with traces and stations; the general band is at 15-30 Hz.

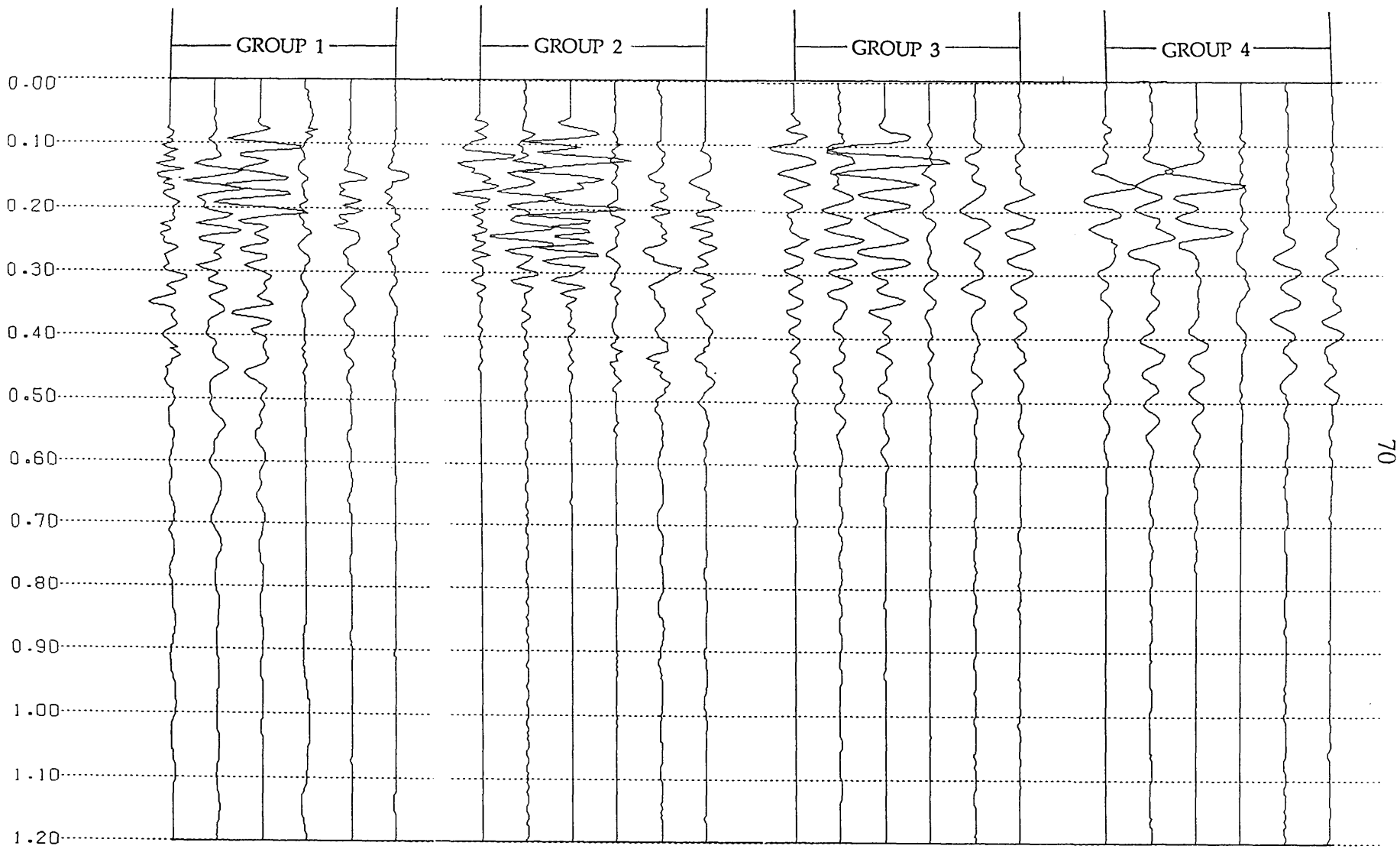

Fig. 3.3.2 Four groups of seismic traces. They are from shots 2, 3, 6, 8 respectively. The first 3 components in each group are from the inner station, the second 3 components are from the outer station.

Suppression of such noise will be discussed in detail in Chapter 4.

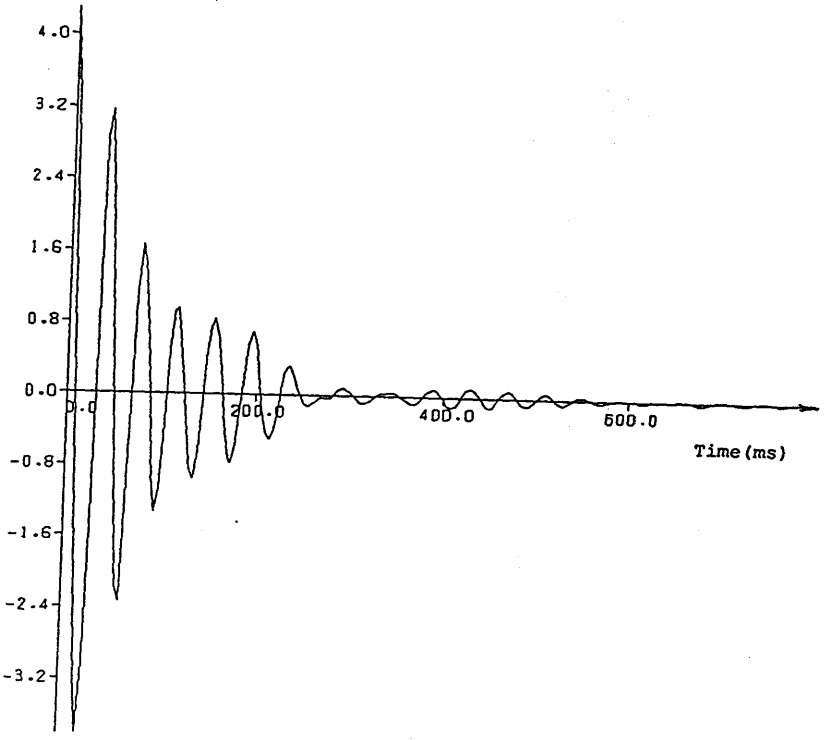

Fig. 3.3.3 Auto-correlation of the horizontal component (North) from station 6 at shot 4. It shows the periodicity of organised noise.

It is hard to see any features of interest from the display of unprocessed seismic data because the later part of a trace is scaled down to such degree that it is nearly invisible. To overcome the problem, before displaying, all the data are coordinate-system transformed, bandpass frequency filtered (20-60 Hz) and finally scaled using the program MAGNPL (refer to Section 2.7.3). Fig. 3.3.4 (a), (b) and (c) show the data from the radial, transverse and vertical components respectively. The data are organised such that the traces from the inner stations are plotted on the left-hand side of the figure (channels 1-60),

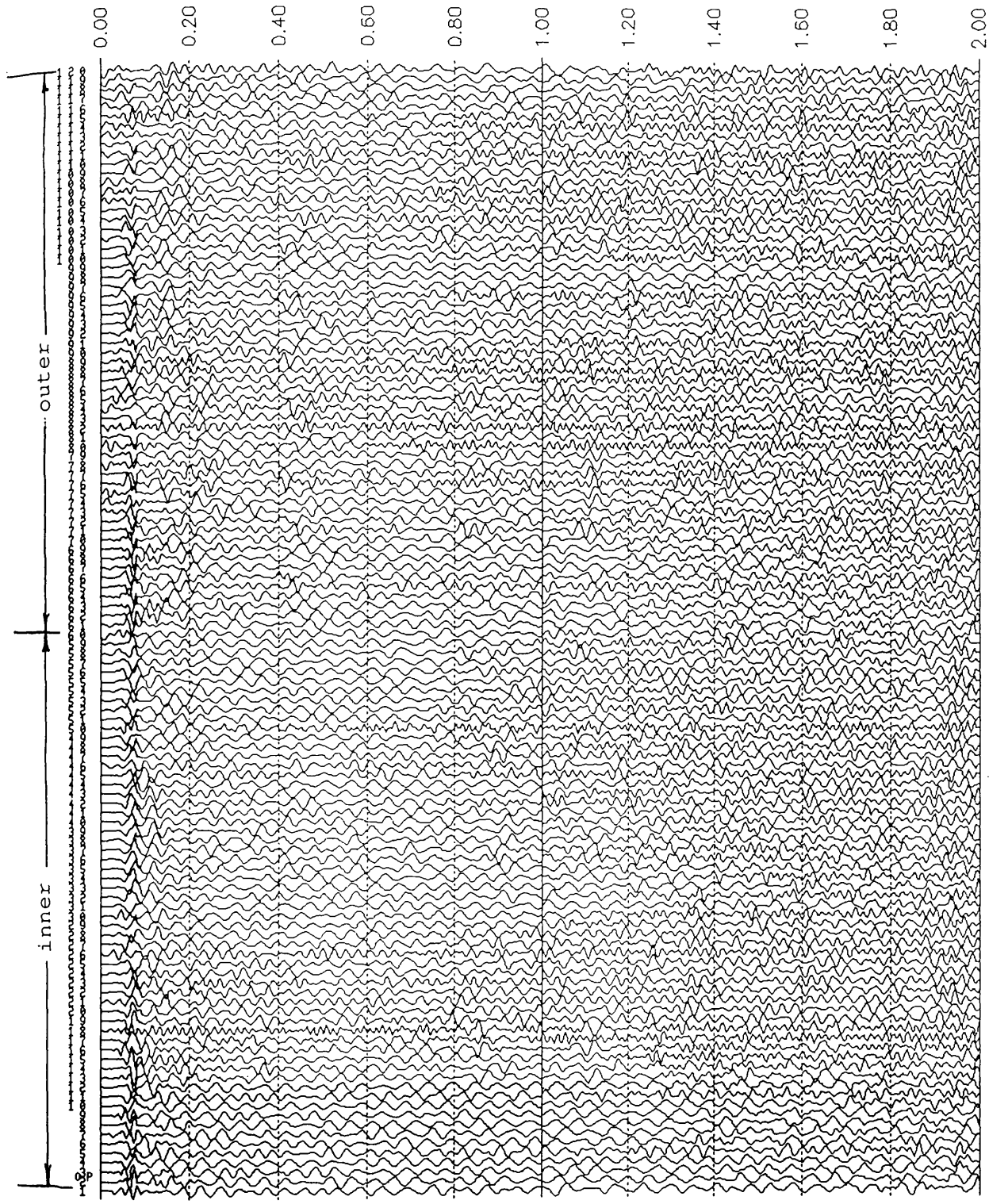

Fig. 3.3.4 (a) The radial components from 10 shots. The traces from the inner stations are on channels 1-60, those from the outer stations are on channels 61-120.

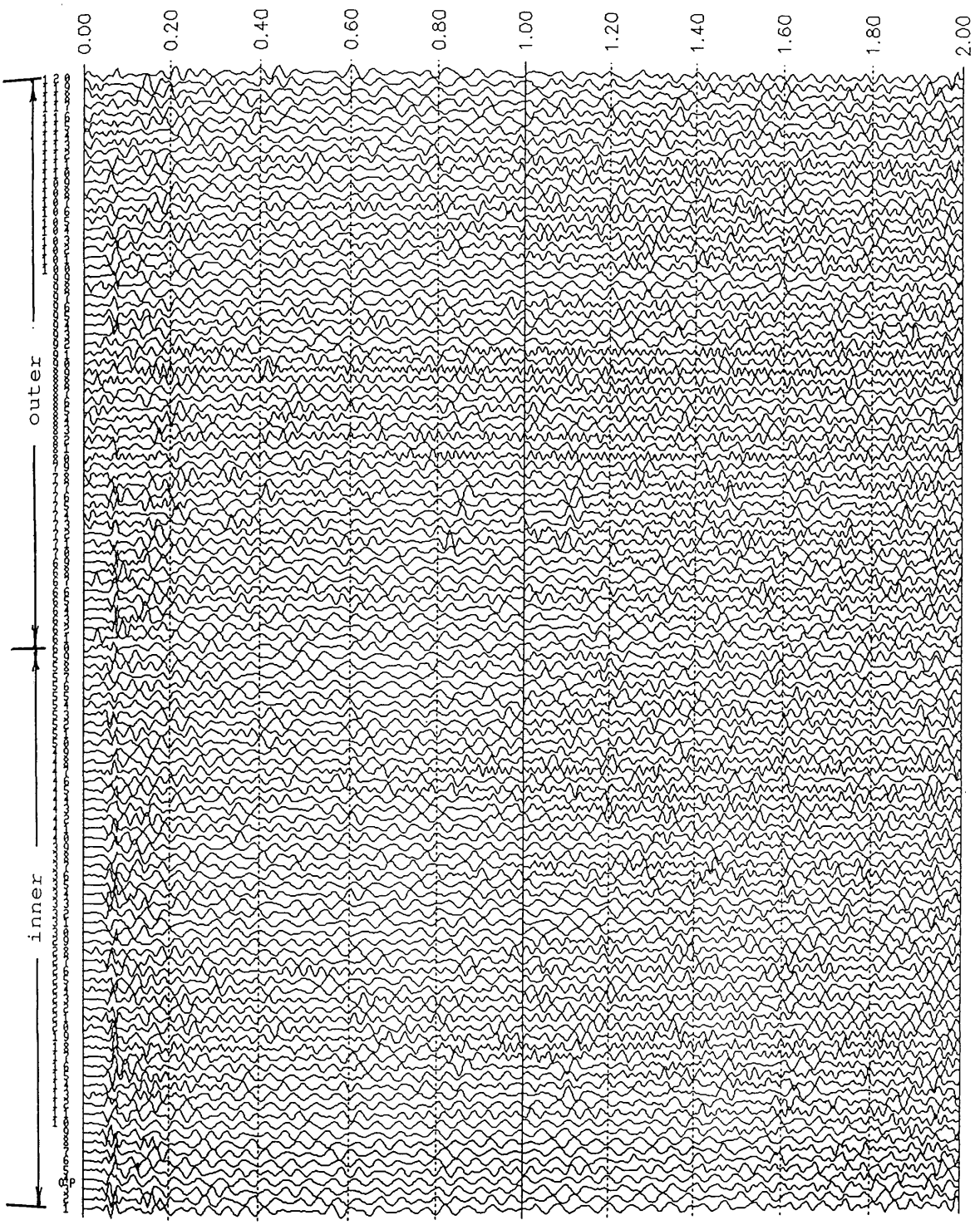

Fig. 3.3.4 (b) The transverse components from 10 shots. The traces from the inner stations are on channels 1-60, those from the outer stations are on channels 61-120.

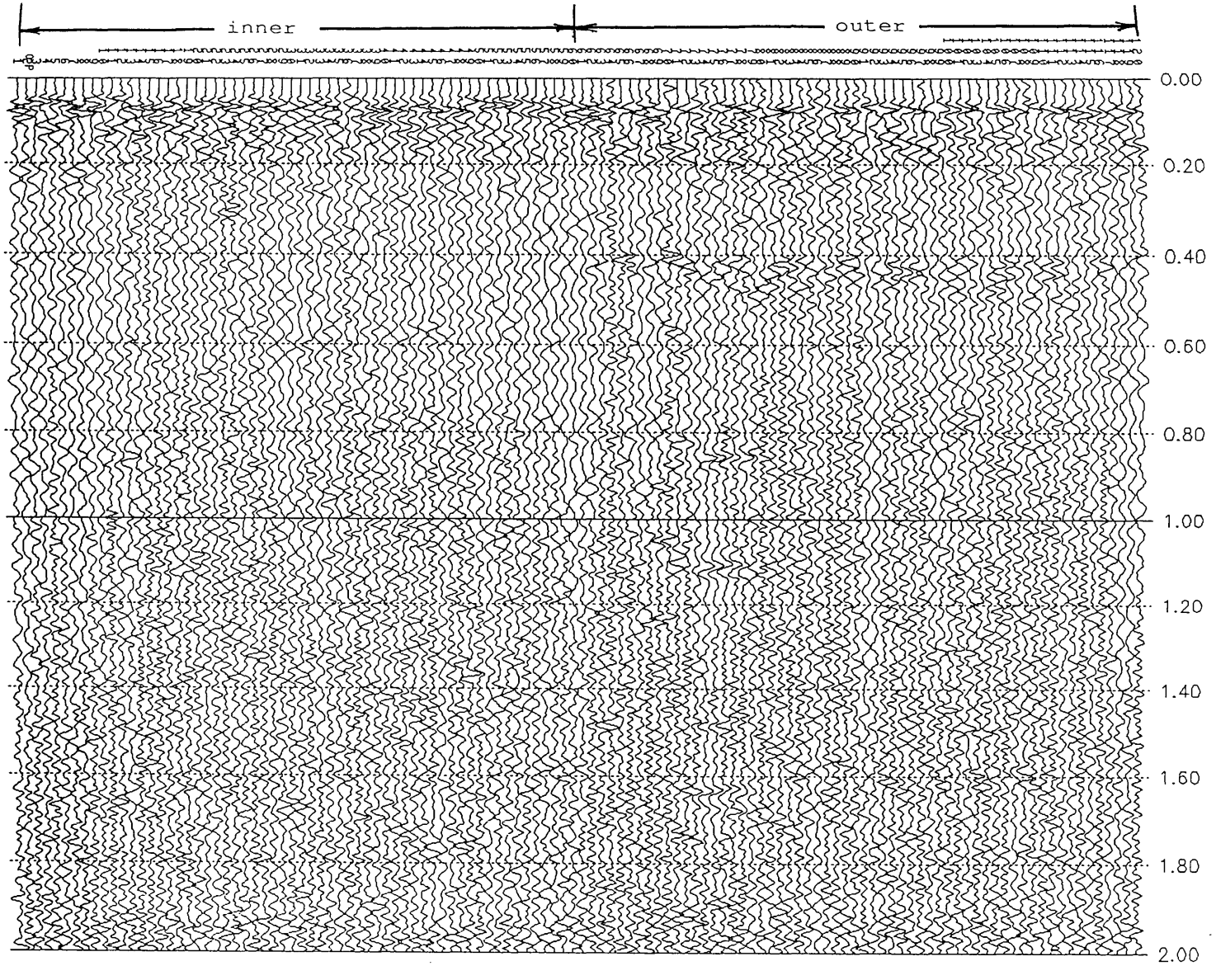

Fig. 3.3.4(c) The vertical components from 10 shots. The traces from the inner stations are on channels 1-60, those from the outer stations are on channels 61-120.

those from the outer stations are plotted on the right-hand side of the figure (channels 61-120). The data from the test shot (we name it shot 0) are also plotted together with the rest (channels 1-6, 61-66). It can be seen that the early part of the traces, down to 1400 ms, is dominated by relatively low frequency content, and the later part of the traces, after 1400 ms, is dominated by high frequency content. Fig. 3.3.4 (a) for the radial component shows some reflections at 420 ms (channels 61-120), which are believed to be P-waves, (b) for the transverse component shows little of interest, (c) for the vertical component shows a line of reflection events at 420 ms from the outer stations (channels 61-120) characterised by the higher frequency. In addition, there are a series of low frequency (about 10 Hz) events at 850, 1100, 1620 ms on channels 73 - 78 at shot 2. These events, however, are not shown at other shots. A detailed analysis and interpretation of the data are given in Chapter 4.

3.4 Detection of seismic source energy distribution using spatial directional filtering

3.4.1 Introduction to the spatial directional filter (SDF)

Seismic recordings contain signals and undesired noise. A direct trace to trace display hardly shows any source and receiver characteristics, although it does tell us roughly about the frequency and shape of the traces. However, 3-component recordings make it possible to analyse the polarisation of particle motions over a time window in three dimensions. Compressional and shear waves (body waves) are well polarised. The trajectories of particle motions have higher rectilinearity and directionality. In contrast, noise shows less polarisation. If we design a filter which preserves the data which are well polarised and rejects the data which are poorly polarised, with a threshold angles from 0^o to 90^o, the corresponding energy distributed on three geophones can be estimated [Cliet, 1987].

3.4.2 Design of the spatial directional filter

The polarisation direction of particle motions over a time window can be determined in several ways. One way is simply to construct a covariance matrix and then determine the principal axis of the matrix. Mathematically, we define the mean for each coordinate as

$$m_x = \frac{1}{N}\sum_{i=1}^{N} x_i$$

$$m_y = \frac{1}{N}\sum_{i=1}^{N} y_i$$

$$m_z = \frac{1}{N}\sum_{i=1}^{N} z_i$$

where x_i, y_i and z_i are observation values, N is the number of observations. The covariance of any two coordinates are:-

$$var(x) = \frac{1}{N}\sum_{i=1}^{N}(x_i - m_x)^2$$

$$var(y) = \frac{1}{N}\sum_{i=1}^{N}(y_i - m_y)^2$$

$$var(z) = \frac{1}{N}\sum_{i=1}^{N}(z_i - m_z)^2$$

$$cov(x, y) = \frac{1}{N}\sum_{i=1}^{N}(x_i - m_x)(y_i - m_y)$$

$$cov(x, z) = \frac{1}{N}\sum_{i=1}^{N}(x_i - m_x)(z_i - m_z)$$

$$cov(y, x) = \frac{1}{N}\sum_{i=1}^{N}(y_i - m_y)(x_i - m_x)$$

$$cov(y, z) = \frac{1}{N}\sum_{i=1}^{N}(y_i - m_y)(z_i - m_z)$$

$$cov(z, x) = \frac{1}{N}\sum_{i=1}^{N}(z_i - m_z)(x_i - m_x)$$

$$cov(z, y) = \frac{1}{N}\sum_{i=1}^{N}(z_i - m_z)(y_i - m_y)$$

The covariance matrix is defined by

$$V = \frac{1}{N}\begin{bmatrix} var\,(x) & cov\,(x\,,\,y) & cov\,(x,\,z) \\ cov\,(y\,,\,x) & var\,(y) & cov\,(y\,,\,z) \\ cov\,(z\,,\,x) & cov\,(z,\,y) & var\,(z) \end{bmatrix}$$

Suppose three eigenvalues of the matrix V are λ_1, λ_2 and λ_3, of which λ_1 is the largest eigenvalue. Its corresponding eigenvector is given by $E=\{e_1, e_2, e_3\}$ which represents the direction of the principal axis. As we defined, the direction of the vector E is the polarisation direction of particle motions over the time window $N \times \Delta t$ (where Δt is the sampling interval).

Having computed the polarisation direction vector $E=\{e_1, e_2, e_3\}$ which has an angle α to the horizontal axis R, an angle β to the horizontal axis T and an angle γ to the vertical axis V, we define a threshold angle ϕ. When any one of the angles α, β and γ is less than or equal to the threshold angle ϕ, the corresponding sample is kept. Fig. 3.4.1 illustrates the principle of spatial directional filtering along the V-direction. The polarisation axis E_{AB} of the response AB is near the V-direction, therefore, part AB will be kept. Part BC will be rejected since its polarisation axis E_{BC} is almost perpendicular to the V-direction.

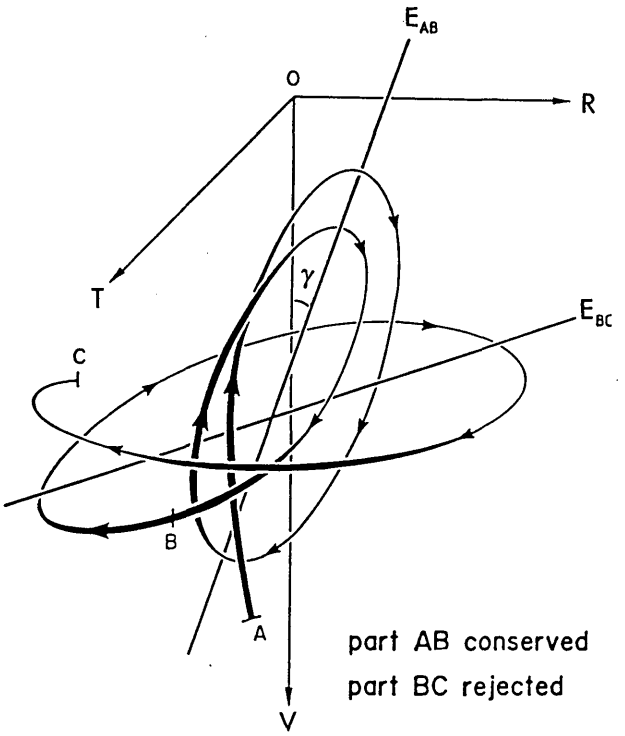

Fig. 3.4.1 Principle of spatial directional filtering along the V-direction. The polarisation axis E_{AB} of the response AB is near the V-direction, therefore, part AB will be kept. Part BC will be rejected since its polarisation axis EBC is almost perpendicular to the V-direction (From Cliet, 1987).

3.4.3 Fortran-77 program MASDF

A Fortran-77 program called MASDF (see Appendices; Fortran-77 program 6) was written by the author to perform the function of the filter. The system-independent program contains a main program and a subroutine. The main program reads the 3-component data into an array, computes the mean value of each variable and covariance of any two variables, and constructs a covariance matrix V. The subroutine EIGEN computes the largest eigenvalue and the corresponding eigenvector of the matrix by the Power method [Churchhouse, 1981]. The program allows the user to define a time window length and a threshold angle ϕ. To run the program under the

VAX/VMS operating system, the program (see Fig. 3.4.2) is modified to call a NAG library routine for calculating the largest eigenvalue and corresponding eigenvector. The data from 12 stations can be processed for each run. A user has to reply to several questions:-

```
$  INPUT FILE NAME FOR FILTERING
   TRST02
$  INPUT NUMBER OF STATIONS IN THE FILE
   12
$  INPUT NUMBER OF SAMPLES IN ONE TRACE
   501
$  INPUT FILE NAME FOR OUTPUT
   EOUT02
$  START READING DATA INTO ARRAY
$  INPUT THRESHOLD ANGLE IN DEGREE
   45
$  INPUT STATION NUMBER TO START (TYPE 0 TO STOP)
   1
   0
$  START WRITING FILTERED DATA INTO OUTPUT FILE
$  FORTRAN STOP
```

For the purpose of a clearer display of the filtered data, we set 0 as a result within the window in which angles α, β and γ are greater than a given threshold angle ϕ, but set a constant 1 for the window in which angles α, β and γ are less than a given threshold angle ϕ.

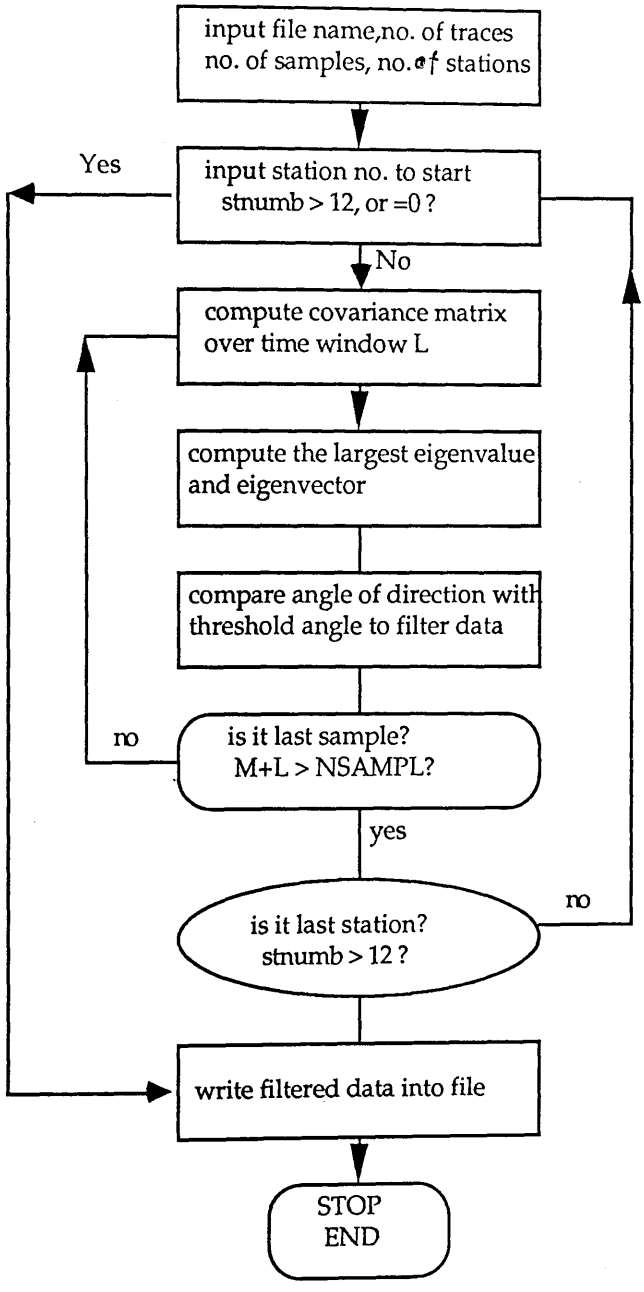

Fig. 3.4.2 Flow diagram of Fortran-77 program MASDF.

3.4.4 *Application of the MASDF filter for analysis of 3-component data*

Applying the MASDF filter to 3-component seismic data provides a means of analysing the polarisation of seismic events, and also enables one to evaluate the energy distribution along the radial, transverse and vertical

directions.

The particle motion of seismic waves is never rectilinear, but is always more elliptical. An elliptical trajectory can be proved by investigating the filtered data. With a threshold angle approaching 0^o, which is an extreme case such that all particle motions are absolutely rectilinear, the three filtered sections show no events passing through the filter. Accordingly, more information appears on the sections as the threshold angle is increased. For a threshold angle of 90^o, which is the case that no polarisation direction is specified, all the events pass through the filter. Fig. 3.4.3. shows the filtered radial, transverse and vertical sections with the threshold angle through 15^o, 30^o, 45^o, 60^o, to 75^o. The data used for processing are from shot 6 on the profile line. By studying 15 diagrams, we are able to see that, for a fixed window length (e.g. 84 ms, see Section 4.5.5) and a fixed threshold angle, the horizontal sections always show more events than the vertical section, moreover, the radial-section exhibits more information passing through the filter than the transverse section. These characteristics may be related to the larger amplitudes on the horizontal components than the vertical component, so that the polarisation direction of particle motions are inclined more towards the horizontal axes. Another feature from the diagrams is that, with a threshold angle of less than 60^o, almost no events pass through the filter on the transverse section at a time down to 300 ms. The absence of events on the first trace for the transverse component is due to a dead trace in this shot record. The patterns on three sections are varied from shot to shot.

By slightly modifying the program MASDF, we can use it to investigate the directionality of particle motions. After a series of threshold angles being input (0^o, 5^o, 10^o, 15^o, 20^o, 25^o, 30^o, 35^o, 40^o, 45^o, 50^o, 60^o, 65^o, 70^o, 75^o, 80^o, 85^o, 90^o), for a specified threshold angle, the program constructs the covariance matrix and computes the eigenvector corresponding to the largest eigenvalue and then filters the data within the window in 3 directions. The number of the windows on one section which pass through the filter is summed and is divided by the total number of windows, finally the result is multiplied by 100 and is

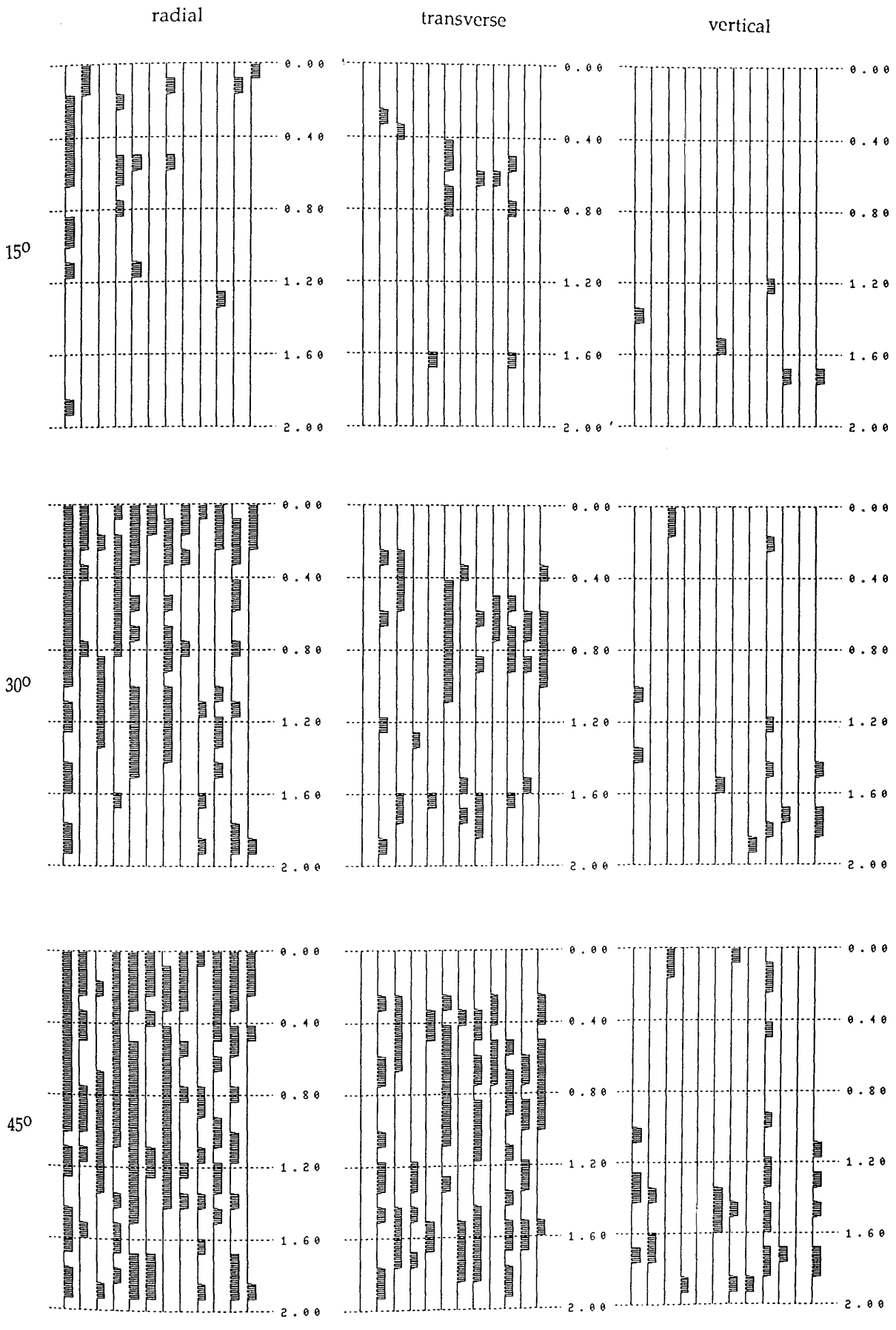

Fig. 3.4.3 Continued (see the next page)

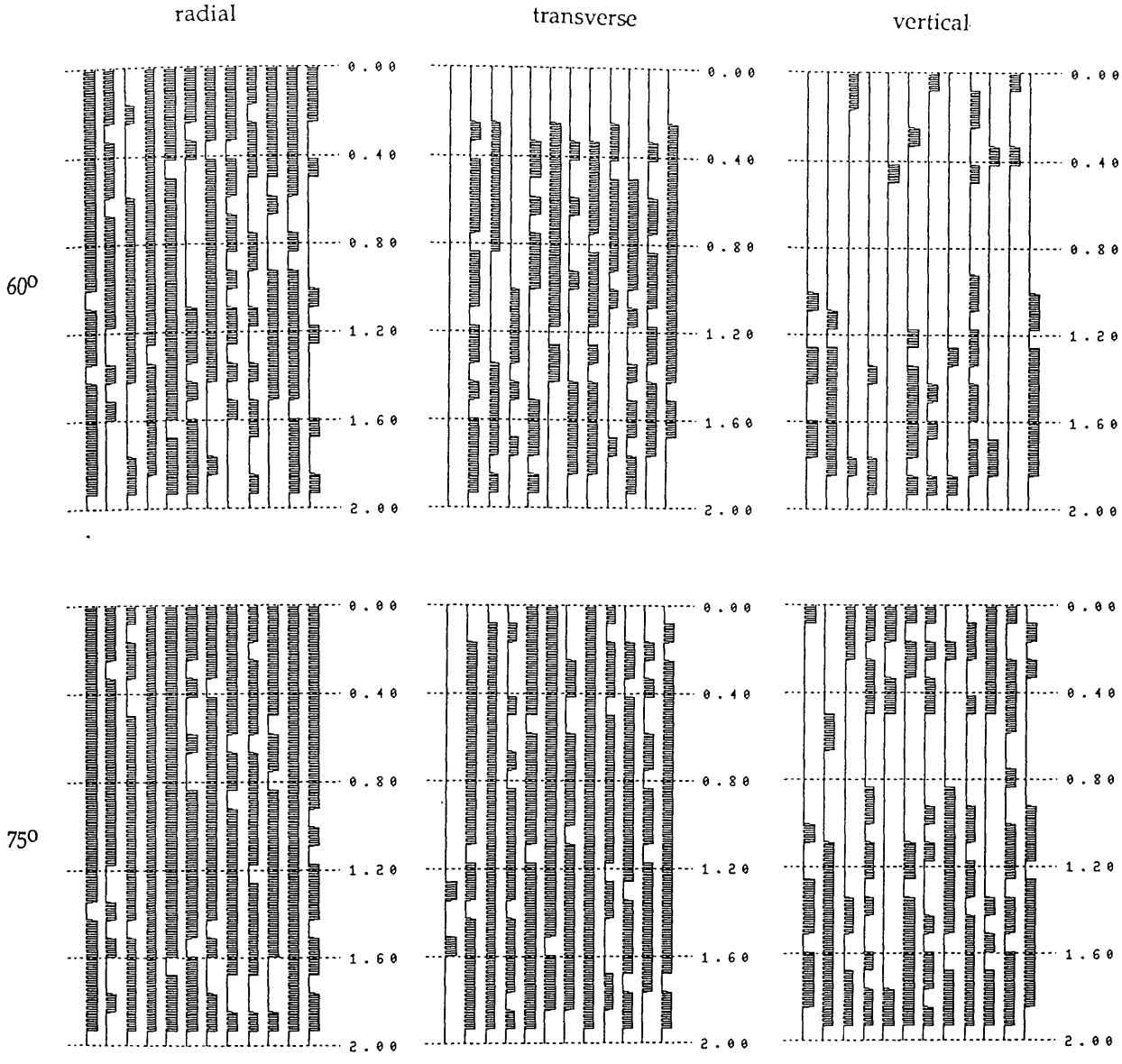

Fig. 3.4.3 The three-component sections of shot 6 after application of the spatial directional filter. The time window for filtering is 84 ms, threshold angles are 15°, 30°, 45°, 60°, and 75°.

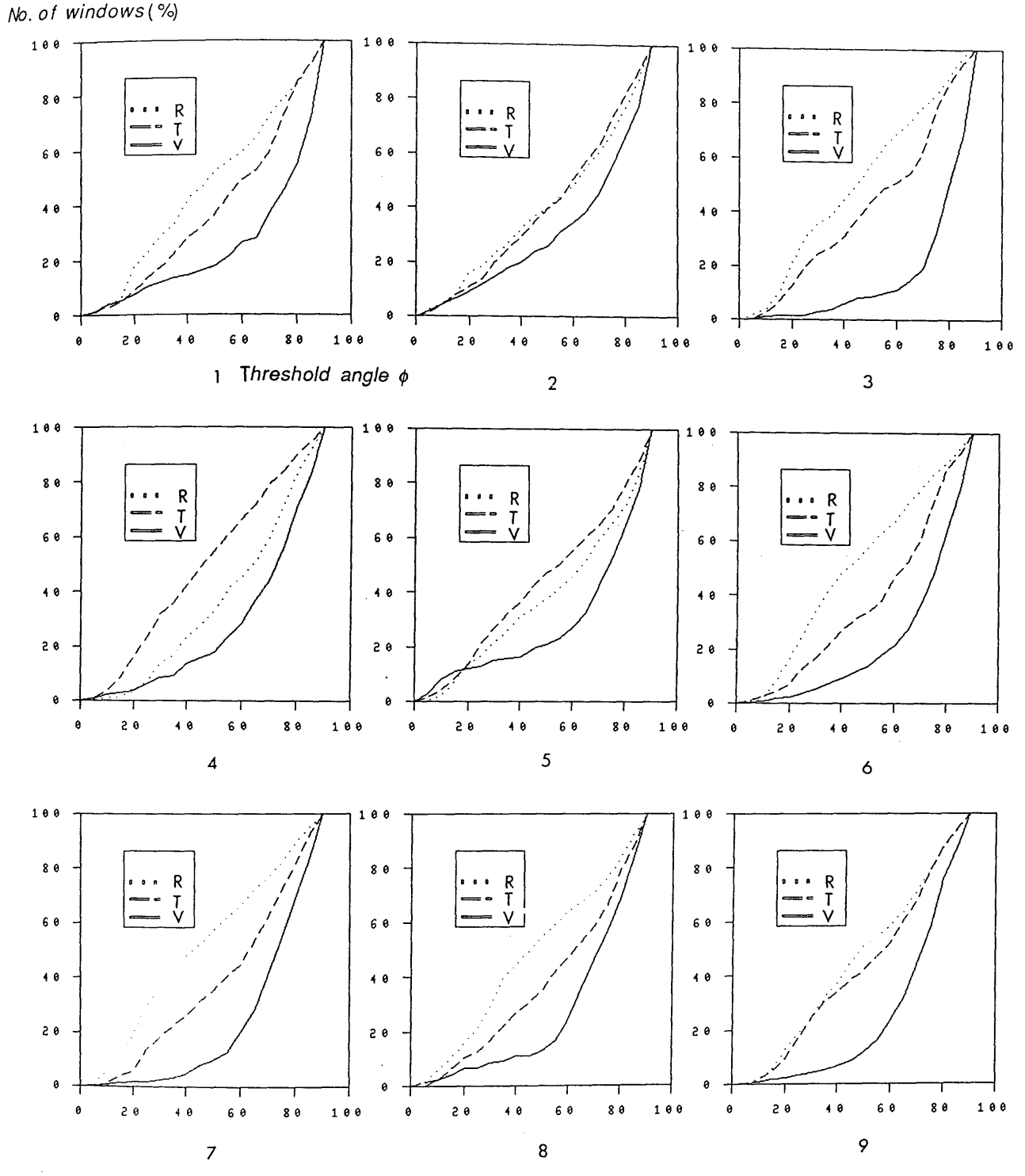

Fig. 3.4.4 The relationship of each component between the number of windows within which the data have passed through the filter and threshold angles. The number of windows is expressed in percent. The data from 9 shots are presented.

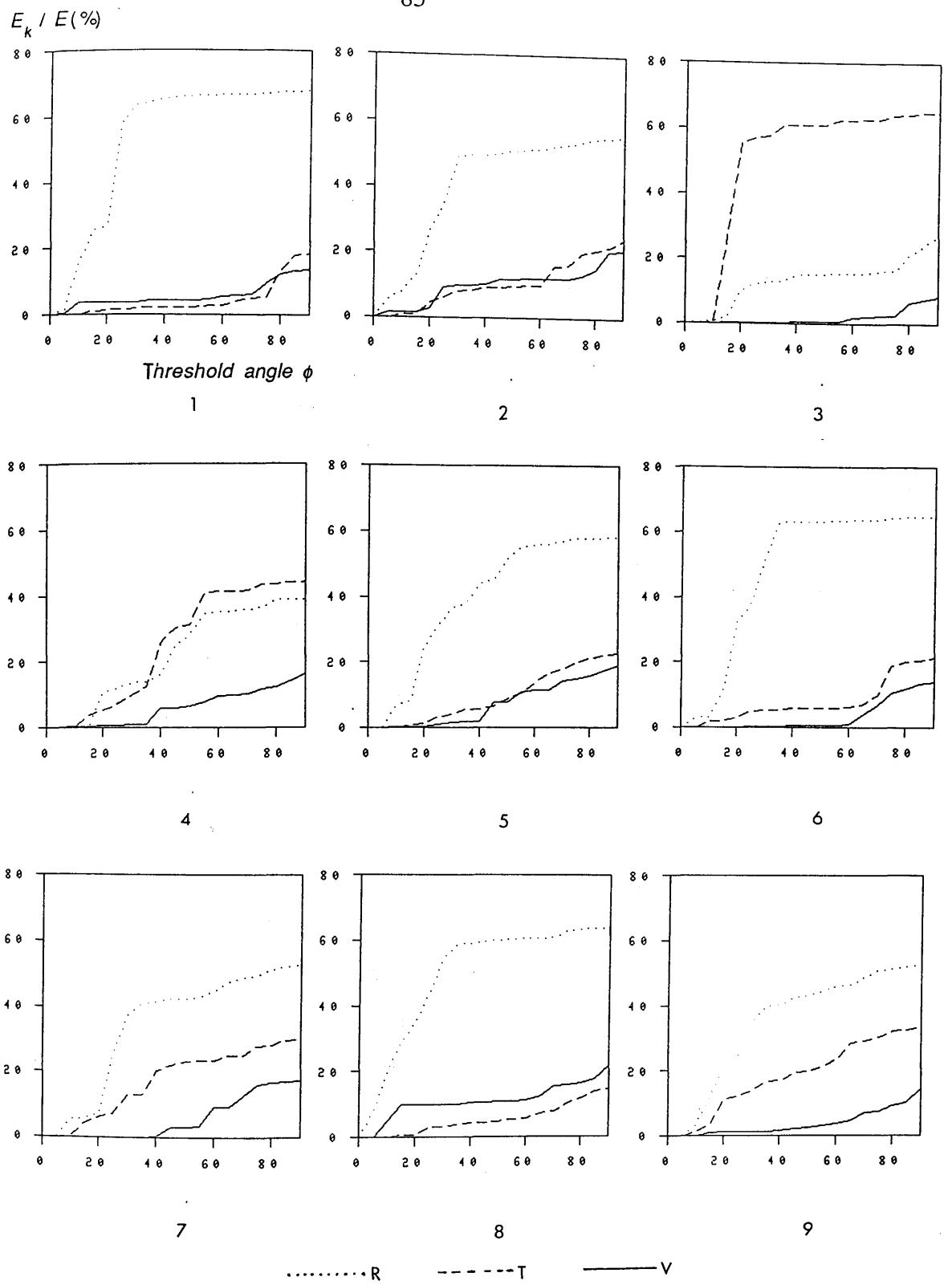

Fig. 3.4.5 Energy variation of each component expressed in percent as a function of threshold angle. The data from 9 shots are presented.

expressed in percent. We plot the results for each shot against the threshold angle. Three different curves for the radial, transverse and vertical sections are shown in Fig. 3.4.4, from which we can see that, with a threshold angle of 0^o, no data pass through the filter, however, with the threshold angle of 90^o, all the data pass through the filter, so the three curves in each plot join together at both ends. The 9 plots all show that the vertical section has the smallest number of windows passing through the filter, so that the curve for the vertical section are all lower than the others. In contrast, seven out of nine plots show that the radial sections indicating the radial direction of particle motions are dominant in the plots at any threshold angles.

Next is an analysis of the energy distribution on different geophones at each shot. The energy density for a harmonic wave is proportional to the density of the medium and to the second power of the frequency and amplitude of the wave. The ratio of energy density, however, only varies with the square of the amplitude [Sheriff & Geldart, 1982]. The program MASDF (see appendices; Fortran-77 program 7) is modified again to calculate the energy density E of seismic waves for 3 sections from one shot and the energy density E_k of seismic waves for one section whose polarisation directions are within the a specified threshold ϕ. The ratio E_k/E is evaluated for each component (12 traces for each shot). As shown in Fig. 3.4.5, the relative energy of each component as a percentage is plotted against the threshold angle in degrees. We can see that although there are some similarities to those in Fig. 3.4.4, the implication is different. The general phenomena are that three curves in each diagram all increase monotonically with the threshold angles, of which the radial components dominate except for shot 3, and the energy distributed on the radial component increases rapidly when the threshold angle is less than 25^o. In contrast, the energy curves for the transverse and vertical components are much lower than the radial component. This indicates that the energy is greatest on the radial component. In spite of that, it cannot be said that these events on the horizontal components are definitely shear waves, as they may be highly organised-noise (for example, multiples) with far larger amplitudes,

which may dominate the polarisation direction.

3.5. Summary

The test shot shows that a doubled size of dynamite in our experiment does not produce better data, indicating that the correlation between the penetration of seismic energy and charge size is not simply linear. Three-component seismic data recorded in a basalt-covered area are characterised by strong reverberations lasting as long as 500 ms. The reverberation patterns vary from station to station. The horizontal components exhibit larger amplitudes and lower frequency than the vertical component. By performing auto-correlations of seismic traces, the frequency of such organised noise is evaluated as about 15-30 Hz. Furthermore, the data from the inner stations are believed to be more affected by surface conditions than the data from the outer stations. The display of the vertical components from the outer stations shows a line of reflection events at about 420 ms. There are no clear events on the transverse section.

By applying the spatial directional filter to each component of seismic data, it is shown that there are more events in the horizontal components passing through the filter than the vertical component. This is attributed to the far larger amplitudes of the horizontal components, which may dominate the polarisation direction of particle motions. The energy variation diagram of each shot shows quantitatively that the radial component receives much more energy than the others.

Chapter 4 Data Processing and Interpretation

4.1 Introduction

Seismic reflection data are usually contaminated with various kinds of noise such as coherent noise (direct wave, refracted wave, diffracted wave and multiples) and random noise. Those data recorded in basalt-covered areas exhibit a very special behaviour, being mixed with high reverberations lasting as long as a second or so. As a result, the reflection signals are severely masked by such organized noise. In order to extract the weak signals from the data in the presence of noise, special processing techniques have to be developed in addition to the existing conventional methods. In this chapter, we firstly attempt to apply the standard processing methods such as frequency filtering and predictive deconvolution filtering to the data, and then we design and apply a signal enhancement polarisation filter. Lastly we present the results of filtering, and give an interpretation.

4.2 Pre-editing 3-component seismic data

On recording 3-component seismic data in the field, some channels were improperly mixed up. For instance, the vertical component was connected to the channel for the horizontal component. Some channels were open-circuit, which caused the dead traces. The electrical connections of some traces were inverted by mistake so that the peak-trough sense of such traces comes out reversed in comparison with the rest of the recording. The SKS package (refer to Section 2.5.1) is used here to zero dead traces and to reverse the polarity of some traces.

The original record length is 5 s with the sampling interval of 1 ms. To

save the storage, the data were re-sampled to 4 ms and data length is reduced to 2 s.

4.3 Frequency filtering

An explosive source also generates unwanted noise. Ground-roll has a frequency lower than 20-25 Hz and its amplitude is very high especially on short-offset records. The air-wave usually has a frequency higher than 50 Hz. A constant zero-phase bandpass frequency filter is used here to attenuate ground-roll and other high-frequency random noise.

The seismic spectrum is subject to absorption along the propagation path because of the intrinsic attenuation of the earth. The higher frequency components are usually attenuated faster by absorption and other natural filtering, so that higher frequency bands of useful signals are confined to the shallow part of the section. In contrast, the lower frequency band of useful signals is confined to the later part of the section. In the exploration industry, a time-variant bandpass filter is commonly used to obtain a cleaner section. However, for our shallow seismic recordings, a constant bandpass filter (20/30 - 60/70) with a low cut-off of 20 Hz and a slope of 30 dB/octave, and a high cut-off of 60 Hz and a slope of 70 dB/octave is used to avoid the difficulties of correlation from record to record induced by varying frequency and phase changes of different filters. Most importantly, the application of a polarisation filter (refer to Section 4.5) to the data requires that frequency filtering 3 components from one station should not change the polarisation characteristics of particle motions of useful signals.

We take the data from shots 5 and 6 as an example, and perform frequency filtering to see how the data are affected. Fig. 4.3.1 (a) shows the unfiltered data (channels 1-3) and filtered data (channels 4-6) from station 7 at shot 6, and Fig. 4.3.1 (b) shows the data from station 10 at shot 5. We can see that high frequency noise, say at 100-200 ms on channel 3 in (a) has been removed. The filtered traces have become smooth. Additionally, the lower frequency components (<20 Hz) have also been removed. Hence the amplitudes

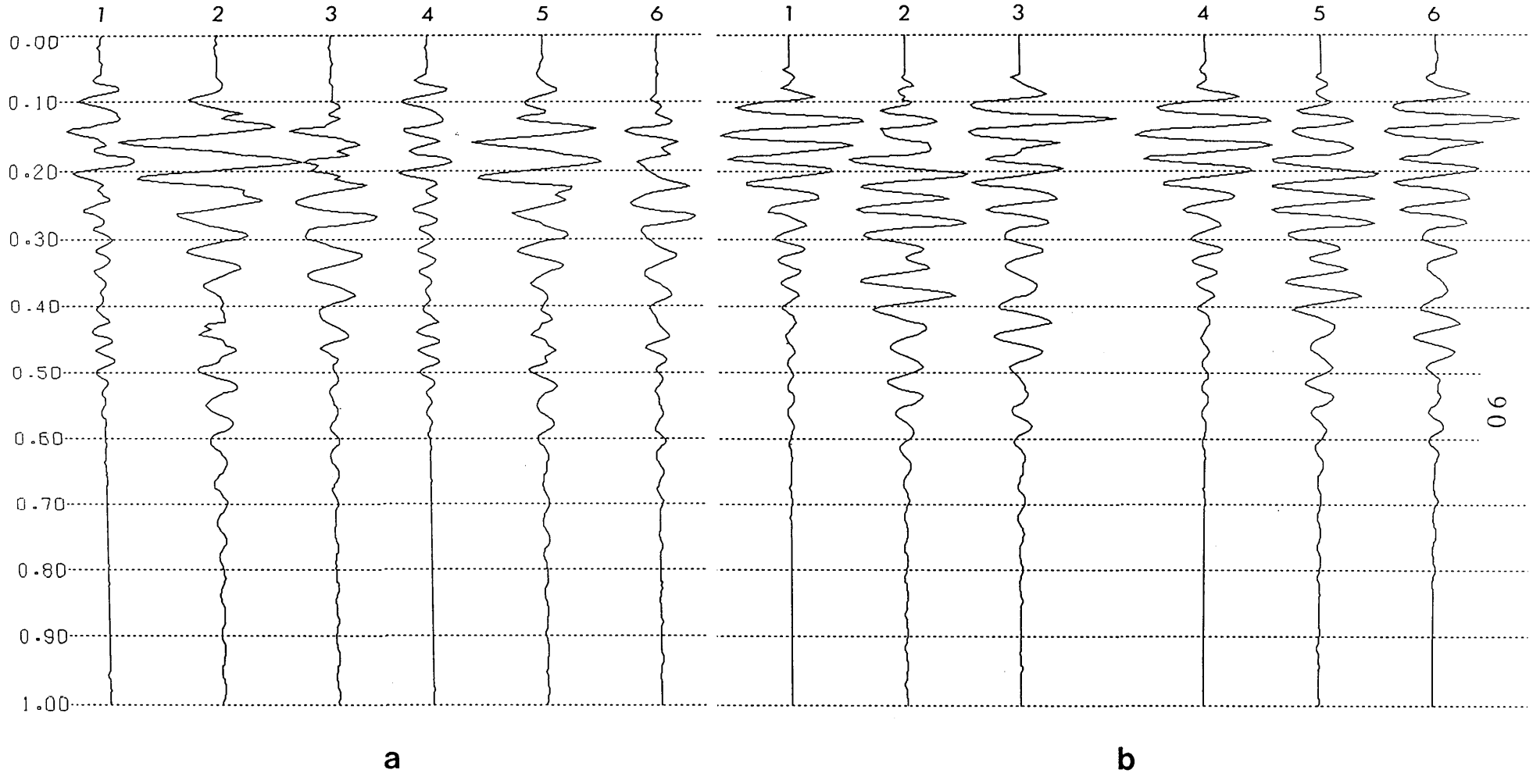

Fig. 4.3.1 (a) The original 3-component seismograms (1-3) from station 7 at shot 6, and the bandpass frequency filtered seismograms (4-6). (b) The original 3-component seismograms (1-3) from station 10 at shot 5, and the frequency filtered seismograms (4-6). Bandpass frequency bandwidth is 20/30-60/70 (Corner frequency/slope in dB/oct).

of filtered data, say channel 5 in (a), have been suppressed. However, for those components within the frequency bandwidth, the filter does little to the data. The unfiltered data (channels 1-3) and filtered data (channels 4-6 in Fig. 4.3.1 (b)) look rather the same because the frequencies of reverberation at this station are higher than 20 Hz.

4.4 Predictive deconvolution filtering

Deconvolution is a general term for data processing methods designed to improve the temporal resolution of seismic data by compressing the basic seismic wavelet (spiking deconvolution) and to remove effects which tend to mask the primary reflected events on a seismogram such as absorption, reverberation, ghosting and multiple reflections (predictive deconvolution). The former process is based on Wiener optimality which states that the seismic wavelet can be restored to any pre-defined shape. The predictive deconvolution is particularly based on the assumption that the reflectivity is a random uncorrelated series, but that the reverberation has a fixed periodicity. Hence the autocorrelation of seismic data is the same as the autocorrelation of the reverberation waveform. From the autocorrelation of the reverberation waveform, a prediction operator can be computed. This operator with prediction distance d will closely predict the reverberation component of the waveform. Therefore, by subtracting the delayed predicted waveform from the received waveform, we can eliminate the reverberation component. However, the above two processes are limited in practical use unless the following conditions are met (Yilmaz, 1988):-

(1) The earth is made up of horizontal layers of constant velocity.

(2) The source generates a compressional plane wave that impinges on layer boundaries at normal incidence. Under such circumstances, no shear waves are generated.

(3) The source waveform does not change as it travels in the subsurface.

(4) The noise component is zero.

(5) Reflectivity is a random process.

(6) The seismic wavelet is minimum phase. Therefore, it has a minimum phase inverse.

The seismic data recorded in our experiment tend to be minimum phase. Additionally, the offset is relatively small. Therefore, we apply a predictive deconvolution filter to the data from shot 6 as an example to show how the predictive deconvolution filter affects the data. When the maximum operator length L, which is sum of a prediction lag and length of operator, is 150 ms and a prediction lag d is 4 ms (sampling interval), the seismic wavelets are compressed, which is usually called spiking deconvolution. Meanwhile, the amplitudes of high reverberation are also suppressed. When d=8 or 16 ms, the filtering does not make additional improvement. When d=24 ms, the filter best attenuates reverberations. With a further increase of the prediction lag d, the vertical resolution is decreased. When d > 60 ms, the filtered data seem untouched. Next, we use a fixed prediction lag d=24 ms, and change the L as 100, 125, 150, 175, 200 ms. The results show that shorter length of L such as 100 and 125 ms introduce "ringing" into the data, and the high reverberations are not adequately suppressed. When the L is too long (> 250 ms), there is no additional improvement. Fig. 4.4.1 (a) and (b) illustrate the original 6 vertical components and deconvolved components respectively. The maximum operator length is chosen to be 150 ms, and the prediction lag 24 ms. We can see that the high amplitudes at early part of the traces are suppressed in addition to the compressed wavelets. However, whether the filtering degrades the useful signal is unknown because the reflections are not clear on the section. In practice, we should test the autocorrelation of each component to choose appropriate parameters. The deconvolution filtering for the vertical and horizontal components should be applied separately.

4.5 Signal enhancement polarisation filtering (SEPF)

4.5.1 Introduction to the SEPF filter

As stated in Section 4.2 and 4.3, a frequency filter can be used to suppress the noise outside the required frequency band. Deconvolution can be

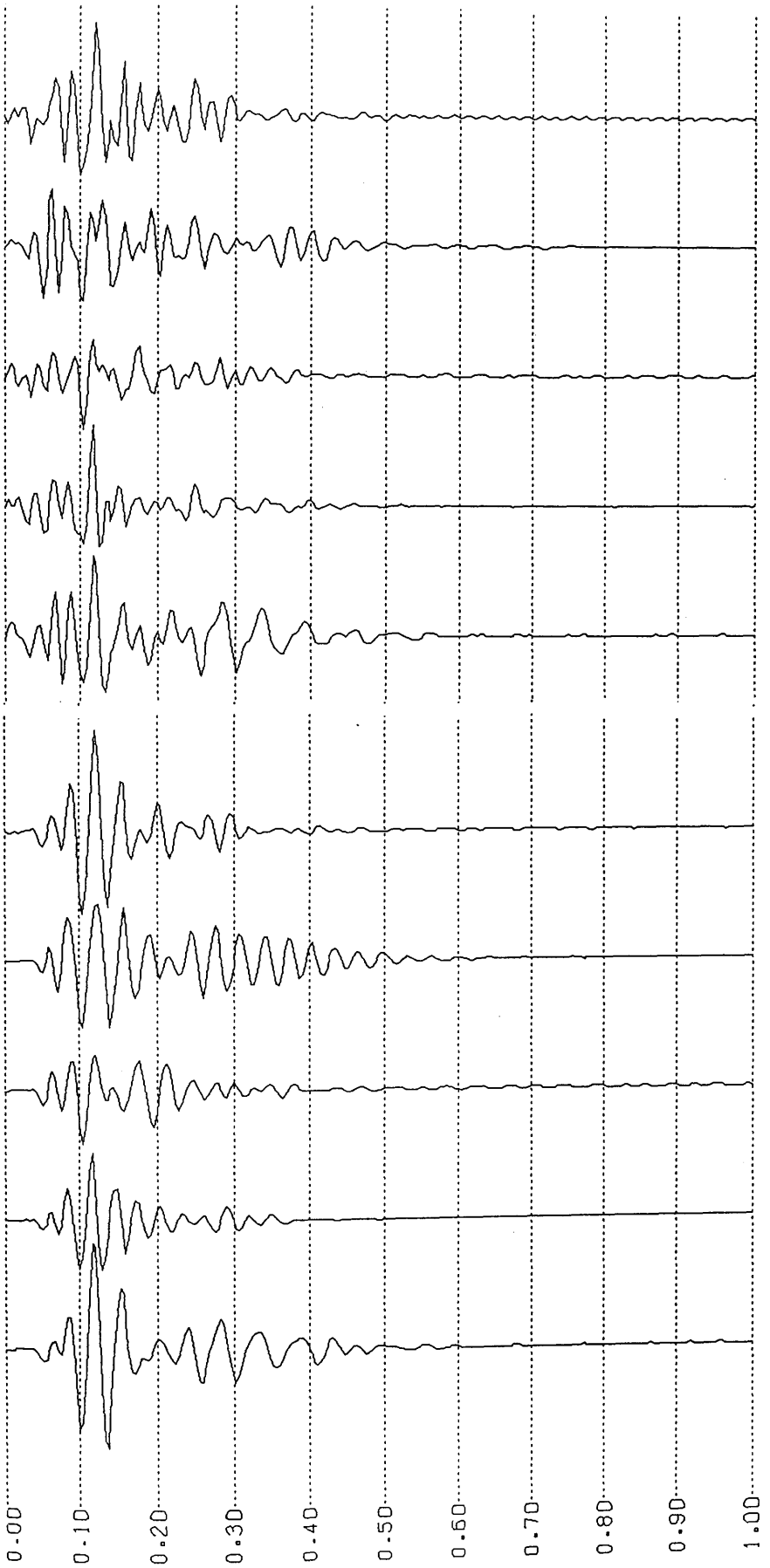

Fig. 4.4.1 Five vertical seismograms (1-5) from stations 15, 21, 28, 34 and 40 at shot 6, and the deconvolved seismograms (6-10). Prediction lag d=24 ms. The maximum operator length L=150 ms.

used to compress a seismic wavelet and also to attenuate multiples. However, its usage is limited by several assumptions, and in practice, field seismic data do not always meet the requirements. Therefore, a predictive deconvolution filter has to be used with great care, otherwise, filtering will have a deleterious effect on data. Velocity filtering has been successfully used to discriminate between primary reflection and multiple reflection or ground-roll. As a result, the low velocity component can be excluded by applying a velocity filter. However, velocity filtering requires the data to be recorded from an appropriate number of stations with different offsets from a shot point. This is because multiples and primaries have no significant moveout difference at near offsets. Regarding the 3-component seismic data recorded in our experiment, it is impossible to apply the velocity filter to such near offset data. In order to suppress the noise which exhibits similar spectral characteristics and similar velocity band to primary reflections, other processing techniques have to be developed. In this section, a signal enhancement polarisation filter is designed and implemented for that purpose.

Signal enhancement polarisation filtering is based on the multiple component recordings of ground motions. The theory is that both compressional and shear waves (body waves) exhibit a high degree of linear polarisation. Noise may also be polarised, but the direction of polarisation is random in nature. Furthermore, surface waves consist of mutually interfering propagation modes arriving from different directions which are also poorly polarised. Three-component recording of ground motions makes it possible to represent the direction of polarisation by the amplitudes of 3 components - vertical, radial and transverse- over a specified time window $N\Delta t$, (where N is number of samples and Δt is the sampling interval). Hence by using various characteristics of polarised particle trajectories, a polarisation filter can be designed to preserve or enhance the data when they are linearly polarised, and to attenuate the data when they are randomly polarised [Kanasewich, 1975].

4.5.2 Design of the SEPF filter

In order to measure the rectilinearity and directionality of particle motions, we construct a covariance matrix of N points taken from each of the 3 components of ground motions and then compute the largest eigenvalue, the second largest eigenvalue and the eigenvector corresponding to the largest eigenvalue of the matrix.

The construction of a covariance matrix follows the same procedures as stated in Chapter 3. We firstly define the mean values of N observations of the random variables x and y,

$$m_x = \frac{1}{N} \sum_{i=1}^{N} x_i$$

$$m_y = \frac{1}{N} \sum_{i=1}^{N} y_i$$

The covariance between N observations of two variables x and y is given by

$$cov(x, y) = \frac{1}{N} \sum_{i=1}^{N} (x_i - m_x)(y_i - m_y)$$

The autocovariance between N observations of the same variable is defined as

$$var(x) = cov(x, x) = \frac{1}{N} \sum_{i=1}^{N} (x_i - m_x)^2$$

The three variables x, y and z correspond to the amplitudes of the radial, transverse and vertical components respectively. From the autocovariance and covariance of above variables, we can construct a covariance matrix V given by

$$V = \frac{1}{N} \begin{bmatrix} var(x) & cov(x, y) & cov(x, z) \\ cov(y, x) & var(y) & cov(y, z) \\ cov(z, x) & cov(z, y) & var(z) \end{bmatrix}$$

If the time window $N\Delta t$ and the amplitudes of 3 traces are given, the covariance matrix V can be found. Thereafter, the rectilinearity of the particle motion trajectory over the specified time window can be estimated from the ratio of principal axes of this matrix, and the direction of polarisation

can be measured by considering the eigenvector of the largest principal axis.

Suppose λ_1 is the largest eigenvalue and λ_2 is the second largest eigenvalue, then a function F is defined by

$$F(\lambda_1, \lambda_2) = 1 - \left(\frac{\lambda_2}{\lambda_1}\right)^n$$

where n is an experimental value. This function would be close to unity when rectilinearity is high ($\lambda_1 >> \lambda_2$) and close to zero when rectilinearity is low (λ_1 and λ_2 approach one another in magnitudes). The rectilinearity function for the time t_0 is given by

$$RL(t_0) = [F(\lambda_1, \lambda_2)]^j$$

where j is an experimental value. If we present the eigenvalue of the principal axis with respect to the radial, transverse and vertical coordinate system by $E=(e_x, e_y, e_z)$, then the direction functions for the time t_0 are represented by

$$D_x(t_0) = (e_x)^k$$
$$D_y(t_0) = (e_y)^k$$
$$D_z(t_0) = (e_z)^k$$

where k is an experimental value. The eigenvector is normalized $|E|=1$, so $0<D_i<1$ (i=x, y, z).

To illustrate rectilinearity, Fig. 4.5.1 shows some computations for sets of data in two dimensions. The data in Fig. 4.5.1 (a) comprise artificial 3-component random noise generated by the ISAN package with a mean of 0 and a root mean square variance of 1000. Forty samples from the radial and transverse components are plotted. We can see that the trajectories of particle motions are random, in other words, the particle motions are poorly polarised. Fig. 4.5.1 (b) shows the polarisation diagram of field 3-component data, the trajectories of particle motions are well polarised. We use the program MASEPF

(refer to Section 4.5.3) to construct a covariance matrix and to compute the largest eigenvalue and the second largest eigenvalue for both noise and field data. As a result, the computation for the random noise gives the largest eigenvalue of 1098211, the second largest eigenvalue of 906572.8 and the rectilinearity function value RL of 0.1745004, the computation for the field data gives the largest eigenvalue of 1148760.4, the second largest eigenvalue of 920788.2 and the rectilinearity function value of 0.9198450. Therefore, the rectilinearity function does tell us about the degree of polarisation of particle motions.

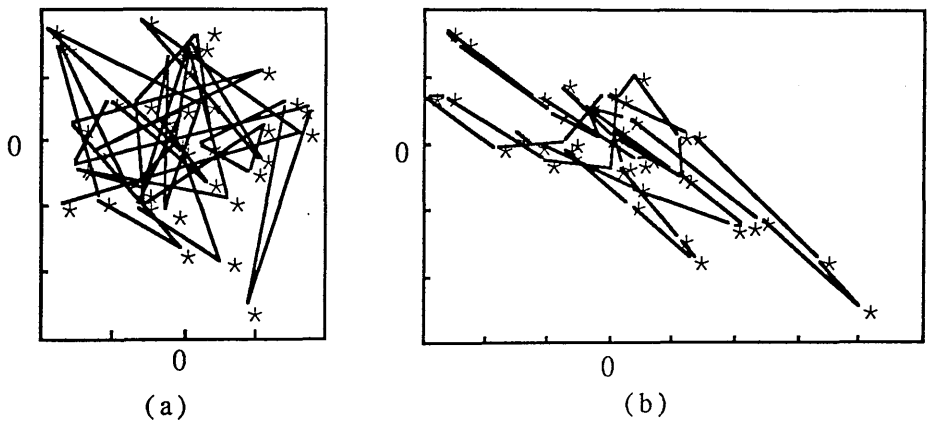

Fig. 4.5.1 (a) Polarisation diagram of random noise RL=0.1745.
(b) Polarisation diagram of field data RL=0.9198.

To subdue the contributions due to any anomalous spike, the rectilinearity and directionality functions are both averaged over a window equal to about half the original window length. If this time window consists of M points (M=N/2), the smooth rectilinearity and directionality functions are given by

$$RL^{*}(t) = \frac{1}{M} \sum_{\tau=-L}^{+L} RL(t+\tau)$$

$$D_i^{*}(t) = \frac{1}{M} \sum_{\tau=-L}^{+L} D_i(t+\tau) \qquad i = x, y, z$$

where L, t, and τ are in ms, but in a program they are sample numbers L=(M-1)/2. Finally we have the filter operators as follows:-

$$F_x = RL^*(t) \cdot D_x^*(t)$$
$$F_y = RL^*(t) \cdot D_y^*(t)$$
$$F_z = RL^*(t) \cdot D_z^*(t)$$

The filtered three seismograms are obtained by multiplying the filter operators by the original seismograms, so we get

$$N_x = x(t) \cdot F_x(t)$$
$$N_y = y(t) \cdot F_y(t)$$
$$N_z = z(t) \cdot F_z(t)$$

4.5.3 Fortran-77 program MASEPF

A Fortran-77 program called MASEPF was written by the author. As shown in Fig. 4.5.2 below, the program reads 3-component seismic data into arrays XX(I), YY(I) and ZZ(I), computes the covariance and autocovariance for various variables over a specified time window, and constructs a covariance matrix V. The largest eigenvalue and a corresponding normalized eigenvector are computed by calling the subroutine EIGEN1 which uses a Power method [Churchhouse, 1981]. The Power method is actually an iterative method in which an arbitrary first approximation to the eigenvector corresponding to the dominant eigenvalue is successively improved until some required precision is reached. The second largest eigenvalue of the matrix is obtained using the same Power method applied to a new matrix B(2, 2) which is constructed from the original matrix, its dominant eigenvalue and the corresponding eigenvector in such a way that it essentially contains only the remaining unknown eigenvalues of the original matrix. A system dependent program (see Appendices; Fortran-77 program 8) was also written by the

author which is run on the VAX/VMS operating system. Here a NAG routine F02ABF is used to calculate the largest eigenvalue, the second largest eigenvalue and the corresponding eigenvectors.

Having found the eigenvalues and the eigenvectors of the matrix V, the program then constructs the rectilinearity and directionality functions for the specified time window. The time window now moves one sample down for the next window until the last sample is reached. However, for the first (N-1)/2 samples and last (N-1)/2 samples, (where N is the number of samples within the window), there are no computed rectilinearity and directionality values, thus the values are taken as the same as those at (N-1)/2 point, and NSAMPL-(N-1)/2 point (NSAMPL is the total number of samples in one trace). The filter operators are obtained by multiplying the rectilinearity functions by the directionality functions. After finishing one station, the program turns to the next station and repeats the computation until the last station has been finished. The final filtered data are obtained by multiplying the original data by the filter operators and are written into a new file. Meanwhile, the operator functions can also be written into a file at the user's request.

To run the program, we have to answer several questions at the beginning (The $ is the command level prompt):-

```
$  INPUT FILE NAME FOR FILTERING
   DATA
$  INPUT NUMBER OF STATIONS
   12
$  INPUT NUMBER OF SAMPLES IN ONE TRACE
   501
$  INPUT FILE NAME FOR OUTPUT
   OUT
$  START READING DATA INTO ARRAY
$  INPUT TIME WINDOW FOR FILTERING(NO. OF SAMPLES)
   21
$  INPUT STATION NUMBER TO START (INPUT 0 TO STOP)
   1
$  INPUT STATION NUMBER TO START (INPUT 0 TO STOP)
```

```
    0
$   START WRITING FILTERED DATA INTO A FILE
$   DO YOU WANT TO KEEP OPERATOR FUNCTIONS(Y/N)
    Y
$   INPUT FILE NAME FOR OPERATOR FUNCTIONS
    OPER
$   START WRITING OPERATOR FUNCTIONS INTO A FILE
$   FORTRAN STOP
```

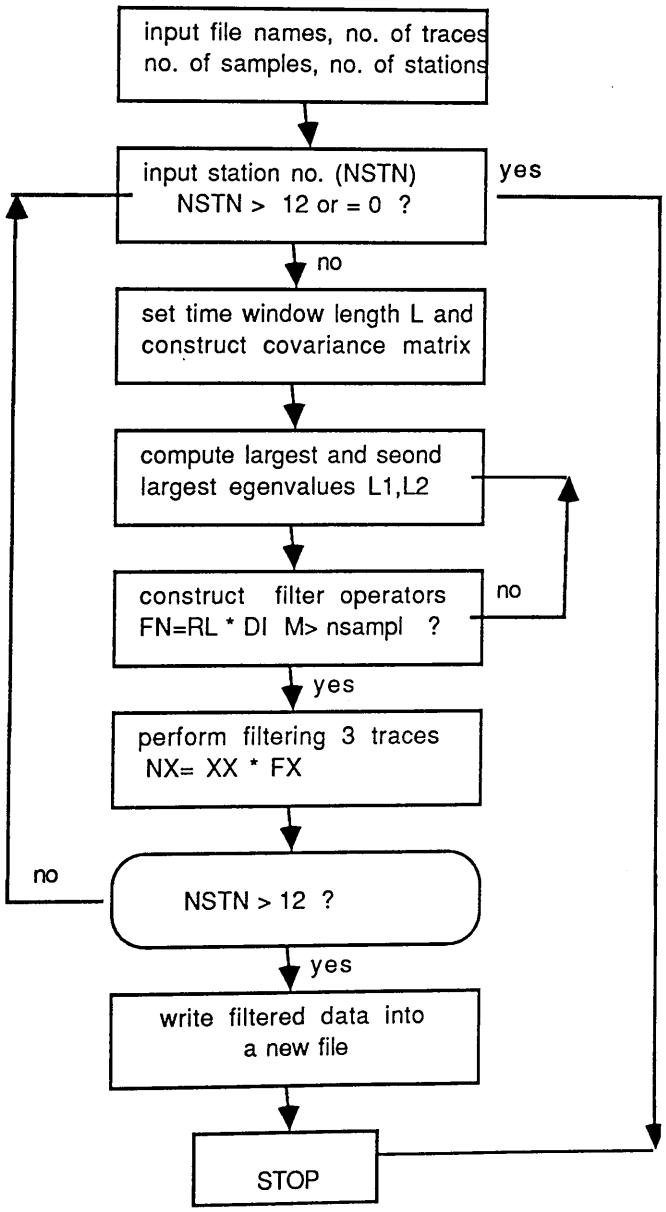

Fig. 4.5.2 Flow Diagram of Fortran-77 program MASEPF.

4.5.4 Program test using noise and field 3-component seismic data

The program test here is based on random noise and field 3-component data. The extensive and sophisticated test on synthetic 3-component data will be discussed in Chapter 5.

The polarisation of noise is random in nature, thus the polarisation filter should suppress it. We firstly generate Gaussian noise by the ISAN package with a mean of 0 and a root mean square variance of 50. The three noise traces are not identical (channels 1-3 in Fig. 4.5.3 (a)). They are then processed by the program MASEPF with a time window of 84 ms (21 samples). We can see from operator functions that the gain values are never higher than 1.00, 80% of them are in the region of 0.10-0.40, which means that the filter does attenuate noise with a degree of nearly 70%. By plotting the filtered traces (channels 4-6) beside the original traces, it confirms that the original unpolarised data have been attenuated from beginning to end.

Secondly, we select 3-component field data to test the filter. The 3-component traces are taken from station 2 at shot 2 which have been edited, bandpass frequency filtered and coordinate system transformed (channels 1-3 in Fig. 4.5.3 (b)). The polarisation filter is now applied to these data and the filtered data are plotted in Fig. 4.5.3 (b) (channels 4-6). To make a comparison, three random noise traces are added into the field data to produce noise-enhanced data which are shown in Fig. 4.5.3 (c) (channels 1-3). After the noise-enhanced field data are filtered by the MASEPF, we can see that the noise, especially in the later part of the traces, has been attenuated significantly, thus the signal to noise ratio has been increased. Furthermore, by comparing the filtered field data with the filtered noise-enhanced field data, we can see that they are still comparable. Therefore the filtered traces have been essentially freed from random noise.

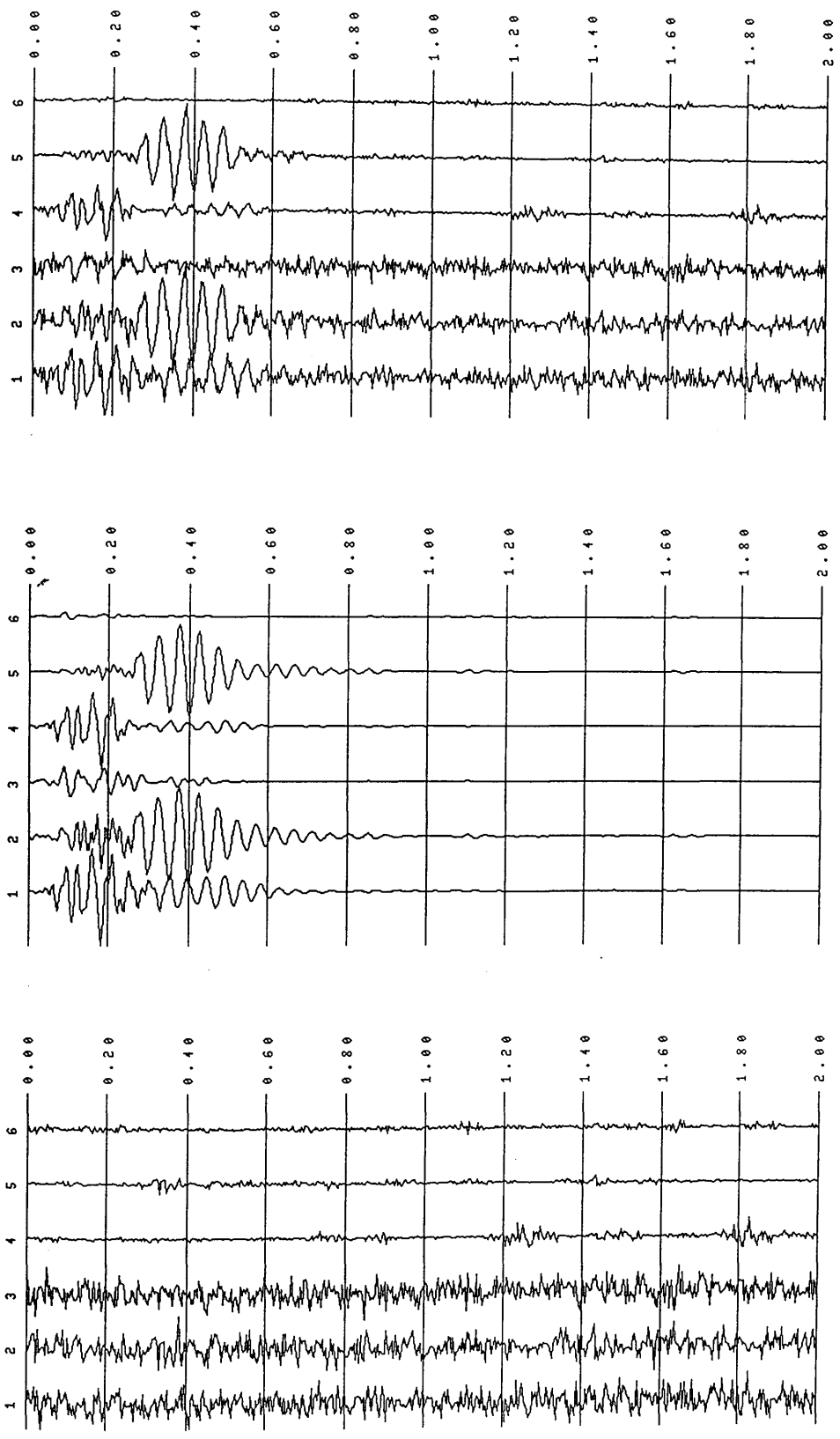

Fig. 4.5.3 (a) Random noise (1-3) and the polarisation filtered traces (4-6). (b) The field 3-components (1-3) from station 2 at shot 2 and the polarisation filtered traces (4-6). (c) Noise-enhanced field data (1-3) and the polarisation filtered noise enhanced data (4-6).

4.5.5 Selection of an appropriate window length for filtering

Selection of an appropriate time window length for the polarisation filter is of equivalent importance to the selection of the operator length and a prediction lag for the predictive deconvolution filter. Improper choice of the time window length can also lead to two extremes - the data are either untouched or the useful signals are degraded after filtering. The general phenomena concerning the window length are as follows: the narrower the time window is, the less the filter will affect the data, thus the use of a very short time window length will not properly perform the function of attenuating random noise. In contrast, the wider the time window is, the greater will be the suppression of arbitrarily polarised noise, but the risk in choosing a wider time window is that it might also suppress useful signals. Trial and error procedures are used to establish a reasonable compromise for the window length such that random noise is attenuated but the useful signals are still kept and not degraded.

We use noise-mixed synthetic 3-component data to test the effect of different time window lengths on the filtered data. The data (channels 1-3 in Fig. 4.5.4) are generated by a modelling package ANISEIS (refer to Section 5.3.1) for an isotropic medium. An explosive source is used. We can see that there are 2 clear reflection events at 0.67 s and 1.50 s on the vertical component and a P-converted S event at 0.93 s on the radial component. The polarisation filter is applied to these 3-components with the varied time window length (12, 36, 60, 84, 124, 180, 244, 324, 404 ms), and the original and the filtered seismograms are plotted together with the same scale in Fig. 4.5.4. This figure indicates that when the time window length L is very small, say 12 ms, the filter does not change the data much; more noise is still contained in the data (see channels 4-6). When L=60 ms, the filtered data give the highest signal to noise ratio. With a further increase of the window length, more and more noise is attenuated, but reflection signals are also degraded. When L=404 ms, the reflection event at 1.5 s is invisible (channels 28-30). In conclusion, the window length of 60-124 ms is appropriate for filtering such data.

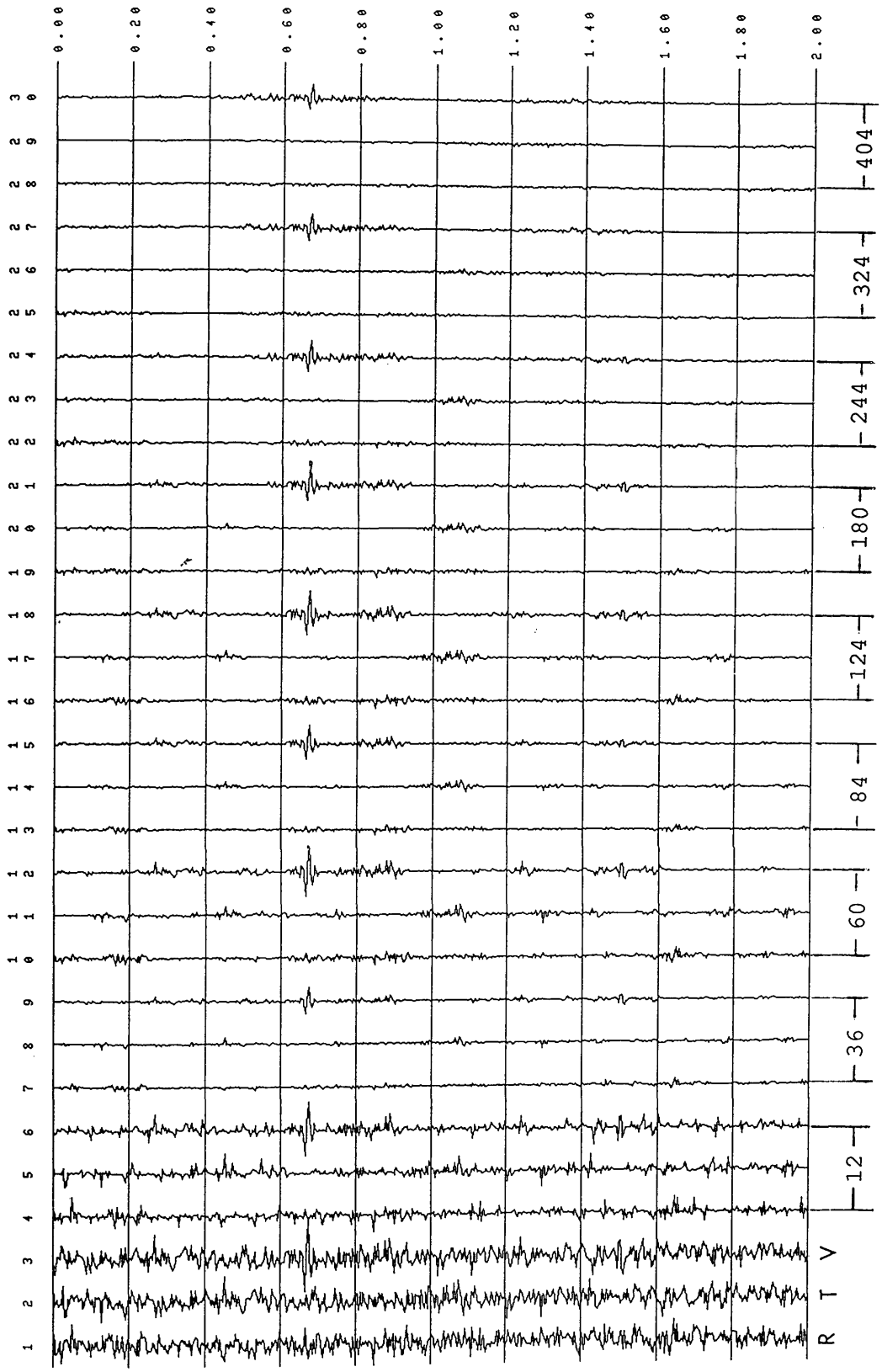

Fig. 4.5.4 Illustration of the effect of different time window length on polarisation filtering. Traces 1-3 are noise mixed synthetic data. Rest are the filtered noise-mixed data with varied window length. They are (from left to right) 12, 36, 60, 84, 124, 180, 244, 324, and 404 ms.

4.5.6 Application of the SEPF filter to the data from the basalt-covered area

The signal enhancement polarisation filter is used here to attenuate surface waves and random noise contained in the data. The time window length is set to 68 ms (17 samples). Ten shot data including the test shot are all processed by the SEPF filter. To illustrate how the filter works on field data, we select 4 vertical traces from the outer stations (3, 5, 7, 9) at shot 5 as an example. Fig. 4.5.5 (a) shows the unfiltered vertical traces. They exhibit not only large amplitudes but complexity in wavelets. Fig. 4.5.5 (b) shows the same data as the above after the application of the polarisation filter. The plotting scale for the filtered data is smaller than for the unfiltered data. We can see that the amplitudes of the filtered data are smaller than the unfiltered data at the same time, i.e., the strong reverberations have been attenuated. Furthermore, the wavelets of filtered data become simple and clear, which indicates that random noise has also been attenuated.

Fig. 4.5.6 (a) shows the processed and scaled radial components. All radial components from the inner circles are plotted on the left-hand side of the figure (channels 1-60), those from the outer circles are plotted on the right-hand side of the figure (channels 61-120). Fig. 4.5.6 (b) and (c) show the processed and scaled transverse and vertical components respectively. We can see from 3 figures that random noise has been attenuated significantly, the processed sections are clearer than the unprocessed sections (refer to Fig. 3.4.4). A line of reflection events at about 420 ms on the vertical section (channels 61-120) are more conspicuous, so are the reflection events on the radial section (channels 61-120). Why the reflections are not in phase may be because of velocity complexity, low-frequency geophones, inaccurate static corrections and most importantly dipping reflectors (refer to Section 6.3 which states that a dipping layer at a great depth will introduce enormous time delays among 12 vertical traces). As stated in Section 3.4, appearance of reflection events on the radial section at the same time as on the vertical section indicates that they are actually P-waves which are projected on the radial components. The reflection event is not a single wavelet but a train of

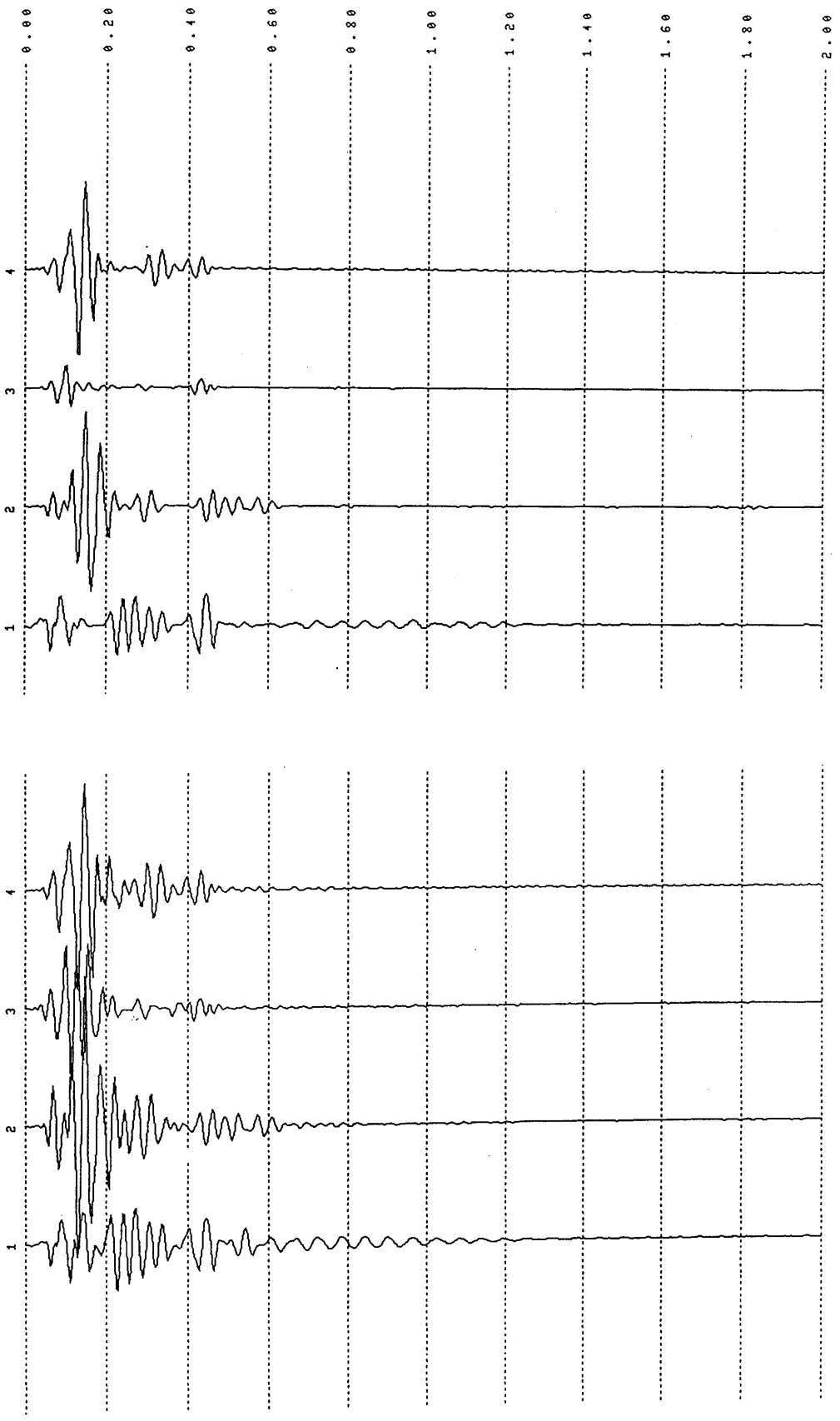

Fig. 4.5.5 (a) The frequency filtered vertical traces from station 3, 5, 7, 9 at shot 5. (b) The same data as in (a) after application of a polarisation filter.

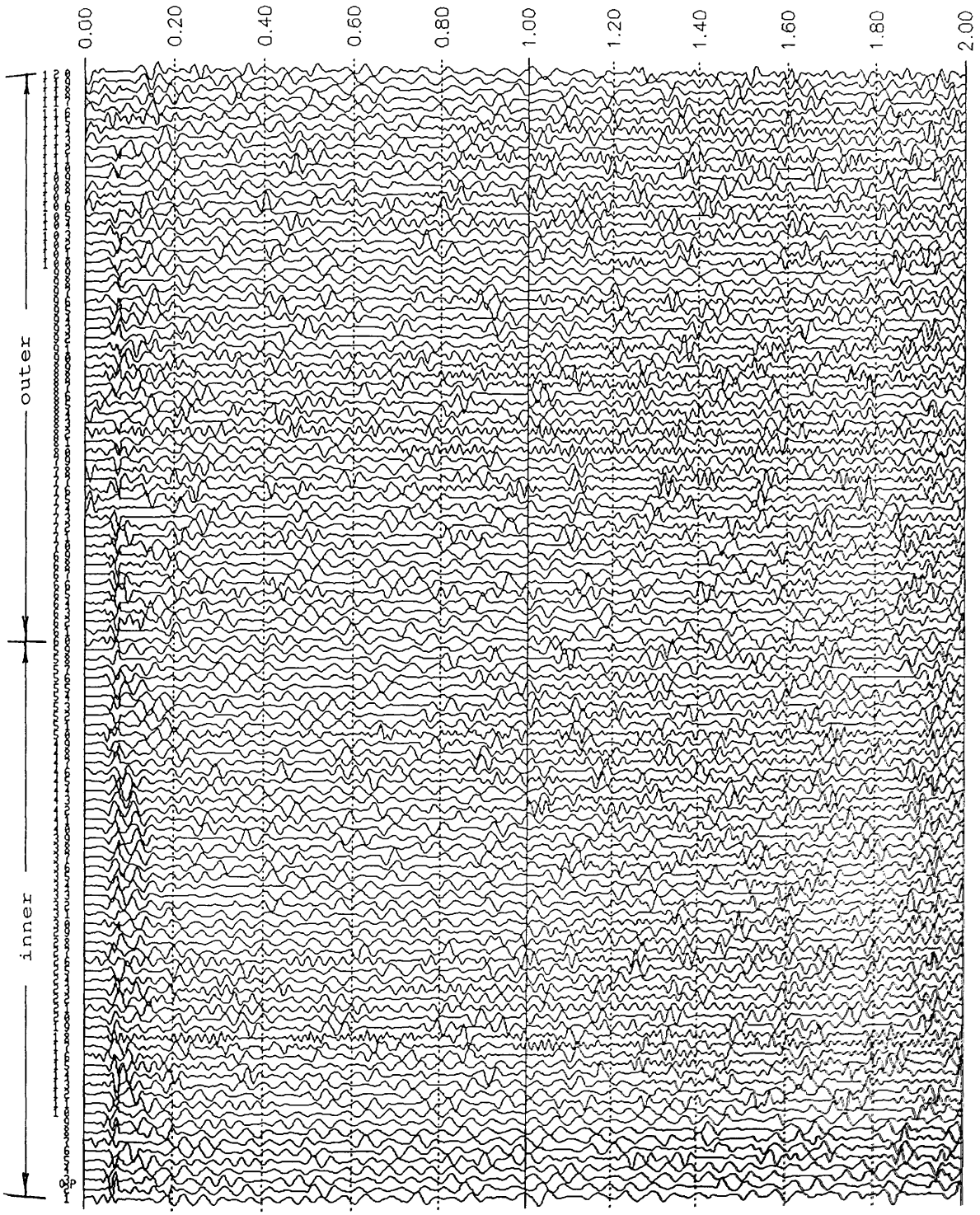

Fig. 4.5.6 (a) The polarisation filtered radial components from 10 shots. Those from the inner circles are plotted on channels 1-60. Those from the outer circles are on channels 61-120. The test shot is also included (1-6, 61-66).

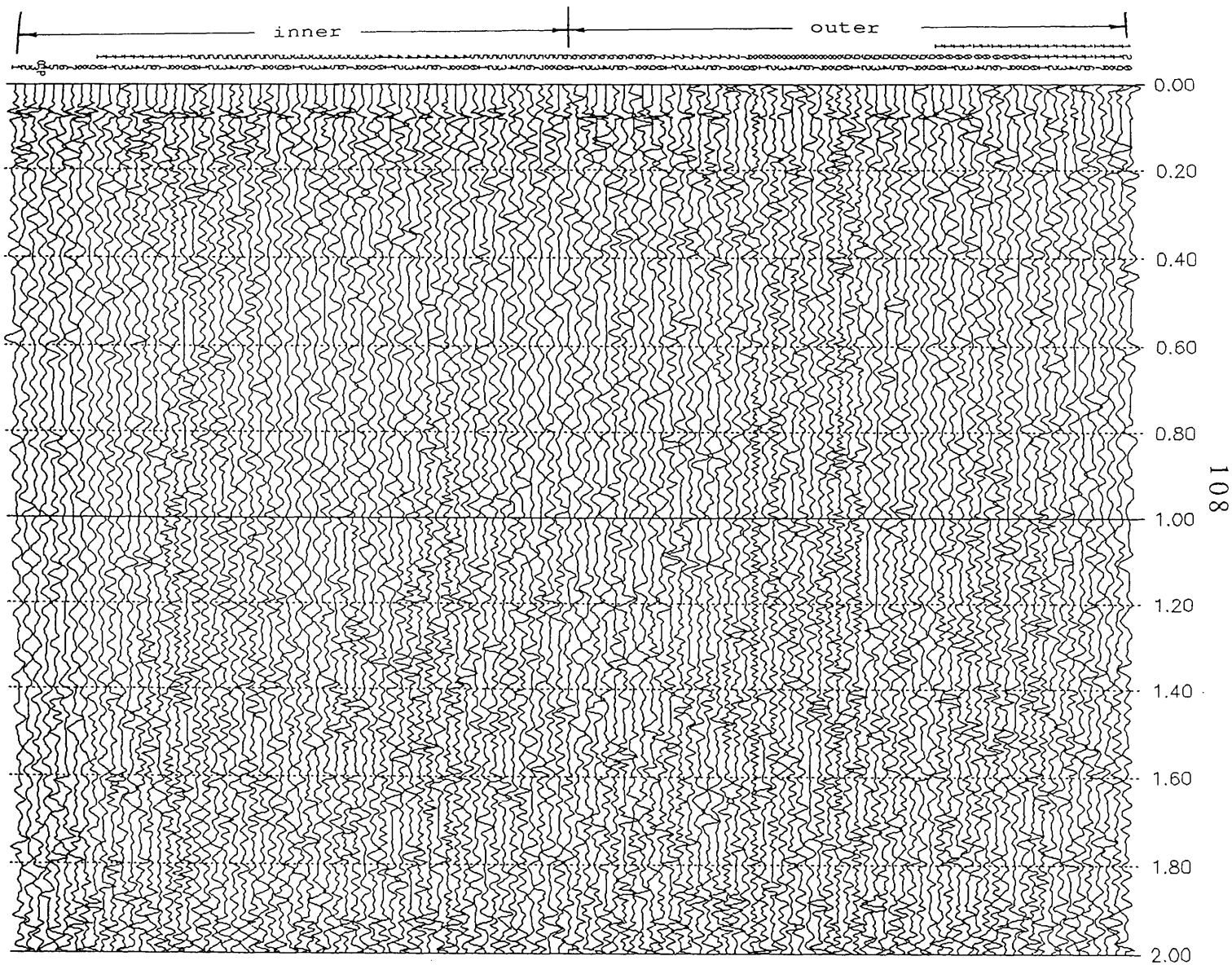

Fig. 4.5.6 (b) The polarisation filtered transverse components from 10 shots. Those from the inner circles are plotted on channels 1-60. Those from the outer circles are on channels 61-120. The test shot is also included (1-6, 61-66).

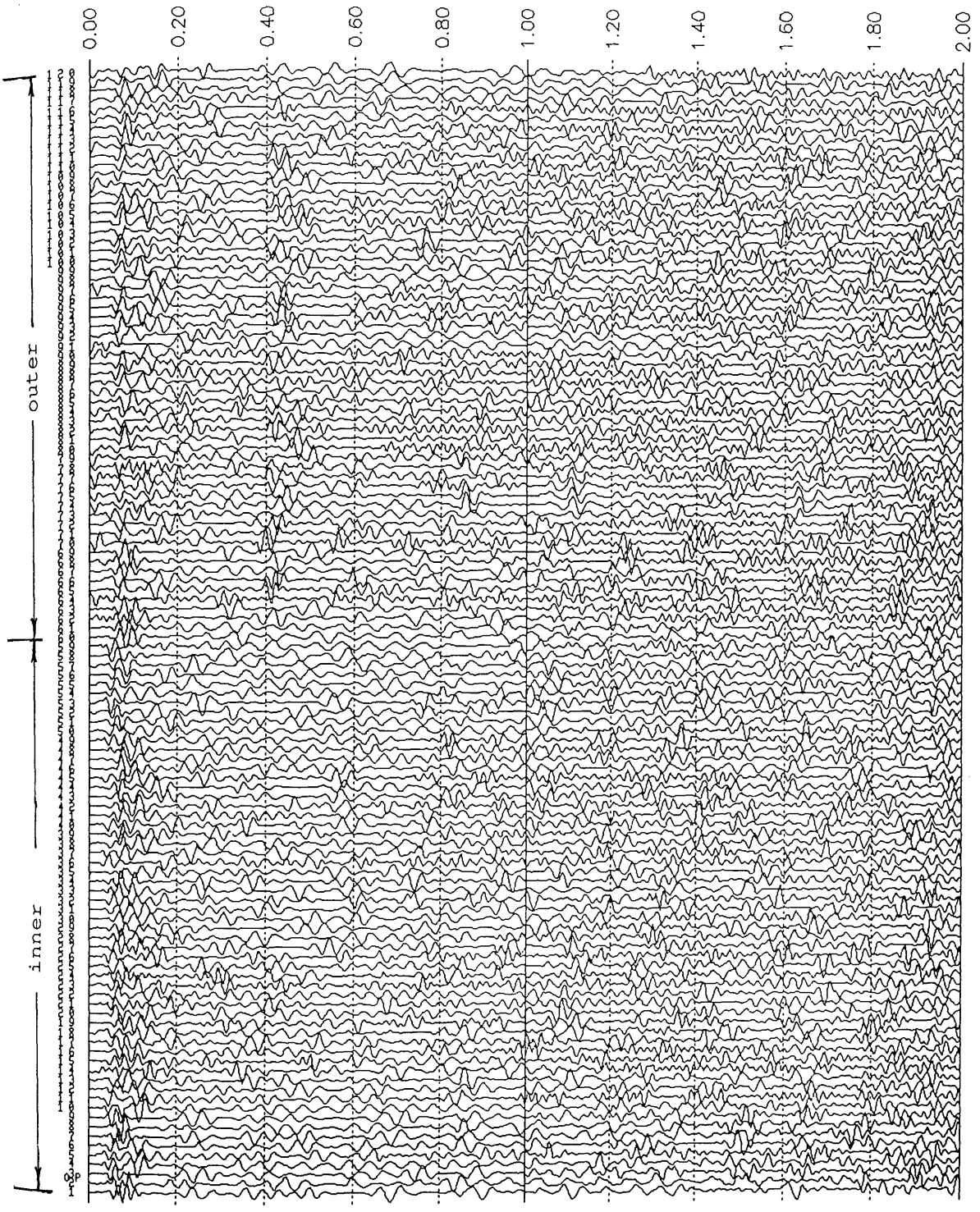

Fig. 4.5.6 (c) The polarisation filtered vertical components from 10 shots. Those from the inner circles are plotted on channels 1-60. Those from the outer circles are on channels 61-120. The test shot is also included (1-6, 61-66).

wavelets, its shape and phase vary from station to station. The transverse section shows little of interest.

4.6 Other data processing

In addition to the techniques stated in the above sections, other methods were also developed and programmed. One of them is to use only two components (R and V) to identify the P-waves by constructing the cross-product of two components over a time window. The theory is that, for a P-wave, the horizontal and vertical components would be exactly in phase if the earth were a uniform half-space, the cross-product will have a big value which gives a measure of the rectilinearity and the total signal power. For S-waves and random noise, the signs of two components are irregular, so the cross-product will be near to zero or have a small value [Shimshoni, 1964]. The filtered seismograms are obtained by multiplying the original seismograms by the cross-product functions. This method however is not implemented here.

After the various of filtering, the 12 vertical components from a single shot are supposed to be stacked together so as to obtain a signal-to-noise ratio improvement of 3.5. The result of summation is not shown here because the number of shots is not adequate enough to draw any conclusions on geological structure. To obtain the structure information, many more shots would be required. Nevertheless, this small-scale shooting is only an experiment mostly for developing new techniques. The large-scale field work can be conducted in the future.

4.7 Interpretation

The most interesting parameters to be obtained from a seismic survey in this area are velocities of formations and the depth of the base of the Clyde Plateau Lavas (CPL). The present techniques based on this areal 'RAZOR' array however cannot derive the interval velocity although it may be possible to do so in the future with the development of this experiment. From the velocity survey conducted by Hall [1974] in the adjacent area, the interval velocity of

the CPL was given as 4420 m/s. We identify a line of events at 420 ms in Fig. 4.5.6 (c) as the primary reflections from the base of the CPL based on the higher frequency of the wavelets compared with those upper and below the wavelets of interest, together with the inverse polarities of wavelets related to the reflections from the top of the CPL (nearly at the surface). This may also indicate an inverse velocity contrast between the CPL and the Old Red Sandstone.

From the two-way travel time 420 ms, we can calculate the depth (or thickness in this case) of the CPL H_{CPL}=928 m below the surface, which is near to 915 m (depth) from the contour map of the base of the CPL and to 900 m (thickness) from the isopach map of the CPL provided by Hall [1974].

4.8 Summary

A bandpass frequency filter is tested and reveals that it can reject part of the low frequency reverberations (<20 Hz) and high frequency noise. For most of high reverberations within the bandwidth, the filter does little to improve the data. Predictive deconvolution filtering test shows that it is very good at compressing the wavelets and attenuating the amplitude of reverberations. Since both multiples and reflections are not clear on the section, the predictive deconvolution filter has to be used with great care, otherwise, it degrades the useful signals. The newly developed polarisation filter can be used to remove the random noise and part of the surface waves arriving from different directions. This filter can also be used to process conventional CDP data, if they are multi-components.

From the interval velocity and the two way travel time, the base of the CPL is found to be at about 928 m below the surface.

Chapter 5 Further Testing of the Polarisation Filter and Optimisation of Array Designing Using Synthetic 3-component Seismic Data

5.1 Introduction

The signal enhancement polarisation filter (SEPF) has been developed and simply tested using the field data as described in chapter 4. To test the filter more thoroughly, there is a need for good quality seismic data in an area with simple geology. In this chapter, we generate synthetic 3-component seismic data in isotropic and anisotropic media by two modelling packages. Random noise has been added to the synthetic data and the noise-mixed data are then filtered by the SEPF filter. We will see how the signal to noise ratio is increased after filtering and stacking.

5.2 Filter testing using the data in an isotropic medium

5.2.1 Introduction to the modelling package "SEIS83"

The program SEIS83 was designed by Vlastislav Cerveny and Ivan Psencik in Charles University, Czechoslovakia for the computation of rays of seismic waves which arrive at a system of receivers distributed regularly or irregularly along the earth's surface. The generation of waves is semi-automatic. At receivers, corresponding travel times are automatically determined. Optionally, amplitudes and phase shifts may be evaluated (effects of slight absorption may also be considered). All these quantities are stored and may be optionally plotted or used for the computation of synthetic seismograms.

The model is 2D, with laterally inhomogenous, curved interfaces.

Interfaces are specified by points read from the input data. They are approximated by cubic spine interpolation. Thus models with vanishing layers, block structures, fractures, isolated bodies may be handled by the program. Within individual layers, the velocity may vary both vertically and horizontally. The source may be situated at any point in the medium. The radiation pattern of the source may be specified independently for P and S waves either from tables or analytically.

All the direct and primary reflected waves P and S, including the converted waves PS and SP at the point of reflection, can be generated automatically. Multiple reflections are optionally generated manually. Refracted waves are considered as special cases of reflected waves with compound ray elements.

The determination of rays which arrive at specified receiver positions along the earth's surface is performed by the modified shooting method. For iterations to the receiver considered, the method of halving of intervals, (REGULA FALSI), or the combination of these methods may be used. The iteration to a receiver continues unless a ray within a distance "REPS" of the receiver is found. The arrival time at the receiver is then obtained by a linear interpolation from arrival times of the ray closest to the ray situated to both sides from the receiver. The amplitude corresponding to the ray closest to receiver is attributed to the receiver.

Two programs called MAVHPL and MAPLOT (see Appendices; Fortran-77 programs 9 and 4) were written by the author to compute and plot synthetic seismograms. The program MAVHPL generates a file which may contain either the vertical displacement component or horizontal displacement component as required.

5.2.2 *Geological model in an isotropic medium*

As one of the initial objectives of this experiment is to investigate new methods of seismic reflection exploration, we firstly construct a model as shown in Fig. 5.2.1. The medium is homogeneously isotropic, the third

interface dips towards East with an angle of 14.5°. The P velocity, S velocity and density of individual layers are given in Table 5.2.1 below.

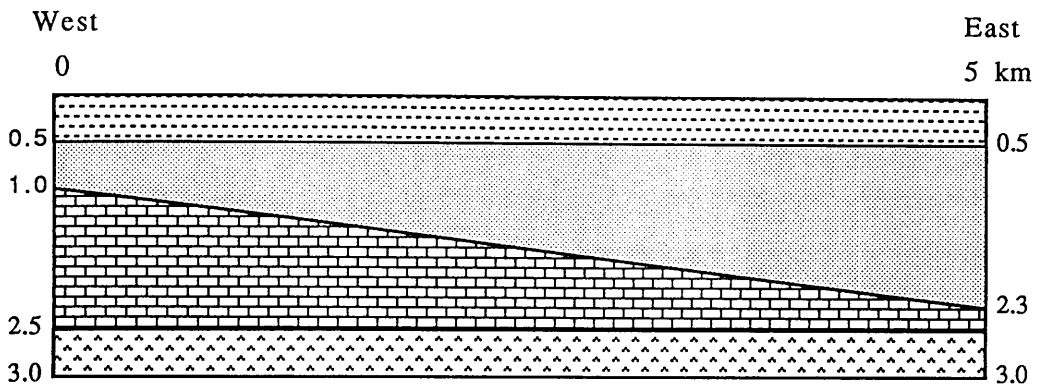

Fig. 5.2.1 Geological model of an isotropic medium.

Layer No.	Thickness (km)	P-velocity (km/s)	S-velocity (km/s)	Density (g/cm^3)
1	0.50	2.00	1.12	2.10
2	0.5 0	2.50	1.40	2.20
3	1.50	3.50	1.97	2.40
4	half space	5.50	3.09	2.80

Table 5.2.1 The parameters of a model in an isotropic medium.

5.2.3 Generating and filtering "one shot - one receiver" data along a profile line

In order to show what the synthetic seismograms from the SEIS83 look like and to test whether the polarisation filter works, we generate synthetic seismograms based on a 2D model. After preparing the input data file which contains parameters needed for constructing the model, we then run the main program SEIS83. The first output file from this program shows how the program works and gives several results, e.g. geometry of interfaces, digitized

velocities, elementary modes, travel times and phases. The second output file from this program, which corresponds to either the vertical component or horizontal component, gives wave modes, travel times, amplitudes, phase shifts, initial angles and so on. This data file is an input file for the program MAVHPL, which generates synthetic seismograms. One shot produces two seismograms (vertical and horizontal) from one station with an offset of 75 m from the shot point. The shot spacing is 75 m. Data for 20 shots along the profile line eastwards have been generated corresponding to a distance of 1.5 km at the surface. The main parameters for a synthetic seismogram are as follows:-

Seismic source type:	explosive source
Frequency of source signal:	35 Hz
Length of recording:	4 s
Sampling interval:	4 ms

Due to the explosive source used in generating synthetic seismograms, there are P-waves, S-waves and P-S converted waves on the vertical and radial components. Let us take the data from shot 1 as an example to inspect the characteristics of the data. As shown on the left-hand sides of Fig. 5.2.2 (a) and Fig. 5.2.2 (b), we can see that there are three P-reflections at 0.50 s, 1.07 s and 1.81 s on the vertical component (channel 1 in Fig. 5.2.2.(a)), and three S-reflections at 0.89 s, 1.91 s and 3.22 s, and three P-S converted waves at 0.70 s, 1.49 s and 2.52 s on the radial component (channel 1 in Fig. 5.2.2.(b)). Meanwhile, the signals on both components are projected on each other but with relatively small amplitudes. Looking at the 20 horizontal and 20 vertical seismograms together, we see clear images of 3 layers in the time and distance domain, with the middle one dipping towards East.

To apply the polarisation filter to the data, there have to be 3-component seismograms at one station which are received at three different orientations. The present package however can generate only one of the horizontal components. To satisfy the conditions, the transverse component is constructed by filling pure random noise.

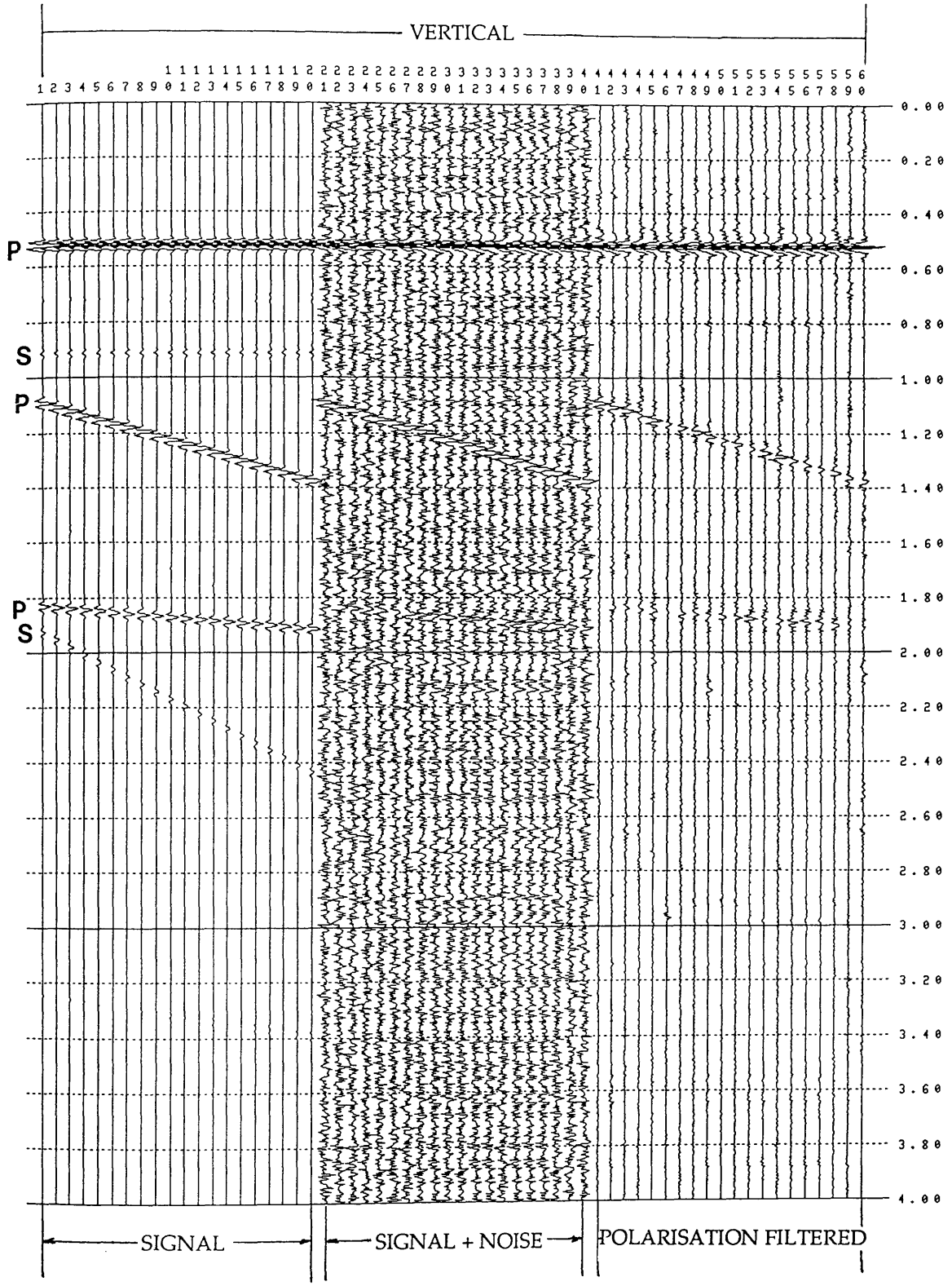

Fig. 5.2.2 (a) The original (channels 1-20), noise-mixed (channels 21-40) and polarisation filtered (channels 41-60) seismograms for the vertical components. The synthetic seismograms are for the model (2D) in an isotropic medium.

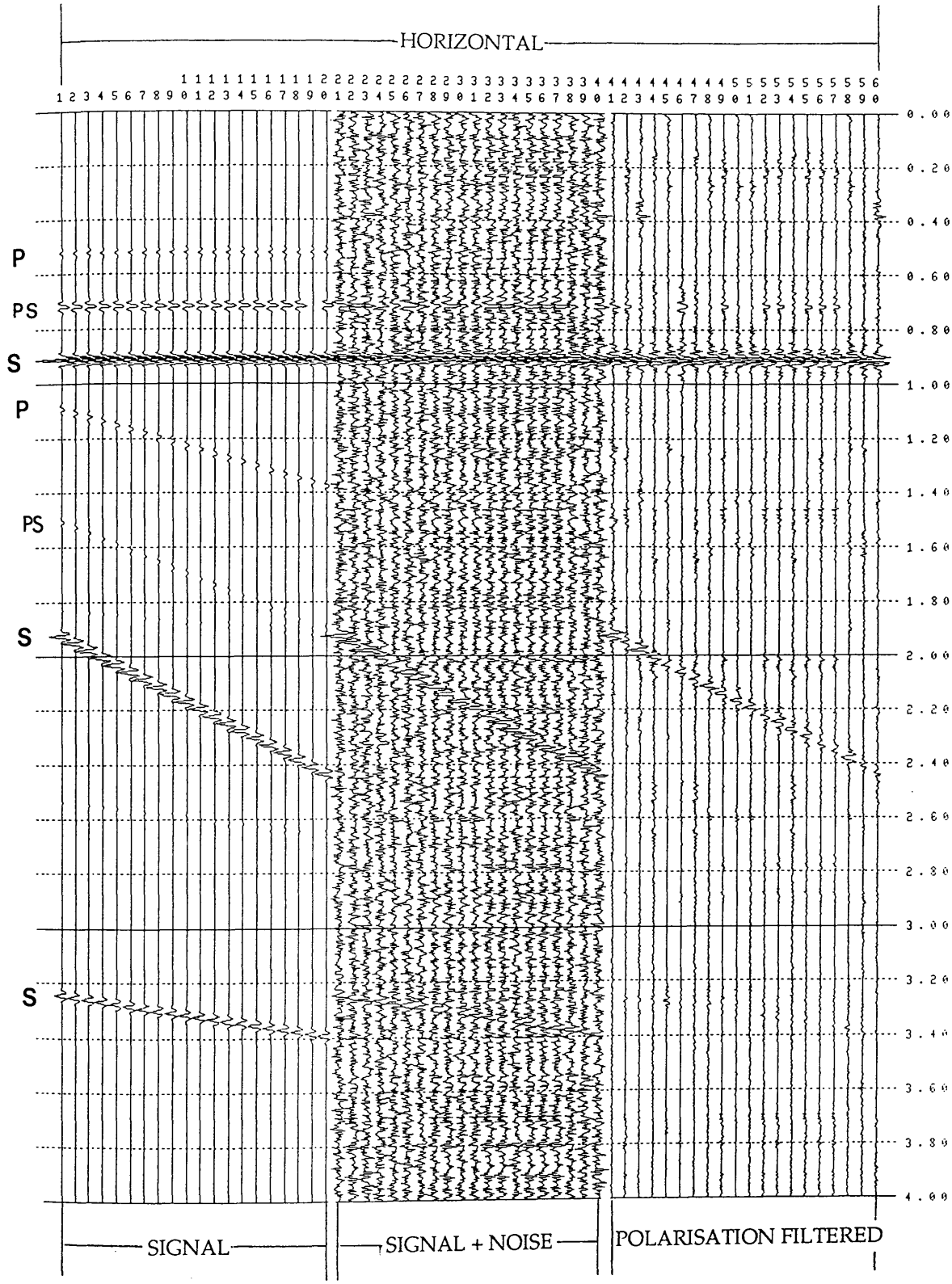

Fig. 5.2.2 (b) The original (channels 1-20), noise-mixed (channels 21-40) and polarisation filtered (channels 41-60) seismograms for the horizontal components. The synthetic seismograms are for the model (2D) in an isotropic medium.

Pure random noise with a mean of 0 and a root mean square variance of 120, generated by the package ISAN, is added to the vertical and radial components, producing noise-mixed data. We can see from the middle panels of Fig. 5.2.2 (a) and Fig. 5.2.2 (b) (channels 21-40) that the signal to noise ratio has been decreased considerably.

The SEPF filter is applied to the 3-component data, the time window for filtering is set to 23 samples (92 ms). The filtered seismograms are plotted on the right-hand sides of Fig. 5.2.2 (a) and Fig. 5.2.2 (b) (channels 41-60). For the horizontal component section, two S-wave and one P-S converted images have been kept, and the P-wave image at 0.50 s has been removed after filtering. However, the S-waves at 3.20-3.40 s are not well separated from noise. It may be because a large scale is used to produce the figure, the S-wave events are then scaled down to an invisible level. Another possibility is that the added noise entirely changes the polarisation direction of particle motions of reflection wavelets, which makes the polarisation filter unable to extract the S-waves (see Section 5.4). For the vertical section, three P wave images have been kept, all the S-wave and P-S converted images are removed because the polarisation directions of these waves are horizontal. By comparing 3 different data - the original, noise-mixed and filtered - in both figures, we can see that the added noise has been attenuated remarkably. The signal, on the other hand, has not been degraded after filtering.

5.2.4 Generating the data based on the areal 'RAZOR' array in an isotropic medium

The areal 'RAZOR' array pattern and its dimensions were described in Chapter 2. For the convenience, the array pattern is shown again in Fig. 5.2.3. We generate synthetic seismograms based on this 3D model to test both the SEPF filter and the optimisation of designing of such an array.

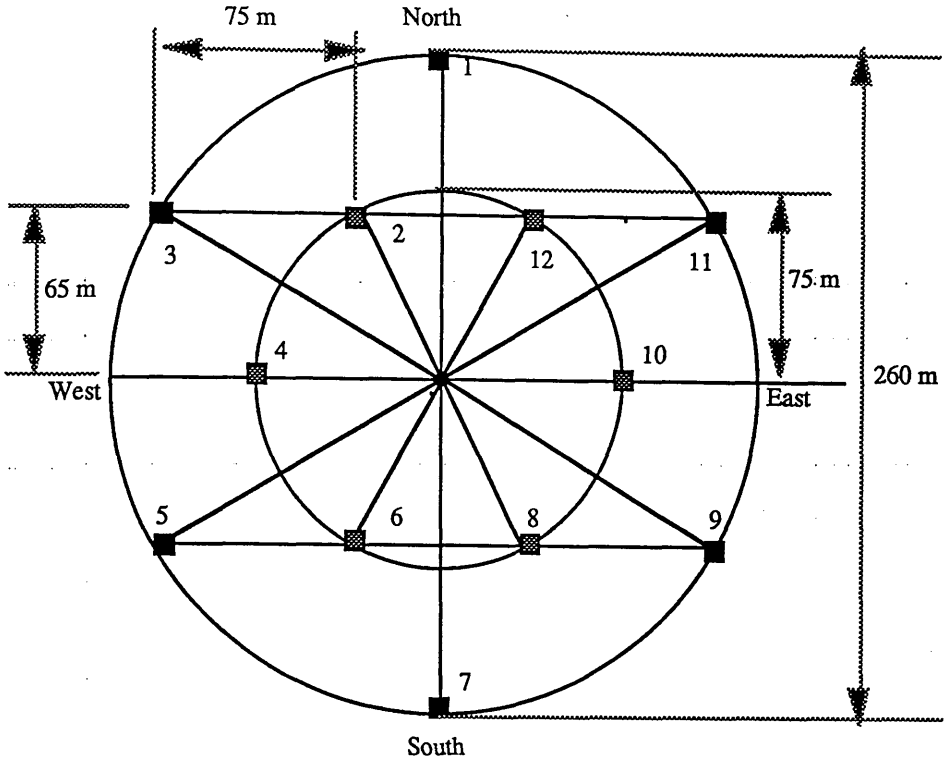

Fig. 5.2.3 Array pattern for generating synthetic seismograms.

The program SEIS83 can only deal with 2D models. If the medium is isotropic and three interfaces are all horizontal, the results calculated by the program SEIS83 would be the same for either the inner or outer stations. However, the dipping layer in the middle medium makes 12 stations receive different responses in terms of travel time and phase shifts. To accommodate this, we decompose one 3D model into six 2D models (or six short profile lines), each line having two stations on both sides of a shot point. The first profile line is set in a north-south direction, the second line is 30^{o} off North (stations 6, 12) clockwise, the third line is 60^{o} off (stations 5, 11), the fourth line is in a west-east direction, and so on. Due to the symmetry of the array, i.e., the lower part of the array is a mirror image of the upper part of the array, we need to calculate for only 4 profile lines. Fig. 5.2.4 shows the geometries of a dipping plane (the second reflector in our 3D model) associated with different profile lines. For profile line 1 in (a), which is in a north-south direction, the vertical

distance of the line to the plane is h_z, the normal distance is h. Thus a new 2D model in (b) is constructed such that the vertical distance to a planar reflector is h. For profile line 4 in (c), which is in a west-east direction, a new 2D model is shown in (d), here ψ is the true dip of the reflector. For profile line 2 and 3 in (e), the geometry of the new models is complicated. The plane OO'N, which is the incident plane of seismic waves, is normal to the dipping plane R, the apparent dip ϕ changes from ψ-0° (ψ is the true dip of the plane R in the 3D model) when the azimuth α of a profile line X changes from 0°-90° (an azimuth of a line is defined as an angle measured clockwise from the west-east line). Hence a new model in (f) for either line 2 or 3 is constructed such that the true dip of a reflector is ϕ and the vertical distance of the line from a shot point at the surface to the reflector is h_x, the normal distance being h. Therefore, by running the program SEIS83 4 times based on different input files, while keeping the source condition untouched, the synthetic data for the 3D model can be generated. Fig. 5.2.5 shows 12 horizontal traces and 12 vertical traces for a shot. We can see a small fluctuation of seismic wavelets between adjacent traces which is introduced by the dipping reflector.

5.2.5 Processing the data based on the areal 'RAZOR' array in the isotropic medium

In this section, we will show how the polarisation filter works on noise-mixed 3-component data based on the areal 'RAZOR' array and how such an array pattern is optimally chosen. At the first stage, we generate the synthetic seismograms in the way described above. The data for 20 shots are generated corresponding to a distance of 1.5 km at the surface. We then add the pure random noise to the data and filter them by the polarisation filter. These original, noise-mixed and filtered data are not presented here, but they look like the data shown in Fig. 5.2.5. At the second stage, we add the filtered seismograms from each shot together so as to increase the signal to noise ratio by 3.5. Specifically, 12 vertical components are stacked together and 12 horizontal components are stacked together for each shot, this stacking will

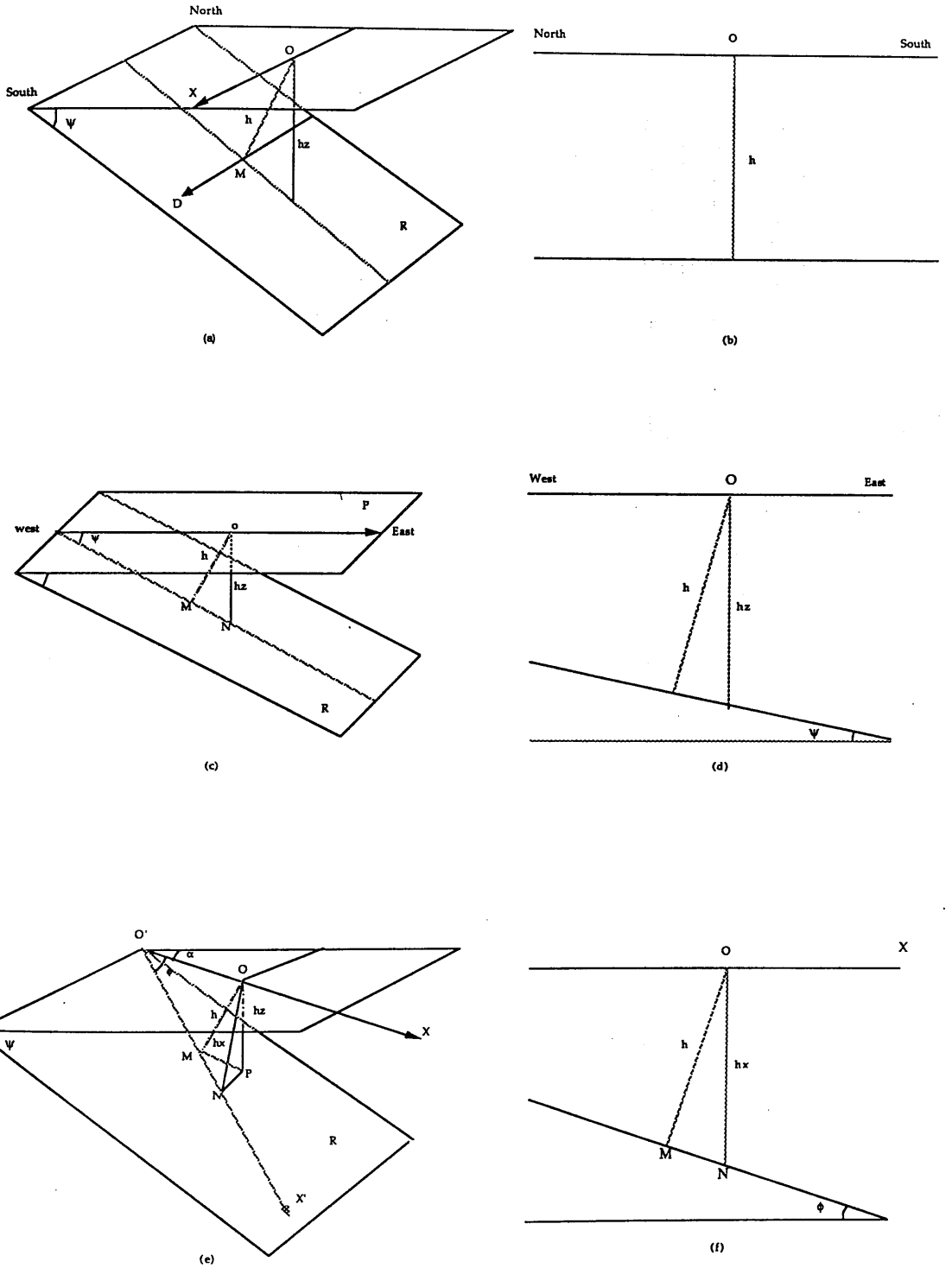

Fig. 5.2.4 The geometries of a dipping reflector related to a line of different azimuths and the new 2D models constructed. (a), (c) and (e) are 3D models, (b), (d) and (f) are new 2D models constructed for the modelling program SEIS83.

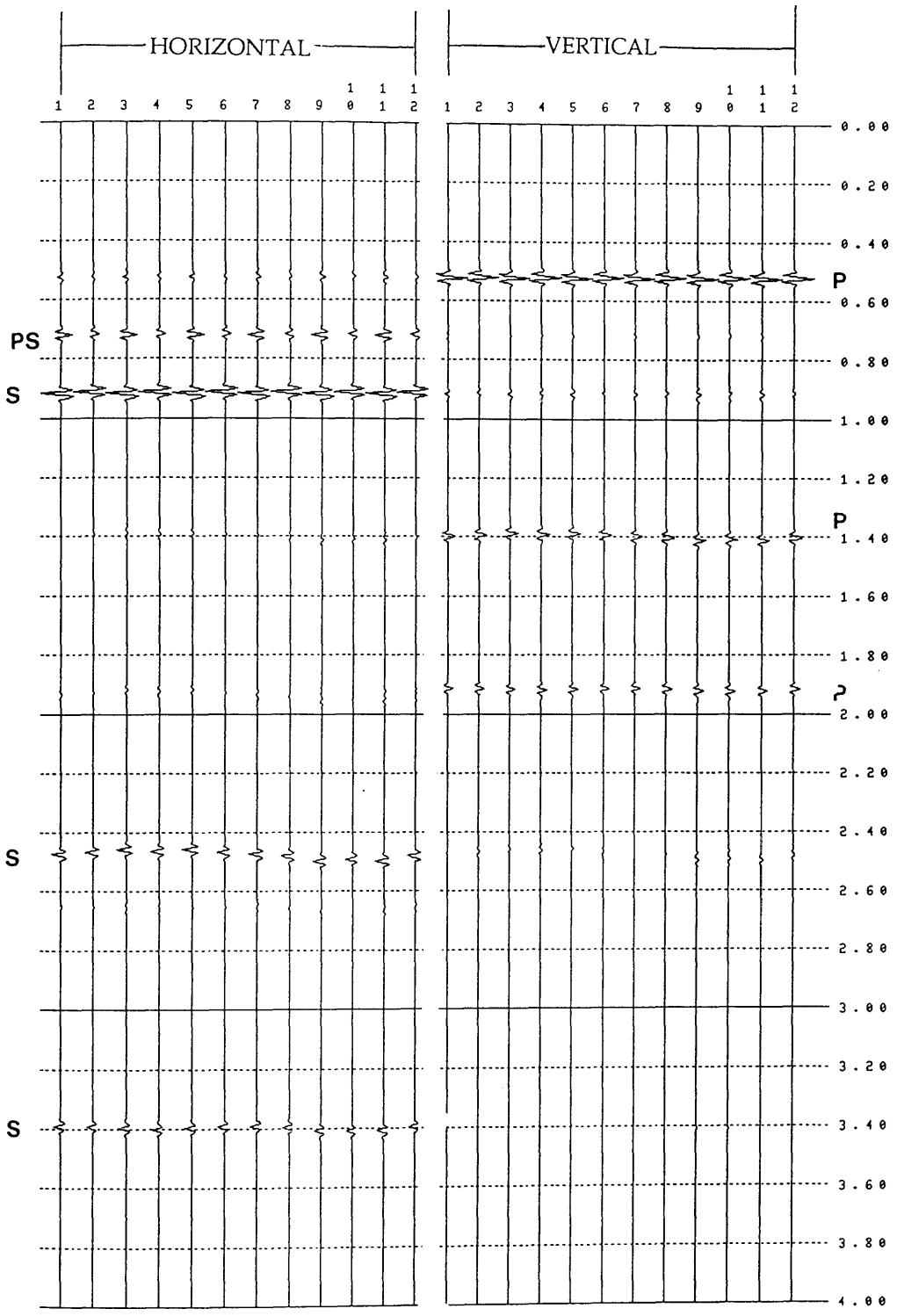

Fig. 5.2.5 The synthetic seismograms based on the array of 3 dimensions. The horizontal components are on the left-hand side. The vertical components are on the right-hand side. The centre of the "RAZOR" array lies at the middle point of the model shown in Fig. 5.2.1, i.e. it is 2.5 km away from west along the profile line. Channel numbers correspond to the station numbers marked in Fig. 5.2.3.

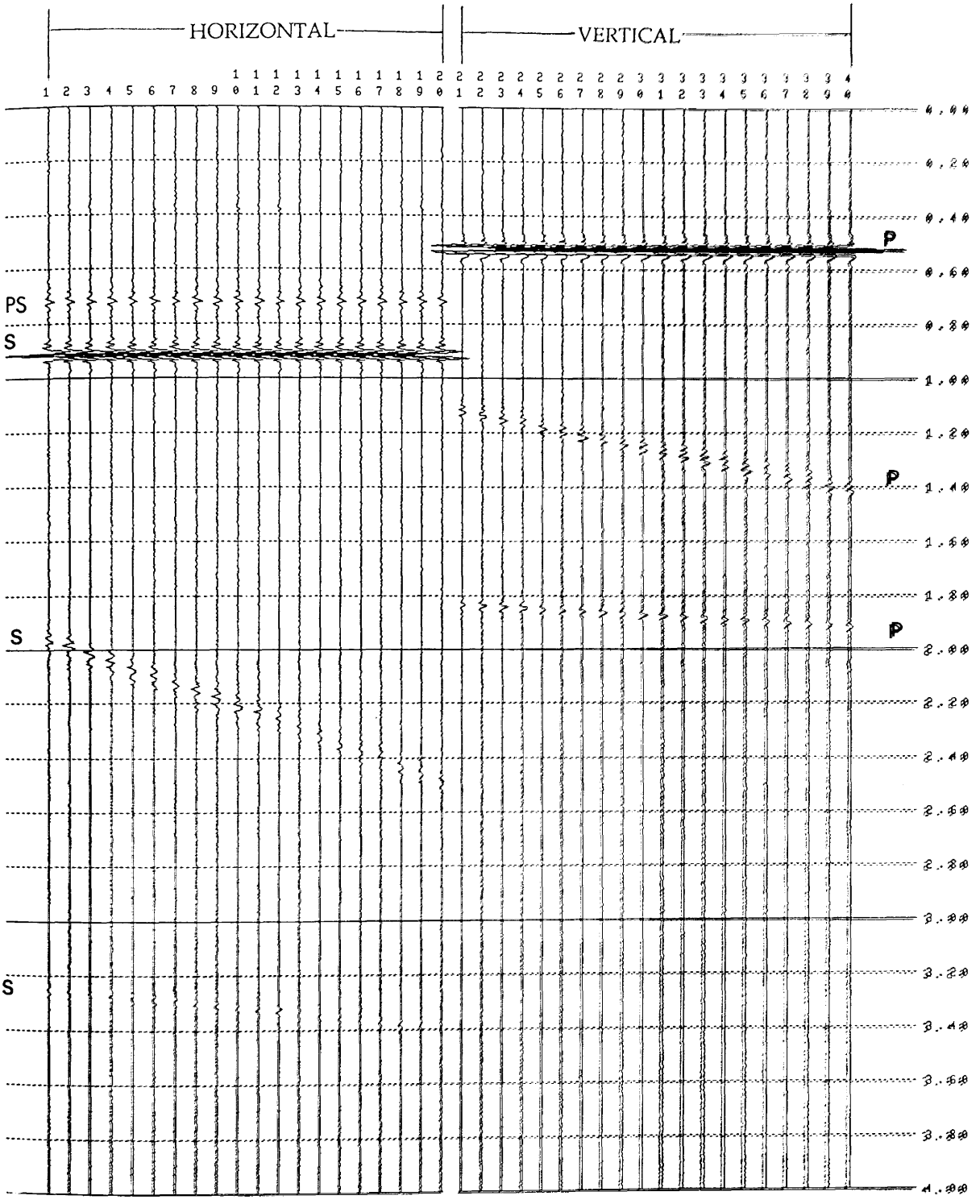

Fig. 5.2.6 The polarisation filtered and stacked seismograms (channels 1-20 for the horizontal components, channels 21-40 for the vertical components).

produce two final composite traces. By carrying out the same process, 20 composite vertical and 20 composite horizontal traces are obtained. They are plotted in Fig. 5.2.6. From this figure, we can see that the residual random noise has been cancelled out after stacking. In contrast, the reflection events from the first horizontal interface are remarkably enhanced; not only because they have large amplitudes but because they are in phase. The later reflections from interfaces 2 and 3 are also revealed and show a better resolution than the section in Fig. 5.2.2.

5.3 Filter testing using the data in an anisotropic medium

5.3.1 Introduction to the modelling package "ANISEIS"

ANISEIS is a flexible computer modelling system for calculating synthetic seismograms from point sources in anisotropic and cracked plane-layers. Vertical seismic profiles, surface to surface reflections, and cross-hole shooting are some of the model geometries that can be accommodated.

The methods used in ANISEIS are based on plane wave analysis and involve use of the reflectivity method or propagator matrix method and accumulation of plane waves along summation paths in both the complex horizontal slowness and complex PHI planes (slowness is the inverse of phase velocity and PHI is an angle in the horizontal plane, measured from the vertical plane which contains the source and geophones). This plane, the (X, Z) plane in a system of right-handed co-ordinates with the Z-axis downwards, will be referred to as the sagittal plane.

The calculation is performed for each of a range of frequencies and the results recorded in the table which the user can update or extend if he wishes to improve the results or add higher frequencies. It is also possible to run frequencies one at a time and to compare results for successive calculations. It is facilities such as this which make interactive use of ANISEIS valuable. While a whole run of 50 to 200 frequencies through a model may be a major computer exercise, the running of one frequency through a simplified but representative model is quickly performed. This feature allows the user to test

the accuracy of sample frequencies before committing himself to a major computer cost. The update facilities allow insufficiently accurate answers to be subsequently replaced without having to re-run other values.

The selection of type of source and a choice of a time window and the number of time sampling points must be made before the displacements at the geophones for the range of frequencies are calculated. The form of the source signal, the shape of a time dependent pulse, can be decided afterwards and synthetic seismograms for a variety of pulse shapes can be generated at normal cost.

5.3.2 Geological model 1 in an anisotropic medium

The synthetic 3-component seismic data from an anisotropic medium are not used to investigate shear wave splitting, but to test the polarisation filter.

Since the modelling package "ANISEIS" cannot deal with a medium with dipping layers, the geological model has to be constructed as one containing horizontal layers with aligned filled cracks within two middle layers (see Fig. 5.3.1). The strike of the aligned cracks is a constant with an angle of 30^{o} from North towards West. The filling of the cracks in the isotropic medium which simulates an anisotropic medium will produce shear wave splitting (one fast S wave, another slow S wave). If the crack parameters in the infinite medium are kept the same, only one shot record is enough to determine the data along the whole profile line. The velocities and densities for this model are given in the table 5.3.1.

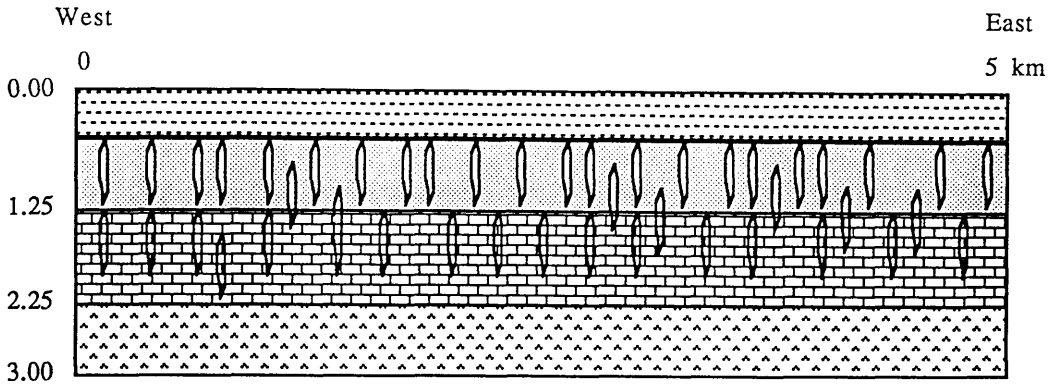

Fig. 5.3.1 The geological model 1 in an anisotropic medium.

No.	Depth (km)	Vp (km/s)	Vs (km/s)	Density (g/cm^3	Thickness (km)	Cracks
1	0.50	1.50	0.84	1.60	0.50	no
2	1.25	1.80	1.00	2.00	0.75	yes
3	2.25	3.00	1.73	2.54	1.00	yes
4	half space	5.55	3.13	2.78	half space	no

Table 5.3.1 The parameters of model 1 in an anisotropic medium.

The parameters of cracks are given as follows:-

Type: Hudson's crack

Fluid: Water

Radius: 0.001 m

ASP Ratio: 0.01

Density: 0.05

Strike: N30°W

Due to the symmetry of the array (see Fig. 5.2.3), there are four stations (1, 7, 3, and 9) which will receive identical signals. Therefore, data for only 4 stations (1, 2, 4 and 5) need to be generated.

5.3.3 Processing the data based on model 1 in the anisotropic medium

To give various types of data, explosive and SH sources are used for model 1. In theory, an explosive source generates strong P-waves on the vertical component, and S-waves and P-converted S waves on the radial component and weak signals on the transverse component. In contrast, an SH source will produce strong S-waves on the transverse component but weak signals on the vertical and radial components. In Fig. 5.3.2, we can see that there are 3 reflection events at 0.66 s, 1.50 s and 2.16 s on the vertical component. Multiples, S-wave and P-S converted waves also appear on the vertical component. The two big events at 0.93 s and 2.14 s on the radial component indicate the P-S converted waves from the first and second interfaces. The appearance of events on the transverse components is due to S wave phase shifting caused by the anisotropic medium. The original data excited by an SH source in Fig. 5.3.3 shows that the transmitted S waves at 2.70 s are a superposition of two pulses which clearly split the arrivals. Both quasi-transverse waves are transmitted strongly except for incident planes of symmetry where the particle motions of transverse wave is pure SH [Keith & Crampin, 1976]. The variation of amplitudes and phase shifts on the horizontal components at different receivers is due to the variation of orientations of different receivers with respect to the crack plane and to the polarisation direction of the SH source.

The data are processed in the same way as described in Section 5.2. Specifically, they are firstly mixed with pure random noise with a mean value of 0 and a root mean square variance of 120. Secondly, the noise mixed data (channels 13-24 in Fig. 5.3.2) are filtered by the SEPF filter, the window length set for the filter is 23 samples (92 ms). Finally, the original, noise-mixed and the filtered seismograms are all plotted together so as to make a clear comparison. From Fig. 5.3.2 (channels 25-36), we see that the random noise mixed in the synthetic seismograms has been attenuated significantly. Meanwhile, the reflection events at 0.60 s and 1.50 s on the vertical component have been extracted. However, the weak arrival at 2.16 s on the vertical

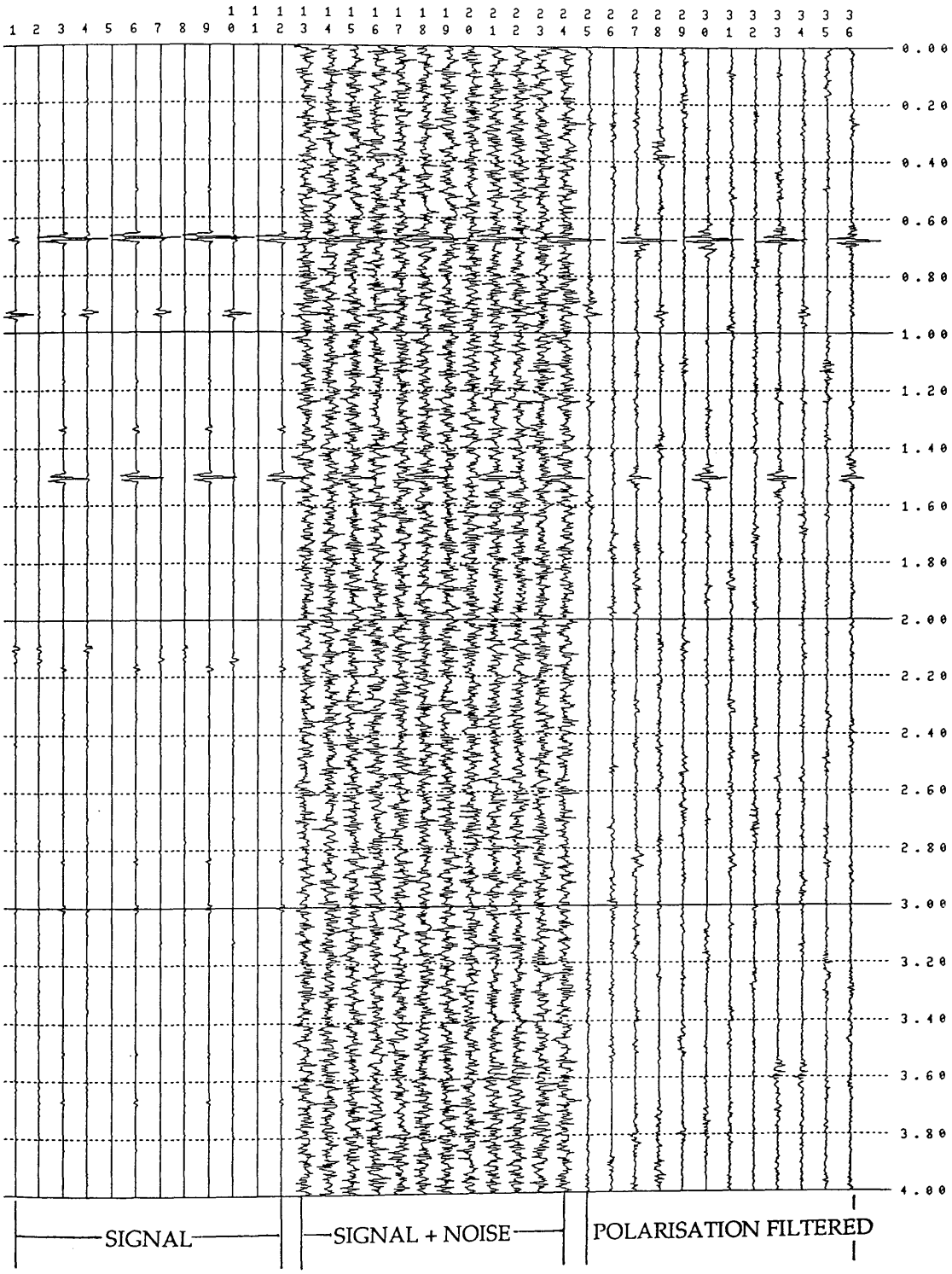

Fig. 5.3.2 The original (channels 1-12), noise-mixed (channels 13-24) and polarisation filtered (channels 25-36) seismograms (explosive source) at 4 stations (1, 2, 4, 5) for model 1 in an anisotropic medium. The order of the traces is the radial, transverse and vertical.

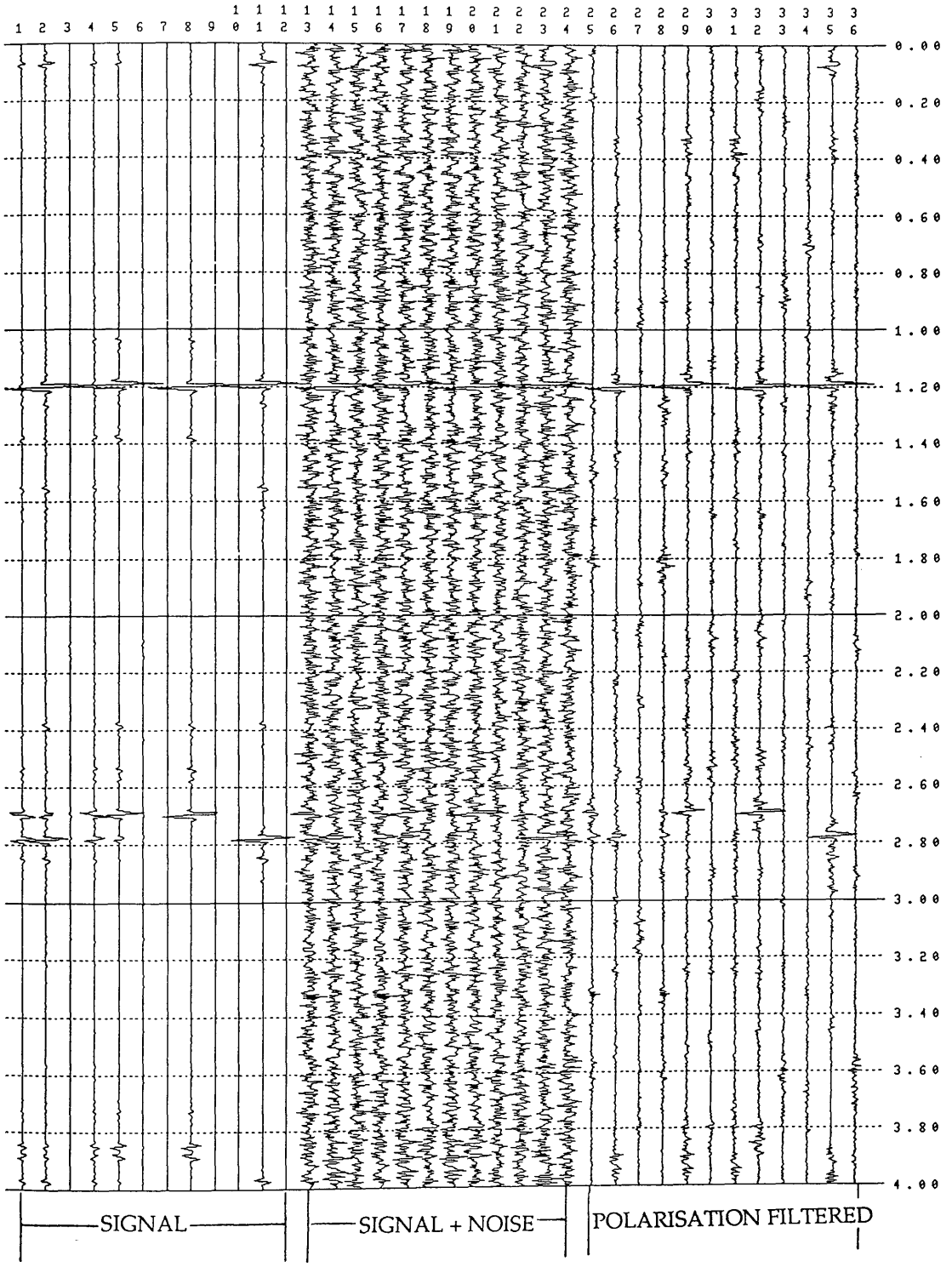

Fig. 5.3.3 The original (channels 1-12), noise-mixed (channels 13-24) and polarisation filtered (channels 25-36) seismograms (SH source) at 4 stations (1, 2, 4, 5) for model 1 in an anisotropic medium. The order of the traces is the radial, transverse and vertical.

component is not clearly shown on the filtered data. This problem is considered in the next section. Fig. 5.3.3 shows the similar data for the SH source. The arrival at 1.19 s for the transverse component corresponds to an SH-SH reflection event propagated through isotropic layer 1, it has been enhanced after filtering. Two arrivals at 2.70 s on the transverse component are the superposed SH and SV waves which have a time delay from one to another. The filtered transverse components exhibit uncommon characteristics varying with stations. For station 1, the first wavelet is removed, the second wavelet is kept (channel 26). For station 3, the first wavelet is kept, the second wavelet is removed (channel 29). We do not know which wavelet is SH or SV, but what we know is that the enhanced wavelet is the one whose polarisation direction is in the transverse direction.

5.3.4 Geological model 2 in an anisotropic medium

In this section, a new geological model is introduced to suit a special case, that is, the second layer is formed by volcanic rocks which have a high velocity of 5.5 km/s. Beneath it is sandstone with a velocity of 3.3 km/s. The characteristics of such seismic data have been described in Section 2.2. The synthetic 3-component seismic data are used here to show whether or not the weak signals beneath hard rocks can be extracted after filtering. Such an exercise is of a great significance in solving many problems in areas covered by volcanic rocks. The velocity and density values for this model in an anisotropic medium are given in Table 5.3.2.

No.	Depth	Vp	Vs	Density	Thickness	Cracks
1	0.50km	2.50 km/s	1.40	1.87	0.50km	no
2	1.25km	5.50	3.13	2.78	0.75	yes
3	2.25km	3.50	1.96	2.54	1.00	yes
4	half space	4.00	2.24	2.60	half space	no

Table 5.3.2 The parameters of model 2 in an anisotropic medium.

5.3.5 Processing the data based on model 2 in the anisotropic medium

Explosive and SH source are used to generate two sets of synthetic data. The data excited by the explosive source (channels 1-12 in Fig. 5.3.4) show a big reflection event at 0.40 s which is the two-way travel time between the surface and first reflector. The second event at 0.50 s is the component of P-S converted wave which has large amplitudes on the radial component. The third event at 0.67 s is the reflection from the second reflector. Event 4 and 5 at 0.80 s and 1.20 s respectively are multiples in the first layer. In addition, there should be another reflection wavelet at 1.24 s from the third reflector. This wavelet is nearly invisible. As predicted, the first reflection and multiples in this model have much larger amplitudes than the later reflection signals, which adds considerable difficulties in processing and interpreting. The data excited by the SH source (channels 1-12 in Fig. 5.3.5) show similar characteristics, that is, the reflections and multiples from the first interface have large amplitudes, the reflections from the third interfaces are invisible.

After the synthetic data are mixed with random noise with a mean of 0 and a root mean square variance of 60, the first and second reflection events are entirely hidden in noise. The polarisation filter is again applied to the noise-mixed data. We can see from Fig. 5.3.4 that the first reflection at 0.40 s and later multiples at 0.80 s and 1.20 s after filtering have been revealed, and the P-S converted waves at 0.55 s and 0.92 s on the vertical component are entirely removed. In addition, the P-waves on the radial component have also been removed. However, the second reflection event at 0.67 s is not very clear although it can still be identified. This problem is investigated in the next section. The filtered data from the SH source in Fig. 5.3.5 show that the weak reflections at 1.19 s from the second interface are revealed.

5.4 Effect of the characteristics of noise on filtering

It is quite understandable that multiples can be preserved after filtering. This is because multiples themselves are also kinds of body waves which are linearly polarised, and they will pass through the polarisation

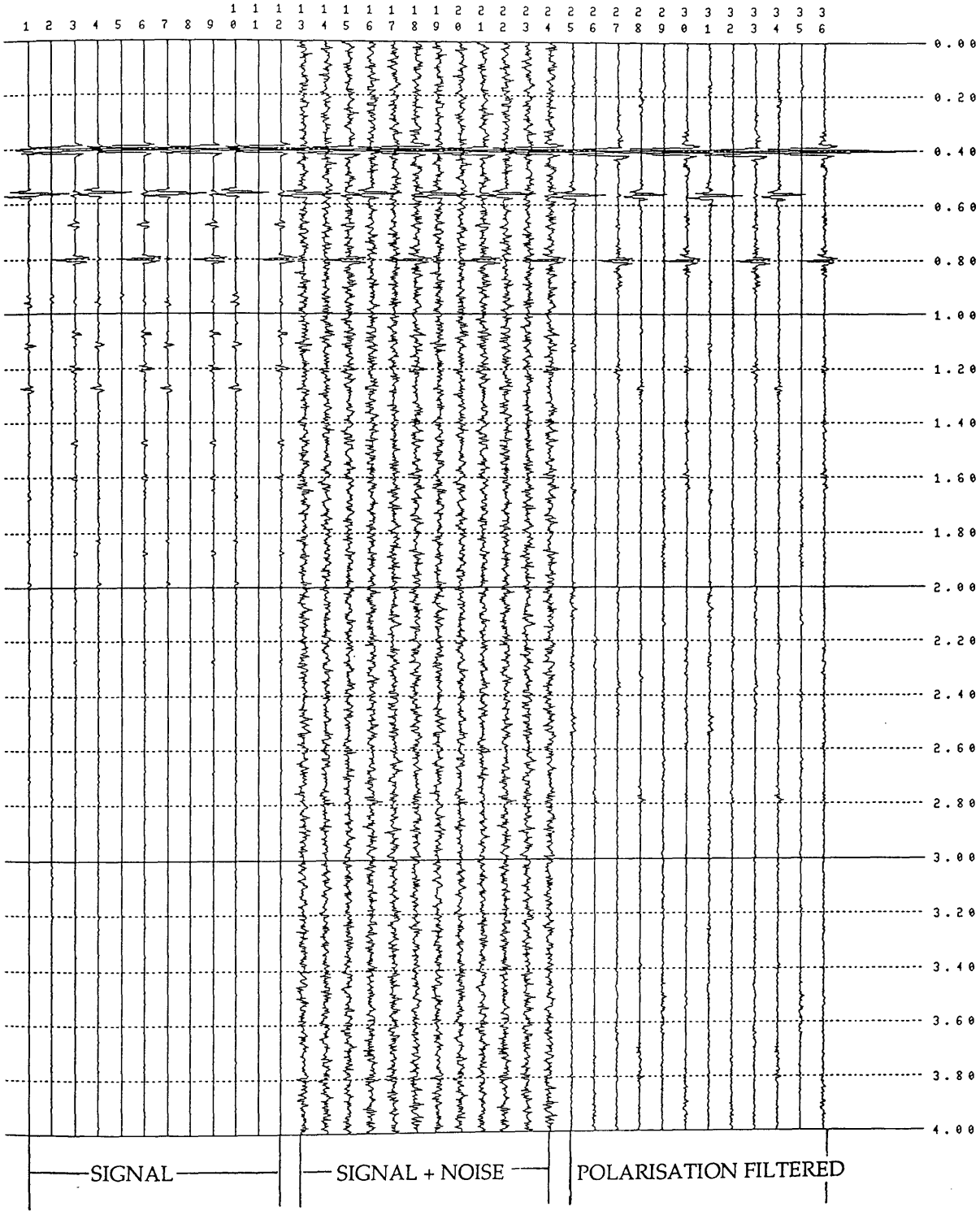

Fig. 5.3.4 The original (channels 1-12), noise-mixed (channels 13-24) and polarisation filtered (channels 25-36) seismograms (explosive source) at 4 stations (1, 2, 4, 5) for model 2 in an anisotropic medium. The order of the traces is the radial, transverse and vertical.

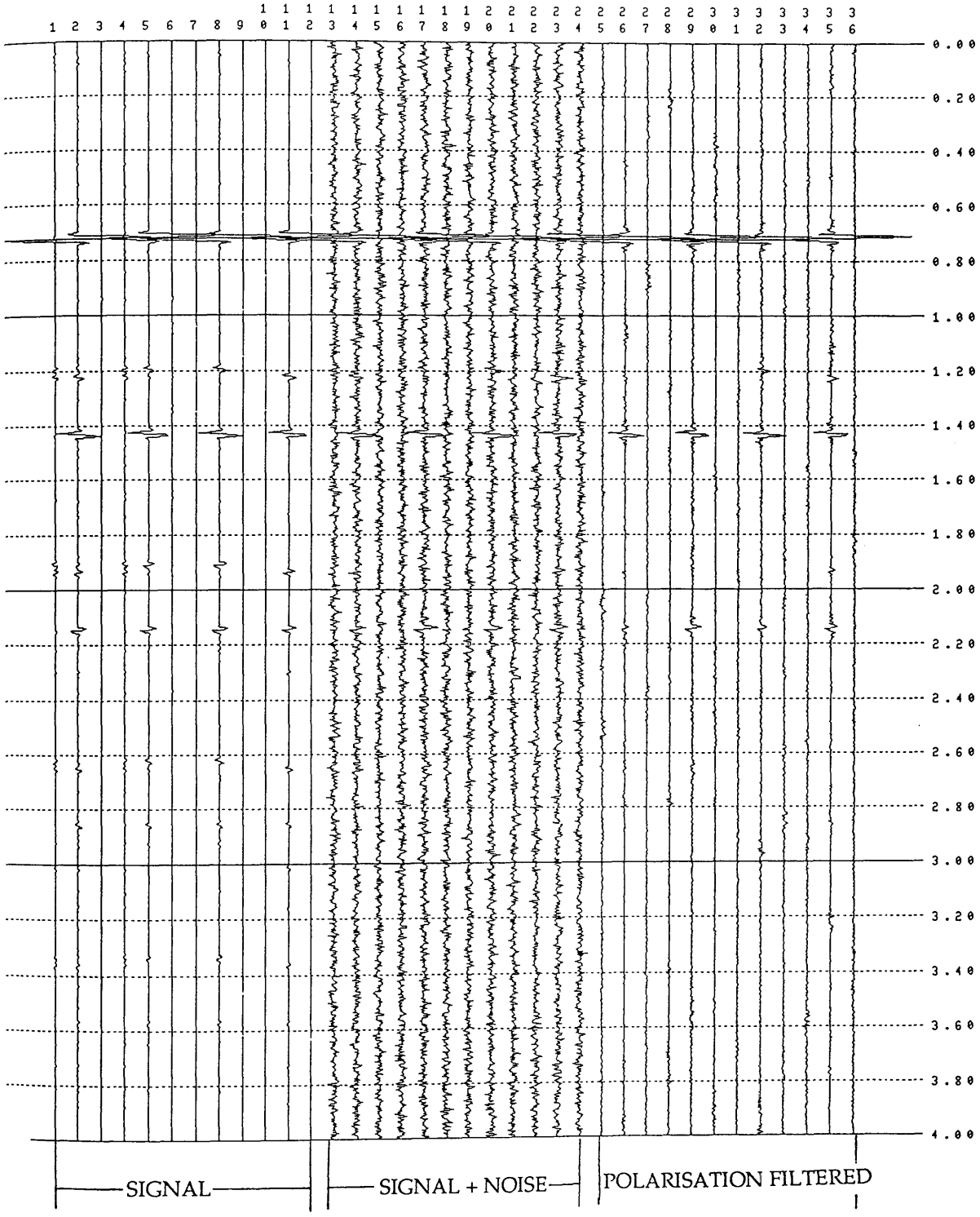

Fig. 5.3.5 The original (channels 1-12), noise-mixed (channels 13-24) and polarisation filtered (channels 25-36) seismograms (SH source) at 4 stations (1, 2, 4, 5) for model 2 in an anisotropic medium. The order of the traces is the radial, transverse and vertical.

filter. To determine why reflection event 2 in model 1, (see Fig. 5.3.1) from the explosive source, has not fully been extracted, we start from the polarisation of particle motions of the original data and noise-mixed data. The particle motions of both the horizontal and vertical components from samples 150-190 (which covers whole reflection event 2 at 0.67 s in Fig. 5.3.4) are plotted. The polarisation diagram for the original data in Fig. 6.3.6 (a) shows the linear polarisation of particle motions in the vertical direction, but the polarisation diagram for noise-mixed data (root mean square variance of noise is 60) in (b) shows random polarisation. The addition of random noise with a big root mean square variance to the data has totally changed the polarisation characteristics of the original data. As a result, this noise-mixed data will provide lower values of rectilinearity and directionality, and they will be attenuated rather than enhanced as hoped for (see channel 3 in Fig 5.3.7).

As we reduce the root mean square variance of random noise to 60%, i.e., the new root mean square variance is 36, in which case the reflection event 2 is still not clearly visible, but this noise-mixed data (channel 4 in Fig. 5.3.7) shows a better polarisation on the vertical direction. The event (channel 5 in Fig. 5.3.7) is clearly revealed after filtering. Therefore, we may conclude that the polarisation filter does extract weaker signals on the condition that the contaminating noise does not entirely change the polarisation of the original data.

The bandwidth of the noise may also affect filtering because the random noise as we use here to contaminate the synthetic data has a very wide range of frequencies, which will strongly change the characteristics of synthetic data. This problem is not investigated further.

5.6 Summary

The modelling package SEIS83 has been used to generate synthetic 3-component seismic data in an isotropic medium. The application of the signal enhancement polarisation filter to these data is successful in terms of suppressing random noise and enhancing signals. In addition, stacking the

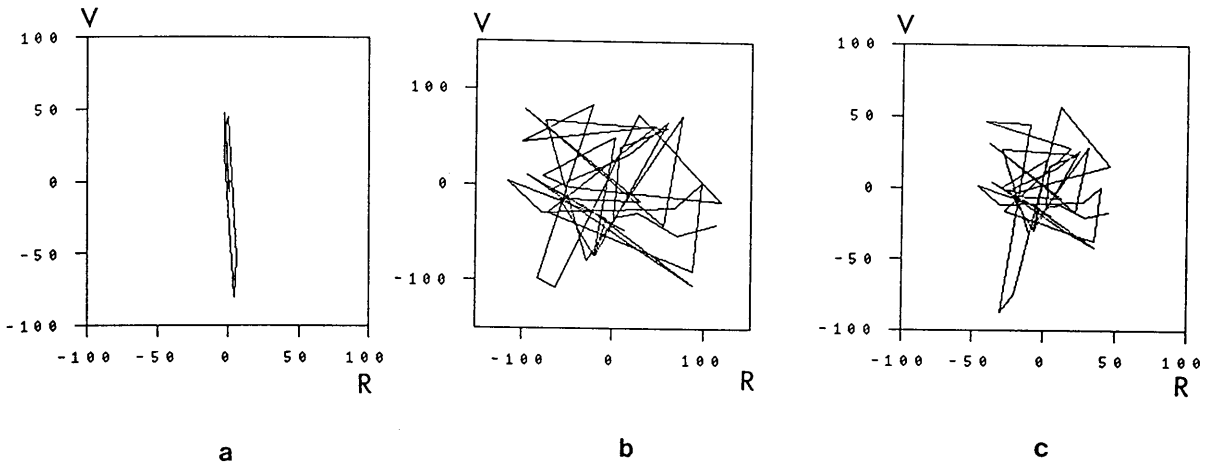

Fig. 5.3.6 (a) The polarisation diagram of the original data from channel 3 in Fig. 5.3.4. (b) The polarisation diagram of the noise-mixed data (root mean square variance of noise is 60). (c) The polarisation diagram of the noise-mixed data (root mean square variance of noise is 36).

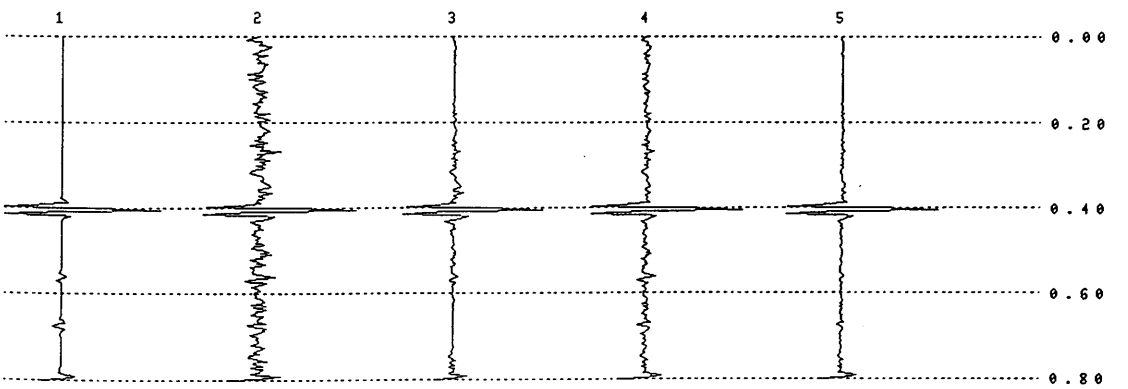

Fig. 5.3.7 Noise-mixed and filtered seismograms. Channel 1 is for the original data, channel 2 is for the noise-mixed data (root mean square variance of noise is 60), channel 3 is for the filtered trace 2, channel 4 is for the noise-mixed data (root mean square variance of noise is 36), channel 5 for filtered trace 4.

filtered data based on the RAZOR array provides a highly resolved section.

To generate 3-component seismograms in an anisotropic medium by the ANISEIS, two geological models are constructed for both a normal case (no reversed velocity contrast) and a special case (low velocity sediments sandwiched between lava at the top and hard rock beneath). The application of the polarisation filter to data based on model 1 gives a good result. However, filtering the data based on model 2 indicates a problem which is investigated by changing amount of noise in the data. The study shows that if the added noise entirely changes the polarisation direction of particle motions of reflection wavelets, the filter may not be able to extract very weak signals from noise, and by reducing the root mean square variance of random noise to a certain degree such that the noise-mixed data exhibit a better polarisation, the filtering will extract the weaker signals.

Chapter 6 Imaging Structure by Slant-stack Processing

6.1 Introduction

At the later stage of conventional seismic data processing, the data are migrated so as to determine the true reflection point. As a result, structural images in the time-offset domain are obtained by displaying zero-offset seismic traces. In this chapter, we present a new idea of imaging structure in 3-dimensions using synthetic data based on the areal 'RAZOR' array. The method can in theory be used to determine the true dip and dip direction of a deep reflector.

6.2 Introduction to conventional slant-stack processing

The slant-stack, also called the τ-p transform, plane wave decomposition, beam-steering etc, is based on the model of a downward moving plane wave. A plane wave propagating at an angle from the vertical can be generated by placing a line of point sources on the surface, exciting the point sources in succession with a time delay and superimposing the responses that are in the form of spherical wavefronts. The transformation of the time-offset domain into the τ-p domain and its usages have been discussed extensively by many authors [Bessonova et al 1974, Stoffa & Buhl 1981, Diebold & stoffa 1981, Treitel el al 1982, Biswell & Konty 1984, Brysk & McCowan 1986, Hake 1986, Mithal & Vera 1987]. Here is a generalized description of how the τ-p transform is performed. As shown in Fig. 6.2.1, a plane wave with an angle θ from the vertical comes up from an interface. The time delay associated with the plane wave is given by

$$\Delta t = (\sin\theta / v) \cdot \Delta x$$

Snell's law says that the quantity sinθ/v, which is the inverse of the horizontal phase velocity, is constant along a raypath in a layered medium. This constant is called the ray parameter. Rewriting above equation gives

$$\Delta t = p \cdot \Delta x$$

For a single p value, the signal is recorded at many offsets. In general, receivers at all offsets record plane waves of many p values. To decompose the offset gather into plane wave components, all the trace amplitudes in the gather must be summed along several slanted paths, each with a unique time delay defined by $\Delta t = p \cdot \Delta x$.

To construct a slant-stack, a linear moveout correction has to be applied to the data through a coordinate transformation

$$\tau = t - px$$

where p is the ray parameter, x is the offset, t is the two-way travel time,

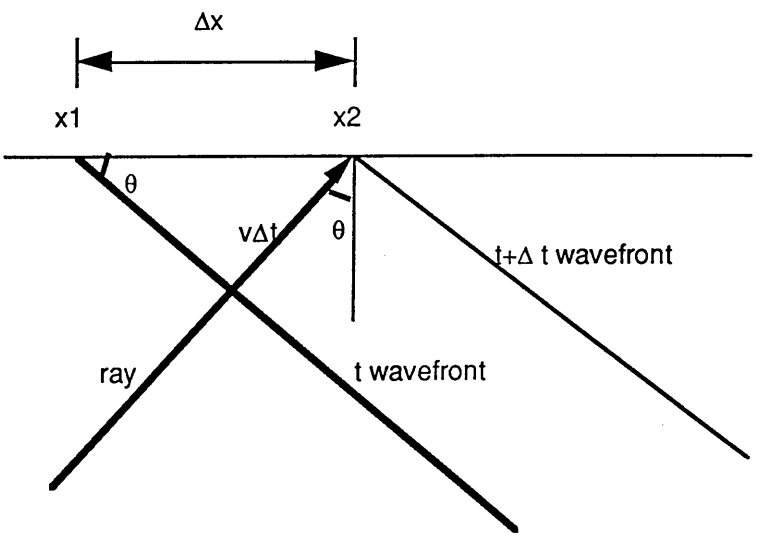

Fig. 6.2.1 The geometry of a plane wavefront and a time delay associated with 2 receivers on the surface

and τ is the linear moveout time (or intercept time). Then, the data are summed

over the offset axis to obtain:-

$$U(p, \tau) = \sum_{i=1}^{N} P(x_i, \tau + px_i)$$

Here, P(x, t) are the observed seismic recordings, and U(p, τ) represents a plane wave with a ray parameter p=sinθ/v. By repeating the linear moveout correction for various values of p and performing the summation, the complete slant-stack gather is constructed. Fig. 6.2.2 shows how a hyperbola in the x-t domain is transformed into an ellipse in the τ-p domain.

The τ-p transformation has successfully been used to suppress multiples based on different characteristics of multiples in two domains. Various filters are found to be more effective if applied to the data in the τ-p domain [Yilmaz, 1988]. In addition, based on downward continuation of a slant stack gather, a technique has been developed to estimate interval velocity [Schultz, 1982].

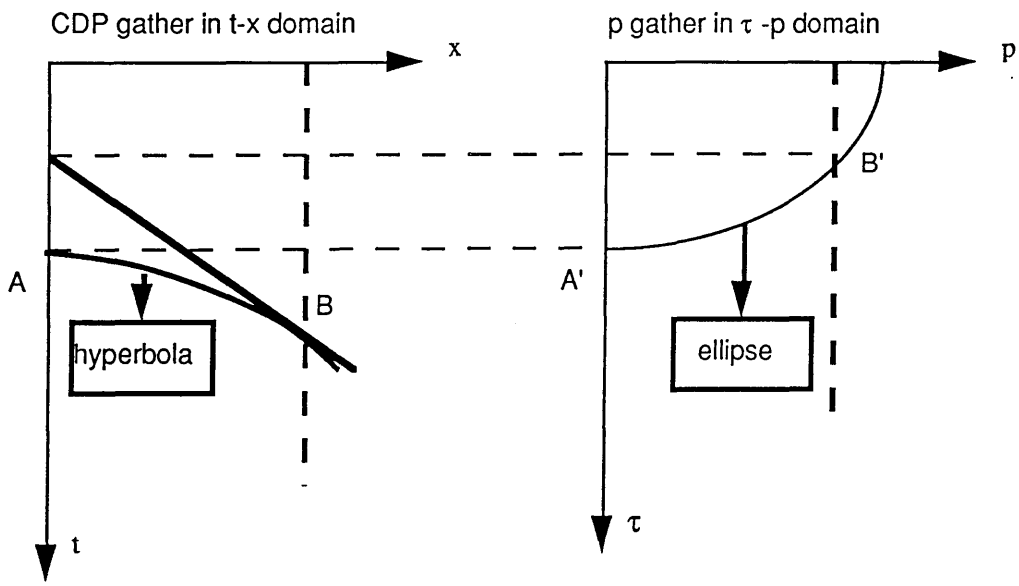

Fig. 6.2.2 A hyperbola in the t-x domain maps onto an ellipse in the τ-p domain

6.3 *Imaging structure by slant-stack processing*

As stated in Section 2.3, the dimension of the 'RAZOR' array is chosen such that the phase difference of a planar arrival will not differ by

more than half a wavelength. It has been found that for a horizontal reflector at a great depth, say 3 km, the time delay introduced by two different offsets (75 m and 130 m in our experiment) is only 0.23 ms assuming that the average velocity of the upper layers is 4.0 km/s. Hence the reflection events from 12 vertical components (refer to Fig. 5.2.3) will almost be located on a horizontal line. This also shows that the assumption that the seismic wavefront behaves as a plane wave across the aerial array is a valid approximation. However, a dipping reflector at a great depth will introduce long time delays between the 12 vertical traces, depending on the true dip of the reflector and the velocities of the upper layers. In other words, the variation of reflection wavelet arrival times on the t-x section is almost entirely due to the dipping of the reflector or structure rather than to the different offsets on the surface [D. K. Smythe, pers. comm., 1989].

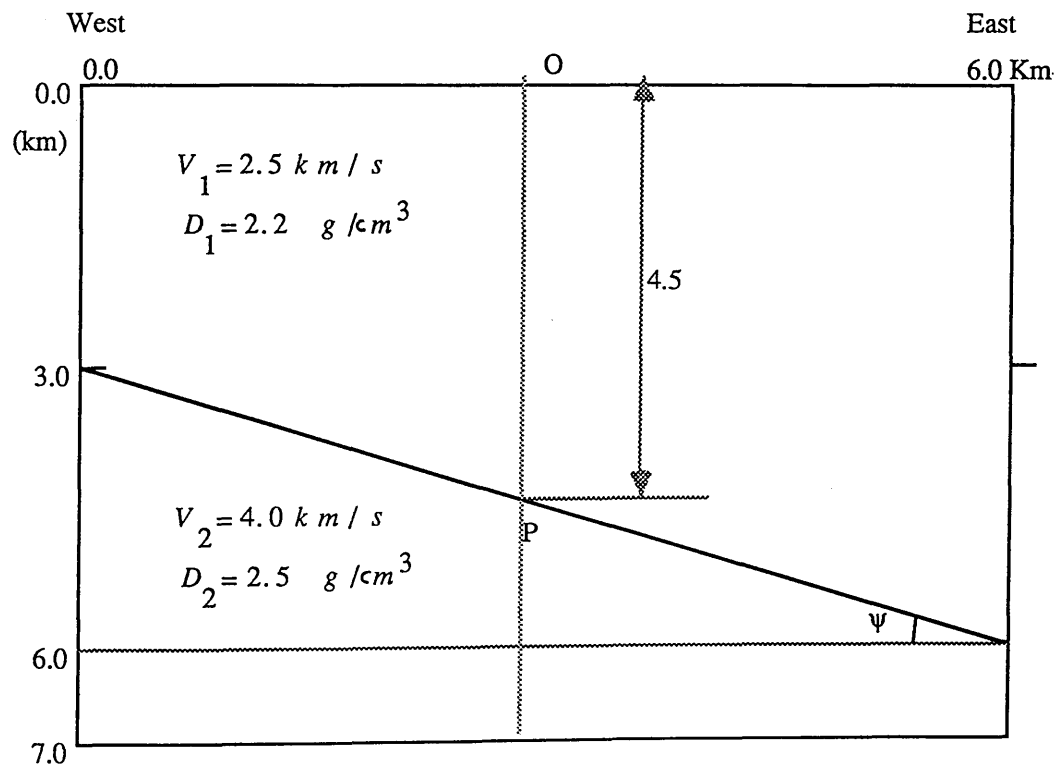

Fig. 6.3.1 Geological model for generating synthetic seismograms. (Horizontal scale is exaggerated, the true dip $\psi=26.6^{O}$)

We generate synthetic seismic data based on a model shown in Fig. 6.3.1 using a seismic modelling package SEIS83 (refer to Section 5.2.1). The model comprises only one interface which dips towards East. The true dip of the interface is 26.6^{o}. The vertical depth from shot point O on the surface to a point P on the dipping interface is 4.5 km. The upper and lower layers have constant velocities of 2.5 km/s and 4.0 km/s, and constant densities of 2.2 g/cm^3 and 2.5 g/cm^3 respectively. This model is used to generate 12 vertical components. The method used to decompose such a 3D model into 6 2D models is the same as that described in Section 5.2.4. The 12 vertical components are plotted in Fig. 6.3.2 in the order of station numbers marked in Fig. 5.2.3. We can see from the figure that the reflection events behave like a cosine wave on the section due to the circular configuration of the array. Additionally, the time delay between two stations, say, stations 3 and 9, reaches up to 40.6 ms, which is more than twice as much as the 20 ms period of a reflection signal (50 Hz). A contour map of two-way travel time associated with 12 station positions is made and shown in Fig. 6.3.3. This figure indicates that the two-way travel time increases towards the dip direction.

We arbitrarily select a straight line L through the shot point at the centre of the array, say, a west-east line, and define the azimuth of a line as an angle measured anticlockwise from x axis (or from East). Here the azimuth of line L is 0^{o}. Then, we "project" 12 stations onto the line L. "Projection" here means that the order of 12 stations is reorganised and their offsets are re-calculated, but the 12 seismic traces themselves are kept untouched. For example, stations 3 and 5 are projected onto the line L, their new offsets are given by

$$x3 = x5 = 130 \cdot \cos 30^{o} = 112.12\ m$$

likewise, the new offsets for station 2 and 6 are given by

$$x2 = x6 = 75 \cdot \cos 60^{o} = 37.50\ m$$

Therefore, a new "profile line" (or projection line) is constructed with 12

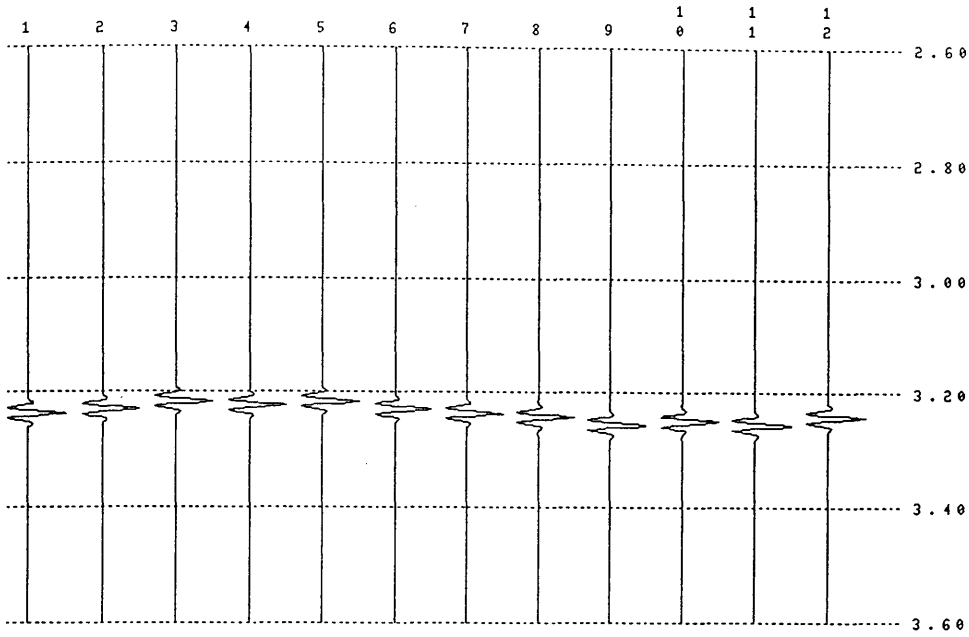

Fig. 6.3.2 Twelve vertical components generated by SEIS83. The data are based on the model in Fig. 6.3.1. Channel numbers correspond to station numbers.

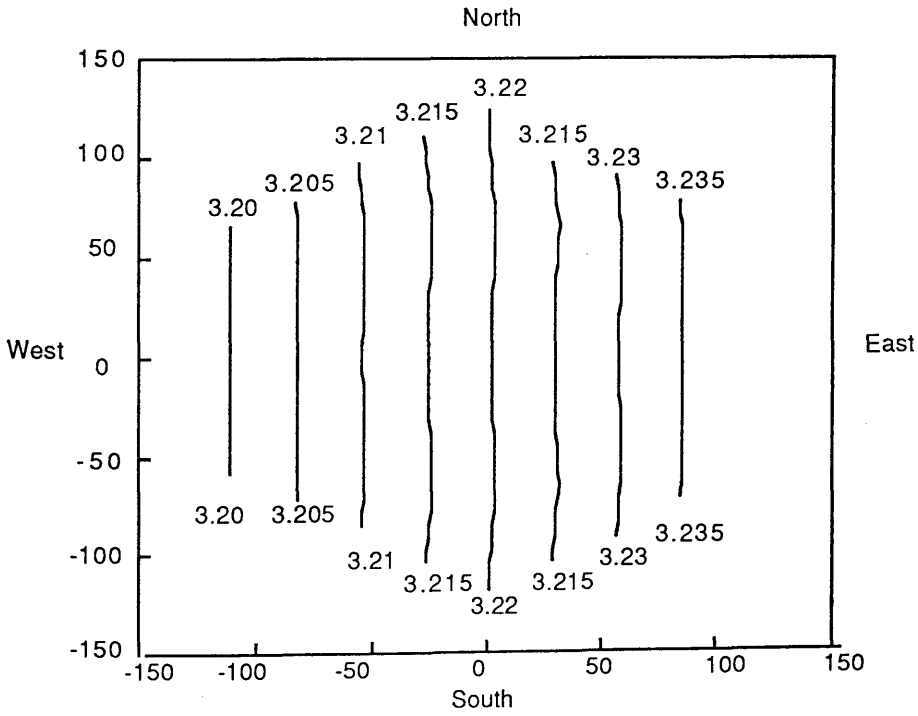

Fig. 6.3.3 The contour map of two way travel time associated with the array.

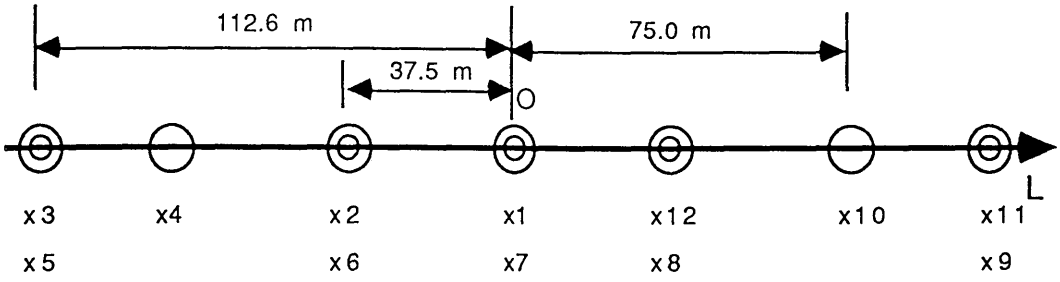

Fig. 6.3.4 Construction of a projection line L with an azimuth $\alpha=0^{o}$.
Two concentric circles indicate that 2 stations are projected at the same point.

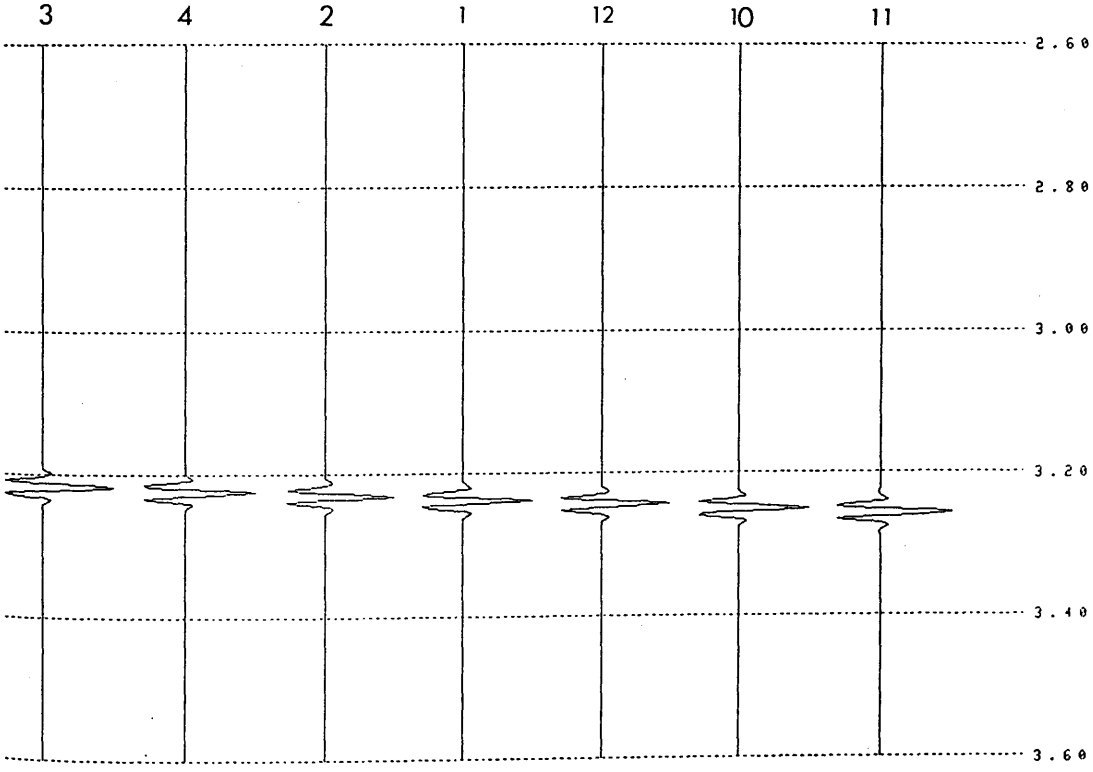

Fig. 6.3.5 Seven seismograms from stations 3, 4, 2, 1, 12, 10, 11 on the projection line L .

stations but only 7 different offsets, this is illustrated in Fig. 6.3.4. By changing the azimuth from 0^0-180^0 anticlockwise, we can obtain a number of projection lines. To demonstrate what seismic events look like on the t-x section, seven seismic traces from stations 3, 4, 2, 1, 12, 10, and 11 along the projection line L are plotted in Fig. 6.3.5. We can see that they form a dipping line.

Conventional slant-stack processing is usually conducted on common-depth point or common-shot point data so that a hyperbola in the t-x domain is transformed into an ellipse in the τ-p domain. However, the transformation requires that the CDP data should have an appropriate number of offsets, so as to reduce the end effects to a minimum. Here, we use the slant-stack technique in an attempt to determine the phase velocity of the upper layer and the true dip and dip direction of a reflector. In other words, we try to image structure in 3 dimensions. If we perform the slant-stack based on the line L shown in Fig. 6.3.4, for a particular intercept time τ and a ray parameter p, which is the slope of the slanted line through peaks of reflection wavelets, the amplitude of the p trace in the τ-p domain will be enhanced, because the reflection events from the dipping layer form a dipping line (see Fig. 6.3.5). By repeating the procedures on different lines, we will be able to obtain a number of τ-p sections. Therefore, p traces with large peak amplitudes on different τ-p sections can be identified.

6.4 Fortran-77 program MASSP

A Fortran-77 program called MASSP was written by the author to carry out the slant-stack processing (see Appendices; Fortran-77 program 10). As shown in the flow diagram in Fig. 6.4.1, the program firstly reads seismic data into arrays U(I, J), and asks the user to input the minimum and maximum values of ray parameters (p) and number of p traces. The increment of p is calculated automatically. The program then performs station projections onto a user-defined line. The new offsets will have both positive and negative values depending on the azimuth α. The slant-stack is carried out using 3 DO

loops and the results are saved in a new file. To run the program on the VAX/VMS operating system, a user has to reply to several questions as shown in the following example.

```
$    INPUT FILE NAME FOR SLANT-STACK
     SHOTDT1
$    INPUT A FILE NAME FOR OUTPUT
     TPOUT
$    INPUT THE MINIMUM AND MAXIMUM RAY PARAMETERS
     -6.6667E-04     +6.667E-04
$    INPUT THE NUMBER OF THE RAY PARAMETERS
     3
$    INPUT AN AZIMUTH FOR PROJECTIONS (IN DEGREES)
     30
$    START SLANT-STACK PROCESSING
$    RAY PARAMETER    1    COMPLETED
$    RAY PARAMETER    2    COMPLETED
$    RAY PARAMETER    3    COMPLETED
$    FORTRAN STOP
```

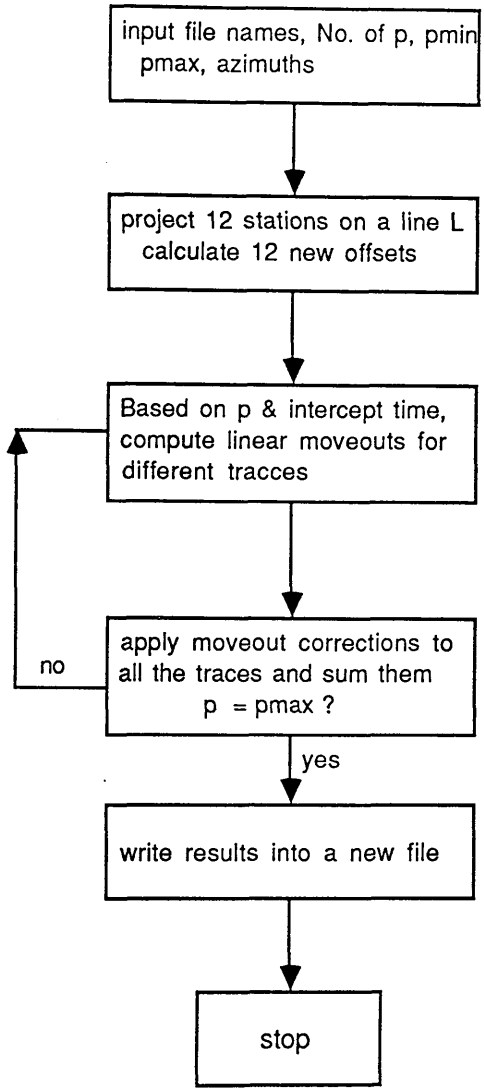

Fig. 6.4.1 Flow diagram of Fortran-77 program MASSP

6.5 The implementation of slant-stack processing on synthetic data to image structure

6.5.1 Determining the true dip of a reflector

To process the synthetic data based on the model in Fig. 6.3.1, we choose the minimum ray parameter p_{min}=-1/1500=-6.667×10^{-4} s/m and the maximum ray parameter p_{max}=1/1500=6.667×10^{-4} s/m. The study of the sampling along the p-axis in constructing a slant-stack gather by Yilmaz [1988] shows that

the p-axis in constructing a slant-stack gather by Yilmaz [1988] shows that undersampling the p value introduces some noise into the reconstructed CDP gather, whereas oversampling in the p-axis does no harm but yields nothing extra either. As a compromise, we choose 60 as the number of p traces. The increment of p will be 2.222×10^{-5} s/m. The azimuths of a line L are chosen as 0^o, 30^o, 45^o, 60^o, 90^o, 120^o, 135^o, 150^o, 180^o. As a result, nine τ-p sections corresponding to each azimuth are produced and shown in Fig. 6.5.1 (a) - (i). We can see from these figures that the events in the τ-p domain are concentrated towards the centre. The end effect is strong at both ends when the ray parameter tends to be either a minimum or a maximum. Fig. 6.5.1 (a) ($\alpha=0^o$) shows that a single wavelet with large peak amplitude by in-phase summation appears on channel 38 corresponding to the ray parameter $p=1.778\times10^{-4}$ s/m. This trace is of great interest to us because it indicates the phase velocity of the upper layer. That is, the dip of a reflector can be determined if the velocity of the upper layer is known. Fig. 6.5.1 (b) (c), (d) also show the positions of the p traces with large peak amplitudes on the sections. They tend to move towards the centre (p=0), this is because when the azimuth increases towards 90^o, the apparent dip associated with the projection line L becomes smaller and smaller, which gives a small ray parameter or large phase velocity. By comparing the single wavelet of interest on different sections, we can see that the peak amplitude decreases when the azimuth increases. When $\alpha=90^o$, the single wavelet with large amplitude disappears because the projection line is parallel to the strike of the dipping layer, and the reflections are no longer in phase, so they do not fill on a dipping line. For the rest of τ-p sections in fig. 6.5.1 when $\alpha>90^o$ and $p<0$, it is found that the p trace with large peak amplitude on a section is the mirror image of the trace formed when the azimuth is $(\alpha-90^o)$ and p is positive. For example, for the section when $\alpha=180^o$, the trace of interest is found to be on channel 22, corresponding to the ray parameter $p=-1.778\times10^{-4}$ s/m.

In practice, the dip direction is unknown, but we can produce a number

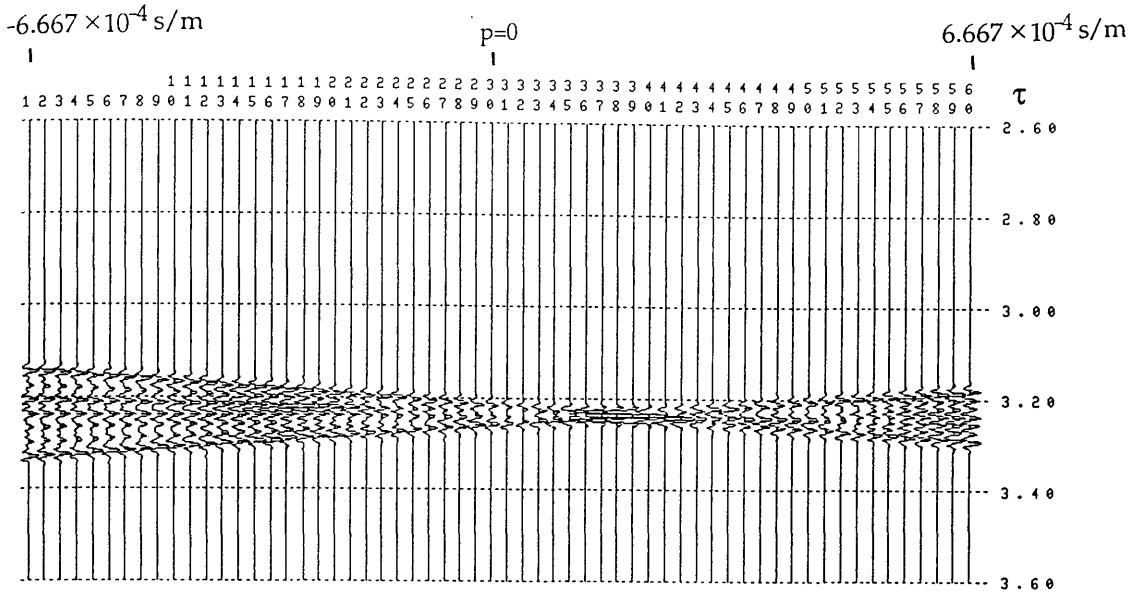

(a) $\alpha=0^o$

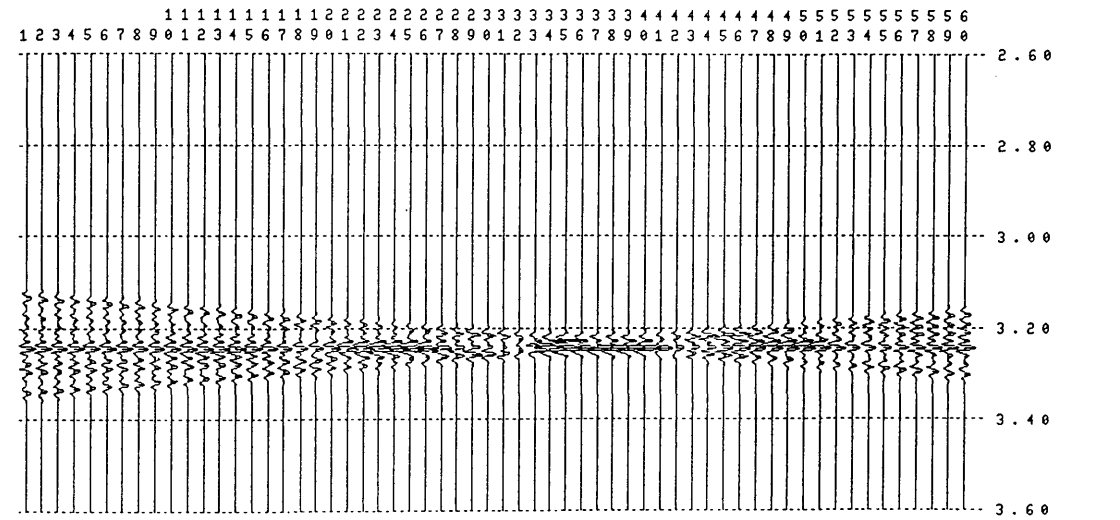

(b) $\alpha=30^o$

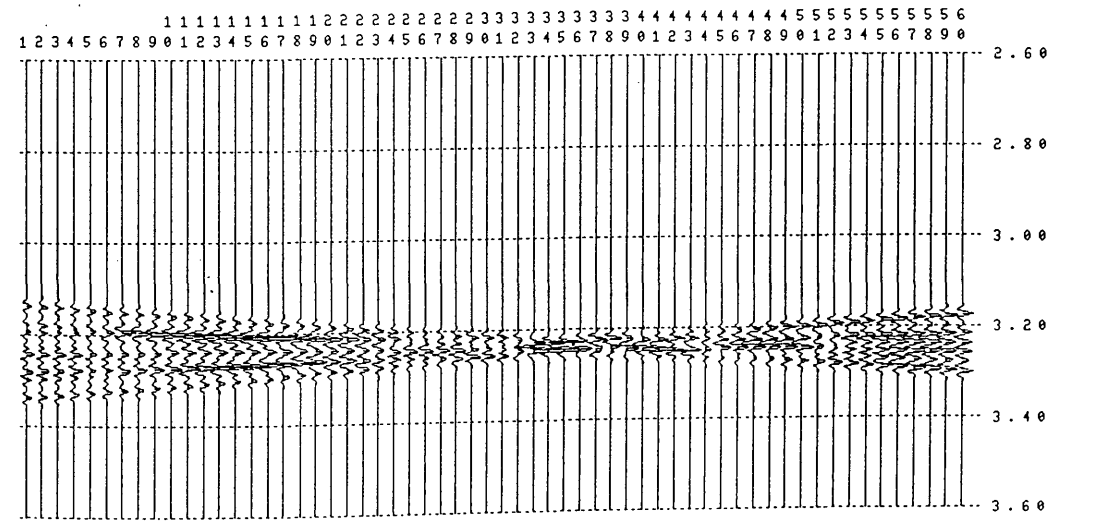

(c) $\alpha=45^o$

Fig. 6.5.1 Continued (see the next page).

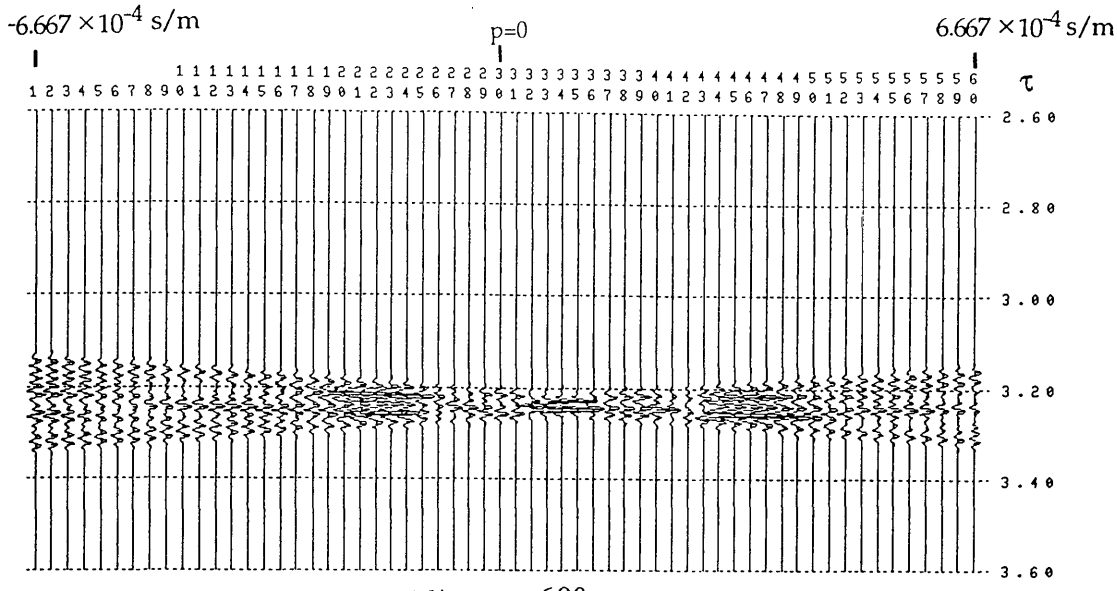

(d) $\alpha=60^{o}$

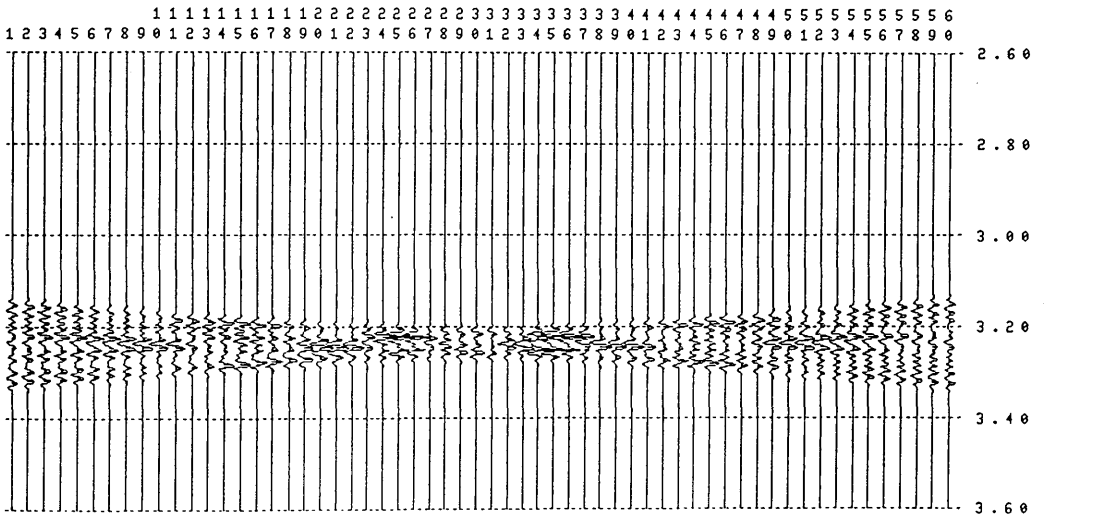

(e) $\alpha=90^{o}$

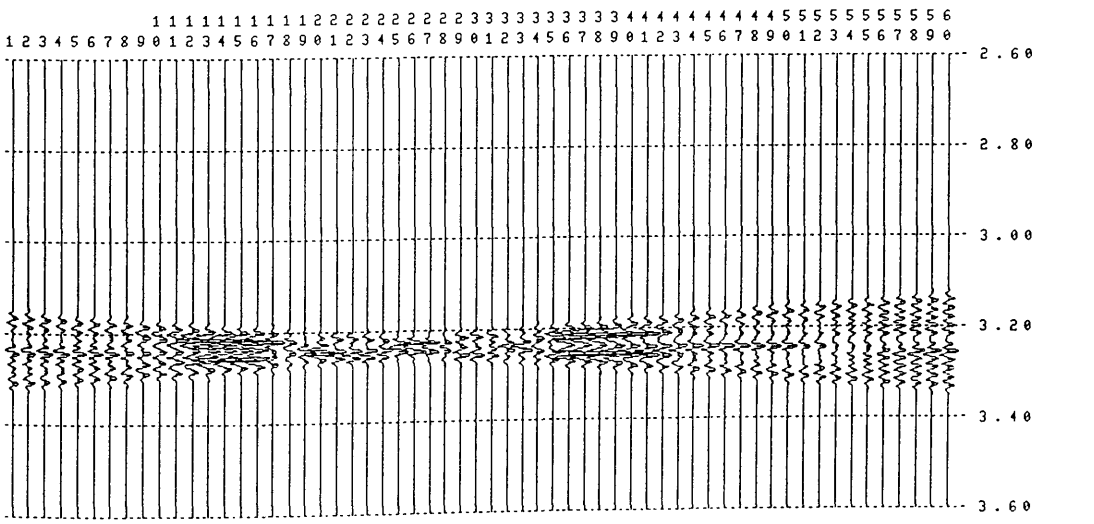

(f) $\alpha=120^{o}$

Fig. 6.5.1 Continued (see the next page).

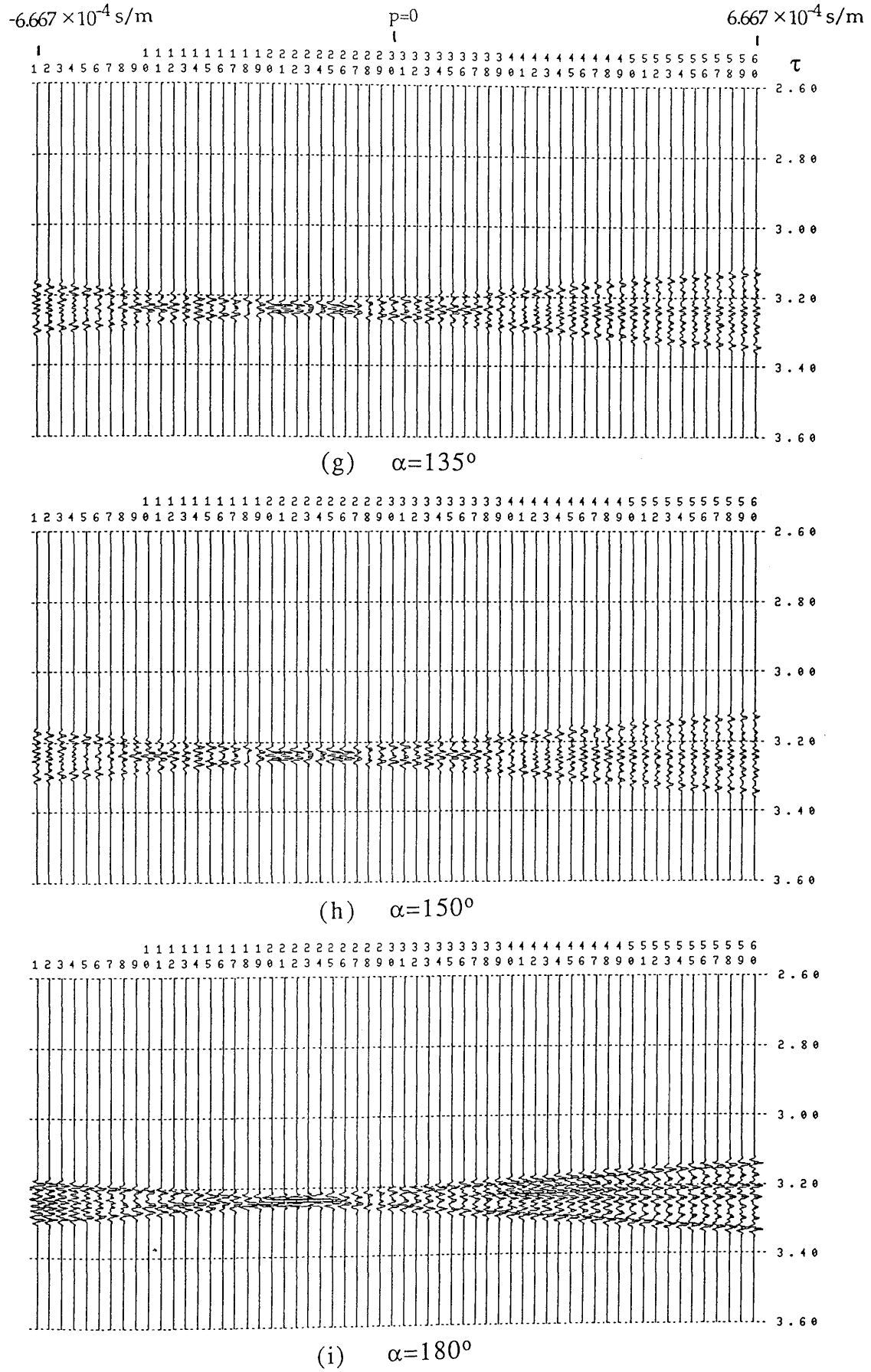

Fig. 6.5.1 Nine τ-p images based on nine projection lines with different azimuths.

of τ-p sections with a small increment of azimuth α ($0^o<\alpha<180^o$). Hence a p trace with a large peak amplitude on each section can be identified. In theory, the biggest ray parameter among the selected p traces of interest on all sections will indicate the largest phase velocity along the projected line. We assume that there is no lateral change in velocity; in fact, the lateral change in velocity will be very small across such a small aerial array. The reflection angle θ from $p=\sin\theta/v$ associated with the projected line may closely approximate the true dip of the reflector. If the average velocity of the upper layers is known, the true dip θ can be determined. Let us take the above nine τ-p sections as an example. We can see that section 1 ($\alpha=0^o$) shows not only the rightmost p trace (channel 38) but also the largest peak amplitude of interest among nine sections. Therefore, the angle θ from phase velocity $p = \sin\theta/v = 1.778\times10^{-4}$ s/m may be calculated as $\theta=26.4^o$ which is near to the true dip of the reflector $\psi=25.6^o$.

6.5.2 Determining the dip direction of a reflector by constructing τ-x images

Above we described how the t-x images can be transformed into the τ-p images as a function of azimuth α. As a result, a striking point (the largest peak amplitude on one p trace) in the τ-p domain, rather than an ellipse as what the conventional slant-stack method shows, is identified by its peak amplitude instead of the time difference. In this section, we try to construct a new image- τ-x section- to derive the dip direction of a deep reflector.

In the field, we usually shoot along a line, say, 50 shots which correspond in our geometry to a distance of 3.75 km on the earth's surface (shot spacing 75 m). After the τ-p sections like those in Fig. 6.5.1 have been constructed as a function of azimuth α_i for a particular shot x_j, a p trace which shows the largest peak amplitude on a τ-p section for each shot is found. We can now plot p traces against x_i while the azimuth α_i is kept constant. The ray parameters in the τ-x domain do not have to be the same, but, if the reflector is

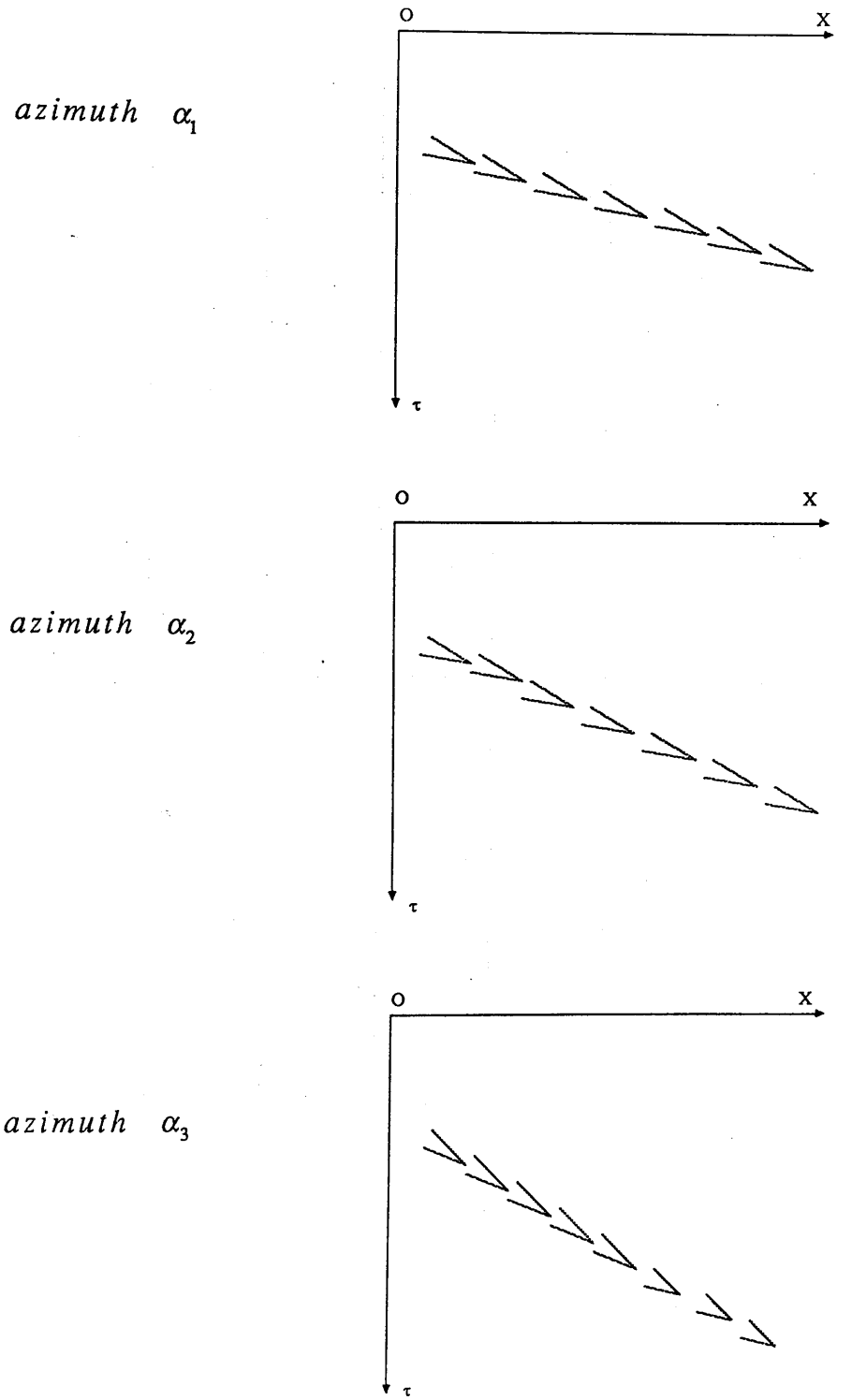

Fig. 6.5.2 Illustration of τ-x images with 3 different azimuths. The ray parameter in each diagram is constant.

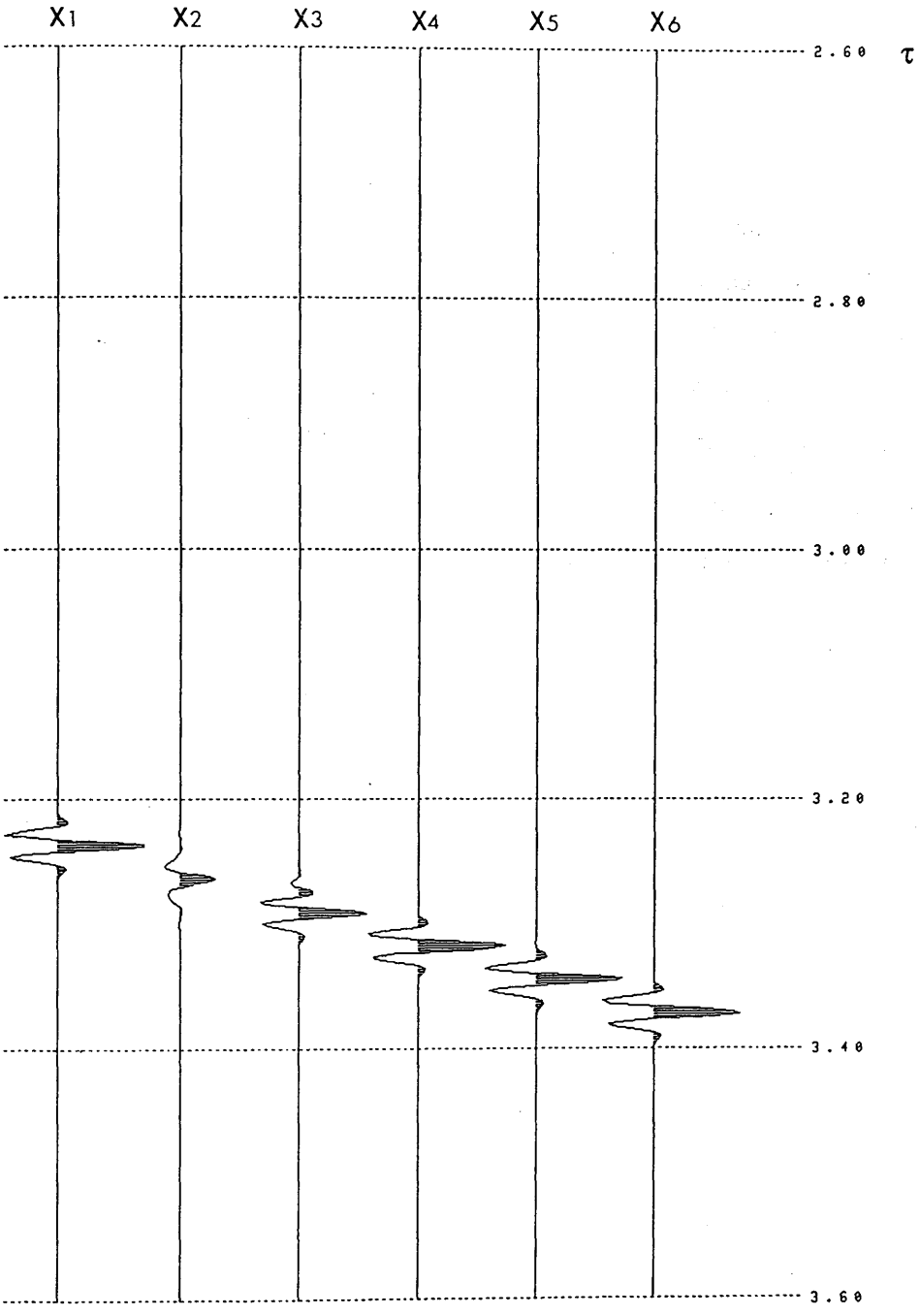

Fig. 6.5.3 A τ-x image constructed by synthetic data based on the model in Fig. 6.3.1. Six shots are presented. The ray parameter p is 1.778×10^{-4} s/m.

absolutely planar, the p values will be identical. Fig. 6.5.2 illustrates what the final τ-x images look like. Three τ-x sections associated with azimuths α_1, α_2 and α_3 are produced, each showing a line of events with dips at different amounts. The largest dip, as shown in Fig. 6.5.2 (c) is most likely to be the true dip of the reflector assuming that the velocity effect has been corrected.

Based on the model in Fig. 6.3.1, we generate 6-shot data and perform the slant-stack processing individually. A azimuth 0^o is used as an example to produce 6 τ-p images. The first image for shot 1 is shown in Fig. 6.5.1 (a), others are not shown here, but they look rather similar, except for the time difference of the p gather. The p traces from 6 τ-p sections are all on channel 38 which corresponds to a ray parameter $p=1.778\times10^{-4}$ s/m so that they are picked up and plotted against offsets. Fig. 6.5.3 tells us about the dip direction of the reflector which is towards East.

6.5.3 Determining the angle of a ray path to optimise polarisation filtering

For a simple geological model with only one layer, the reflection angle θ of a ray can be determined by the method described in Section 6.5.1. If the angle is near to the true dip of a reflector, the polarisation direction P of a compressive wave can be derived as illustrated in Fig. 6.5.4 (a). On the other hand, by constructing a covariance matrix over a time window and calculating the eigenvalues and eigenvectors of the matrix, we can determine the polarisation direction E of particle motions recorded by 3-component geophones (refer to Section 3.4). Fig. 6.5.4 (b) shows the polarisation directions P and E. The vector E is constructed by 3-component recordings. It can represent the polarisation direction either of a shear wave or a compressional wave, depending on seismic source type and geological conditions.

To preserve those trajectory parts whose polarisation direction is the same as or near to the vector P, we define a fixed cone around the vector P. Thus P is the cone's axis and the desired filtering direction. The vertex half

angle of the cone is the criterion of filtering sharpness. If this angle is small, the cone is narrow and the filter is very selective, since only those events that are well polarised along the cone's axis are preserved [Benhama & Cliet, 1988].

In practice, we can use the matrix method to determine the polarisation direction E over a time window. If the E lies inside the defined cone, the particle motions are kept or enhanced, otherwise they are rejected. Therefore, we will be able to get a section on which the reflection events present only those whose polarisation directions are along the vector P.

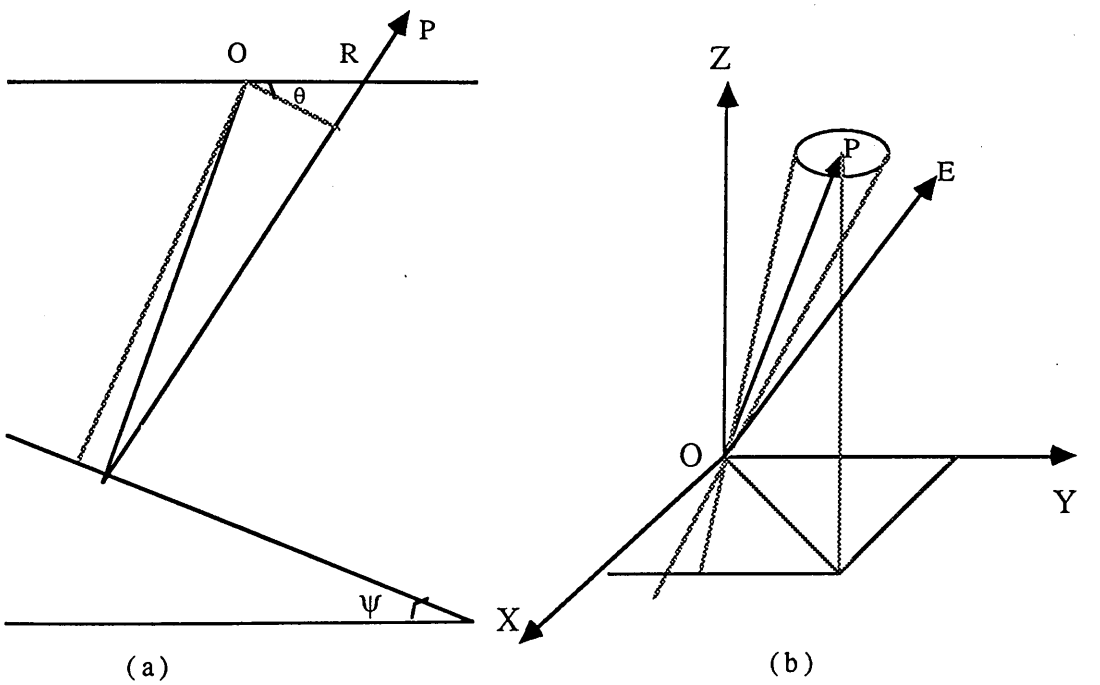

Fig. 6.5.4 (a) Geometry of a ray path showing the polarisation of a compressional wave P. (b) Polarisation direction P of a compressional wave obtained by the slant-slack method and polarisation direction E of particle motions obtained by the matrix method.

6.6 Summary and discussion

In above sections, the conventional slant-stack method used to transform t-x data into τ-p data has been reviewed. A new approach of using the slant-slack processing to image 3D structure, based on the 'RAZOR'

array, has been demonstrated by synthetic data. The result further proves that the dimension of the . array is appropriate for receiving reflected plane waves from deep interfaces. The true dip and dip direction of a reflector may be derived from τ-p images and τ-x images respectively, assuming that the velocity of the upper layer is known. The computer program MASSP was designed to perform the slant-stack processing from the original t-x data. The plotting program can display either τ-p images or τ-x images in various ways. This method can additionally be used to optimise the polarisation filtering, which keeps and enhances the compressional waves of interest according to the polarisation directions of waves.

In reality, the geological conditions are complicated. There will be many reflectors, with dips in different directions, and the velocities of layers are no longer constant but are a function of depth. Nevertheless, we can treat the geology as a model consisting of several layers, within each layer the velocity can be considered as constant. Thus the slant-stack processing will produce more than one line of events on both τ-p image and τ-x image. The angle θ derived from the phase velocity can no longer represent the true dip or apparent dip of an individual layer but a contribution of several layers. The true dip of individual layers can also be determined, if corrections are made. Therefore, this slant-stack method, different from the conventional, is potentially of great importance for imaging complex structure.

Chapter 7 The RAZOR Array, General Discussion and Future Work

The RAZOR array, a new array for acquiring seismic reflection data, has been tested in a basalt-covered area. The radius of the outer circle is an appropriate dimension for recording the weak reflection events from below basalts because Ground-roll and reverberations can be suppressed. The study of the characteristics of seismic reflection data from a basalt-covered area not only confirms with the results by other workers, but also reveals additional characteristics. The horizontal components exhibit larger amplitudes and lower frequency than the vertical component. Application of a newly designed spatial directional filter to the three component of seismic data shows that more information passes through the filter on the horizontal component. The energy variation diagram for each shot shows that the radial component receives much more energy than the others. The newly developed signal enhancement polarisation filter can be used to suppress random noise and a portion of reverberations. The synthetic data based on this array demonstrates that seismic wavefronts can reasonably be considered as planes, which allows slant-stacking to be carried out. As a result, the true dip and dipping direction of a deep reflector can possibly derived. This method can also be used to optimise the polarisation filtering, which passes compressional waves of interest according to the polarisation directions of the waves.

However, the field data from the inner stations were very poor. One explanation could be that these data are more severely affected by the surface materials than the data from the outer stations. Other possibilities are that the radius of the inner circle is too small, the inner stations interfere with the firing of the shots, or the MDS-10 channels are overloaded because of explosive charges close to geophones. From the data processing point of view, the conventional methods such as frequency filtering and predictive

deconvolution filtering cannot be applied with the same degree of success compared to conventional seismic reflection data. The polarisation filter cannot completely cancel all reverberations, especially when the data quality is so poor that the the polarisation of the useful signals is lost in the presence of noise. Apart from the above, it is dangerous to stack the data across the array, because problems may arise by summing reflection events with different phases when reflectors are very deep and the dipping angles are large. The technique of imaging geological structure in 3 dimensions is only based on the synthetic data of a simple model. To test the method thoroughly, there is a need to use the data from a more complicated model, and more sophisticated processing methods need to be developed.

With the further development of techniques, the areal RAZOR array will have its great potential in imaging geological structure. Below are listed several areas for future work:

(a) We need to modify the dimensions of the RAZOR array and to test the developed techniques for commercial use. We should empirically determine the appropriate radius of the inner circle of the array and acquire seismic reflection data in an area of simple geology (a normal case). The shot hole should be drilled as deep as possible into bedrock. The size of explosive charge for each hole should also be determined empirically. It is hoped that good shear waves can be received from an explosive source, so that some lithology information of the crust can be obtained as it is indicated by Vp/Vs.

(b) Instead of stacking data across the array, we can fire a number of shots, say 10, at one location, and then stack the individual channels. Thus, we face no danger of stacking reflection signals with different phases. Random noise will be greatly attenuated.

(c) We can generate the synthetic data based on a more complicated model to test the new techniques stated in Chapter 6, using more than one interface, with different layer velocities. Software can be produced to determine the true dips and dipping directions of reflectors after correction are made. Various kinds of images such as x-t, τ-p, x-τ and offset-depth can be displayed on

modern Sun Workstations.

(d) Having been fully tested by the field data from an area of simple geology, this method can then be applied to the area covered by volcanic rocks. In addition to the existing processing methods (frequency filtering, deconvolution filtering, polarisation filtering, τ-p transform, etc.), more advanced processing techniques need to be developed for extracting the weak signals in the presence of noise.

(e) It is well known that the study of shear wave splitting is of great potential in exploration geophysics. With the further development, we can use 3-component geophones and an S source to record very good shear waves. The anisotropic characteristics of the crust can systematically be analysed by studying shear wave splitting. In addition to using polarisation diagrams which are the main tools at present to characterise the data, we can develop a new means of processing 3-component data to identify the orientations of aligned cracks in the crust. One possibility is to study the energy distribution on the 3-components as a function of orientation of geophones. The correlation between them may help us to derive the crack orientations. Another possibility is to construct a new domain in which shear wave splitting shows a great anomaly, from which further information may be obtained.

The RAZOR array, with further modification and development, will have a promising future.

References

Agocs, W. B., 1951. Least squares residual anomaly determination, Geophysics, Vol. 16, 686-696.

Al-Sadi, H. N. 1980. Seismic Exploration Technique and Processing. Birkhauser Verlag Basel.

Arnold, M. E., 1977. Beam forming with vibrator arrays. Geophysics, Vol. 42, No. 7, 1321 - 1338.

Benhama, A. and Cliet, C., 1988. Study and application of spatial directional filtering in three-component recordings. Geophysical Prospecting, 36, 591-613.

Benoliel, S. D., 1987. Frequency wavenumber approach of the τ-p transform: Some applications in seismic data processing. Geophysical Prospecting, 35, 517-538.

Bessonova, E. N. and Fishman, V. M., 1974. The tau method for inversion of travel times- I. Deep seismic sounding data. Geophy. J. Astr. Soc. 36, 377-398.

Biswell, D. E. and Konty, L. F., 1984. A geophone subarray beam-steering process. Geophysics, Vol. 49, No. 11, 1838 - 1849.

Blais, J. A. R., Lodwick, G. D. and Ferland.R., 1983. Gravimetric terrain corrections in west Canada. Can. J. Earth Sci. 20, 259-265.

Blais, J. A. D. and Ferland, R. 1984. Optimization in gravimetric terrain corrections. Can. J. Earth Sci. 21, 505-515.

Bott, M. H. P., 1959. The use of electronic digital computers for the evaluation of gravimetric terrain corrections. Geophysical Prospecting 8 45-54.

Bott, M. H. P. and Masson-smith, D., 1960. A gravity survey of the Criffell granodiorite and the New Red Sandstone deposits near Dumfries. Proceedings of the Yorkshire Geological Society. 32, 317-332.

Bott, M. H. P., 1962. A simple criterion for interpreting negative gravity anomalies. Geophysics, Vol. 27, 376-381.

Bott, M. H. P., 1964. Gravity measurements in the North-Eastern part of the Irish Sea. Quart. J. Geol. Soc. Lond. 120, 369-396.

Bott, M. H. P. and Smithson, S. B., 1967. Gravity investigations of subsurface shape and mass distributions of Granite Batholiths. Geological Society of America Bulletin, Vol. 78, 859-878.

Brysk, H. and McCowan, D. W., 1986. A slant-stack procedure for point-source data. Geophysics, Vol. 51, No. 7, 1370-1386.

Carrion, P. M. and Hassanzadeh, S., 1985. Direct estimation of shear-wave interval velocities from seismic data. Geophysics, Vol 50, No. 4, 530-538.

Cerveny, V. and Psencik, I., 1983. Numerical modelling of seismic wavefield in 2-D laterally varying layered structures by the ray method (Manual).

Churchhouse R. F., 1981. Handbook of Applicable Mathematics. Volume 3 Numerical Methods John Wiley & sons.

Cliet, C. and Dubesset, M., 1987. Three-component recordings: Interest for land seismic source study. Geophysics, Vol. 52, No. 8, 1408-1059.

Darby, E. K. and Davies, E. B., 1967. The analysis and design of two-dimensional filters for two-dimensional data, Geophysical Prospecting, Vol. XV, No. 3, 383-406.

Danes, Z. F., 1960. On a successive approximation method for interpreting gravity anomalies.

Geophysics, Vol. XXV, No. 6, 1215-1228.

Danes, Z. F. and Oncley, L. A., 1962. An analysis of some second derivative methods. Geophysics, Vol. XXVII, No. 5, 611-615.

Dankbaar, J. W. M., 1987. Vertical seismic profiling-separation of P- and S-waves. Geophysical Prospecting, 35, 803-814.

Dankbaar, J. W. M., 1985. Separation of P- and S-waves. Geophysical Prospecting, 33, 970-986.

Diebold J. B. and Stoffa, P. L., 1981. The traveltime equation, tau-p mapping, and inversion of common midpoint data. Geophysics, Vol. 46, No. 3, 238 - 254.

Dobrin, M. B., 1988. Introduction to Geophysical Prospecting. Fourth Edition. McGraw-hill Book Company.

Dohr, G. and Janel, H., 1980. Improvements in the observation of shear waves. Geophysical Prospecting, 28, 208-220.

Douma, J. and Helbig, K., 1987. What can the polarization of shear waves tell us. First Break, Vol. 5, No. 3.

Evan, R., 1984. Effects of the free surface on shear wavetrains. Geophys. J. R. Soc., 76, 165-172.

Elkins, T. A., 1951. The second derivative method of gravity interpretation. Geophysics, Vol. 16, 29-50.

Evjen, H. M., 1936. The place of the vertical gradient in gravitational interpretations. Geophysics, Vol. 1, 127-136.

Faddeev D. K. and Faddeeva V. N., 1963. Computational Methods of Linear Algebra. Translated by Robert C. Williams.

Fertig, J., 1984. Shear waves by an explosive point-source: The Earth surface as a generator of converted P-S waves. Geophysical Prospecting, 32, 1-17.

Flinn, E. A., 1965. Signal analysis using rectilinearity and direction of particle motion. Proceedings of the IEEE (December).

Geldart, L. P., Gill, D. E. and Sharma, B., 1966. Gravity anomalies of two dimensional faults. Geophysics, Vol. XXI, No. 2, 372-397.

Granar L., 1966-1967. On topographic correction. Geoexploration, 4-5, 65-70.

Granser, H., 1987. Topographic reduction of gravity measurements by numerical Integration of boundary integrals. Geophysical Prospecting, 35, 71-82.

Grant, F. S., 1954. A theory for the regional correction of potential filed data. Geophysics, Vol. 1, 23-45.

Grant, F., 1957. A problem in the analysis of geophysical data. Geophysics, Vol. XXII, No. 2, 309-344.

Grant, F. S. and Elsahaty, A. F.,1962. Bouguer gravity corrections using a variable density. Geophysics, Vol. XXVII, No. 5, 616-626.

Grant, F. S., 1972. Review of data processing and interpretation methods in gravity and magnetics, 1964-71. Geophysics, 37, 647-661.

Green, R., 1976. Accurate determination of the dip angle of a geological contact using the gravity method, Geophysical Prospecting 24, 265-272.

Hake, H., 1986. Slant stacking and its significance for anisotropy. Geophysical Prospecting, 34, 595-608.

Hall, J. 1970. The correlation of seismic velocities with formations on the South-west of Scotland. Geophysical Prospecting 18, 134-148.

Hall, J., 1971. Seismic studies in the region of the Firth of Clyde, University of Glasgow, Ph. D. Thesis.

Hall, J., 1974. A seismic reflection survey of the Clyde Plateau Lavas in North Airshire and Renfrewshire. Scottish J. of Geology, 9 (4) 253-279.

Hammer, S., 1939. Terrain corrections for gravimeter stations. Geophysics, Vol. 4, 184-194.

Hansen, O., 1988. Signal-noise-ratio estimation and image processing of seismograms using two-dimensional coherence techniques. M. Sc thesis in information technology systems. University of Strathclyde.

Hatton, L., Worthington, M. H. and Makin, J., 1986. Seismic Data Processing: Theory and Practice. Oxford Blackwell Scientific.

Helbig, K. and Mesdag, C. S., 1982. The potential of shear-wave observations. Geophysical Prospecting, 30, 413-431.

Henderson, R. G., 1960. A comprehensive system of automatic computation in magnetic and gravity interpretation. Geophysics, Vol. XXV, No. 3, 569-585.

Hipkin, R. G. and Hussain, A., 1983. Regional gravity anomalies. 1 Northern Britain. Report 82/10. Institute of Geological Sciences, NERC.

Kane, M. F., 1962. A comprehensive system of terrain corrections using a digital computer. Geophysics, 27, 455-462.

Kanasewich, E. R., 1975. Time sequence analysis in Geophysics. Edmonton University of Alberta Press.

Kantas, K, and Zych, D., 1967. Reduction of gravity observations with digital computer. Pure and Applied physics. 68, 12-18.

Karlemo B., 1963. Calculation of terrain correction in gravity studies using the electric computer. Geoexploration, 1 (1), 56-66.

Kelamis, P. G. and Mitchell, A. R., 1989. Slant-stacking process. First Break, Vol. 7, No. 2, 43-54.

Ketelaar, A. C. R., 1976. A system for computer-calculation of the terrain correction. Geoexploration, 14, 57-65.

Ketelaar, A. C. R., 1987. Terrain correction for gravity measurement, using a digital terrain model (DTM). Geoexploration, 24, 109-124.

Lagios, E., 1979. Gravity and other geophysical studies relating to the crustal structure of South-east Scotland. PhD Thesis, University of Edinburgh.

Lagios, E. and Hipkin, R. G., 1981. Gravity measurements in South-east Scotland. Geophys. J. R. Astr. Soc. , 65, 505-506.

Lagios, E. and Hipkin, R. G., 1979. The Tweeddale Granite- a newly discovered batholith in the Southern Uplands. Nature, Vol. 280, 672-675.

Lash, C. C., 1985. Shear waves produced by explosive sources. Geophysics, Vol. 50, No. 9, 1399-1409.

Linsser, H., 1965. A generalized form of Nettleton's density determination, Geophysical Prospecting 13, 245-258.

Linsser, H., 1967. Investigation of tectonics by gravity detailing. Geophysical Prospecting, Vol.

XV, No. 3, 480-515.

Lu, J. M., 1982. The principle of seismic exploration (in Chinese). Published by the Petroleum Industry Press, Beijing.

Malzac, J. and Rousseau, A., 1978. A "processing density" to calculate marine Bouguer gravity free of topographic variations in case of unknown bottom density, Geophysical Prospecting, 26, 853-867.

Mansfield, J., and Kennett. P. 1963. A gravity survey of the Stranraer sedimentary basin. Proceedings of the Yorkshire Geological Society, 34, 139-151.

Mclean, A. C. and Qureshi, I. R., 1964-1965. Regional gravity anomalies in the Western Midland Valley of Scotland. Trans. Roy. Soc. Edin., Vol. LXVI., No. 11.

Mcmechan, G. A. and Ottolini, R., 1980. Direct observation of a p-t curve in a slant stacked wave field. Bulletin of the SEIS. Soci. America. Vol. 70, N0. 3, 775-789.

McMechan, G. A., 1983. p-x imaging by localized slant stacks of t-x data. Geophys. J. R. astr. Soc. 72. 213-221.

Merlin Geophysical (Research) Ltd. SKS Users Manual.

Mithal, R. and Vera, E. E., 1987. Comparison of plane-wave decomposition and slant stacking of point-source seismic data. Geophysics, Vol. 52, No. 12, 1631-1638.

Mu, Y. G., 1981. Seismic data processing methods (in Chinese). Published by the Petroleum Industry Press, Beijing.

Nagy, D., 1966. The gravitational attraction of a right rectangular prism. Geophysics, 31, 362-371.

Nettleton, L. L., 1939. Determination of density for reduction of gravimeter observations. Geophysics, 4, 176-183.

Nettleton, L. L., 1954. Regionals, residuals, and structures. Geophysics, Vol. XIX, No. 1, 1- 23.

Oldham, C. H. G., 1954. The correlation between Pre-cambrain rock densities and Bouguer gravity anomalies near parry sound, Ontario. Geophysics, Vol. 1, 76-88.

Parslow, G. R. and Randall, B. A. O., 1973. A gravity survey of the Cairnsmore of Fleet granite and its environs. Scott. J. Geol. 9 (3), 219- 231.

Pujol, J. and Fuller. B. N., 1989. Interpretation of a vertical seismic profile conducted in the Columbia Plateau basalts. Geophysics, Vol. 54, No. 10, 1258-1266.

Rene, R. M., et al, 1986. Multicomponent seismic studies using complex trace analysis. Geophysics, Vol. 51, No. 6, 1235-1251.

Robinson, E. A. and Durrani, T. S., 1986. Geophysical Signal Processing. The University Press, Cambridge.

Rosenbach, O., 1953. Quantitative studies concerning the vertical gradient and second derivative methods of gravity interpretation. Geophysical Prospecting, II, 128-138.

Rosenbach, O., 1953. A contribution to the computation of the "second derivative" from gravity data. Geophysics, Vol. 18, 894-912

Sandberg, C. H., 1958. Terrain corrections for an inclined plane in gravity computations. Geophysics,18, 701-711.

Schultz, P. S., 1982. A method for direct estimation of interval velocities. Geophysics, Vol. 47, No. 12, 1657-1671.

Selem. A. M. and Monnet, C., 1953. Application of vertical gradients and comparison of different geophysical methods in a difficult area. Geophysical Prospecting, Vol. 1, No.3, 208-219.

Shimshoni, M. and Smith, S. W., 1964. Seismic signal enhancement with three-component detectors. Geophysics, Vol. XXIX, No. 5, 664-671.

Simpson, S. M., 1954. Least squares polynomial fitting to gravitational data and density plotting by digital computers. Geophysics, Vol. 19, 255-269.

Sissons, B. A., 1981. Densities determined from surface and subsurface gravity measurements. Geophysics, Vol. 46, No. 11, 1568-1571.

Smithson, S. B., Fuller, B., Pujol, J. and Woods, T., 1986. Final Report for 1985. University of Wyoming Volcanic Reflection Research Project.

Smythe, D. K., 1988. A note on BIRPS S-wave experiment 1988 - Field layout of the Glasgow piggyback experiment (unpublished).

Stoffa, L. P. and Buhl, P., 1981. Direct mapping of seismic data to the domain of intercept time and ray parameter- A plane-wave decomposition. Geophysics, Vol. 46, No. 3, 255 - 267.

Swartz, C. A., 1954. Some geometrical properties of residual maps. Geophysics, Vol. 1, 46-70.

Takin, M. and Talwani, M., 1966. Rapid computation of the gravitation attraction of topography on a spherical earth. Geophysical Prospecting, Vol. XIV, 119-142.

Talwani, M., Worzel, J. L. and Landisman, M., 1959. Rapid gravity computations for two-dimensional bodies with application to the Mendocino Submarine Fracture Zone. J. of Geophysical research, Vol. 64, No. 1, 49-59 .

Talwani, M. and Ewing, M., 1960. Rapid computation of gravitational attraction of three-dimensional bodies of arbitrary shape. Geophysics, Vol. XXV, No. 1, 203-225.

Taner, M. T., et al, 1979. Complex seismic trace analysis. Geophysics, Vol. 44, No. 6, 1041-1063.

Tatham, R. H., et al, 1976. Vp/Vs - A potential hydrocarbon indicator. Geophysics, Vol. 41, No. 5, 837-849.

Tatham, R. H., 1982. Vp/Vs and lithology. Geophysics, Vol. 47, No. 3, 336-344.

Tatham, R. H., et al, 1983. Seismic shear-wave observations in a physical model experiment. Geophysics, Vol. 48, No. 6, 688-701.

Tatham, R. H., et al, 1984. Separation of S-wave and P-wave reflections offshore western Florida. Geophysics, Vol. 49, No. 5, 493-508.

Tompkins, C. B. and Willson W. L. 1969. Elementary Numerical Analysis.

Treitel, S., Gutowski, P. R. andWagner, D. E., 1982. Plane-wave decomposition of seismograms. Geophysics, Vol. 47, No. 10, 1375-1401.

Trejo, C. A., 1954. A note on downward continuation of gravity. Geophysics, Vol. 1, 71-75.

Vajk, R., 1956. Bouguer corrections with varying surface density. Geophysics, Vol. XXI, No. 4, 1004-1020.

Waters. K. H., 1978. Reflection seismology. A tool for energy resource exploration. A Wiley-interscience Publication.

Wiggins, R. A., 1967. Use of expected error in the design of least-squares optimum filters. Geophysical Prospecting, Vol. XV, No. 2, 288-296.

Yilmaz, O., 1988. Seismic data processing. (Investigation in Geophysics, Volume 2), Society of Exploration Geophysicists.

Appendices

FORTRAN-77 PROGRAM 1 - MATERRAIN

```
c     ********************************************************
c     Bougeur anormaly calculation program on VAX/UNIX: MATERRAIN   *
c     Designed and written by                                       *
c     XIN-QUAN MA                                                   *
c     at the Department of Geology & Applied Geology,               *
c     University of Glasgow Glasgow G12 8QQ ( in 1987).             *
c     This program is used for automatic Bougeor anomaly calculation.*
c     The distinctive advantage is its automatic terrain correction.*
c     ********************************************************
      parameter(m=708,n=4528)
      integer N,L,K,I,Q,J(m),W(n)
      real E(n),F(n),den(n),H(n),z1(n),z2(n),z3(n),z4(n),XX(m),YY(m),
     z d(m),h1(m),h2(m),h3(m),h4(m),h5(m),h6(m),h7(m),h8(m),lati(n),
     z h9(m),h10(m),h11(m),h12(m),h13(m),h14(m),h15(m),h16(m),x(16),
     z y(16),r(16),b(16),G(4),r0,lati(n),g0(n),gb(n),ga(n),gt(n),
     z gf(n),go(n),a1,a2,a3,a4,b1,b2,b3,b4,c1,c2,c3,c4,c5,c6,RT,
     z c7,c8,d1,d2,d3,d4,d5,d6,d7,d8,t11(n),t22(n),ht1,ht2,ht3,u,
     z ht4,z11(n),z22(n),z33(n),z44(n),GG,GG1,GG2,GG3,GG4,t33(n),
     z k1,k2,k3,k4,k11,k22,k33,k44,l1,l2,l3,l4,l11,l22,l33,l44,
     z O,O1,O2,O3,O4,P,P1,P2,P3,P4,S,S1,S2,S3,S4,T,T1,T2,T3,T4,
     z x1,x2,x3,x4,y1,y2,y3,y4,TDK
      open(unit=1,file='stdata5',form='formatted',access='sequential',
     z status='old')
      open(unit=2,file='bldata2',form='formatted',access='sequential',
     z status='old')
      open(unit=3,file='output',form='formatted',access='sequential',
     z status='new')
      open(unit=4,file='correct',form='formatted',access='sequential',
     z status='new')
c     read station discription data and block discription data into
c     related arrays
      do 20 K=1,n
      read(unit=1,fmt=10) W(K),lati(K),E(K),F(K),H(K),z11(K),z22(K),
     z  z33(K),z44(K),den(K),go(K)
10    format(I5,F9.4,F8,F8,F7.1,4(F7.1),F5.2,F8.2)
```

```
20    continue
      do 50 I=1,m
      read(unit=2,fmt=30)  J(I),XX(I),YY(I),d(I),h1(I),h2(I),h3(I),
     z h4(I),h5(I),h6(I)
      read(unit=2,fmt=40)  h7(I),h8(I),h9(I),h10(I),h11(I),h12(I),
     z h13(I),h14(I),h15(I),h16(I)
30    format(I5,2X,F7,2X,F7,2X,F4.2,6(2X,F6.1))
40    format(10(2X,F6.1))
50    continue
      write(unit=3,fmt=55)  'no.','E','F','gt','gf','gb',
     z 'go','g0','ga'
55    format(2X,A3,4X,A1,8X,A1,9X,A2,6X,A2,7X,A2,7X,A2,8X,A2,9X,A2)
      do 300 K=1,n
      do 200 I=1,m
      b(1)=h1(I)
      b(2)=h2(I)
      b(3)=h3(I)
      b(4)=h4(I)
      b(5)=h5(I)
      b(6)=h6(I)
      b(7)=h7(I)
      b(8)=h8(I)
      b(9)=h9(I)
      b(10)=h10(I)
      b(11)=h11(I)
      b(12)=h12(I)
      b(13)=h13(I)
      b(14)=h14(I)
      b(15)=h15(I)
      b(16)=h16(I)
c     dividing terrain into 7 zones: 1. r0<0.5km;     2. 0.5<r0<2km;
c     3. 2<r0<15km;  4. 15<r0<20km;  5. 20<r0<30km;  6. 30<r0<50km;
c     7. r0>50km.
      r0=sqrt((XX(I)-E(K))**2+(YY(I)-F(K))**2)
      if(r0.LE.15000) go to 60
      if(r0.LE.20000) go to 100
      if(r0.LT.30000) go to 58
      if(r0.LT.50000) go to 56
      go to 200
c     approximating terrain(prism) as a line with all mass centraled
c     on it. formula: gt=G*D*A*h**2/2*r**3.
56    u=(h1(I)+h2(I)+h3(I)+h4(I)+h5(I)+h6(I)+h7(I)+h8(I)+h9(I)+
     z h10(I)+h11(I)+h12(I)+h13(I)+h14(I)+h15(I)+h16(I))/16
```

```
      TDK=abs(3336*16*d(I)*(u-H(K))**2/r0**3)
       t33(K)=t33(K)+TDK
      gt(K)=gt(K)+TDK
      go to 200
c     approximating terrain as prism with 4km long sides.
c     formula:  gt=G*D*A*h**2/2*r**3-r*4E06).
58    u=(h1(I)+h2(I)+h3(I)+h4(I)+h5(I)+h6(I)+h7(I)+h8(I)+h9(I)+
     z h10(I)+h11(I)+h12(I)+h13(I)+h14(I)+h15(I)+h16(I))/16
      TDK=abs(3336*16*d(I)*(u-H(K))**2/(r0**3-r0*4E6))
      t33(K)=t33(K)+TDK
      gt(K)=gt(K)+TDK
      go to  200
60    x(1)=XX(I)-1500
      y(1)=YY(I)-1500
      r(1)=sqrt((x(1)-E(K))**2+(y(1)-F(K))**2)
      x(2)=XX(I)-500
      y(2)=YY(I)-1500
      r(2)=sqrt((x(2)-E(K))**2+(y(2)-F(K))**2)
      x(3)=XX(I)-1500
      y(3)=YY(I)-500
      r(3)=sqrt((x(3)-E(K))**2+(y(3)-F(K))**2)
      x(4)=XX(I)-500
      y(4)=YY(I)-500
      r(4)=sqrt((x(4)-E(K))**2+(y(4)-F(K))**2)
      x(5)=XX(I)+500
      y(5)=YY(I)-1500
      r(5)=sqrt((x(5)-E(K))**2+(y(5)-F(K))**2)
      x(6)=XX(I)+1500
      y(6)=YY(I)-1500
      r(6)=sqrt((x(6)-E(K))**2+(y(6)-F(K))**2)
      x(7)=XX(I)+500
      y(7)=YY(I)-500
      r(7)=sqrt((x(7)-E(K))**2+(y(7)-F(K))**2)
      x(8)=XX(I)+1500
      y(8)=YY(I)-500
      r(8)=sqrt((x(8)-E(K))**2+(y(8)-F(K))**2)
      x(9)=XX(I)-1500
      y(9)=YY(I)+500
      r(9)=sqrt((x(9)-E(K))**2+(y(9)-F(K))**2)
      x(10)=XX(I)-500
      y(10)=YY(I)+500
      r(10)=sqrt((x(10)-E(K))**2+(y(10)-F(K))**2)
```

```
      x(11)=XX(I)-1500
      y(11)=YY(I)+1500
      r(11)=sqrt((x(11)-E(K))**2+(y(11)-F(K))**2)
      x(12)=XX(I)-500
      y(12)=YY(I)+1500
      r(12)=sqrt((x(12)-E(K))**2+(y(12)-F(K))**2)
      x(13)=XX(I)+500
      y(13)=YY(I)+500
      r(13)=sqrt((x(13)-E(K))**2+(y(13)-F(K))**2)
      x(14)=XX(I)+1500
      y(14)=YY(I)+500
      r(14)=sqrt((x(14)-E(K))**2+(y(14)-F(K))**2)
      x(15)=XX(I)+500
      y(15)=YY(I)+1500
      r(15)=sqrt((x(15)-E(K))**2+(y(15)-F(K))**2)
      x(16)=XX(I)+1500
      y(16)=YY(I)+1500
      r(16)=sqrt((x(16)-E(K))**2+(y(16)-F(K))**2)
      do 80 Q=1,16
      if(E(K).GT.(x(Q)-500).AND.E(K).LT.(x(Q)+500).AND.
     z F(K).GT.(y(Q)-500).AND.F(K).LT.(y(Q)+500)) go to 85
      if(r(Q).GE.2000)  go to 83
c     calculating terrain correction in the inner zone(0.5<r0<2 km)
c     approximate terrain to a vertical prism with horizontal lower
c     face and slopping upper surface whose slop is constant toward
c     the station point.
c     formula:  g=G*p*(1-cosa)*D*K(i,j)
c     1-cosa=0.5*tan(a)**2
      TDK=6672*d(I)*(1/r(Q)-1/sqrt((b(Q)-H(K))**2+r(Q)**2))
      t22(K)=t22(K)+TDK
      gt(K)=gt(K)+TDK
      go to 80
83    TDK=3336*d(I)*(b(Q)-H(K))**2/(r(Q)**3-r(Q)*2.5E05)
      t33(K)=t33(K)+TDK
      gt(K)=gt(K)+TDK
      go to 80
c     calculating terrain correction for the most inner zone(r0<0.5km) by
c     dividing square into four triangle prisms.
85    z1(K)=abs(z11(K)-H(K))
      z2(K)=abs(z22(K)-H(K))
      z3(K)=abs(z33(K)-H(K))
      z4(K)=abs(z44(K)-H(K))
      x1=x(Q)-E(K)+500
```

```
y1=y(Q)-F(K)-500
x2=x1
y2=500+y(Q)-F(K)
x3=x(Q)-E(K)-500
y3=y2
x4=x3
y4=y1
a1=(z1(K)*y2-z2(K)*y1)/(x1*y2-x2*y1)
b1=(x1*z2(K)-x2*z1(K))/(x1*y2-x2*y1)
a2=(z2(K)*y3-z3(K)*y2)/(x2*y3-x3*y2)
b2=(x2*z3(K)-x3*z2(K))/(x2*y3-x3*y2)
a3=(z3(K)*y4-z4(K)*y3)/(x3*y4-x4*y3)
b3=(x3*z4(K)-x4*z3(K))/(x3*y4-x4*y3)
a4=(z4(K)*y1-z1(K)*y4)/(x4*y1-x1*y4)
b4=(x4*z1(K)-x1*z4(K))/(x4*y1-x1*y4)
c1=(z1(K)*y2+z2(K)*y1)/(x1*y2-x2*y1)
d1=(-x1*z2(K)-x2*z1(K))/(x1*y2-x2*y1)
c2=(-z1(K)*y2-z2(K)*y1)/(x1*y2-x2*y1)
d2=(x1*z2(K)+x2*z1(K))/(x1*y2-x2*y1)
c3=(z2(K)*y3+z3(K)*y2)/(x2*y3-x3*y2)
d3=(-x2*z3(K)-x3*z2(K))/(x2*y3-x3*y2)
c4=(-z2(K)*y3-z3(K)*y2)/(x2*y3-x3*y2)
d4=(x2*z3(K)+x3*z2(K))/(x2*y3-x3*y2)
c5=(z3(K)*y4+z4(K)*y3)/(x3*y4-x4*y3)
d5=(-x3*z4(K)-x4*z3(K))/(x3*y4-x4*y3)
c6=(-z3(K)*y4-z4(K)*y3)/(x3*y4-x4*y3)
d6=(x3*z4(K)+x4*z3(K))/(x3*y4-x4*y3)
c7=(z4(K)*y1+z1(K)*y4)/(x4*y1-x1*y4)
d7=(-x4*z1(K)-x1*z4(K))/(x4*y1-x1*y4)
c8=(-z4(K)*y1-z1(K)*y4)/(x4*y1-x1*y4)
d8=(x4*z1(K)+x1*z4(K))/(x4*y1-x1*y4)
k1=y1/x1
k2=y2/x1
k3=y2/x3
k4=y4/x3
k11=1/k1
k22=1/k2
k33=1/k3
k44=1/k4
l1=-c1/d1
l2=-c3/d3
l3=-c5/d5
```

```
      l4=-c7/d7
      l11=1/l1
      l22=1/l2
      l33=1/l3
      l44=1/l4
c     using subroutines to calculate terrain correction produced by
c     four triangle prisms
c     triangle prism 1.
      call INNERZONE1(a1,b1,k2,k1,x1,GG1)
c     triangle prism 2.
      call INNERZONE1(b2,a2,k22,k33,y2,GG2)
c     triangle prism 3.
      call INNERZONE1(a3,b3,k3,k4,x3,GG3)
c     triangle prism 4.
      call INNERZONE1(b4,a4,k11,k44,y1,GG4)
      GG=GG1+GG2+GG3+GG4
c     considering symboles of four height values in the four conners
c     of that square,overestimated terrain correction must be substracted
c     by the values resulting from central triangle prisms.
c     central triangle prism 1.
      call INNERZONE2 (c1,d1,l1,k1,x1,P1)
      call INNERZONE2 (a1,b1,l1,k1,x1,P2)
      call INNERZONE2 (c2,d2,k2,l1,x1,P3)
      call INNERZONE2 (a1,b1,k2,l1,x1,P4)
      P=P1-P2+P3-P4
c     central triangle prism 2.
      call INNERZONE2 (d4,c4,l22,k33,y2,O1)
      call INNERZONE2 (b2,a2,l22,k33,y2,O2)
      call INNERZONE2 (d3,c3,k22,l22,y2,O3)
      call INNERZONE2 (b2,a2,K22,l22,y2,O4)
      O=O1-O2+O3-O4
c     central triangle prism 3.
      call INNERZONE2 (c6,d6,l3,k4,x3,S1)
      call INNERZONE2 (a3,b3,l3,k4,x3,S2)
      call INNERZONE2 (c5,d5,k3,l3,x3,S3)
      call INNERZONE2 (a3,b3,k3,l3,x3,S4)
      S=S1-S2+S3-S4
c     central triangle prism 4.
      call INNERZONE2 (d7,c7,l44,k44,y1,T1)
      call INNERZONE2 (b4,a4,l44,k44,y1,T2)
      call INNERZONE2 (d8,c8,k11,l44,y1,T3)
      call INNERZONE2 (b4,a4,k11,l44,y1,T4)
      T=T1-T2+T3-T4
```

```
c       comparing the four heights of prism corners with station
c       height,deciding the exact correction value for the inner zone.
        ht1=z11(K)-H(K)
        ht2=z22(K)-H(K)
        ht3=z33(K)-H(K)
        ht4=z44(K)-H(K)
        if(ht1.gt.0) go to 500
        if(ht2.gt.0) go to 480
        if(ht3.gt.0) go to 450
        if(ht4.gt.0) go to 430
        RT=GG
        go to 900
430     RT=GG-S-T
        go to 900
450     if(ht4.gt.0) go to 460
        RT=GG-O-S
        go to 900
460     RT=GG-O-T
        go to 900
480     if(ht3.gt.0) go to 490
        if(ht4.gt.0) go to 485
        RT=GG-P-O
        go to 900
485     RT=GG-P-O-S-T
        go to 900
490     if(ht4.gt.0) go to 495
        RT=GG-P-S
        go to 900
495     RT=GG-P-T
        go to 900
500     if(ht2.gt.0) go to 600
        if(ht3.gt.0) go to 550
        if(ht4.gt.0) go to 530
        RT=GG-P-T
        go to 900
530     RT=GG-P-S
        go to 900
550     if(ht4.gt.0) go to 580
        RT=GG-P-S-O-T
        go to 900
580     RT=GG-P-O
        go to 900
```

```
600   if(ht3.gt.0) go to 700
      if(ht4.gt.0) go to 650
      RT=GG-O-T
      go to 900
650   RT=GG-O-S
      go to 900
700   if(ht4.gt.0) go to 800
      RT=GG-S-T
      go to 900
800   RT=GG
900   TDK=abs(0.006672*d(I)*RT)
      t11(K)=t11(K)+TDK
      gt(K)=gt(K)+TDK
 80   continue
      go to 200
c     approximating terrain as prisms with 2km long sides.
c     formula:  gt=G*D*A*h**2/2*(r**3-r*1E06).
 100  r(1)=sqrt((XX(I)-1000-E(K))**2+(YY(I)-1000-F(K))**2)
      r(2)=sqrt((XX(I)+1000-E(K))**2+(YY(I)-1000-F(K))**2)
      r(3)=sqrt((XX(I)-1000-E(K))**2+(YY(I)+1000-F(K))**2)
      r(4)=sqrt((XX(I)+1000-E(K))**2+(YY(I)+1000-F(K))**2)
      G(1)=(h1(I)+h2(I)+h3(I)+h4(I))/4
      G(2)=(h5(I)+h6(I)+h7(I)+h8(I))/4
      G(3)=(h9(I)+h10(I)+h11(I)+h12(I))/4
      G(4)=(h13(I)+h14(I)+h15(I)+h16(I))/4
      do 110 L=1,4
      TDK=abs(3336*4*d(I)*(G(L)-H(K))**2/(r(L)**3-r(L)*1E6))
      t33(K)=t33(K)+TDK
      gt(K)=gt(K)+TDK
110   continue
 200  continue
      write(4,220)  W(K),t11(K),t22(K),t33(K),gt(K)
 220  format(I5,5X,4(F8.4,5X))
c     calculating normal gravity by using international formula
      g0(K)=978031.85*(1+0.0053024*(sin(lati(K)*3.1416/180))**2
     z -0.0000059*(sin(lati(K)*3.1416/90))**2)
c     Free-air correction
      gf(K)=0.3086*H(K)
c     Bouguer correction
      gb(K)=0.04193*den(K)*H(K)
c     calculating Bouguer anomaly
      ga(K)=(go(K)+980000)+gt(K)+gf(K)-gb(K)-g0(K)
      print 250,  W(K),E(K),F(K),H(K),gt(K),gf(K),gb(K),go(K),g0(K),ga(K)
```

```
      write(3,250)  W(K),E(K),F(K),H(K),gt(K),gf(K),gb(K),go(K),g0(K),ga(K)
250   format(I4,1X,2(1X,F7),F7.1,3(2X,F6.2),2X,F7.2,2X,F9.2,2X,F6.2)
300   continue
      close(unit=3)
      close(unit=4)
      stop
      end
c
c     ************************************************************
c     subprogram for calculating the terrain correction of triangle volume
c     with the horizontal lower face and the sloping upper face.
      subroutine INNERZONE1(aa,bb,kk,ll,ss,FF)
      real  aa,bb,gg,hh,kk,ll,oo,pp,qq,rr,ss,tt,FF
      oo=aa*aa+1
      pp=bb*bb+1
      tt=1/sqrt(pp)
      gg=kk+sqrt(1+kk*kk)
      hh=ll+sqrt(1+ll*ll)
      qq=sqrt((kk+aa*bb/pp)**2+oo/pp-aa*aa*bb*bb/(pp*pp))
      rr=sqrt((ll+aa*bb/pp)**2+oo/pp-aa*aa*bb*bb/(pp*pp))
      FF=ss*(log(gg/hh)-tt*log((kk+aa*bb/pp+qq)/(ll+aa*bb/pp+rr)))
      return
      end
c     ************************************************************
c     &&&&&&&&&&&&&&&&&&&&&&&&&&&&&&&&&&&&&&&&&&&&&&&&&&&&&&&&&&
      subroutine INNERZONE2(aa,bb,kk,ll,ss,FF)
      real  aa,bb,kk,ll,oo,pp,qq,rr,ss,tt,FF
      oo=aa*aa+1
      pp=bb*bb+1
      tt=1/sqrt(pp)
      qq=sqrt((kk+aa*bb/pp)**2+oo/pp-aa*aa*bb*bb/pp**2)
      rr=sqrt((ll+aa*bb/pp)**2+oo/pp-aa*aa*bb*bb/pp**2)
      FF=ss*tt*log((kk+aa*bb/pp+qq)/(ll+aa*bb/pp+rr))
      return
      end
c     &&&&&&&&&&&&&&&&&&&&&&&&&&&&&&&&&&&&&&&&&&&&&&&&&&&&&&&&&&
```

FORTRAN-77 PROGRAM 2 - MASEGY

```
C*************************************************************
C       CHANGING SEGY FORMAT PROGRAM ON VAX/VMS SYSTEM, MASEGY      *
C       ORIGINALLY WRITTEN BY                                       *
C       OVE HANSEN,  IN 1988.                                       *
C       MODIFIED BY                                                 *
C       XIN-QUAN MA                                                 *
C       AT THE DEPARTMENT OF GEOLOGY & APPLIED GEOLOGY,             *
C       UNIVERSITY OF GLASGOW GLASGOW Q12 8QQ (IN 1989)             *
C       THIS PROGRAM IS TO CHANGE SEGY FORMAT INTO ANY REQUIRED ASCII *
C       CODED FORMAT BY CALLING SKS SUBROUTINES.                    *
C*************************************************************
        INCLUDE 'PROCCOM.FOR'
        INCLUDE 'CONSTANTS.FOR'
        INCLUDE 'RHWCOM.FOR'
        CHARACTER * ( 30  ) QUAL
        CHARACTER * ( 30 ) FILE
        CHARACTER * ( 10 ) STATUS
        CHARACTER * (7)   FILEOUT
        CHARACTER * ( ULNPTH ) PATH
        INTEGER LFC, IOTABL( 18 ), ITRACE, NSAMPL, HEADER(200), LHEAD,
     : IEOF, IERR, IASG1, IASG2, NREC, LRECL, IMODE, TRACE
        INTEGER LTRACE,STRACE
        REAL    BUFFER( 800, 800 ), HOST( 5000 ), TAPE( 5000 )
        EXTERNAL DEFLFC,UDEFIN,DSKINQ,DSKOPN,DSKHED
C       INITIALIZE THE INPUT & OUTPUT TABLES TO ZERO
        DO 10 I=1,18
        IOTABL(I)=0
10      CONTINUE
        WRITE(*,*)  '--FILE QUALIFIER :'
        READ (*,'( A )')  QUAL
        write (*,*) '--FILE NAME : '
        READ (*, '( A )') FILE
        UTRCLN = 160
        CALL DEFLFC ( LFC )
        CALL UDEFIN ( LFC, NREC, LRECL, IMODE, IOTABL )
        CALL DSKINQ ( QUAL, FILE, IERR, IASG1, IASG2 )
        IF ( IERR .NE. 1 ) THEN
        WRITE (*,*) '*** INPUT FILE NOT FOUND ***'
        ENDIF
        CALL DSKOPN ( LFC, IOTABL, QUAL, FILE )
```

```
      CALL DSKHED ( LFC, IOTABL, QUAL, FILE, HEADER, RHWLEN )
      WRITE(*,*) 'TRACE COMMON LENGTH (UTRCLN)=',UTRCLN
      WRITE(*,*) 'LENGTH OF TRACE HEADER(RHWTHL)=',RHWTHL
      WRITE(*,*) 'SAMPLES PER TRACE(RHWNSM) =          ',RHWNSM
      WRITE(*,*) 'NUMBER OF TRACES IN FILE(RHWNRC) =   ',RHWNRC
      IF ( RHWTHL .GT. 160 ) THEN
      WRITE(*,*) 'NON-STANDARD HEADER LENGTH(>160) '
      ERROR = .TRUE.
      ENDIF
      WRITE(*,*) '--INPUT FIRST TRACE NUMBER YOU WANT TO READ'
      READ ( *, * ) ITRACE
      NTRACE = RHWNRC - ITRACE + 1
      STRACE = ITRACE
      WRITE(*,*) '--INPUT LAST TRACE NUMBER YOU WANT TO READ '
      READ(*, *)  LTRACE
      WRITE(*,*) ' --INPUT FIRST SAMPLE YOU WANT TO READ  '
      READ ( *, * ) ISAMPL
      NSAMPL = RHWNSM - ISAMPL + 1
      JTRACE = ITRACE - 1
      ITRACE = ITRACE - 1
100   ITRACE = ITRACE + 1
      CALL DSKTIN ( LFC, IOTABL, ITRACE, HOST, TAPE, RHWNSM,
     : IEOF, HEADER )
      CALL DSKFMT ( HOST, TAPE, RHWNSM )
      DO 200 I = 1, NSAMPL
      BUFFER ( ITRACE - JTRACE, I ) =
     : HOST ( I + ISAMPL - 1)
200   CONTINUE
      IF ( IEOF .EQ. 0 .AND. ITRACE .GE. LTRACE ) GO TO 999
      GO TO 100
C     WRITE DATA IN THE BUFFER INTO FILE
999   WRITE(*,*) '--INPUT FILE NAME FOR OUTPUT'
      READ(*,'(A)') FILEOUT
      OPEN(1,FILE=FILEOUT,FORM='FORMATTED',STATUS='NEW')
      PRINT*,'NO. OF TRACES TO WRITE=',LTRACE-STRACE+1
      PRINT*,'NSAMPL=',NSAMPL
      DO 888 I=1,LTRACE-STRACE+1
      DO 777 J=1,NSAMPL
      WRITE(1,889)  I,J,BUFFER(I,J)
889   FORMAT( 2I5,E18.8)
777   CONTINUE
      PRINT*,' THE TRACE ', I, '  COMPLETED'
```

```
888   CONTINUE
      CLOSE ( 1 )
      STOP
      END
```

FORTRAN-77 PROGRAM 3 - MATRAN

```
C     ************************************************************
C     THREE-COMPONENT SEISMIC DATA ROTATION PROGRAM ON            *
C     THE VAX/VMS SYSTEM: MATRAN                                  *
C     DESIGNED AND WRITTEN BY                                     *
C     XIN-QUAN MA                                                 *
C     AT THE DEPARTMENT OF GEOLOGY & APPLIED GEOLOGY              *
C     UNIVERSITY OF GLASGOW GLASGOW G12 8QQ (IN 1989)             *
C     THE PURPOSE OF THIS PROGRAM IS TO TRANSFORM FEILD COORDINATE *
C     SYSTEM (VERT, NORTH, EAST) INTO A REQUIRED SYSTEM (VERTICAL, *
C     RADIAL,TRANSVERSE). VERTICAL TRACE IS KEPT INTACT. THE OTHER *
C     TRACES AS A VECTOR AT A SPECIFIC TIME HAVE BEEN PROJECTED   *
C     ONTO NEW SYSTEM. FOR ONE SHOTPOINT, 12 ANGLES OF RADIAL LINES *
C     TO MAGNETIC NORTH ARE SET IN THE PROGRAM. AFTER THE OLD DATA *
C     HAVE BEEN INPUT, THE NEW DATA IN THE DIFFERENT ORDER ARE THE *
C     OUTPUTS.                                                    *
C     ************************************************************
      REAL  XYZ(100,800),XX(20,800),YY(20,800),ZZ(20,800)
      REAL  ALPHA,PI
      INTEGER  STNUMB,NORTHCH,EASTCH,VERTCH,NSAMPL,NTRACE
      INTEGER  III
      CHARACTER * 8  INFILE,OUTFILE
      PRINT*,'--INPUT FILE NAME TO BE TRANSLATED'
      READ(*,'(A)')  INFILE
      NTRACE = 48
      NSAMPL = 501
      OPEN(1,FILE=INFILE,STATUS='OLD')
      PRINT*,'--INPUT FILE NAME FOR OUTPUT'
      READ(*,'(A)')  OUTFILE
      OPEN(2,FILE=OUTFILE,STATUS='NEW')
      PRINT*,'--START READING DATA INTO ARRAY '
C     READ THE 3-COMPONENT DATA INTO ARRAY XYZ(I,J)
C     THE DATA IN THE ARRAY XYZ(I,J) ARE PRODUCED BY PROGRAM
C     MARDDISK.FOR, I IS  CHANNEL, J IS SAMPLE
      DO 200 I=1, NTRACE
      DO 100 J=1, NSAMPL
      READ(1,50) M, N, XYZ(I,J)
50    FORMAT(2I5,E18.8)
100   CONTINUE
200   CONTINUE
```

```
      PI=3.14159/180
C     INPUT STATION NUMBER
      III=0
99    PRINT*,'--INPUT STATION NUMBER(TYPE "0" TO STOP) '
      READ*, STNUMB
      III=III+ 1
      IF(STNUMB.EQ.1) GO TO   300
      IF(STNUMB.EQ.2) GO TO   400
      IF(STNUMB.EQ.3) GO TO   500
      IF(STNUMB.EQ.4) GO TO   600
      IF(STNUMB.EQ.5) GO TO   700
      IF(STNUMB.EQ.6) GO TO   800
      IF(STNUMB.EQ.7) GO TO   900
      IF(STNUMB.EQ.8) GO TO   1000
      IF(STNUMB.EQ.9) GO TO   1100
      IF(STNUMB.EQ.10) GO TO  1200
      IF(STNUMB.EQ.11) GO TO  1300
      IF(STNUMB.EQ.12) GO TO  1400
      IF(STNUMB.EQ.0) GO TO   9999
300   PRINT*,'--INPUT VERTICAL,NORTH,EAST TRACE NUMBERS'
C     THE ORIGINAL DATA HAVE SEQUENCES FROM  VERTICAL,NORTH,EAST
C     WHICH ARE CORRESPONDING FIELD CHANNEL SEQUENCES.
C     REMEMBER INPUTING  DATA IN CORRECT ORDER.
      READ*, VERTCH,NORTHCH,EASTCH
C     A IS ANGLE OF ROTATION IN THE POSITIVE DIRECTION
      ALPHA=346.5*PI
      DO 350 J=1,NSAMPL
      CALL TRANSLT(ALPHA,XYZ(NORTHCH,J),XYZ(EASTCH,J),XX(STNUMB,J),
     Z            YY(STNUMB,J) )
      ZZ(STNUMB,J)=XYZ(VERTCH,J)
350   CONTINUE
      GO TO 99
400   PRINT*,'--INPUT VERTICAL NORTH AND EAST TRACE NUMBER'
      READ*, VERTCH,NORTHCH,EASTCH
C     A IS ANGLE OF ROTATION IN THE POSITIVE DIRECTION
      ALPHA = 316.5*PI
      DO 450 J=1,NSAMPL
      CALL TRANSLT(ALPHA,XYZ(NORTHCH,J),XYZ(EASTCH,J),XX(STNUMB,J),
     Z            YY(STNUMB,J) )
      ZZ(STNUMB,J)=XYZ(VERTCH,J)
450   CONTINUE
      GO TO 99
500   PRINT*,'--INPUT VERTICAL NORTH AND EAST TRACE NUMBER'
```

```
      READ*, VERTCH,NORTHCH,EASTCH
C     A IS ANGLE OF ROTATION IN THE POSITIVE DIRECTION
      ALPHA = 286.5*PI
      DO 550 J=1,NSAMPL
      CALL TRANSLT(ALPHA,XYZ(NORTHCH,J),XYZ(EASTCH,J),XX(STNUMB,J),
     Z          YY(STNUMB,J) )
      ZZ(STNUMB,J)=XYZ(VERTCH,J)
550   CONTINUE
      GO TO 99
600   PRINT*,'--INPUT VERTICAL NORTH AND EAST TRACE NUMBER'
      READ*, VERTCH,NORTHCH,EASTCH
C     A IS ANGLE OF ROTATION IN THE POSITIVE DIRECTION
      ALPHA = 256.5*PI
      DO 650 J=1,NSAMPL
      CALL TRANSLT(ALPHA,XYZ(NORTHCH,J),XYZ(EASTCH,J),XX(STNUMB,J),
     Z          YY(STNUMB,J) )
      ZZ(STNUMB,J)=XYZ(VERTCH,J)
650   CONTINUE
      GO TO 99
700   PRINT*,'--INPUT VERTICAL NORTH AND EAST TRACE NUMBER'
      READ*, VERTCH,NORTHCH,EASTCH
C     A IS ANGLE OF ROTATION IN THE POSITIVE DIRECTION
      ALPHA = 226.5*PI
      DO 750 J=1,NSAMPL
      CALL TRANSLT(ALPHA,XYZ(NORTHCH,J),XYZ(EASTCH,J),XX(STNUMB,J),
     Z          YY(STNUMB,J) )
      ZZ(STNUMB,J)=XYZ(VERTCH,J)
750   CONTINUE
      GO TO 99
800   PRINT*,'--INPUT VERTICAL NORTH AND EAST TRACE NUMBER'
      READ*, VERTCH,NORTHCH,EASTCH
C     A IS ANGLE OF ROTATION IN THE POSITIVE DIRECTION
      ALPHA = 196.5*PI
      DO 850 J=1,NSAMPL
      CALL TRANSLT(ALPHA,XYZ(NORTHCH,J),XYZ(EASTCH,J),XX(STNUMB,J),
     Z          YY(STNUMB,J) )
      ZZ(STNUMB,J)=XYZ(VERTCH,J)
850   CONTINUE
      GO TO 99
900   PRINT*,'--INPUT VERTICAL NORTH AND EAST TRACE NUMBER'
      READ*, VERTCH,NORTHCH,EASTCH
C     A IS ANGLE OF ROTATION IN THE POSITIVE DIRECTION
```

```
      ALPHA = 166.5*PI
      DO 950 J=1,NSAMPL
      CALL TRANSLT(ALPHA,XYZ(NORTHCH,J),XYZ(EASTCH,J),XX(STNUMB,J),
     Z          YY(STNUMB,J) )
      ZZ(STNUMB,J)=XYZ(VERTCH,J)
950   CONTINUE
      GO TO 99
1000  PRINT*,'--INPUT VERTICAL NORTH AND EAST TRACE NUMBER'
      READ*, VERTCH,NORTHCH,EASTCH
C     A IS ANGLE OF ROTATION IN THE POSITIVE DIRECTION
      ALPHA = 136.5*PI
      DO 1050 J=1,NSAMPL
      CALL TRANSLT(ALPHA,XYZ(NORTHCH,J),XYZ(EASTCH,J),XX(STNUMB,J),
     Z          YY(STNUMB,J) )
      ZZ(STNUMB,J)=XYZ(VERTCH,J)
1050  CONTINUE
      GO TO 99
1100  PRINT*,'--INPUT VERTICAL NORTH AND EAST TRACE NUMBER'
      READ*, VERTCH,NORTHCH,EASTCH
C     A IS ANGLE OF ROTATION IN THE POSITIVE DIRECTION
      ALPHA = 106.5*PI
      DO 1150 J=1,NSAMPL
      CALL TRANSLT(ALPHA,XYZ(NORTHCH,J),XYZ(EASTCH,J),XX(STNUMB,J),
     Z          YY(STNUMB,J) )
      ZZ(STNUMB,J)=XYZ(VERTCH,J)
1150  CONTINUE
      GO TO 99
1200  PRINT*,'--INPUT VERTICAL NORTH AND EAST TRACE NUMBER'
      READ*, VERTCH,NORTHCH,EASTCH
C     A IS ANGLE OF ROTATION IN THE POSITIVE DIRECTION
      ALPHA=76.5*PI
      DO 1250 J=1,NSAMPL
      CALL TRANSLT(ALPHA,XYZ(NORTHCH,J),XYZ(EASTCH,J),XX(STNUMB,J),
     Z          YY(STNUMB,J) )
      ZZ(STNUMB,J)=XYZ(VERTCH,J)
1250  CONTINUE
      GO TO 99
1300  PRINT*,'--INPUT VERTICAL NORTH AND EAST TRACE NUMBER'
      READ*, VERTCH,NORTHCH,EASTCH
C     A IS ANGLE OF ROTATION IN THE POSITIVE DIRECTION
      ALPHA=46.5*PI
      DO 1350 J=1,NSAMPL
      CALL TRANSLT(ALPHA,XYZ(NORTHCH,J),XYZ(EASTCH,J),XX(STNUMB,J),
```

```
     Z          YY(STNUMB,J) )
        ZZ(STNUMB,J)=XYZ(VERTCH,J)
1350    CONTINUE
        GO TO 99
1400    PRINT*,'--INPUT VERTICAL NORTH AND EAST TRACE NUMBER'
        READ*, VERTCH,NORTHCH,EASTCH
C       A IS ANGLE OF ROTATION IN THE POSITIVE DIRECTION
        ALPHA = 16.5*PI
        DO 1450 J=1,NSAMPL
        CALL TRANSLT(ALPHA,XYZ(NORTHCH,J),XYZ(EASTCH,J),XX(STNUMB,J),
     Z          YY(STNUMB,J) )
        ZZ(STNUMB,J)=XYZ(VERTCH,J)
1450    CONTINUE
        GO TO 99
9999    PRINT*,'--START WRITING DATA INTO FILE '
C       THE SEQUENCES OF OUTPUT DATA HAVE BEEN CHANGED INTO XX,YY,ZZ
C       WHICH ARE IMPORTANT FOR NEXT PROGRAM TO KEEP THEM SAME.
        DO 8888 I=1, III-1
        DO 8888 J=1,NSAMPL
        WRITE(2,7777)  I,J,XX(I,J),YY(I,J),ZZ(I,J)
7777    FORMAT(2I5,E18.8,E18.8,E18.8)
8888    CONTINUE
        STOP
        END
C
C       $$$$$$$$$$$$$$$$$$$$$$$$$$$$$$$$$$$$$$$$$$$$$$$$$$$$$$$$$$$$$$$$
C       @@@@@@@@@@@@@@@@@@@@@@@@@@@@@@@@@@@@@@@@@@@@@@@@@@@@@@@@@@@@@@@@
C       THE NEW COORDINATE SYSTEM IS THAT X AXIS POINTS TO THE              @
C       RADICAL DIRECTION FROM THE SHOT POINT, Y AXIS IS                    @
C       PERPENDICULAR TO THE X AXIS 90 DEGREE ANTICLOCKWISE FROM  IT        @
C       THE ROTATING FORMULA IS                                             @
C       X=XO COS A + YO SIN A                                               @
C       Y=-XO SIN A + YO COS A                                              @
C       @@@@@@@@@@@@@@@@@@@@@@@@@@@@@@@@@@@@@@@@@@@@@@@@@@@@@@@@@@@@@@@@
        SUBROUTINE  TRANSLT ( A, XXO,YYO,XXN,YYN)
        REAL A,XXO,YYO,XXN,YYN,B,C
        XXN=XXO*COS(A)+YYO*SIN(A)
        YYN=-XXO*SIN(A)+YYO*COS(A)
        RETURN
        END
C       $$$$$$$$$$$$$$$$$$$$$$$$$$$$$$$$$$$$$$$$$$$$$$$$$$$$$$$$$$$$$$$$
```

FORTRAN-77 PROGRAM 4 - MAPLOT

```
C     ********************************************************
C     SEISMIC DATA DISPLAY PROGRAM ON VAX/VMS:  MAPLOT        *
C     DESIGNED AND WIRRTEN BY                                 *
C     XIN-QUAN  MA                                            *
C     AT THE DEPARTMENT OF GEOLOGY & APPLIED GELOGY,          *
C     UNIVERSITY OF GLASGOW  GLASGOW  G12  8QQ (IN 1989)      *
C     THIS PROGRAM IS TO PLOT SEISMIC DATA AS VAIABLE AREA WIGGLE *
C     TRACES USING POWERFUL UNIRAS GRAPHICS FLIBRARYN ROUTINES *
C     WHICH IC MOUNTED ON VAX/VMS AT THE COMPUTER CENTRE,     *
C     UNVERSITY OF GLASGOW.                                   *
C     THE PROGRAM IS DESIGNED TO DISPLAY 3-COMPONENT SEISMIC DATA *
C     WHICH ARE STORED IN FREE ASCII-CODED FORMAT. THE CHOICE FOR *
C     X, Y, Z DATA DISPLAY IS DETERMINED BY THE USER.         *
C     ********************************************************
      REAL  TRACD,X(501),Y(501),Z(501)
      CHARACTER* 8  COMP,INFILE
      INTEGER   KTYPE,KSLINE
      PRINT*,'--INPUT DATA FILE NAME FOR DISPLAY'
      READ(*,'(A)')   INFILE
      OPEN(1,FILE=INFILE,STATUS='OLD')
11    PRINT*,'--DO YOU WANT TO PLOT WIGGLE LINE WITH VAIABLE '
      PRINT*,'  AREA, INPUT 0 FOR YES, 1 FOR JUST LINE '
      READ*,  KTYPE
      IF(KTYPE.EQ.0) GO TO 18
      IF(KTYPE.EQ.1) GO TO 21
      PRINT*,'--YOU INPUT A WRONG INTEGER, TRY AGAIN!'
      GO TO 11
18    PRINT*,'--DO YOU WANT TO KEEP LINE AND VAIABLE AREA,'
      PRINT*,'  INPUT 0 FOR LINE & AREA, 1 FOR ONLY AREA, NO LINE'
      READ*, KSLINE
      IF((KSLINE.EQ.1).OR.(KSLINE.EQ.0)) GO TO 21
      PRINT*,'--YOU INPUT A WRONG INTEGER, TRY AGAIN!'
      GO TO 18
21    PRINT*,'--INPUT SCALLING VALUE E.G 999.999'
      READ*, TRACD
C     DATA FILE CONSISTS OF 4 COLUMNS I,X,Y,Z
22    PRINT*,'--INPUT DATA COMPONENT FOR DISPLAY(X,Y.OR Z)'
      READ(*,'(A)')  COMP
      IF(COMP.EQ.'X') GO TO 156
      IF(COMP.EQ.'Y') GO TO 250
```

```
      IF(COMP.EQ.'Z') GO TO 350
      PRINT*,'--YOU INPUT A WRONG CHARACTER, TRY IT AGAIN!'
      GO TO 22
156   CALL GROUTE ('S VT4014;E')
      CALL GMSLEV('I',' ',' ',' ')
      CALL GOPEN
      CALL  SPRIMA(1)
      CALL SDIR(1,-1)
      CALL SSMPSI(10.0,0.40,TRACD)
      CALL STYPEW(KTYPE,1,KSLINE)
      DO 200 I=1, 12
      READ(1,100) X
100   FORMAT(5X,E12.4)
      CALL SWIGG(X,501)
      CALL STRNMB(I)
200   CONTINUE
      CALL SWIGG(X,9999)
      CALL SNUMBS(-1)
      GO TO 999
250   CALL GROUTE ('S VT4014;E')
      CALL GMSLEV('I',' ',' ',' ')
      CALL GOPEN
      CALL  SPRIMA(1)
      CALL SDIR(1,-1)
      CALL SSMPSI(10.0,0.40,TRACD)
      CALL STYPEW(KTYPE,1,KSLINE)
      DO 210 I=1, 12
      READ(1,190) Y
190   FORMAT(17X,E12.4)
      CALL SWIGG(Y,501)
      CALL STRNMB(I)
210   CONTINUE
      CALL SWIGG(Y,9999)
      GO TO 999
350   CALL GROUTE ('S VT4014;E')
      CALL GMSLEV('I',' ',' ',' ')
      CALL GOPEN
      CALL  SPRIMA(1)
      CALL SDIR(1,-1)
      CALL SSMPSI(10.0,0.40,TRACD)
      CALL STYPEW(KTYPE,1,KSLINE)
      DO 310 I=1, 12
```

```
      READ(1,180) Z
180   FORMAT(29X,E12.4)
      CALL SWIGG(Z,501)
      CALL STRNMB(I)
310   CONTINUE
      CALL SWIGG(Z,9999)
999   CALL STIMEE(1.0,1.0)
      CALL GDASH(4)
      CALL STIMEL(0.0,0.2,50,2)
      CALL GCLOSE
      STOP
      END
```

FORTRAN-77 PROGRAM 5 - MAGNPL

```
C     ************************************************************
C     SCALLING SEISMIC TRACE PROGRAM ON THE VAX/VMS: MAGNPL       *
C     DESIGNED AND WRIITEN BY                                     *
C     XIN-QUAN MA                                                 *
C     AT THE DEPERTMENT OF GEOLOGY & APPLIED GEOLOGY,             *
C     UNIVERSITY OF GLASGOW GLASGOW G12 8QQ (IN 1989)             *
C     THIS PROGRAM IS TO DESIGN A GAIN FUNCTION FOR EACH TRACE,   *
C     WHICH VARIES WITH THE AMPLITUDES IN A TRACE. THE SCALED TRACE *
C     IS OBTAINED BY MULTIPLYING THE ORIGINAL TRACE BY THE GAIN   *
C     FUNCTIONS. THE NUMBER OF TRACES FOR PROCESSING CAN BE DEFINED *
C     AS REQUIRED.                                                *
C     ************************************************************
C
      INTEGER  T,II,JJ,NSTN,NSAMPL
      PARAMETER(NSTN=12, NSAMPL=501)
      REAL  X(7000),Y(7000),Z(7000)
      REAL XX(NSTN,NSAMPL),YY(NSTN,NSAMPL),ZZ(NSTN,NSAMPL)
      REAL DX(NSTN,NSAMPL),DY(NSTN,NSAMPL),DZ(NSTN,NSAMPL)
      REAL FX(NSTN,NSAMPL),FY(NSTN,NSAMPL),FZ(NSTN,NSAMPL)
      REAL MX,MY,MZ
      CHARACTER* 8 INFILE,OUTFILE,COMP
      INTEGER  KTYPE,KSLINE
      PRINT*,'--INPUT THE FILE NAME TO BE PLOTTED'
      READ (*,'(A)') INFILE
      OPEN(1,FILE=INFILE,STATUS='OLD')
      L = 21
C     READ 3- COMPONENT DATA INTO ARRAY
C     THE DATA ARE OUTPUT FROM PROGRAM MATRSFM.FOR WHICH ARE
C     IN ORDER OF XX,YY,ZZ
      DO 15 I=1,NSTN
      DO 25 J=1,NSAMPL
      READ(1,222)  XX(I,J),YY(I,J),ZZ(I,J)
222   FORMAT(5X,3E12.4)
25    CONTINUE
15    CONTINUE
      PRINT*,'--START SCALLING TRACES'
      DO 991 I=1,NSTN,2
      M=0
100   M=M+L
```

```
      MX=0
      MY=0
      MZ=0
      DO 150 J=M-L+1, M
      MX=MX+ABS(XX(I,J))
      MY=MY+ABS(YY(I,J))
      MZ=MZ+ABS(ZZ(I,J))
150   CONTINUE
      DO 160 J=M-L+1, M
      FX(I,J)=MX/L
      FY(I,J)=MY/L
      FZ(I,J)=MZ/L
160   CONTINUE
      IF(M.LE.(NSAMPL-L)) GO TO 100
C     COMPUTE MEAN VALUES FOR LAST (NSAMPL-M) SAMPLES
      MX=0
      MY=0
      MZ=0
      DO 250 J=M+1, NSAMPL
      MX=MX+ABS(XX(I,J))
      MY=MY+ABS(YY(I,J))
      MZ=MZ+ABS(ZZ(I,J))
250   CONTINUE
      DO 350 J=M+1, NSAMPL
      FX(I,J)=MX/L
      FY(I,J)=MY/L
      FZ(I,J)=MZ/L
350   CONTINUE
991   CONTINUE
C     TO WEIGHT OPERATOR FUNCTION
      DO 666 I=1,NSTN,2
      DO 555 J=1,NSAMPL
      DX(I,J)=0
      DY(I,J)=0
      DZ(I,J)=0
555   CONTINUE
      N=(41-1)/2
      DO 434 J=1+(41-1)/2, NSAMPL-(41-1)/2
      DO 433 T=-N,N
      DX(I,J)=DX(I,J)+FX(I,J+T)
      DY(I,J)=DY(I,J)+FY(I,J+T)
      DZ(I,J)=DZ(I,J)+FZ(I,J+T)
433   CONTINUE
```

```
      DX(I,J)=DX(I,J)/41
      DY(I,J)=DY(I,J)/41
      DZ(I,J)=DZ(I,J)/41
434   CONTINUE
666   CONTINUE
      DO 567 I=1,NSTN,2
      DO  567  J=1,(41-1)/2
      DX(I,J)=FX(I,J)/1
      DY(I,J)=FY(I,J)/1
      DZ(I,J)=FZ(I,J)/1
567   CONTINUE
      DO 568 I=1,NSTN,2
      DO  568  J=NSAMPL-(41-1)/2 , NSAMPL
      DX(I,J)=FX(I,J)/1
      DY(I,J)=FY(I,J)/1
      DZ(I,J)=FZ(I,J)/1
568   CONTINUE
      K = 0
      DO 700 I=1,NSTN,2
      DO 700 J=1,NSAMPL
      K = K + 1
      X(K)=XX(I,J)/DX(I,J)
      Y(K)=YY(I,J)/DY(I,J)
      Z(K)=ZZ(I,J)/DZ(I,J)
700   CONTINUE
      PRINT*,' '
      PRINT*,'--START PLOTTING TRACES'
      PRINT*, ' '
      PRINT*,'--INPUT GAIN FOR SCALLING(E.G.999.999)'
      READ*, TRACD
11    PRINT*,'--DO YOU WANT TO PLOT WIGGLE LINE WITH VAIABLE '
      PRINT*,'  AREA, INPUT 0 FOR YES, 1 FOR JUST LINE '
      READ*,  KTYPE
      IF(KTYPE.EQ.0) GO TO 18
      IF(KTYPE.EQ.1) GO TO 22
      PRINT*,'--YOU INPUT A WRONG INTEGER, TRY AGAIN!'
      GO TO 11
18    PRINT*,'--DO YOU WANT TO KEEP LINE AND VAIABLE AREA,'
      PRINT*,'  INPUT 0 FOR LINE & AREA, 1 FOR ONLY AREA, NO LINE'
      READ*, KSLINE
      IF((KSLINE.EQ.1).OR.(KSLINE.EQ.0)) GO TO 22
      PRINT*,'--YOU INPUT A WRONG INTEGER, TRY AGAIN!'
```

```
      GO TO 18
C     DATA FILE CONSISTS OF 4 COLUMNS I,X,Y,Z
 22   PRINT*,'--INPUT DATA COMPONENT FOR DISPLAY(X,Y,OR Z)'
      READ(*,'(A)') COMP
      IF(COMP.EQ.'X') GO TO 156
      IF(COMP.EQ.'Y') GO TO 251
      IF(COMP.EQ.'Z') GO TO 351
      PRINT*,'--YOU INPUT A WRONG CHARACTER, TRY IT AGAIN!'
      GO TO 22
156   CALL GROUTE ('S VT4014;E')
      CALL GMSLEV('I',' ',' ',' ')
      CALL GOPEN
      CALL SPRIMA(1)
      CALL SDIR(1,-1)
      CALL SSMPSI(12.0,0.45,TRACD)
      CALL STYPEW(KTYPE,1,KSLINE)
      K = 0
      DO 200 I=1, NSTN,2
      IF(I.GT.1) K=K+501
      CALL SWIGG(X(K),501)
      CALL STRNMB(I)
200   CONTINUE
      CALL SWIGG(X,9999)
      GO TO 999
251   CALL GROUTE ('S VT4014;E')
      CALL GMSLEV('I',' ',' ',' ')
      CALL GOPEN
      CALL SPRIMA(1)
      CALL SDIR(1,-1)
      CALL SSMPSI(12.0,0.45,TRACD)
      CALL STYPEW(KTYPE,1,KSLINE)
      K = 0
      DO 210 I=1, NSTN,2
      IF(I.GT.1) K=K+501
      CALL SWIGG(Y(K),501)
      CALL STRNMB(I)
210   CONTINUE
      CALL SWIGG(Y,9999)
      GO TO 999
351   CALL GROUTE ('S VT4014;E')
      CALL GMSLEV('I',' ',' ',' ')
      CALL GOPEN
      CALL SPRIMA(0)
```

```
      CALL GVPORT(32.0, 5.0, 200.0,200.0)
      CALL SNTRAC(12)
      CALL SDIR(1,1)
      CALL SSMPSI(10.0,0.40,TRACD)
      CALL STYPEW(KTYPE,-1,KSLINE)
      K = 0
      DO 310 I=1, NSTN,2
      IF(I.GT.1) K=K+501
      CALL SWIGG(Z(K),501)
      CALL SNUMBS(-1)
      CALL STRNMB(I)
310   CONTINUE
      CALL SWIGG(Z,9999)
      CALL SNUMBS(1)
999   CALL GDASH(2)
      CALL STIMEL(0.0,0.2,50,2)
      CALL GDASH(0)
      CALL STIMEL(0.0,1.0,250,2)
      CALL GCLOSE
      STOP
      END
```

FORTRAN-77 PROGRAM 6 - MASDF

```
C     ********************************************************
C     SPATIAL DIRECTION FILTER ON VAX/VMS: MASDF                *
C     DEDSIGNED AND WRITTEN BY                                  *
C     XIN-QUAN MA,                                              *
C     DEPARTMENT OF GEOLOGY & APPLIED GEOLOGY,                  *
C     UNIVERSITY OF GLASGOW.(IN 1988)                           *
C     THIS PROGRAM IS TO FILTER THE DATA WHICH POLARIZE IN THE   *
C     DEFINED DIRECTIONS BY EVALUATING THE LARGEST EIGENVECOTOR OF *
C     A MATRIX OVER A TIME WINDOW.                              *
C     ********************************************************
      INTEGER NN,CHANN1,CHANN2,CHANN3,IFAIL,IV,NSTN,NTRACE,NSAMPL
      DOUBLE PRECISION XX(20,1500),YY(20,1500),ZZ(20,1500),X(1500),
     Z Y(1500),Z(1500),AL,BL,CL,DL,RR,R(3),V(3,3),T(3),MX,MY,
     Z MZ,A(3,3)
      CHARACTER * 8 INFILE,OUTFILE
      EXTERNAL  F02ABF
      PRINT*,' '
      PRINT*,' ****************************************'
      PRINT*,' *                                      *'
      PRINT*,' * SPATIAL DIRECTIONAL FILTERING        *'
      PRINT*,' *                                      *'
      PRINT*,' ****************************************'
      PRINT*,' '
      PRINT*,'--INPUT THE FILE NAME TO BE FILTERED'
      READ (*,'(A)') INFILE
      OPEN(1,FILE=INFILE,STATUS='OLD')
      PRINT*,'--INPUT FILE NAME FOR OUTPUT'
      READ(*,'(A)') OUTFILE
      OPEN(2,FILE=OUTFILE,STATUS='NEW')
      PRINT*,'--INPUT NUMBER OF STATIONS IN THE FILE'
      READ*, NSTN
      PRINT*,'--INPUT NUMBER OF SAMPLES PER TRACE'
      READ*, NSAMPL
      PRINT*,'--INPUT THE LENGTH OF TIME WINDOW(NO.OF SAMPLES)'
      READ*, L
      PRINT*,'--START READING DATA INTO ARRAY'
C     READ 3- COMPONENT DATA INTO ARRAY
C     THE DATA ARE OUTPUT FROM PROGRAM MATRSFM.FOR WHICH ARE
C     ORDER OF XX,YY,ZZ
      DO 15 I=1,NSTN
```

```
      DO 25 J=1,NSAMPL
      READ(1,222)  II,JJ,XX(I,J),YY(I,J),ZZ(I,J)
222   FORMAT(2I5,3E18.8)
25    CONTINUE
15    CONTINUE
C     INPUT A THRESHOLD ANGLE IN DEGREE
      PRINT*,'--INPUT A THRESHOLD ANGLE IN DEGREE'
      READ*,  DL
      DL=DL*3.1416/180
999   PRINT*,'--INPUT THE STATION NUMBER TO START'
      READ*,  I
      IF(I.EQ.0 .OR. I.GT.NSTN) GO TO 9999
C     TO CREATE A MATRIX A(3,3)
      M=0
100   NN=M/L + 1
      M=M+L
C     SET MX,MY,MZ INTO ZEROS
      MX=0
      MY=0
      MZ=0
      DO 45 J=M-L+1,M
      MX=MX+XX(I,J)
      MY=MY+YY(I,J)
      MZ=MZ+ZZ(I,J)
 45   CONTINUE
      MX=MX/L
      MY=MY/L
      MZ=MZ/L
C     SET MATRIX A INTO ZERO
      DO 455 J=1,3
      DO 455 K=1,3
      A(J,K)=0
455   CONTINUE
      DO 60 J=M-L+1,M
      A(1,1)=A(1,1)+(XX(I,J)-MX)**2
      A(1,2)=A(1,2)+(XX(I,J)-MX)*(YY(I,J)-MY)
      A(1,3)=A(1,3)+(XX(I,J)-MX)*(ZZ(I,J)-MZ)
      A(2,1)=A(2,1)+(YY(I,J)-MY)*(XX(I,J)-MX)
      A(2,2)=A(2,2)+(YY(I,J)-MY)**2
      A(2,3)=A(2,3)+(YY(I,J)-MY)*(ZZ(I,J)-MZ)
      A(3,1)=A(3,1)+(ZZ(I,J)-MZ)*(XX(I,J)-MX)
      A(3,2)=A(3,2)+(ZZ(I,J)-MZ)*(YY(I,J)-MY)
```

```
      A(3,3)=A(3,3)+(ZZ(I,J)-MZ)**2
60    CONTINUE
      DO 70 J=1,3
      DO 70 K=1,3
      A(J,K)=A(J,K)/L
70    CONTINUE
C     £££££££££££££££££££££££££££££££££££££££££££££££
C     AFTER CREATING A MATRIX A, THEN COMPUTE THE EIGENVECTOR          £
C     CORRESPONDING TO THE LARGEST EIGENVALUE OF  MATRIX A(3,3)        £
C     THAT VECTOR IN THEORY IS CONSIDERED AS A DIRECTIONAL VECTOR      £
C     OF MAIN POLARIZATION AXIS DURING A PERIOD OF TIME.               £
C     £££££££££££££££££££££££££££££££££££££££££££££££
C     %%%%%%%%%%%%%%%%%%%%%%%%%%%%%%%%%%%%%%%%%%%%%%
C     NAG ROUTINE F02ABF CALCULATES EIGENVALUES AND EIGENVECTORS
C     OF SYMMETRIC MATRIX. HERE
C     A(3,3) STANDING FOR SYMMETRIC MATRIC
C     R(3)   STANDING FOR 3 EIGENVALUES
C     V(3,3) STANDING FOR 3 EIGENVECTORS
      IA = 3
      N  = 3
      IFAIL = 1
      IV = 3
      CALL  F02ABF(A,IA,N,R,V,IV,E,IFAIL)
      R(1)  =  ABS(R(1))
      R(3)  =  ABS(R(3))
C     TO FIND OUT THE LARGEST EIGENVALUE AMONG 3 AND EIGENVECTOR
C     CORRESPONDING TO THE LARGEST EIGENVALUE.
      IF(R(3).LT.R(1))  THEN
      T(1)  =  ABS(V(1,1))
      T(2)  =  ABS(V(2,1))
      T(3)  =  ABS(V(3,1))
      ELSE
      T(1)  =  ABS(V(1,3))
      T(2)  =  ABS(V(2,3))
      T(3)  =  ABS(V(3,3))
      ENDIF
C     %%%%%%%%%%%%%%%%%%%%%%%%%%%%%%%%%%%%%%%%%%%%%%
c     **************************************************
C     AFTER THE DIRECTIONAL VECTOR OF MAIN POLARIZATION AXIS           *
C     {T(1),T(2),T(3)} HAS BEEN FOUND, WE CALCULATE THE ANGLES         *
C     OF POLARIZATION AXIS WITH THREE AXISES, MATHEMATICALLY           *
C     (COSAL)**2 + (COSBL)**2 + (COSCL)**2 = 1                         *
C     COSAL=T(1)/SQRT(T(1)**2+T(2)**2+T(3)**2)                         *
```

```
C       COSBL=T(2)/SQRT(T(1)**2+T(2)**2+T(3)**2)                          *
C       COSCL=T(3)/SQRT(T(1)**2+T(2)**2+T(3)**2)                          *
C       *****************************************************************
        RR=SQRT(T(1)**2+T(2)**2+T(3)**2)
        AL=ACOS(ABS(T(1))/RR)
        BL=ACOS(ABS(T(2))/RR)
        CL=ACOS(ABS(T(3))/RR)
C       ^^^^^^^^^^^^^^^^^^^^^^^^^^^^^^^^^^^^^^^^^^^^^^^^^^^^^^^^^^^^^^^^^
C       IF WE SELECT THE FILTERING DIRECTIONS AS X,Y,Z AXIAL              ^
C       DIRECTIONS(THIS IS GENERAL CASE AND COMMONLY USED),THEN           ^
C       WE HAVE TO GIVE A THRESHOLD ANGLE. THE FILTERING THEORY           ^
C       IS THAT IF THIS ANGLE IS LESS THAN THE GIVEN THRESHOLD            ^
C       ANGLE,THE CORRESPONDING PART OF THE TRAJECTORY IS KEPT,           ^
C       OTHERWISE, IT IS REJECTED.                                        ^
C       ^^^^^^^^^^^^^^^^^^^^^^^^^^^^^^^^^^^^^^^^^^^^^^^^^^^^^^^^^^^^^^^^^
C       FILTERING IN X DIRECTION
        IF (AL.GT.DL) go to 250
C       KEEPING THIS PART OF TRAJECTORY.
        DO 232 K=M-L+1, M
        X(K)=1000
232     CONTINUE
        GO TO 255
250     DO 233 K=M-L+1,M
233     X(K)=0
C       FILTERING IN Y DIRECTION
255     IF(BL.GT.DL) go to 300
        DO 258 K=M-L+1,M
258     Y(K)=1000
        GO TO 310
300     DO 311 K=M-L+1,M
311     Y(K)=0
C       FILTERING IN Z DIRECTION
310     IF(CL.GT.DL) GO TO 560
        DO 350 K=M-L+1,M
350     Z(K)=1000
        GO TO 660
560     DO 570 K=M-L+1,M
570     Z(K)=0
660     IF((M+L).GT.NSAMPL) GO TO 661
        GO TO 100
C       WRITE FILTERED DATA INTO A  FILE
661     DO 550 K=1,NSAMPL
```

```
      WRITE(2,500)  K,X(K),Y(K),Z(K)
500   FORMAT(I5,3E12.4)
550   CONTINUE
      GO TO 999
9999  STOP
      END
```

FORTRAN-77 PROGRAM 7 - MAENERGY

```
C     ********************************************************
C     SEISMIC SOURCE ENERGY EVALUATION PROGRAM: MAENERGY      *
C     ON THE VAX/VMS SYSTEM.                                  *
C     DEDSIGNED AND WRITTEN BY                                *
C     XIN-QUAN  MA                                            *
C     AT THE DEPARTMENT OF GEOLOGY & APPLIED GEOLOGY,         *
C     UNIVERSITY OF GLASGOW. GLASGOW  G12  8QQ (IN 1988)      *
C     THIS PROGRAM IS TO CALCULATE THE TOTAL ENERGY FROM SINGLE SHOT *
C     AND THE ENERGY ON EACH COMPONENT OF INDIVIDUAL STATIONS. THE   *
C     GIVES THE RATIO OF THEM.                                *
C     ********************************************************
C
      INTEGER NN,THRESH,IFAIL,IV,NSTN,NTRACE,NSAMPL
      DOUBLE PRECISION XX(20,1500),YY(20,1500),ZZ(20,1500),X(1500),
     Z        Y(1500),Z(1500),AL,BL,CL,DL,RR,R(3),V(3,3),T(3),MX,MY,
     Z     MZ,NWX,NWY,NWZ,LL(20),ENX,ENY,ENZ,A(3,3)
      CHARACTER * 8 INFILE,OUTFILE
      DATA  LL/0,5,10,15,20,25,30,35,40,45,50,55,60,65,70,
     Z        75,80,85,90,999/
      EXTERNAL  F02ABF
      PRINT*,'--INPUT THE FILE NAME TO BE PROCESSED'
      READ  (*,'(A)')  INFILE
      OPEN(1,FILE=INFILE,STATUS='OLD')
      PRINT*,'--INPUT FILE NAME FOR OUTPUT'
      READ(*,'(A)')  OUTFILE
      OPEN(2,FILE=OUTFILE,STATUS='NEW')
      PRINT*,'--INPUT NUMBER OF STATIONS IN THE FILE'
      NSTN = 12
      PRINT*,'--INPUT NUMBER OF SAMPLES PER TRACE'
      NSAMPL = 501
      PRINT*,'--INPUT THE LENGTH OF TIME WINDOW(NO.OF SAMPLES)'
      READ*, L
C     COMPUTE TOTAL NUMBER OF WINDOWS IN ONE SECTIONS(12 TRACES)
      PRINT*,'--START READING DATA INTO ARRAY'
C     READ 3- COMPONENT DATA INTO ARRAY
C     THE DATA ARE OUTPUT FROM PROGRAM MATRSFM.FOR WHICH ARE
C     IN ORDER OF XX,YY,ZZ
      DO 15 I=1,NSTN
      DO 25 J=1,NSAMPL
```

```
      READ(1,222)  II,JJ,XX(I,J),YY(I,J),ZZ(I,J)
      NWX = NWX + XX(I,J)**2
      NWY = NWY + YY(I,J)**2
      NWZ  = NWZ + ZZ(I,J)**2
222   FORMAT(I3,I5,3E12.4)
25    CONTINUE
15    CONTINUE
1111  THRESH = THRESH +1
      ENX = 0
      ENY = 0
      ENZ = 0
      KK = 0
      I = 0
      IF(LL(THRESH).EQ.999) GO TO 9999
      KK = KK + 1
      DL=LL(THRESH)*3.1416/180
999   I = I + 1
      IF(I.GT.NSTN) GO TO 661
C     TO CREATE A MATRIX A(3,3)
      M=0
100   NN=M/L + 1
      M=M+L
C     SET MX,MY,MZ INTO ZEROS
      MX=0
      MY=0
      MZ=0
      DO 45 J=M-L+1,M
      MX=MX+XX(I,J)
      MY=MY+YY(I,J)
      MZ=MZ+ZZ(I,J)
45    CONTINUE
      MX=MX/L
      MY=MY/L
      MZ=MZ/L
C     SET MATRIX A INTO ZERO
      DO 455 J=1,3
      DO 455 K=1,3
      A(J,K)=0
455   CONTINUE
      DO 60 J=M-L+1,M
      A(1,1)=A(1,1)+(XX(I,J)-MX)**2
      A(1,2)=A(1,2)+(XX(I,J)-MX)*(YY(I,J)-MY)
      A(1,3)=A(1,3)+(XX(I,J)-MX)*(ZZ(I,J)-MZ)
```

```
      A(2,1)=A(2,1)+(YY(I,J)-MY)*(XX(I,J)-MX)
      A(2,2)=A(2,2)+(YY(I,J)-MY)**2
      A(2,3)=A(2,3)+(YY(I,J)-MY)*(ZZ(I,J)-MZ)
      A(3,1)=A(3,1)+(ZZ(I,J)-MZ)*(XX(I,J)-MX)
      A(3,2)=A(3,2)+(ZZ(I,J)-MZ)*(YY(I,J)-MY)
      A(3,3)=A(3,3)+(ZZ(I,J)-MZ)**2
 60   CONTINUE
      DO 70 J=1,3
      DO 70 K=1,3
      A(J,K)=A(J,K)/L
 70   CONTINUE
C
C     &&&&&&&&&&&&&&&&&&&&&&&&&&&&&&&&&&&&&&&&&&&&&&&&&&&&&&&&&&&&&&&&
C     AFTER CREATING A MATRIX A, THEN COMPUTE THE EIGENVECTOR          &
C     CORRESPONDING TO THE LARGEST EIGENVALUE OF  MATRIX A(3,3)        &
C     THAT VECTOR IN THEORY IS CONSIDERED AS A DIRECTIONAL VECTOR      &
C     OF MAIN POLARIZATION AXIS DURING A PERIOD OF TIME.               &
C     ##################################################################
C     %%%%%%%%%%%%%%%%%%%%%%%%%%%%%%%%%%%%%%%%%%%%%%%%%%%%%%%%%%%%%%%
C     NAG ROUTINE F02ABF CALCULATES EIGENVALUES AND EIGENVECTORS
C     OF SYMMETRIC MATRIX. HERE
C     A(3,3) STANDING FOR SYMMETRIC MATRIC
C     R(3)  STANDING FOR 3 EIGENVALUES
C     V(3,3) STANDING FOR 3 EIGENVECTORS
      IA = 3
      N  = 3
      IFAIL = 1
      IV = 3
      CALL  F02ABF(A,IA,N,R,V,IV,E,IFAIL)
      R(1) = ABS(R(1))
      R(3) = ABS(R(3))
C     TO FIND OUT THE LARGEST EIGENVALUE AMONG 3 AND EIGENVECTOR
C     CORRESPONDING TO THE LARGEST EIGENVALUE.
      IF(R(3).LT.R(1))  THEN
      T(1) = ABS(V(1,1))
      T(2) = ABS(V(2,1))
      T(3) = ABS(V(3,1))
      ELSE
      T(1) = ABS(V(1,3))
      T(2) = ABS(V(2,3))
      T(3) = ABS(V(3,3))
      ENDIF
```

```
C     %%%%%%%%%%%%%%%%%%%%%%%%%%%%%%%%%%%%%%%%
C
C     ****************************************************
C     AFTER THE DIRECTIONAL VECTOR OF MAIN POLARIZATION AXIS      *
C     {T(1),T(2),T(3)} HAS BEEN FOUND, WE CALCULATE THE ANGLES     *
C     OF POLARIZATION AXIS WITH THREE AXISES, MATHEMATICALLY       *
C     (COSAL)**2 + (COSBL)**2 + (COSCL)**2 = 1                     *
C     COSAL=T(1)/SQRT(T(1)**2+T(2)**2+T(3)**2)                     *
C     COSBL=T(2)/SQRT(T(1)**2+T(2)**2+T(3)**2)                     *
C     COSCL=T(3)/SQRT(T(1)**2+T(2)**2+T(3)**2)                     *
C     ****************************************************
      RR=SQRT(T(1)**2+T(2)**2+T(3)**2)
      AL=ACOS(ABS(T(1))/RR)
      BL=ACOS(ABS(T(2))/RR)
      CL=ACOS(ABS(T(3))/RR)
C     ^^^^^^^^^^^^^^^^^^^^^^^^^^^^^^^^^^^^^^^^^^^^^^^^^^^^^^^^^^^^^^^^^^^^^^^^^^^^^^^
C     IF WE SELECT THE FILTERING DIRECTIONS AS X,Y,Z AXIAL          ^
C     DIRECTIONS(THIS IS GENERAL CASE AND COMMONLY USED),THEN       ^
C     WE HAVE TO GIVE A THRESHOLD ANGLE. THE FILTERING THEORY       ^
C     IS THAT IF THIS ANGLE IS LESS THAN THE GIVEN THRESHOLD        ^
C     ANGLE,THE CORRESPONDING PART OF THE TRAJECTORY IS KEPT,       ^
C      OTHERWISE, IT IS REJECTED.                                   ^
C     ^^^^^^^^^^^^^^^^^^^^^^^^^^^^^^^^^^^^^^^^^^^^^^^^^^^^^^^^^^^^^^^^^^^^^^^^^^^^^^^
C     FILTERING IN X DIRECTION
      IF (AL.GT.DL) go to 255
C     KEEPING THIS PART OF TRAJECTORY.
      DO 232 K=M-L+1, M
      ENX = ENX + XX(I,K)**2
232   CONTINUE
C     FILTERING IN Y DIRECTION
255   IF(BL.GT.DL) go to 300
      DO 258 K=M-L+1, M
      ENY = ENY +YY(I,K)**2
258    CONTINUE
C     FILTERING IN Z DIRECTION
300   IF(CL.GT.DL) GO TO 660
      DO 350 K=M-L+1, M
      ENZ = ENZ + ZZ(I,K)**2
350   CONTINUE
660   IF((M+L).GT.NSAMPL) GO TO 999
      GO TO 100
C     WRITE FILTERED DATA INTO A  FILE
661   ENX = 100*ENX/(NWX+NWY+NWZ)
```

```
      ENY = 100*ENY/(NWX+NWY+NWZ)
      ENZ = 100*ENZ/(NWX+NWY+NWZ)
      WRITE(2,500) THRESH,LL(THRESH),ENX,ENY,ENZ
500   FORMAT(I5,F6.2,3E12.4)
      GO TO 1111
9999  STOP
      END
```

FORTRAN-77 PROGRAM 8 - MASEPF

```
C     ************************************************************
C     SIGNAL ENHANCEMENT POLARISATION FILTER: MASEPF               *
C     ON THE VAX/VMS SYSEM                                         *
C     DESIGNED AND WRITTEN BY                                      *
C     XIN-QUAN MA                                                  *
C     AT THE DEPARTMENT OF GEOLOGY & APPLIED GEOLOGY,              *
C     UNIVERSITY OF GLASGOW  GLASGOW  G12  8QQ  (IN 1988)          *
C     THIS SOFTWARE COMPUTES THE COVARIANCE MATRIX OVER A TIME      *
C     WINDOW AND THEN CALCULATES THE LARGEST AND THE SECOND        *
C     LARGEST EIGENVALUES OF THIS MATRIX AND THE EIGENVECTOR       *
C     CORRESPONDING THE LARGEST EIGENVALUE BY CALLING NAG ROUTINE  *
C     F02ABF. THE REACTILINEARITY AND DIRECTIONALITY FUNCTIONS      *
C     ARE CONSTRUCTED, WHICH FORMS THE FILTER OPERATORS. THE       *
C     FILTERED SEISMOGRAMS ARE OBTAINED BY MULTIPLYING THE         *
C     ORIGINAL SEISMOGRAMS BY FILTER OPERATORS.                    *
C     ************************************************************
C
      INTEGER  MN,LL,T,L,II,IJK,III,NN,KK,JJ,JJJ,WW,NSTN,NSAMPL,
     Z       MM,LTH,RN,CN,IFAIL,IV,N,IA,QQ
      PARAMETER (RN=15,CN=1500)
      DOUBLE PRECISION A(3,3),F(2),G(3),MX,MY,MZ,V(3,3),E(3),R(3),
     Z P(3),FTN(RN,CN),RLL(RN,CN),XX(RN,CN),YY(RN,CN),ZZ(RN,CN),
     Z FF,FNT(RN,CN),RL(RN,CN),DX(RN,CN),DY(RN,CN),DZ(RN,CN),
     Z FX(RN,CN),FY(RN,CN),FZ(RN,CN),NX(RN,CN),NY(RN,CN),
     Z NZ(RN,CN),DXX(RN,CN),DYY(RN,CN),DZZ(RN,CN)
      CHARACTER*8 INFILE,OUTFILE,OPFILE,YORN
      EXTERNAL  F02ABF
      PRINT*,' '
      PRINT*,' '
      PRINT*,'        ****************************************'
      PRINT*,'   *                                            *'
      PRINT*,'   * SIGNAL ENHANCEMENT POLARISATION FILTER     *'
      PRINT*,'   *                                            *'
      PRINT*,'        ****************************************'
      PRINT*,' '
      PRINT*,' '
      PRINT*,'--INPUT DATA FILE NAME FOR FILTERING '
      READ(*,'(A)')     INFILE
      OPEN(1,FILE=INFILE,STATUS='OLD')
      PRINT*,'--INPUT NUMBER OF STATIONS IN THE FILE'
```

```
      NSTN = 1
      PRINT*,'--INPUT THE NUMBER OF SAMPLES IN ONE TRACE '
      NSAMPL = 1001
      PRINT*,'--INPUT THE FILE NAME FOR OUTPUT '
      READ(*,'(A)')   OUTFILE
      OPEN(2,FILE=OUTFILE,STATUS='NEW')
C     INPUT THE TIME WINDOW ( NO OF SAMPLES )
555   PRINT*,'--INPUT TIME WINDOW(NO.OF SAMPLES) '
      READ*, L
      PRINT*,'--START READING DATA INTO ARRAY '
C     READ THE 3-COMPONENT DATA INTO ARRAY XX(I,J),YY(I,J),ZZ(I,J)
C     THE DATA ARE OUTPUT FROM PROGRAM MATRSFM.FOR WHICH HAS ORDER
C     OF X,Y,Z.
      DO 333  I=1,  NSTN
      DO 222  J=1,  NSAMPL
      READ(1,111)   QQ, XX(I,J),YY(I,J), ZZ(I,J)
111   FORMAT(I5,3E12.4)
222   CONTINUE
333   CONTINUE
7777  PRINT*,'--INPUT STATION NUMBER FOR FILTERING(TYPE 0 TO STOP) '
      READ*,  I
      IJK=IJK+1
      IF((I.EQ.0) .OR. (I.GT.NSTN)) GO TO 8888
C     TO CREATE COVARIANCE MATRIX A OVER THE TIME L*DT.
      LL=L
27    LL=LL+1
      MX=0
      MY=0
      MZ=0
      DO 33 J= LL-L, LL-1
      MX=MX+XX(I,J)
      MY=MY+YY(I,J)
      MZ=MZ+ZZ(I,J)
33    CONTINUE
      MX=MX/L
      MY=MY/L
      MZ=MZ/L
C     SET ELEMENTS OF MATRIX INTO ZEROS
      DO 6112 J=1,3
      DO 6112 K=1,3
      A(J,K) = 0
6112  CONTINUE
```

```
      DO 44 J=LL-L,LL-1
      A(1,1)=A(1,1)+(XX(I,J)-MX)**2
      A(1,2)=A(1,2)+(XX(I,J)-MX)*(YY(I,J)-MY)
      A(1,3)=A(1,3)+(XX(I,J)-MX)*(ZZ(I,J)-MZ)
      A(2,1)=A(2,1)+(YY(I,J)-MY)*(XX(I,J)-MX)
      A(2,2)=A(2,2)+(YY(I,J)-MY)**2
      A(2,3)=A(2,3)+(YY(I,J)-MY)*(ZZ(I,J)-MZ)
      A(3,1)=A(3,1)+(ZZ(I,J)-MZ)*(XX(I,J)-MX)
      A(3,2)=A(3,2)+(ZZ(I,J)-MZ)*(YY(I,J)-MY)
      A(3,3)=A(3,3)+(ZZ(I,J)-MZ)**2
44    CONTINUE
      DO 55 J=1,3
      DO 55 K=1,3
      A(J,K)=A(J,K)/L
55    CONTINUE
C     !!!!!!!!!!!!!!!!!!!!!!!!!!!!!!!!!!!!!!!!!!!!!!!!!!!!!!!!!!!!!!!!!!!!!!!!!!!!!!!!!!!!!!!!!!!!!!!!!!!!!!!!!!!!!!!
C     ***********************************************************
C     AFTER CREATING MATRIX A(3,3), THE NAG ROUTINE F02ABF IS           *
C     USED TO CALCULATE THREE EIGENVALUES AND CORRESPONDING THREE       *
C     EIGENVECTORS.HOWEVER, ONLY THE LARGEST AND THE SECOND             *
C     LARGEST EIGENVALUES ARE USED IN THIS PROGRAM. SO IS THE           *
C     EIGENVECTOR CORRESPONDING THE LARGEST EIGENVALUE.                 *
C     NAG ROUTINE F02ABF CALCULATES EIGENVALUES AND EIGENVECTORS        *
C     OF SYMMETRIC MATRIX. HERE                                         *
C     A(3,3) STANDING FOR SYMMETRIC MATRIX                              *
C     R(3)   STANDING FOR 3 EIGENVALUES                                 *
C     V(3,3) STANDING FOR 3 EIGENVECTORS                                *
C     ***********************************************************
      IA = 3
      N  = 3
      IFAIL = 1
      IV = 3
      CALL  F02ABF(A,IA,N,R,V,IV,E,IFAIL)
      R(1)  =  ABS(R(1))
      R(2)  =  ABS(R(2))
      R(3)  =  ABS(R(3))
C     TO FIND OUT THE LARGEST EIGENVALUE AMONG 3 AND EIGENVECTOR
C     CORRESPONDING TO THE LARGEST EIGENVALUE.
      IF(R(3).LT.R(1))  THEN
      F(1)  =  R(1)
      G(1)  =  ABS(V(1,1))
      G(2)  =  ABS(V(2,1))
      G(3)  =  ABS(V(3,1))
```

```
      F(R(2).LT.R(3)) GO TO 6109
      F(2) = R(2)
      GO TO 7009
6109  F(2) = R(3)
7009  CONTINUE
      ELSE
      F(1) = R(3)
      G(1) = ABS(V(1,3))
      G(2) = ABS(V(2,3))
      G(3) = ABS(V(3,3))
      IF(R(2).LT.R(1)) GO TO 7109
      F(2) = R(2)
      GO TO 7209
7109  F(2) = R(1)
7209  ENDIF
C     !!!!!!!!!!!!!!!!!!!!!!!!!!!!!!!!!!!!!!!!!!!!!!!!!!!!!!!!!!!!!!!!!!!!!!!!!!!!!!!!!!!!!!!!!!!!!!!!!!!!!!!!!!!!!!!!!!!!!!!!
C     AFTER FINDING THE LARGEST AND SECOND LARGEST EIGENVALUES
C     WE NOW CONSTRUCT A FUNCTION CALLED FTN.
      II=LL-1-(L-1)/2
      NN=1
      JJ=1
      KK=1
      FTN(I,II)=1-(F(2)/F(1))**NN
C     TO MEASURE THE RECTILINEARITY AT TIME To, A NEW FUNC-
C     TION CALLED RL IS NOW CONSTRUCTED.
      RL(I,II)=FTN(I,II)**JJ
C     TO CREATE THE DIRECTION FUNCTIONS AT TIME To, WE CONS-
C     TRUCT DX,DY AND DZ.
      DX(I,II) = G(1)**KK
      DY(I,II) = G(2)**KK
      DZ(I,II) = G(3)**KK
      IF(II.LE.(NSAMPL-(L-1)/2)) GO TO 27
C     NOTICE THAT WE CAN NOT OBTAIN THE FILTER OPERATORS FOR
C     FIRST (L/2 -1) POINTS, BUT TAKEN THEM AS SAME AT THAT OF
C     POINT L/2.
      III=1+(L-1)/2
      DO 888 N=1,(L-1)/2
      RL(I,N)=RL(I,III)
      DX(I,N)=DX(I,III)
      DY(I,N)=DY(I,III)
      DZ(I,N)=DZ(I,III)
888   CONTINUE
```

```
C       NOTICE THAT WE CAN NOT OBTAIN THE FILTER OPERATORS FOR
C       THE LAST (L-1)/2 POINTS, BUT TAKEN THEM AS SAME AS THAT
C       OF POINT (MN-(L-1)/2).
C       JJJ IS LT CENTRE POINT IN ABOVE LOOP
        JJJ=II-1
        DO 950 MM=II,NSAMPL
        RL(I,MM)=RL(I,JJJ)
        DX(I,MM)=DX(I,JJJ)
        DY(I,MM)=DY(I,JJJ)
        DZ(I,MM)=DZ(I,JJJ)
950     CONTINUE
C       TO WEIGHT OPERATOR FUNCTIONS
C       TO SET WINDOW LENGTH FOR SMOOTHING THE FUCTIONS.
        LTH = 11
        M=(LTH-1)/2
        DO 434 J=1+(LTH-1)/2, NSAMPL-(LTH-1)/2
        DO 433 T=-M,M
        RLL(I,J)=RLL(I,J)+RL(I,J+T)
        DXX(I,J)=DXX(I,J)+DX(I,J+T)
        DYY(I,J)=DYY(I,J)+DY(I,J+T)
        DZZ(I,J)=DZZ(I,J)+DZ(I,J+T)
433     CONTINUE
        RL(I,J)=RLL(I,J)/LTH
        DX(I,J)=DXX(I,J)/LTH
        DY(I,J)=DYY(I,J)/LTH
        DZ(I,J)=DZZ(I,J)/LTH
434     CONTINUE
C       OPERATOR FUNCTIONS FX,FY,FZ
        DO 553 J=1,NSAMPL
        FX(I,J)=RL(I,J)*DX(I,J)
        FY(I,J)=RL(I,J)*DY(I,J)
        FZ(I,J)=RL(I,J)*DZ(I,J)
553     CONTINUE
C       THE GAIN FUNCTIONS FX,FY AND FZ ARE CONSIDERED AS THE
C       FILTER OPERATORS. THE FILTERED SEISMOGRAMS ARE OBTAINED
C       BY MULTIPLYING THE ORIGINAL SEISMIGRAMS BY FILTER OPERATORS.
        DO 890 J= 1, NSAMPL
        NX(I,J)=XX(I,J)*FX(I,J)
        NY(I,J)=YY(I,J)*FY(I,J)
        NZ(I,J)=ZZ(I,J)*FZ(I,J)
890     CONTINUE
C       SO FAR, THE 3 TRACES FOR ONE STATION HAVE BEEN FILTERED
C       NEXT IS IF COMMAND ASKING FOR NEXT TRACES TRACES TO BE
```

```
C       FILTERED.
        GO TO  7777
C       AFTER NSTRN STATIONS HAVE BEEN FINISHED, THIS PROGRAM IS TO
C       WIRIT FILTERED DATA INTO FILE
8888    PRINT*,'--START WRITING FILTERED DATA INTO FILE '
        DO 8890  J = 1, IJK-1
        DO 8890  K = 1, NSAMPL
        WRITE(2,8889)  K,  NX(J,K),NY(J,K),NZ(J,K)
8889    FORMAT( I5, )
8890    CONTINUE
444     PRINT*,'--DO YOU WANT TO KEEP OPERATOR FUNCTIONS(Y/N)'
        READ(*,'(A)')   YORN
        IF(YORN.EQ.'N') GO TO 9999
        IF(YORN.EQ.'Y') GO TO 666
        PRINT*,'--YOU INPUT A WRONG LETTER,TRY AGAIN!'
        GO TO 444
666     PRINT*,'--INPUT FILE NAME FOR OPERATOR FUNCTIONS '
        READ(*,'(A)')  OPFILE
        OPEN(3,FILE=OPFILE,STATUS='NEW')
        PRINT*,'--START WRITING FILTER FUNCTIONS INTO FILE '
        DO 7790  J = 1, IJK-1
        DO 7790  K = 1, NSAMPL
        WRITE(3,7789)  K,  FX(J,K),FY(J,K),FZ(J,K)
7789    FORMAT( I5, 3E12.4)
7790    CONTINUE
9999    CLOSE(2)
        CLOSE(3)
        STOP
        END
```

FORTRAN-77 PROGRAM 9 - MAVHPL

```
C     ********************************************************
C     GENERATION SYNTHETIC SEISMOGRAM PROGRAM: MAVHPL          *
C     ON THE VAX/VMS SYSTEM.                                   *
C     DESIGNED AND WRIITEN BY                                  *
C     XIN-QUAN  MA                                             *
C     AT THE DEPARTMENT OF GEOLOGY & APPLIED GEOLOGY,          *
C     UNIVERSITY OF GLASGOW  GLASGOW  G12  8QQ  (IN 1989)      *
C     THIS PROGRAM IS USED IN CONJUNCTION WITH MODELLING PACKAGE *
C     SEIS83 AND VERTPL. TRACE LENGTH IS 4 SEC, SAMPLING RATE IS 4 MS. *
C     ********************************************************
C
      REAL  TO,L1,L2,NP,Y(200,20)
      INTEGER LO,NN,NO,X(200,20)
      CHARACTER* 10 INFILE,OUTFILE
      CHARACTER* 70 B
      OPEN(1,FILE='SEISGRAM',STATUS='OLD')
      OPEN(2,FILE='VMA',STATUS='NEW')
      DO 30 I=1,3
      READ(1,89),B
89    FORMAT(A70)
30    CONTINUE
      NN = 0
333   NN = NN +1
      IF(NN.EQ.3) STOP
C     TO IS THE TIME OF THE FIRST POINT IN SYNTHETIC SEISMOGRAM.
C     NP IS NUMBER OF POINTS IN SYNTHETIC SEISMOGRAM.
      READ(1,90) TO,NP
90    FORMAT(25X, F10.5, F5.0)
      NO = NINT(TO/0.004)
      L1 = NP/18
      L2 = ANINT(NP/18)
      IF((L1-L2).GT.0.0)  THEN
      LO = NINT(L2) + 1
      ELSE
      LO = NINT(L2)
      END IF
 5    DO 100 I=1,LO
      READ(1,10)  X(I,1),X(I,2),X(I,3),X(I,4),X(I,5),
     Z          X(I,6),X(I,7),X(I,8),X(I,9),X(I,10),
     Z          X(I,11),X(I,12),X(I,13),X(I,14),X(I,15),
```

```
      Z         X(I,16),X(I,17),X(I,18)
        Y(I,1) = X(I,1)
        Y(I,2) = X(I,2)
        Y(I,3) = X(I,3)
        Y(I,4) = X(I,4)
        Y(I,5) = X(I,5)
        Y(I,6) = X(I,6)
        Y(I,7) = X(I,7)
        Y(I,8) = X(I,8)
        Y(I,9) = X(I,9)
        Y(I,10) = X(I,10)
        Y(I,11) = X(I,11)
        Y(I,12) = X(I,12)
        Y(I,13) = X(I,13)
        Y(I,14) = X(I,14)
        Y(I,15) = X(I,15)
        Y(I,16) = X(I,16)
        Y(I,17) = X(I,17)
        Y(I,18) = X(I,18)
10      FORMAT(18I4)
100     CONTINUE
        DO 260 I = 1, NO-1
        WRITE(2,200)  I, 0.0
260     CONTINUE
        K = NO-1
        DO 300 I=1,LO
        DO 300 J=1,18
        K=K+1
        WRITE(2,200)  K,Y(I,J)
200     FORMAT(I5,E12.4)
300     CONTINUE
        DO 360 I = NO+LO*18, 1001
        WRITE(2,200)  I, 0.0
360     CONTINUE
        GO TO 333
 99     CLOSE(UNIT=2)
        STOP
        END
```

FORTRAN-77 PROGRAM 10 - MASSP

```
C     ********************************************************
C     SLANT-STACK PROCESSING PROGRAM ON THE VAX/VMS SYSTEM: MASSP *
C     DESIGNED AND WRITTEN BY                                    *
C     XIN-QUAN MA                                                *
C     AT THE DEPARTMENT OF GEOLOGY & APPLIED GEOLOGY,            *
C     UNIVERSITY OF GLASGOW, GLASGOW G12 8QQ (IN 1989)           *
C     THIS PROGRAM IS TO PROJECT ALL THE 12 STATIONS TO A        *
C     SPECIFIED LINE WITH CERTAIN ANGLE TO THE EAST DEFINED      *
C     BY THE USER AND THEN TO CALCULATE THE NEW OFFSETS OF       *
C     DIFFERET STATIONS ACCORDING TO ARRAY GEOMETRY.FINALLY,     *
C     TO CARRY OUT SLANT STACKING OR BEAM STEERING PROCESS.      *
C     THE ARRAY CONSISTS OF 12 3-CONPONENT GEOPHONES WITH        *
C     UNIT DIMENSION D.                                          *
C     ********************************************************
C
      REAL  D,RATE,UPD,LOD,ALPHA,U(100,5000),Z(20,5000)
      REAL  B(12),DT(12),P(100),UPP,PIC,TAU,LOP,PI
      INTEGER  NP,TA,NSAMPL
      CHARACTER*8 FILEOUT,FILEIN,YON
      DATA B /90,120,150,180,210,240,270,300,330,0,30,60/
      PRINT*,' '
      PRINT*,' '
      PRINT*,'       ******************************************'
      PRINT*,'  *                                              *'
      PRINT*,'  *  SLANT STACKING FORTRAN PROGRAM              *'
      PRINT*,'  *                                              *'
      PRINT*,'       ******************************************'
      PRINT*,' '
      PRINT*,' '
      DO 789 I= 1,12
      DO 789 J=2002,3000
      Z(I,J) = 0.00000
789   CONTINUE
      PRINT*,'-INPUT FILE NAME FOR PROCESS PLEASE!'
      READ(*,'(A)') FILEIN
      OPEN(1,FILE=FILEIN,FORM='FORMATTED',STATUS='OLD')
C     INPUT THE ALL PARAMETERS
      NSAMPL = 2001
      LOP =-6.66667E-4
      UPP = 6.66667E-4
```

```
      PRINT*,'-INPUT NUMBER OF RAY PARAMETERS YOU NEED PLEASE!'
      READ*,NP
C     CALCULATE THE RAY PARAMETER INCREMENT PIC
      PIC=(UPP-LOP)/NP
      D = 75
C     DEFINE A 2-DIMENSION ARRAY,INPUT 12 TRACE SEISMIC DATA
C     INTO THIS ARRAY--Z(I,J)
      PRINT*,' '
      PRINT*, '-START READING 12-TRACE DATA INTO ARRAY U(I,J)'
      PRINT*,' '
      DO 100 I = 1, 12
      DO 100 J = 1, 2001
      READ(1,50)  Z(I,J)
 50   FORMAT(5X,E12.4)
100   CONTINUE
      GO TO 889
776   PRINT*,'-DO YOU WANT TO TRY MORE ALPHA(Y/N)EG."Y" OR "N"?'
777   READ(*,'(A)'),YON
      IF(YON.EQ.'N') GO TO 999
      IF(YON.EQ.'Y') GO TO 889
      PRINT*,'-YOU INPUT A WRONG CHARACTER,TRY AGAIN!'
      GO TO 777
889   PRINT*, '-INPUT ARIMUTH ALPHA PLEASE!'
      READ*, ALPHA
      PRINT*,'-INPUT FILE NAME FOR OUTPUT PLEASE! '
      READ(*,'(A)'),FILEOUT
      OPEN(2,FILE=FILEOUT,FORM='FORMATTED',STATUS='NEW')
C     CALCULATE THE OFFSET DISTANCE OF THE FIRST GEOPHONE
      PRINT*,' '
      PRINT*,'-START COMPUTE OFFSET DISTANCES(PROJECTION)'
      PRINT*,' '
      LOD=D
      UPD = 130
      PI = 3.1416/180
      DT(1) = UPD*COS((ALPHA-B(1))*PI)
      DT(2) = LOD*COS((ALPHA-B(2))*PI)
      DT(3) = UPD*COS((ALPHA-B(3))*PI)
      DT(4) = LOD*COS((ALPHA-B(4))*PI)
      DT(5) = UPD*COS((ALPHA-B(5))*PI)
      DT(6) = LOD*COS((ALPHA-B(6))*PI)
      DT(7) = UPD*COS((ALPHA-B(7))*PI)
      DT(8) = LOD*COS((ALPHA-B(8))*PI)
```

```
      DT(9) = UPD*COS((ALPHA-B(9))*PI)
      DT(10) = LOD*COS((ALPHA-B(10))*PI)
      DT(11) = UPD*COS((ALPHA-B(11))*PI)
      DT(12) = LOD*COS((ALPHA-B(12))*PI)
C     FOR THIS SHOT POINT,12 STATIONS HAVE BEEN PROJECTED INTO
C     A LINE WITH ANGLE ALPHA DEFINED BY USER. THE 12 OFFSET
C     DISTANCES HAVE BEEN OBTAINED X01,X02,X03.....X11,X12.
C     TO CARRY OUT BEAM STEERING WE NEED RAY PARAMETER p,AND OFFSET
C     TIME TAU,IT MEANS THAT WE SUM ALL WAVE APLITUDE WITH SLOPE P
C     OFFSET TIME TAU--A DECLINED LINE.
C     THE FORMULA IS AS FOLLOWING:
C     U(P,TAU)= SIGMA (U(Xj,T=TAU+P*Xj))
C     IN THIS PROGRAM WE USE THREE LOOPS TO SUM THE VALUES.
      PRINT*,' '
      PRINT*,'-START SLANT STACKING PROCESS'
      PRINT*,' '
      P(0)=LOP
C     THE FIRST LOOP DEFINES NUMBER OF P TRACES,IT ALSO MEANS
C     NO. OF DIFFERENT SLOPES GIVEN.
      DO 500 I=1,NP
      P(I)=P(I-1)+PIC
C     THIS LOOP DEFINES INTERCEPT TIME VALUES-TAU FOR PROCESSING.
      TAU = 0.0
      DO 300 J=1,NSAMPL
      TAU=TAU+2*0.001
      TA = TAU/(2*0.001)
C     TO INITIALIZE COUNTER M
      M=0
      DO 200 K=1,12
      N=TAU/(2*0.001)+NINT((P(I)*DT(K))/(2*0.001))
      M=M+1
96    U(I,TA)=U(I,TA)+Z(K,N)
200   CONTINUE
C     TO NORMOLIZE STACKED DATA----THE SUMMED DATA DIVIDED BY
C     NUMBER OF TRACES(M)
97    U(I,TA)=U(I,TA)/M
300   CONTINUE
      DO 101 J = 1301, 1801
98    WRITE(2,99)  J,U(I,J)
99    FORMAT(I5,E12.4)
101   CONTINUE
      PRINT*,'-RAY PARAMETER',I,'     COMPLETED'
500   CONTINUE
```

```
      PRINT*,' '
      GO TO 776
999   PRINT*,'-CALCULATION COMPLETED'
      CLOSE(2)
      STOP
      END
```

FORTRAN-77 PROGRAM 11 - MAPRISM

```
c     ********************************************************
c     Computing the gravity effect of a prism, a line mass and sylinder on  *
c     VAX/UNIX: MAPRISM                                                     *
c     Written by                                                            *
c     XIN-QUAN MA                                                           *
c     at the Department of Geology & Applied Geology,                       *
c     Univrsity of Glasgow,  Glasgow G12 8QQ (in 1987)                      *
c     This program calculates the gravity effect from a vertical prism with *
c     horizontal upper and lower faces, expressed by a 24-term formula;     *
c     from a prism with a horizontal lower face and a sloping upper face;   *
c     from a line mass; and from a sector of a hollow sylinder.             *
c     ********************************************************
      real  x1,x2,y1,y2,h,t1,t2,t3,t4,t5,t6,t7,t8,t9,
     z 10,t11,t12,Fz,i,j,K,g1,g2,g3,c,cosa,r,P,g4
      print*,'input  x1,y1,h'
      read*,x1,y1,h
      x2=x1+1000
      y2=y1+1000
      t1=log((y2+sqrt(x2*x2+y2*y2))/(y2+sqrt(x2*x2+y2*y2+h*h)))
      t2=log((y1+sqrt(x2**2+y1**2))/(y1+sqrt(x2**2+y1**2+h**2)))
      t3=log((y2+sqrt(x1**2+y2**2))/(y2+sqrt(x1**2+y2**2+h**2)))
      t4=log((y1+sqrt(x1**2+y1**2))/(y1+sqrt(x1**2+y1**2+h**2)))
      t5=log((x2+sqrt(x2**2+y2**2))/(x2+sqrt(x2**2+y2**2+h**2)))
      t6=log((x1+sqrt(x1**2+y2**2))/(x1+sqrt(x1**2+y2**2+h**2)))
      t7=log((x2+sqrt(x2**2+y1**2))/(x2+sqrt(x2**2+y1**2+h**2)))
      t8=log((x1+sqrt(x1**2+y1**2))/(x1+sqrt(x1**2+y1**2+h**2)))
      t9=asin((y2**2+h**2+y2*sqrt(x2**2+y2**2+h**2))/((y2+
     z sqrt(x2**2+y2**2+h**2))*sqrt(y2**2+h**2)))
      t10=asin((y2**2+h**2+y2*sqrt(x1**2+y2**2+h**2))/((y2+
     z sqrt(x1**2+y2**2+h**2))*sqrt(y2**2+h**2)))
      t11=asin((y1**2+h**2+y1*sqrt(x2**2+y1**2+h**2))/((y1+
     z sqrt(x2**2+y1**2+h**2))*sqrt(y1**2+h**2)))
      t12=asin((y1**2+h**2+y1*sqrt(x1**2+y1**2+h**2))/((y1+
     z sqrt(x1**2+y1**2+h**2))*sqrt(y1**2+h**2)))
      Fz=x2*(t1-t2)-x1*(t3-t4)+y2*(t5-t6)-y1*(t7-t8)+
     z h*(t9-t10-t11+t12)
      print*,'Fz=',Fz
      i=(x1+500)/1000
      j=(y1+500)/1000
      r=sqrt((x1+500)**2+(y1+500)**2)
```

```
      c=sqrt(r**2+h**2)
      cosa=r/c
      K=(i+0.5)*log((j+0.5)+sqrt((i+0.5)**2+(j+0.5)**2))
     z -(i-0.5)*log((j+0.5)+sqrt((i-0.5)**2+(j+0.5)**2))
     z +(j+0.5)*log((i+0.5)+sqrt((i+0.5)**2+(j+0.5)**2))
     z -(j+0.5)*log((i-0.5)+sqrt((i-0.5)**2+(j+0.5)**2))
     z -(i+0.5)*log((j-0.5)+sqrt((i+0.5)**2+(j-0.5)**2))
     z +(i-0.5)*log((j-0.5)+sqrt((i-0.5)**2+(j-0.5)**2))
     z -(j-0.5)*log((i+0.5)+sqrt((i+0.5)**2+(j-0.5)**2))
     z +(j-0.5)*log((i-0.5)+sqrt((i-0.5)**2+(j-0.5)**2))
      P=1/sqrt(i**2+j**2)
      print*,'K=',K
      print*,'P=',P
      print*,'      '
      g1=abs(0.006672*2.70*Fz)
      g2=6.672*2.70*(1-cosa)*K
      g3=6672*2.70*(1/r-1/c)
      g4=3336*2.70*h**2/(r**3-r*2.5E05)
      print*,'r=',r
      print*,'prism=',g1
      print*,'slopping   prism=',g2
      print*,'line   mass=',g3
      print*,'sylinder=',g4
      stop
      end
```

FORTRAN-77 PROPGRAM 12 - MAEIGEN

```
C     ********************************************************
C     THE FOLLOWING TWO SUNROUTINES ARE USED TO CALCULATE THE      *
C     EIGENVALUES AND EIGENVECTORS OF A SYMMETRIC MATRIX. THE      *
C     EIGENVALUES ARE, ON OUPUT, IN DECEANT ORDER.C                *
C     ********************************************************
      SUBROUTINE JACOBI(A,N,NP,D,V,NROT)
      PARAMETER (NMAX=100)
      DIMENSION  A(NP,NP),D(NP),V(NP,NP),B(NMAX),Z(NMAX)
      DO 12 IP=1,N
      DO 11 IQ=1,N
      V(IP,IQ)=0.
11    CONTINUE
      V(IP,IP)=1.
12    CONTINUE
      DO 13 IP=1,N
      B(IP)=A(IP,IP)
      D(IP)=B(IP)
      Z(IP)=0.
13    CONTINUE
      NROT=0
      DO 24 I=1,50
      SM=0.
      DO 15 IP=1,N-1
      DO 14 IQ=IP+1,N
      SM=SM+ABS(A(IP,IQ))
14    CONTINUE
15    CONTINUE
      IF(SM.EQ.0.)RETURN
      IF(I.LT.4)  THEN
      THRESH=0.2*SM/N**2
      ELSE
      THRESH=0.
      ENDIF
      DO 22 IP=1,N-1
      DO 21 IQ=IP+1,N
      G=100.*ABS(A(IP,IQ))
      IF((I.GT.4) .AND. (ABS(D(IP))+G  .EQ.ABS(D(IP)))
     * .AND. (ABS(D(IQ))+G .EQ. ABS(D(IQ)))) THEN
      A(IP,IQ)=0.
      ELSE IF(ABS(A(IP,IQ)).GT.THRESH)THEN
```

```
      H=D(IQ)-D(IP)
      IF(ABS(H)+G .EQ. ABS(H))THEN
      T=A(IP,IQ)/H
      ELSE
      THETA=0.5*H/A(IP,IQ)
      T=1./(ABS(THETA)+SQRT(1.+THETA**2))
      IF(THETA.LT.0.)T=-T
      ENDIF
      C=1./SQRT(1+T**2)
      S=T*C
      TAU=S/(1.+C)
      H=T*A(IP,IQ)
      Z(IP)=Z(IP)-H
      Z(IQ)=Z(IQ)+H
      D(IP)=D(IP)-H
      D(IQ)=D(IQ)+H
      A(IP,IQ)=0.
      DO 16 J=1,IP-1
      G=A(J,IP)
      H=A(J,IQ)
      A(J,IP)=G-S*(H+G*TAU)
      A(J,IQ)=H+S*(G-H*TAU)
16    CONTINUE
      DO 17 J=IP+1,IQ-1
      G=A(IP,J)
      H=A(J,IQ)
      A(IP,J)=G-S*(H+G*TAU)
      A(J,IQ)=H+S*(G-H*TAU)
17    CONTINUE
      DO 18 J=IQ+1,N
      G=A(IP,J)
      H=A(IQ,J)
      A(IP,J)=G-S*(H+G*TAU)
      A(IQ,J)=H+S*(G-H*TAU)
18    CONTINUE
      DO 19 J=1,N
      G=V(J,IP)
      H=V(J,IQ)
      V(J,IP)=G-S*(H+G*TAU)
      V(J,IQ)=H+S*(G-H*TAU)
19    CONTINUE
      NROT=NROT+1
```

```
      ENDIF
21    CONTINUE
22    CONTINUE
      DO 23 IP=1,N
      B(IP)=B(IP)+Z(IP)
      D(IP)=B(IP)
      Z(IP)=0.
23    CONTINUE
24    CONTINUE
      PAUSE '50 ITERATIONS SHOULD NEVER HAPPEN'
      RETURN
      END
c
      SUBROUTINE EIGSRT(D,V,N,NP)
      DIMENSION  D(NP),V(NP,NP)
      DO 13 I=1,N-1
      K=I
      P=D(I)
      DO 11 J=I+1, N
      IF(D(J).GE.P) THEN
      K=J
      P=D(J)
      ENDIF
11    CONTINUE
      IF(K.NE.I)THEN
      D(K)=D(I)
      D(I)=P
      DO 12 J=1,N
      P=V(J,I)
      V(J,I)=V(J,K)
      V(J,K)=P
12    CONTINUE
      ENDIF
13    CONTINUE
      RETURN
      END
```